MONITORING AND MODELING OF ACID MINE DRAINAGE FROM WASTE ROCKS DUMPS

La Mine Doyon Case Study

MEND Report 1.14.2 g

June 1994

GREGI

RAPPORT GREGI 1994-12

MONITORING AND MODELING OF ACID MINE DRAINAGE FROM WASTE ROCKS DUMPS

LA MINE DOYON CASE STUDY

By

Pierre Gélinas, René Lefebvre, Marc Choquette, Denis Isabel, Jacques Locat and Roger Guay

UNIVERSITÉ LAVAL

MONITORING AND MODELING OF ACID MINE DRAINAGE FROM WASTE ROCK DUMP - LA MINE DOYON CASE STUDY

EXECUTIVE SUMMARY

This report presents a summary of work done on the monitoring and modeling of acid mine drainage from the South waste rock dump at La Mine Doyon for the period between September 1991 and December 1993. The main purpose of the study was to measure physical and chemical properties of an actual waste dump and to identify the key processes contributing to the generation of acid rock drainage: hydrology, geochemistry, microbiology, and physical processes such as oxygen, mass, and heat transfer.

Important physical parameters such as climatic data, temperature profiles within the dump, total discharge of acid drainage from collecting ditches and chemical composition of the effluents were monitored on a regular basis. Other parameters were measured once or at irregular intervals: gas composition, piezometric levels, leachate composition in the unsaturated zone, infiltration rates, particle size, surface temperature. It is the first time that such a coherent and comprehensive set of parameters is assembled in a large waste rock dump.

The data collected were presented in a progress report in November 1992 (Gélinas *et al.* 1992) and a series of interim reports on specific topics from February 1993 to March 1994: Guay, 1993 (procedure to enumerate iron bacteria); Choquette *et al.*, 1993a (rapid chemical techniques to monitor acid drainage) and 1993b (chemical monitoring data at Mine Doyon); Lefebvre *et al.*, 1993 (heat transfer analysis); Locat *et al.*, 1994 (physico-chemical and mechanical properties of waste rocks); Choquette and Gélinas, 1994 (mineralogy and geochemical processes); Isabel *et al.*, 1994 (hydrology and water budget); Guay, 1994 (microbiological diversity). Reports from Phase I of the project are also used here to present data on monitoring installations and complete chemical analyses (including trace metals) of selected monitoring points (Gélinas *et al.* 1991).

Again, this report does not present all the data available at the site but rather integrates the information and analyses from the above sources, to present a general synthesis of physical and chemical processes active in an acid generating waste rock dump. We are also presenting some new information on numerical modeling of acid mine drainage production in waste dumps.

SURVEILLANCE ET MODÉLISATION DU DRAINAGE MINIER ACIDE DANS UNE HALDE DE STÉRILES - ÉTUDE DU CAS DE LA MINE DOYON

SOMMAIRE

Voici un résumé du travail de surveillance et de modélisation du drainage minier acide dans la halde sud de la mine Doyon, entre septembre 1991 et décembre 1993. Le but premier de l'étude était de mesurer les propriétés physiques et chimiques d'une halde de stériles et de déterminer les principaux processus qui contribuent au drainage minier acide : hydrologique, géochimique et microbiologique ainsi que les processus physiques comme le transfert d'oxygène, le transfert de masse et la dissipation de la chaleur.

On a surveillé régulièrement l'évaluation des paramètres physiques importants comme les données climatiques, les profils de température dans la halde, la quantité totale du drainage acide dans les fossés collecteurs et la composition chimique des effluents. Les autres paramètres qui ont été mesurés une fois ou à intervalles irréguliers sont : la composition des gaz, les niveaux piézométriques, la composition du lixiviat dans la zone non saturée, les taux d'infiltration, la granulométrie et la température de la surface. C'est la première fois que l'on constitue un ensemble de paramètres aussi cohérent et aussi complet pour une halde de stériles aussi vaste.

Les données recueillies ont été présentées dans un rapport d'étape en novembre 1992 (Gélinas et coll. 1992) et dans une série de rapports provisoires sur des projets précis remis entre février 1993 et mars 1994 : Guay, 1993 (procédure pour le dénombrement des bactéries du fer); Choquette et coll., 1993a (techniques chimiques rapides pour la surveillance du drainage minier acide) et 1993b (données de surveillance chimique à la mine Doyon); Lefebvre et coll. 1993 (analyse des transferts thermiques); Locat et coll., 1994 (propriétés physico-chimiques et mécaniques des stériles); Choquette et Gélinas, 1994 (minéralogie et processus géochimiques); Isabel et coll., 1994 (hydrologie et bilan hydrologique); Guay, 1994 (diversité microbiologique). On s'est aussi servi des rapports de la première phase du projet pour obtenir des données sur les installations de surveillance et des analyses chimiques complètes (y compris sur les métaux-trace) des points de surveillance choisis (Gélinas et coll., 1991).

Je vous rappelle que le rapport ne fournit pas toutes les données disponibles à la mine, mais regroupe les renseignements et les analyses fournis par les sources susmentionnées afin de présenter une synthèse générale des processus physiques et chimiques actifs dans une halde de stériles qui produit du drainage acide. Nous vous donnons aussi de nouveaux renseignements sur la modélisation numérique de la production du drainage acide dans les haldes de stériles.

Table of contents

List of tables

Chapter 6.

Chapter 7.

List of figures

Chapter 5.

Chapter 6

Chapter 7.

1 / Introduction

1.1   SCOPE AND OBJECTIVES OF THE MINE DOYON PROJECT

The Mine Doyon monitoring and modeling project originated in September 1989 when an agreement between Centre de Recherches Minérales (Ministry of Energy and Resources, Québec), La Mine Doyon (Lac Minerals and Cambior) and GREGI from Université Laval was signed to undertake a long term project on the characterization of the south waste rock dump of La Mine Doyon that had been showing signs of increasing acid production only a few years after it had been constructed. Since data were lacking on the actual processes controlling acid generation in waste rock dumps and that no baseline information was available, a program was established to provide minimal monitoring capacity to help in decision making over the future of the dump.

Phase I of the project lasted from January 1990 to September 1991. During that period a system of collecting ditches was built and three weir stations were put in place. Six boreholes were drilled in the dump during the winter of 1991 providing complete geological logs, and were equiped with piezometers, thermistors chains, and air tubes. A similar set of observation wells were installed around the dump to identify any leaks in the collecting system. Data collection for a few months were included in a final report for that phase. Chemical analyses of the acid drainage were done on samples of groundwater from observation wells, and samples of surface water collected at the weir stations. Major ions (Fe, SO_4, Al, Mg, Ca), minor ions (Na, K, Mn, Si), and trace metals (Cd, Cu, Ni, Pb, Zn) were determined. Monitoring changes with time relied mainly on physico-chemical parameters such as pH, Eh, conductance, acidity, specific gravity, and total dissolved solids.

Objectives

One overall goal of the MEND research program is to contribute establishing guidelines for engineering decisions related to AMD production from waste rock dumps. These decisions may range from waste dumps siting and design to minimize AMD production, monitoring programs for the effective evaluation of the magnitude of AMD production and its environmental impact at a given site, as well as the choice and design of control measures to economically limit or eliminate AMD production.

To reach that goal, it is important that comprehensive physical and chemical data be collected in a major waste rock dump to provide insights on key parameters that control acid rock drainage. The Mine Doyon South waste rock dump was chosen as a study site because of several favorable

features: large size (>20 million tonnes), simple hydrologic setting, important acid production, rapid development of ARD, and extensive monitoring facilities already in place.

The primary scientific goal of this study is to predict acid leachate composition and its evolution in time and space. The leachate chemical characteristics are largely controled by reactions occurring in a thick unsaturated zone. Using a comprehensive monitoring data base, the research program concentrated on two major problems:

- To evaluate acid rock drainage generation processes based on physico-chemical conditions prevailing within the unsaturated zone, physical characterization of waste rock, changes in mineralogy (alteration, formation of new minerals, deposition of amorphous reaction products), chemical characterization of the leachate as a function of depth and its relation to leachate composition in the saturated zone.

- To model transport mechanisms in the unsaturated zone. Emphasis is put on heat generation and dissipation, gas flow (mainly oxygen) by diffusion and thermally induced convection, and fluid flow. Fluid flow models are used to establish mass balances in the system.

1.2   SITE CHARACTERISTICS

1.2.1   LOCATION

La Mine Doyon is a gold mine located in the Bousquet Township in Abitibi, Quebec. It lies 40 km east of Rouyn-Noranda and 60 km west of Val-d'Or (Figure 1.1). From the beginning in 1978 the mine operated as an open pit until 1989 at which time 47 million tonnes of waste rock and overburden were excavated. Overburden was used partly to build roads and dams for tailing ponds, and the rest was deposited in the north waste dump. The south waste dump was built from 1983 to 1988 from material coming from the main pit (Figure 1.2) with minor amounts of overburden and less reactive rocks from the west pit. The south dump covers approximately 53 hectares and contains an estimated 21 million tonnes of waste rocks. The total volume is an estimated 11,5 million cubic meters with an average thickness of 30 m. It occupies a rectangular area of approximately 600 m by 900 m and it partly covers a small hydrologic basin that used to drain toward the west (Figure 1.3).

1.2.2   GENERAL GEOLOGY OF THE MINE DOYON SITE

The different lithologies in the main pit and the west pit have been summarized by Savoie *et al.*, (1991). Mine Doyon is located in Archean metavolcanic rocks of the Blake River Group within the Abitibi Greenstone Belt. The regional metamorphic grade is greenschist. We make only a brief description of the geological units found in the waste dump. Two important zones of gold ore were mined from the main pit, the source of most of the waste rocks found on the south dump. A typical cross-section of the pit is shown on Figure 1.4. Three main rock types occur in that portion of the mine (in order of decreasing importance): 1) Sericitic schists (Unit 4B), 2) Intermediate tuffs (Unit 3), and 3) Felsic volcanoclastics (Unit 4A).
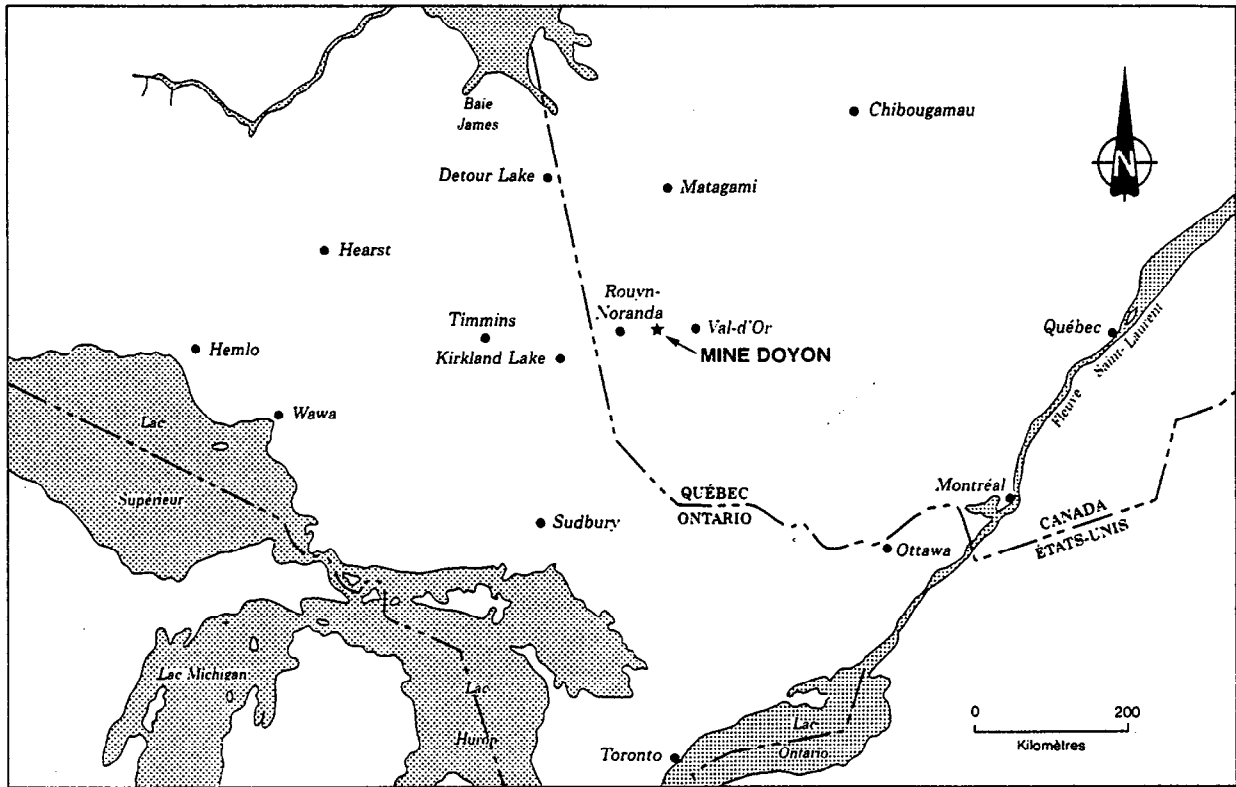
Fig. 1 Location of La Mine Doyon

Sericitic schists (Unit 4B)

The sericitic shists are composed of quartz, mica (muscovite mainly), pyrite, rutile and chlorite. They have a well defined penetrative schistosity which obliterated all original textures. Based on 45 total sulphur analyses made by Savoie *et al.* (1991), the sulfide content of that unit is estimated at 7% and the calcite content at 2%. More than 99% of sulfides is pyrite. Sericite is a variety of muscovite with a silky luster. Approximately 50% of the waste rocks in the south dump are sericitic schists.

Intermediate tuffs (Unit 3)

Intermediate tuffs are composed mainly of quartz, plagioclase feldspar, chlorite and variable amounts of carbonate (5,5% equivalent calcite). The sulfide content calculated from 15 chemical analyses is 1,8%. This unit accounts for about 30% of the waste dump.
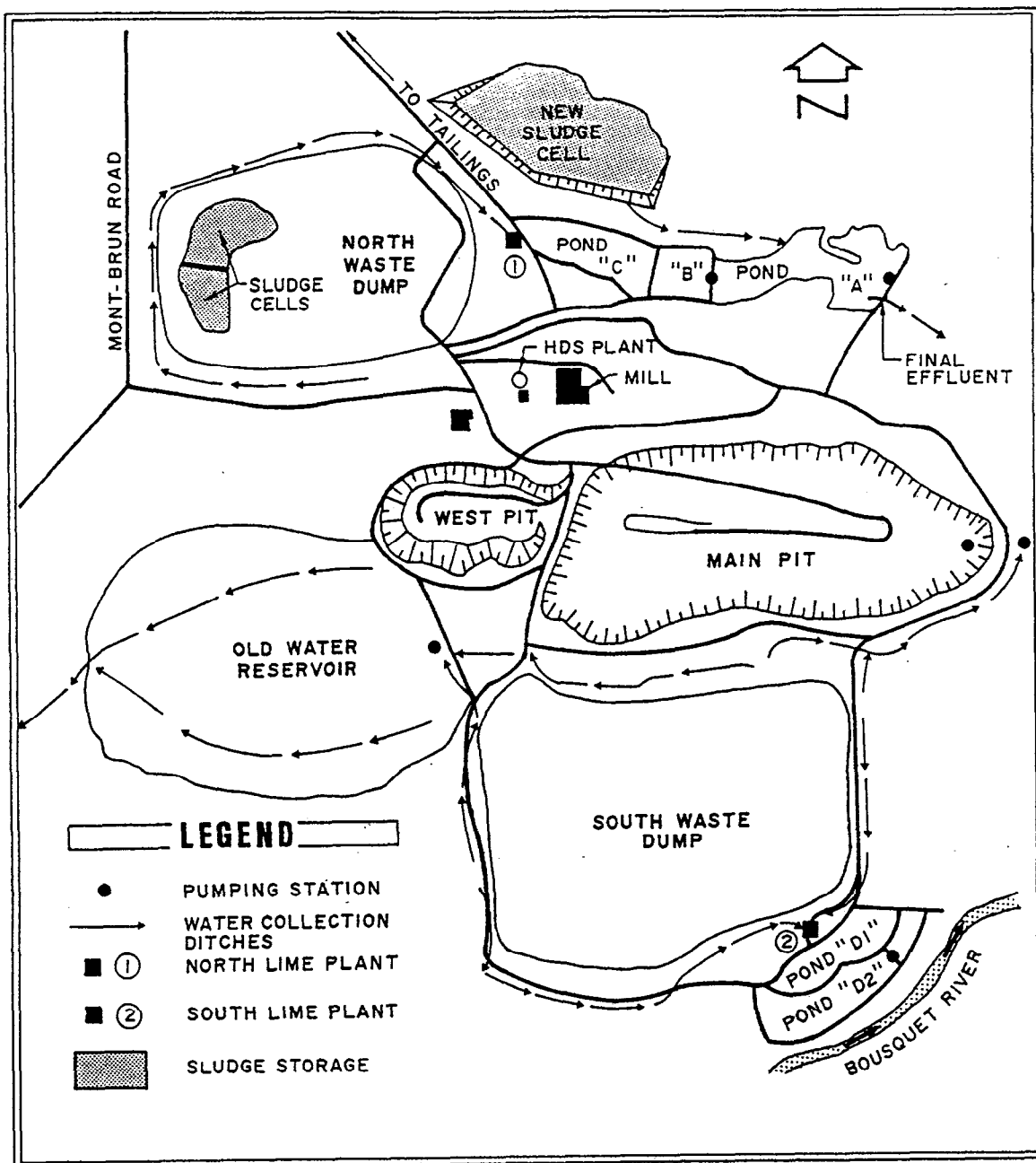
Fig. 1.2 Schematic plan of the site
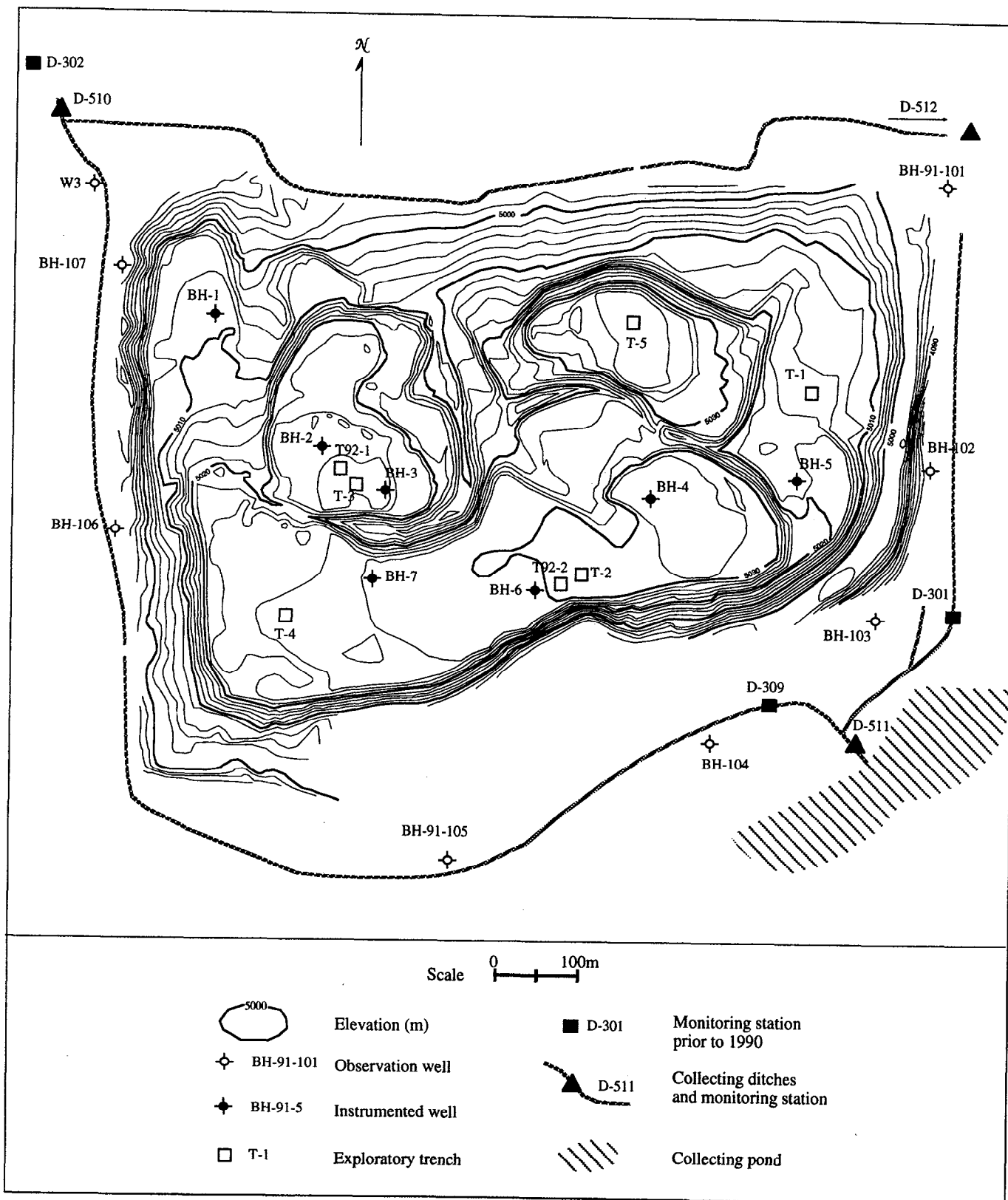
Fig 1.3 Location map of the South Dump
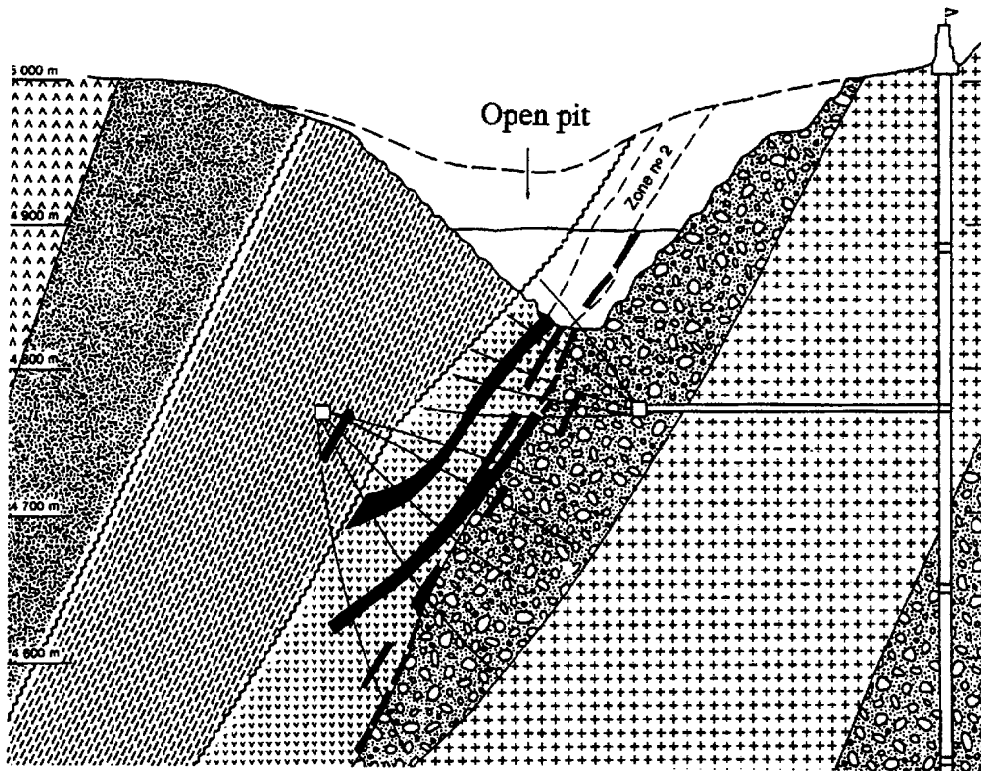
Unit

3 ▨ Intermediate tuffs

4a ▨ Felsic volcanoclastics

4b ▨ Sericitic schists

0 ——————————— 200

meters

Fig 1.4 Schematic cross-section through the main pit (from Savoie et al. 1991)

Felsic volcanoclastics (Unit 4A)

This unit is composed of plagioclase feldspar and quartz with traces of chlorites and micas. A penetrative schistosity is present but it is not as intense as in Unit 4B. This rock type is concentrated in a specific pile inside the south dump and is a potential very low grade gold ore. The pyrite content is estimated at 5.5% based on 43 samples and the calcite content is 2%. This unit accounts for about 15% of the waste rocks of the dump.

Smaller quantities of other rock types (less than 5% of the total mass) are composed of diorite and other intrusive rocks coming from the west open-pit. These rocks are located as a small layer on the top of the NE corner of the dump.

Smaller quantities of other rock types (less than 5% of the total mass) are composed of diorite and other intrusive rocks coming from the west open-pit. These rocks are located as a small layer on the top of the NE corner of the dump.

Sulfides other than pyrite are not found in any significant amounts in the waste pile. In the ore zones chalcopyrite and sphalerite may be found in very small amounts. Based on the relative proportion of the waste rock types, the total mass of pyrite in the whole dump is 1,05 million tonnes.

1.3   ACID ROCK DRAINAGE AT MINE DOYON

1.3.1   EARLY OBSERVATIONS

Beaudoin and McMullen (1990) made a summary of the acid generation problem at Mine Doyon and the corrective measures that were designed. Acid drainage from the south dump was first noticed in 1985, two years after beginning the construction of the pile. Acid generation increased steadily from 1985 to 1988 when the dump construction stopped and Mine Doyon continued as an underground operation. The monitoring network was not well developed at this time and it is
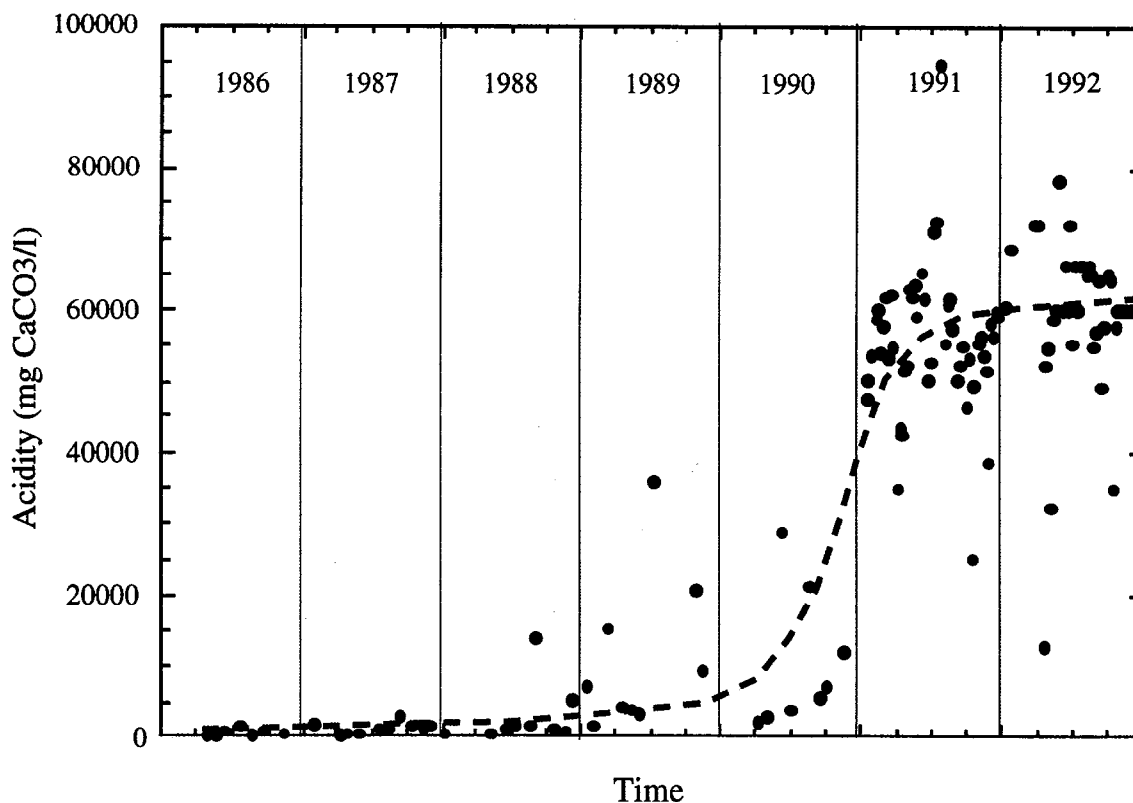
Fig. 1.5 Evolution of acidity at station 510 from 1986 to 1992

1.3.2 ESTIMATES OF ACID/BASE ACCOUNTING AND PYRITE CONTENT

Sulfides in the waste rocks of La Mine Doyon consist mainly of pyrite (for more than 99% of the total). Minor amounts of other sulfides such as chalcopyrite and sphalerite occur in these rocks. However in the gold-mineralized veins, chalcopyrite is often present. Based on lithology and mine records, the mass of each rock type can be estimated for the waste dump. Sericitic schists (7% pyrite) accounts for 50% of the waste rocks, intermediate tuffs (1,8% pyrite) is 30% of the waste rocks, and felsic volcanoclastics (5,5% pyrite) is 15% of the waste rocks, Other non-acid generating rocks from the west pit accounts for about 5% of the waste rocks. A weighted average gives 5% pyrite. This estimate is based on more than a one hundred chemical analyses for sulphur in the three principal units. However, the proportions of each rock type in the waste dump are still approximate.

Net neutralization potential (NNP) for unweathered rocks were calculated from chemical analysis and are presented in Table 1.1. The sericitic schists (Unit 4B) and felsic volcanoclastics (Unit 4A) are net acid producers with respective NNP values of -97 kg/t and -71 kg/t. Unit 3, the intermediate tuffs, has a NNP of +25 kg/t. Similar data were collected by Firlotte et al. (1991) for sericitic schists with a mean value (from 11 samples) of NAP (net acid potential) of 116 kg/t; a wide variation of NAP from -20 to +207 kg/t was observed.

1.4 ORGANIZATION OF THE REPORT

This report is divided in several sections corresponding to the different parameters and processes that were studied. Chapter 2 presents field instrumentation and monitoring procedures that were put in place to characterize an active waste rock dump. Chapter 3 analyzes the waste rocks themselves with particular attention to their strength and durability against physical and chemical weathering. Chapter 4 looks at the water budget and identifies the major processes of water transport in a waste dump. Chapter 5 deals with the monitoring data on water and leachate composition at different points in the Mine Doyon dump; it also presents studies of mineralogical and microbiological transformation of sulfides in an active waste dump. Chapter 6 studies the thermal regime of the dump and explains the heat flux and heat production in terms of rates of oxidation. Chapter 7 is used to present a numerical model of AMD production processes in the dump and to validate it with field data. Chapter 8 lists the main findings of this project. This report summarizes findings already documented in interim reports that have to be referred to for more detailed explanations as well as for the tabulation of data.

Table 1.1 Maximum potential acidity from sulfides content and neutralization potential from carbonate analysis.

	Unit 3 Intermediate tuffs	Unit 4A Felsic volcanoclastics	Unit 4B Sericitic schists
Calculated Sulfides [*] *(%)*			
Chalcopyrite	0.041	0.023	0.013
Galena	0.001	0.002	0.002
Sphalerite	0.008	0.004	0.007
Pyrite	1.759	5.452	6.950
Calculated Carbonate [**] *(%)*			
Calcite	5.46	1.98	1.96
Maximum Potential Acidity (from %S) (MPA in eq. kg $CaCO_3$/tonne of rock)			
	29.67	91.25	116.25
Carbonate Analysis (CA in kg $CaCO_3$/tonne of rock)			
	54.60	19.80	19.60
Net Neutralization Potential (CA-MPA in kg $CaCO_3$)			
	24.93	**-71.45**	**-96.65**

[*]: Chalcopyrite from Cu, Galena from Pb, Sphalerite from Zn and Pyrite from S - S attributed to the Cu, Pb and Zn sulfides. [**]: Calcite from CO_2.

2/ Field instrumentation, characterization and monitoring

2.1   INTRODUCTION

A major goal of this project is to gather fundamental field data on a comprehensive scale to study all the physico-chemical processes which have been recognized as important in controling acid mine drainage generation. Data have been obtained outside the waste dump location (weather data, surface water samples), inside the dump (rock and mineral samples, groundwater and unsaturated zone moisture, temperature data, gas samples), at the surface (surface temperature, precipitation and infiltration), and around the waste dump (seepage at surface and underground). A large part of the field equipment was put in place during Phase I of this project and only a summary is given here.

2.2   INSTRUMENTATION

2.2.1   EXPLORATION TRENCHES

Rock sampling was done from trenches 3 to 5 meters deep located in such a way as to represent the major lithologies present. Figure 1.3 shows the location of these trenches: three are located in a zone where the sericitic schists are the main lithology (T1, T2 and T4) including the oldest part of the pile (T1); one is located in the very low grade ore pile (T3), and one in a non-reactive zone of "green" rocks (T5). Bulk samples were taken in stratigraphic succession to yield mineralogical evidence of alteration in the top 5 meters of the dump. Two larger trenches (T92-1, T92-2) were used to collect larger samples for particle size and mineralogical analyses, and water content determination. These were equipped with gravity lysimeters. Description of the material collected is given in *Gélinas et al., 1991*. In the first meter, the rocks are usually at a near neutral pH and most oxidation features become abundant past 3 meters. Several other samples were collected at the surface and along the slopes of the waste rock dump.

2.2.2 BOREHOLES INSTALLATION

Drilling was done under the supervision of Golder Associates Ltd in the winter and spring of 1991. Reverse-circulation air-drilling with an excentric bit was used to recover rock fragments smaller less than 2 cm as composite samples taken every 1,5 meters. A 6-inch (0.15 m) steel casing was used to maintain the borehole walls until the underlying bedrock was reached. The entire thickness of the dump, the underlying original soil and 5 to 10 meters in underlying bedrock were penetrated in 6 boreholes labeled BH-91-1 to BH-91-6. The layout of these boreholes reflects the former drainage basin and represents conditions in three subbasins. Seven other boreholes were dug on the outside perimeter of the dump to monitor acid groundwater seeping into the peripheral ditch system. These are labeled BH-91-101 to BH-91-107 and are shown on Figure 2.1. Samples collected during the drilling operations were analyzed to determine lithology, mineralogy (unweathered and oxidized minerals, newly formed minerals), porewater geochemistry and physical toughness of fragments.

2.2.3 BOREHOLES EQUIPMENT

Each borehole has multiple functions; it is used to study hydrology and hydrogeology, to sample groundwater, to measure temperature profiles with depth, to sample gases and measure their properties. A typical borehole instrumentation is illustrated in Figure 2.1.

Typically, two piezometers are installed in each borehole, isolated with a clay and bentonite plug. The deeper piezometer is a 19 mm PVC tube fitted with a PVC screen reaching approximately 5 meters into sound regional bedrock. A silty clay layer overlies most of the bedrock except in a few areas representing small hills before the dump was filled. The other piezometer (38 mm in diameter) is terminated at the interface between waste rock and the original soil surface. The free (phreatic) groundwater surface is usually located very close to the original soil surface or slightly below it. Precise elevation of piezometers and water levels are used to calculate hydraulic gradients and were used for the hydrogeologic model. Around the dump, boreholes only penetrate soil and bedrock and two piezometers were installed and sealed from each other when the soil layer was thick enough to have a groundwater table.

Polyethylene gas sampling tubes are taped to the higher piezometer tube at 8 different depths from the surface. When the steel casing was removed, a sand pack was placed in the annular space between the borehole and the tubes. Air sampling was done at a few occasions in 1991 and 1992 to measure gas composition in the dump. Physical measurements of air density, pressure and temperature were also performed using these tubes in the summer of 1992.

Strings of thermistors (11 in a typical borehole) were also installed in each drill hole in the dump (Figure 2.2). Each borehole is completed at surface by a PVC casing extending one meter above ground and covered with a cap to prevent water and dust from entering the boreholes. Thermal data is treated in details in Chapter 6.

ø = 38 mm   ø = 19 mm
0.66 m ———   ——— 0.65 m   Surface

1.3 m
1.8 m
2.8 m

4.8 m

Éch. horiz.: 1: 10
Éch. vert.: 1: 250

0.2 m

5 m

9.8 m

14.8 m

19.8 m

Waste

29.8 m

34.1 m

Silt

Bedrock

39.6 m

0.15 m
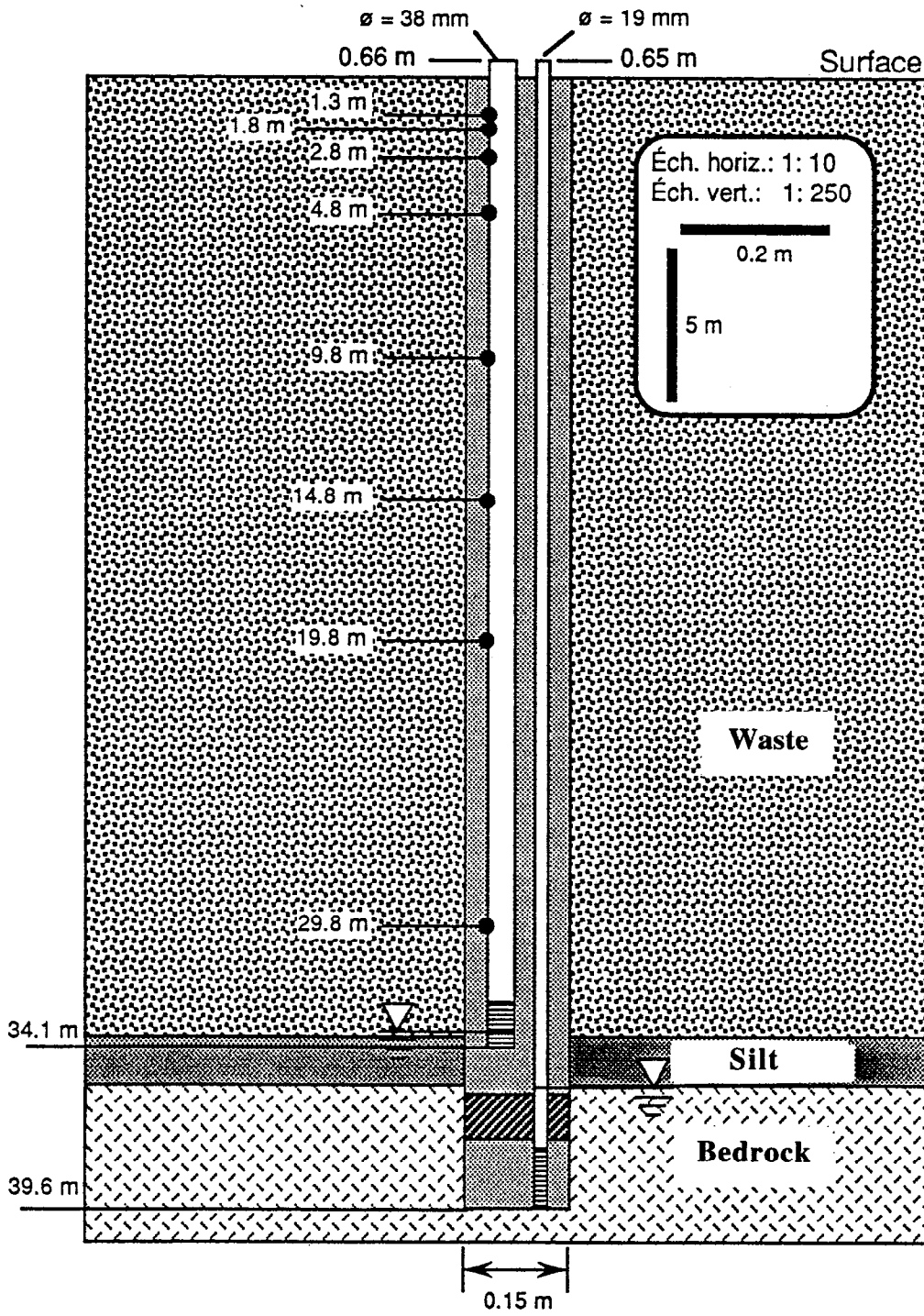
● : Air sampling port and thermistor

Fig. 2.1 Typical borehole instrumentation

2.2.4   LYSIMETERS INSTALLATION

In 1992 it was decided to install gravity lysimeters at two locations to help understand the surface hydrology of the dump and get some data on infiltration. Two large excavations 15 meters wide and 5 meters deep (T92-1 and T92-2) were equiped with polyethylene half-barrels, 60 cm in diameter and 60 cm high at three different levels, two on each level. A PVC tube from the bottom of the barrel to surface allows the measurement of water level and water sampling with a peristaltic pump. Each excavation was carefully backfilled with waste rocks to the original surface. Calibration was done on each lysimeter by measuring the water volume corresponding to a change in level by injecting or pumping water. This simple instrumentation is essential to estimate surface evaporation and infiltration. Water sampling at three different levels is important in understanding chemical transformations occurring in the interstitial water near the top of an active dump. A typical installation is illustrated on Figure 2.2.

Vertical scale (m)

Non-reactive waste rocks (2cm Ø)
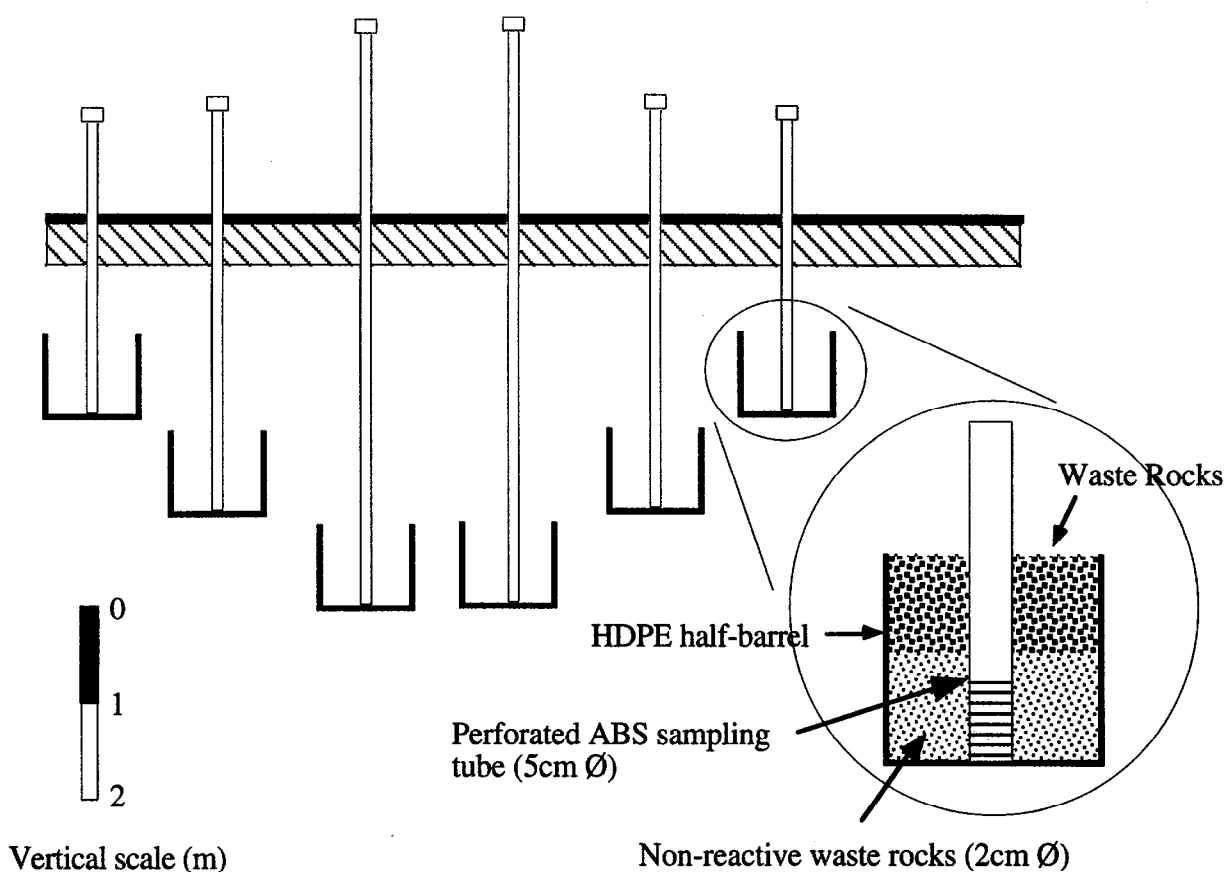
Fig. 2.2 Schematic representation of a group of lysimeters

2.2.5   COLLECTION DITCHES AND WEIR STATIONS

Seepage of acid leachate is collected trough a ditch system in three segments. Location of weir stations 510, 511, and 512 is illustrated in Figure 1.3. In terms of basin size and the portion of the waste dump being drained, station 510 is the most important since it drains 72% of the waste rock,

station 511 takes 23% of the acid drainage and station 512 only 5%. Precipitation on surfaces outside the dump tends to dilute acid drainage as will be seen in Chapter 4. Ditches were dug in soil for most of their length but small sections on the south side of the dump are intersecting bedrock. Part of the water drained in each branch is coming from runoff generated outside the dump. In Chapter 5, a hydrograph analysis is used to distinguish between the portion of total flow generated by the dump and by surface runoff. Three automatic weir stations have been installed and calibrated to measure total flow as a function of time. During the monitoring period, frequent power failures of short durations made it very difficult to get accurate short-time-interval measurements of flow. Continuous flow measurement are collected on a chart recorder producing a long string of calibrated paper each month. This type of analog record is not easily interpreted since for major flow events, the flow rate can be out of range. Even though instantaneous flow rates are not always available, cumulative flow volumes are also recorded. Weekly measurements of total flow are thus available for analysis as well as selected short events when rainfall and flow rates were measured simultaneously. New equipment is now in place with an independent logger that takes accurate measurements with an absolute time reference.

2.2.6   WATER SAMPLES COLLECTION

Acid mine drainage was collected by different methods according to the sampling location. Surface water samples were collected at the weir stations by a programmable automatic sampler and several samples were collected manually by a technician when freezing prevented the operation of the sampler. For a two-year period, weekly samples were collected. Special sampling intervals were also used for some events such as the spring melt.

Groundwater was sampled using an inertial Wa-Terra pump. With this instrument, dedicated sampling tools are used for each monitoring point and it is possible to recover acid leachate even when it is very concentrated or contains sediments.

In the unsaturated zone, the gravity lysimeters were sampled with a peristaltic pump operated from the surface. Starting in 1993, after the backfilled material had reached equilibrium, sample frequency was approximately every month. A one-time evaluation of water quality in the unsaturated zone can be obtained from drill cuttings by extracting soluble salts with distilled water as will be discussed in Chapter 4. A small number of water samples from the unsaturated zone were also recovered by squeezing moist soil samples collected in open excavations.

2.2.7   WEATHER STATION

Climatic data was collected on-site by a weather station installed at the mill. Data on precipitation, temperature, relative humidity, and atmospheric pressure are collected at 15-minute intervals. This station has started operating in the summer of 1992. Temperature correlates fairly well with regional weather stations in Rouyn-Noranda, Val-d'Or and Amos. Precipitations, especially snowfall is not accurate enough for many purposes because the instruments were installed on the roof of the mill building. For water budgets on an annual basis, the statistical analysis of weather

data from the three regional stations is considered more significant. This point is discussed in Chapter 5.

2.3   PHYSICAL CHARACTERIZATION

2.3.1   PARTICLE SIZE

Particle size distribution of waste rock is difficult to measure because very large blocks (1 meter or more) are present. Field determinations of larger particle sizes were done during lysimeters installation. Using a backhoe, a large canvas and a field scale (1000 kg capacity), four large samples were collected near the surface in two contrasting area: an area of low reactivity (acid volcanoclastic rocks) and another one with very reactive material (sericitic schists). Discarding blocks larger than 0,5 m, waste rocks were divided in the field in two fractions using a cross-bar sieve with 70-mm openings. Between 17 and 60% of fragments are larger than 70 mm, the higher figure representing more rigid volcanoclastic rocks. The sericitic schists unit that forms about 50% of the waste rock dump is more brittle and produces greater amounts of fines. The smaller-than-70-mm fractions were quartered and brought to the lab for standard sieve analysis. Figure 2.3 illustrates particle size curves for samples taken at surface and at a depth of 1 m at the two locations where lysimeters were installed. The mean particle size d_{50} varies between 15 and 100 mm. The finer 10% of samples is usually between 0,5 and 1,0 mm. However for all properties depending on specific surface (m^2/kg) the 10% fine fraction has approximately 50 times more surface area than larger blocks. Thus water content, degree of saturation, oxidation rates and relative permeability are dominated by the relative abundance of the fine fraction.
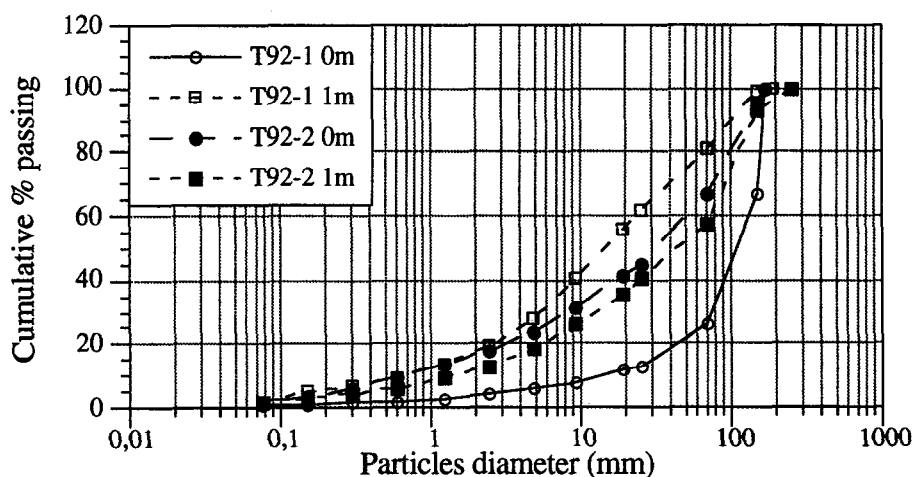
Fig. 2.3   Particles size curves for samples taken at lysimeter stations T92-1 and T92-2

2.3.2   WATER CONTENT

Water content can be defined on a mass basis w_C as the weight of water divided by the weight of solids (geotechnical definition) or on a volume basis T as the volume of water over the total volume of a sample. Since samples taken in the field are disturbed, water content on a mass basis were measured. Conversion to volumetric water content is made if porosity and rock density are known. Water content was measured on 28 samples collected in the two trenches used for lysimeters installation. In the very low grade ore pile T-92-1, the average water content to a depth of 4 meters is 0,038 (3,8%) and in the very reactive zone T-92-2, where sericitic schists dominate, the average water content is 0.075 (7.5%).

2.3.3   BULK DENSITY

Bulk density is an important parameter to estimate porosity and water saturation if the density of solids is known. A standard method to determine bulk density is to weigh a sample coming from a known volume of soil or rock. In waste dumps, this method is not applicable because very large blocks are present and it is very difficult to evaluate with precision the volume of an excavation. For that reason a geophysical method was used to estimate the bulk density of the whole dump.

Based on the theory of gravity (Grant and West, 1965), the value of the constant of acceleration g on earth depends on latitude, altitude and topography. The change in gravity with elevation may be related to the density of the underlying material. The corrected change in gravity is called a Bouguer anomaly and is a function of the elevation h (in meters) above a reference plane, G the gravitational constant $(6,666 \times 10^{-6}$ m^3/kg $s^2)$ and the density ρ_b (kg/m^3) of the material. The difference of gravity Δg is measured in milligals $(1$ mgal $= 10^{-5}$ $m/s^2)$. During a microgravimetric survey, Δg is measured as a function of elevation at a series of stations where location and elevation have to be measured with accuracy. A plot of Δg versus elevation h yields a slope m used to calculate ρ_b using the following relationships:

$$\Delta g = 2\ \pi\ G\ h\ \rho_b \quad \text{and} \quad m = \Delta g / h = 4,19 \times 10^{-5}\ \rho_b$$

Figure 2.4 shows three line segments over which a microgravimetric survey was done, and Figure 2.5 illustrates a vertical profile of the dump. A plot of Δg versus difference in elevation is given on Figure 2.6. Two slopes are drawn for the west and the east section because their base elevations (reference) are not the same. The slope m is 0,0818 mgal/m which yields a mean density ρ_b of 1950 kg/m^3. These data have been checked with a program which makes corrections to take into account topographic features around the waste rock dump; these corrections are not significant in this case. The dry bulk density is estimated at 1840 kg/m^3 from the total mass of the south waste dump (21 million tonnes, from mine records) and its volume (11,5 million m^3 determined from accurate surveys of the dump before and after its construction). The difference between this value and the bulk density is 110 kg/m^3. This difference is attributed to water retained in the pore space of the dump.
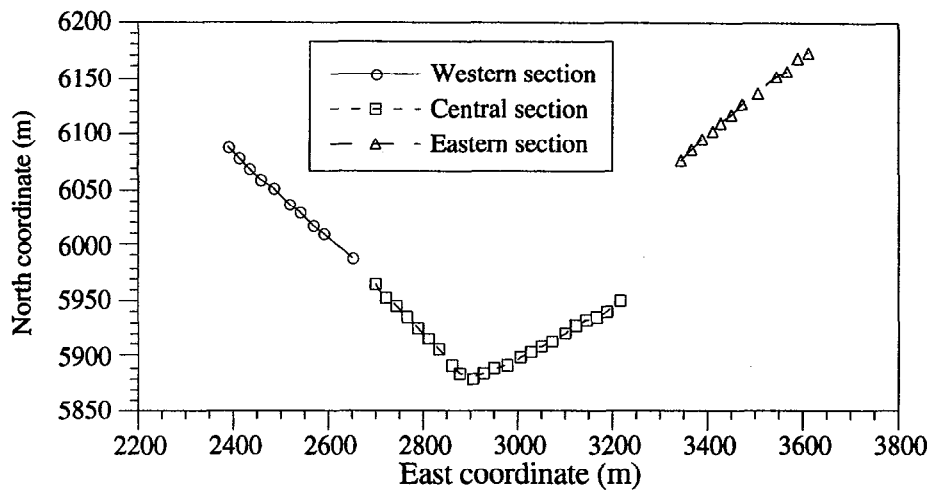
Fig 2.4 Localisation of gravimetric station
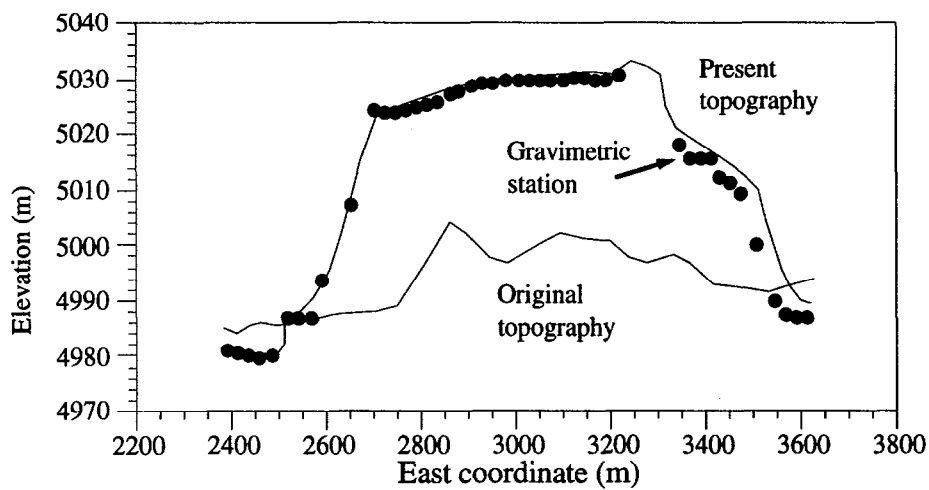
Fig. 2.5 Vertical profile of the dump below gravimetric stations
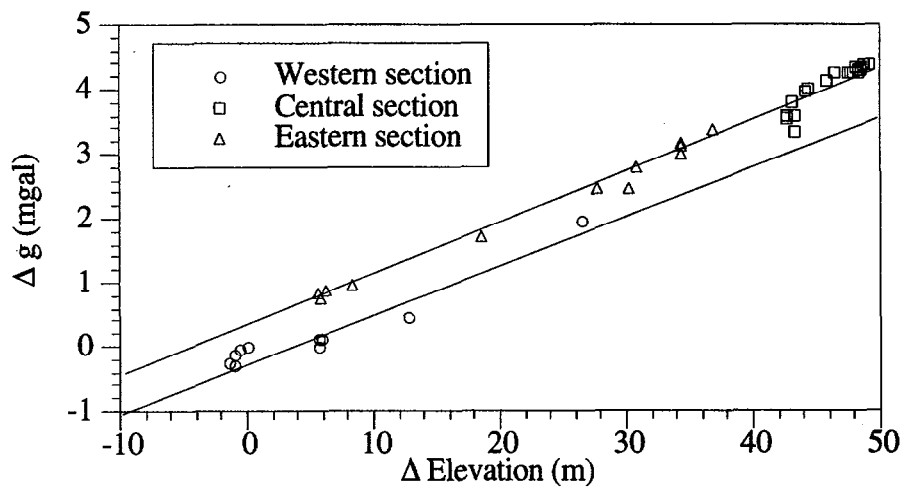
Fig. 2.6 Bouguer anomaly Δg as a function of elevation

2.3.4   POROSITY

Bulk density derived from gravimetric survey takes into account partial saturation in water. Water content and rock density values measured in the lab must be used to calculate dry density, porosity and degree of saturation of the waste rocks. The following relationships between parameters are used.

For a unit volume, water content w_c is the mass of water M_w over the mass of solids M_s; Water saturation S_w is the volume of water V_w over the volume of pores V_p; porosity n is defined as the volume of pores V_p over the total volume V_t.

$$W_c = \frac{M_w}{M_s} = \frac{V_w \rho_w}{V_s \rho_s} \qquad (1)$$

$$S_w = \frac{V_w}{V_p} \qquad (2)$$

$$n = \frac{V_p}{V_t} \quad \text{and} \quad (1-n) = \frac{V_s}{V_t} \qquad (3)$$

where ρ_w is the density of water and ρ_s the density of solids. From equations (1) to (3) the following relation between w_c and S_w is derived:

$$S_w = \frac{W_c(1-S)\rho_s}{n\rho_w} \qquad (4)$$

The definition of bulk density ρ_b for a partially-saturated porous medium uses the same parameters:

$$\rho_b = (1 - n)\,\rho_s + n\,S_w\,\rho_w \qquad (5)$$

or

$$n = \frac{\rho_s - \rho_b}{\rho_s - \rho_w S_w} \qquad (6)$$

With equations (4) and (6), it is possible to derive porosity in the following form:

$$n = \frac{\rho_s(W_p + 1) - \rho_b}{\rho_s(W_p + 1)} \qquad (7)$$

Finally, S_w is calculated from this value of n in equation (4). Dry bulk density can also be calculated from porosity using the following relation:

$$\rho_{b\ dry} = (1 - n)\,\rho_s \qquad (8)$$

Using these equations, with a water content of 7,5%, the porosity is 0,33 and the dry density is 1836 kg/m^3. In rock piles, porosity does not vary over a wide range and it is usually between 0.3 and 0.4. Porosity can also be estimated from the total volume of the waste dump, the mass of waste rock and the dry unit weight of the rocks. During the exploitation of the main pit, Mine Doyon kept records of total rock mass displaced and average bulk unit weight of crushed rocks. The bulk unit weight used by the mine is from 1,80 and 1,85 t/m^3 and the total mass of the waste dump is equal to 21,1 million tonnes. The total volume calculated from these figures is 11,5 million m^3. This volume was checked using planimetry; two detailed topographic surveys were done before placing the rock waste and after closing the dump. The volume was then calculated by integrating between these two surfaces. The result was within 3% of the calculated volume from bulk dry weight. The volume of solids is calculated from the mass of solids divided by the specific gravity of the solid rock fragments. Specific gravity was measured on 15 samples coming from different lithologies with a weighted average of 2740 kg/m^3. Dividing the total mass by the specific gravity, the volume of solids is obtained as 7,7 million m^3. The calculated value for porosity has a meaning for the whole waste dump; locally under different conditions, porosity may vary.

2.3.5   DEGREE OF SATURATION

An other important parameter is the degree of saturation of the dump. That parameter controls the relative permeability to air and water, and it also affects the water budget. Degree of saturation eventually reaches a nearly constant value called field capacity. Under hydrodynamic conditions where infiltration occurs, the degree of saturation may exceed field capacity. Using the data calculated for bulk density, water content and solids density, the difference in mass between dry and wet rock is 110 kg/m^3 or an equivalent volume of 0.11 m^3 of water per m^3 of waste rock since the density of fresh water is 1000 kg/m^3. Since the porosity is 0.33, it represents the volume of voids in a 1 m^3 sample of rock. The degree of saturation S_W is the ratio between the volume of water to the volume of voids. With the values calculated above, S_W is then 0.33 or 33% of the voids is filled with water. This is a mean value for the whole waste rock dump. Near surface, S_W varies between 0.21 (in the low reactive area of T-92-1) to 0.42 in the very reactive area near T-92-2. This difference can be partly explained by the fact that the waste is finer in the second case and that more water is retained by capillarity. Also, the sericitic schists tend to swell in the presence of water which allows for a greater water content inside blocks rather than between blocks. There is no data on the variation of the degree of saturation with time but it should continue to increase slightly because oxidation of sulfides lead to rock weathering, the creation of more fine particles that increase the capillary retention properties of the whole mass.

2.3.6   GAS COMPOSITION AND PRESSURE

Gas composition

Gas composition was analyzed on samples collected in 1991 and 1992. The purpose of obtaining data on gas composition in the dump is to evaluate oxygen transport mechanisms and to understand reactions producing gases, such as the production of CO_2 following neutralization of
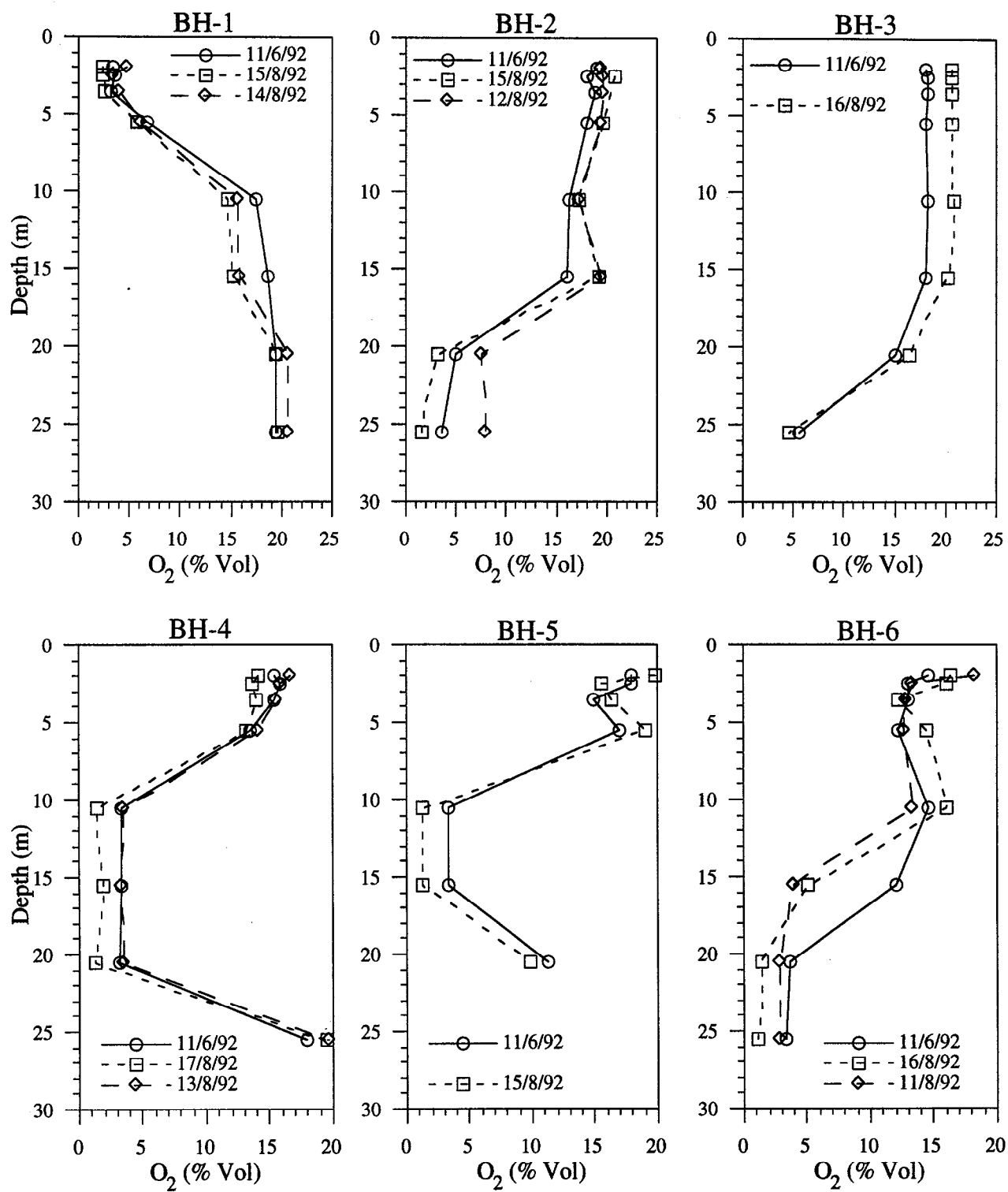
Fig. 2.7 Oxygen concentration versus depth in boreholes

acid by carbonates. Gas tubes are attached to piezometers and terminate at 8 different depths (1.5, 2, 3, 5, 10, 15, 20, and 30 m). Sampling was done with a hand pump and gas was collected in syringes. Water vapor from gas samples was removed in line by filtration through an anhydrite capsule. Field monitoring uses an oxygen sensor (model GC 502 from GC Industries) with a precision of 1% in the interval between 0-25% O_2. Gas chromatography was used to analyze samples for nitrogen, oxygen, carbon dioxide, and water vapor; traces gases were not analyzed. Details of procedures are discussed in Phase I reports (Gélinas et al., 1991).

Figure 2.7 show the oxygen concentrations in the dump in June and August of 1992. These values are similar to the one taken in 1991 and are quite stable with time. Well BH-1 is atypical since oxygen concentration is very low at surface and is almost atmospheric at the base; this type of behavior is predicted by models for points located near the toe of slopes where convection of air is upward. Wells BH-2, BH-4, BH-5, and BH-6 show similar patterns with an oxygen concentration close to atmospheric near surface and a very rapid decrease to less than 10% between 10 and 15 meters. These profiles are not typical of air diffusion where oxygen concentration would decrease exponentially with depth. They are better explained by convection cells located near surface and along the slopes of the dump that transport atmospheric oxygen inside to replace oxygen consumed by oxidation of pyrite. BH-3 shows a different pattern with a very slow decrease of oxygen concentration below 20 meters. This borehole is located in an area of very low reactivity and shows also a thermal profile that is quite different from the other observation wells. Temperature and gas composition data are used to establish a model of air circulation in the dump (Chapters 6 and 7).

Gas pressure

Measurements of differential air pressure between surface and the tips of air tubes were done to complete the set of physical parameters affecting air circulation in the dump and to measure variations of differential air pressure as a function of variations in atmospheric pressure; this type of data can be used to evaluate air permeability of the dump using a technique developed by Weeks (1979).

Instrumentation used in the field is illustrated in Figure 2.13. Gas sampling tubes in each borehole are connected to a valve manifold system that allows the selection of any point and connect it to a gas pressure transducer. A differential pressure is measured between atmosphere and a point in the waste dump. The gas pressure sensor is a Model PX 154 from Omega Engineering measuring pressure values between 0 an 10 inches of water with a precision of 0.1% (or 0,25 mm of water, or 2,5 Pa).

During the field experiments, atmospheric pressure variations were too small to conclude if changes in differential pressures can be generated in a short period of time ; hence it was not possible to verify if this technique can be used to estimate air permeability using the natural gradient method. It indicates however that air permeability is large since atmospheric pressure variations are transmitted almost instantaneously at depth. Future work is planned to use automatic loggers and dedicated pressure cells to verify this technique.
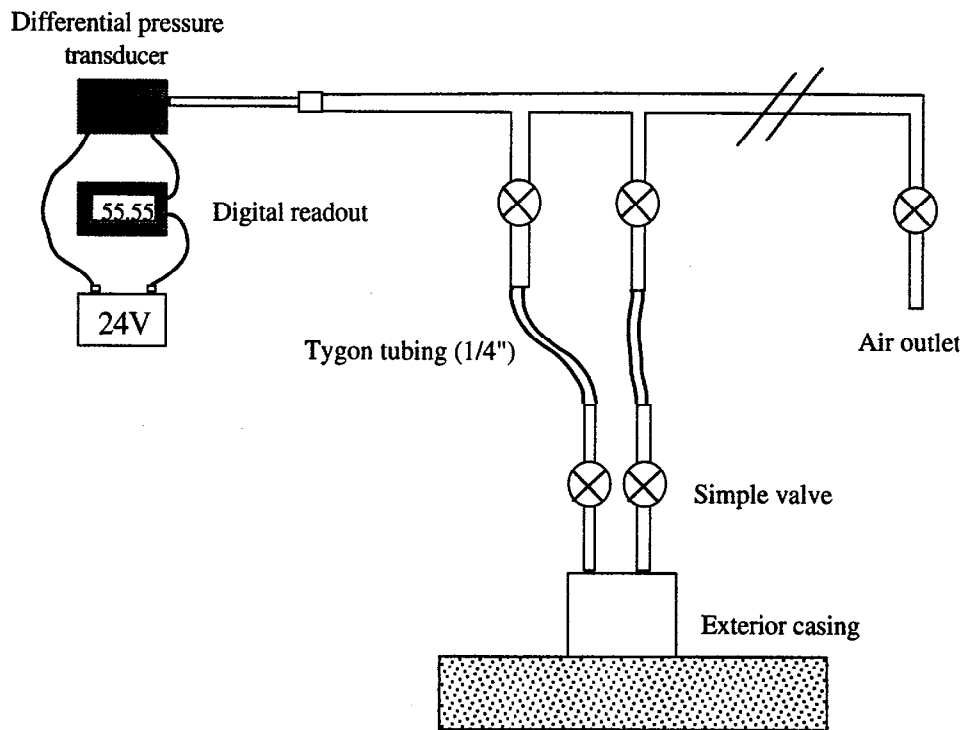
Fig 2.8 Field instrumentation used to measure differential air pressure

Air pressure measurements with time are illustrated for observation well BH-6 where several measurements were taken with time (Figure 2.14). For a given time, differential pressures can be calculated and corrected for temperature and depth. These pressures are illustrated on Figure 2.15 for well BH-6. The meaning of that curve is that the pressure gradient exceeds the hydrostatic gradient and that air flow is definitely upward in BH-6. Similar patterns were observed in BH-1 and BH-4. In three boreholes (BH-2, BH-3, BH-5), the gradients are inverted and indicate downward flow of air. These important observations are used in conjunction with thermal gradients to model convection cells in a waste rock dump (Chapters 6 and 7).

2.3.7 INFRARED THERMOGRAPHY

Thermally driven convection is the key mechanism controlling oxygen flow through waste rock dumps. Temperature profiles suggest that strong upward thermal gradients and oxygen profiles in rock dumps are often not typical of transport mechanisms by diffusion alone. Field observations during cold seasons show the presence of "hot spots" in different parts of the dump, frequently near the edges on the top of slopes. Often fumes caused by vapor condensation, are observed during cold days. Snow-free spots may be observed at the surface of several waste dump for part of the winter. Local measurements between rock fragments indicate temperatures of 10 to 20°C even when the air temperature is below freezing.
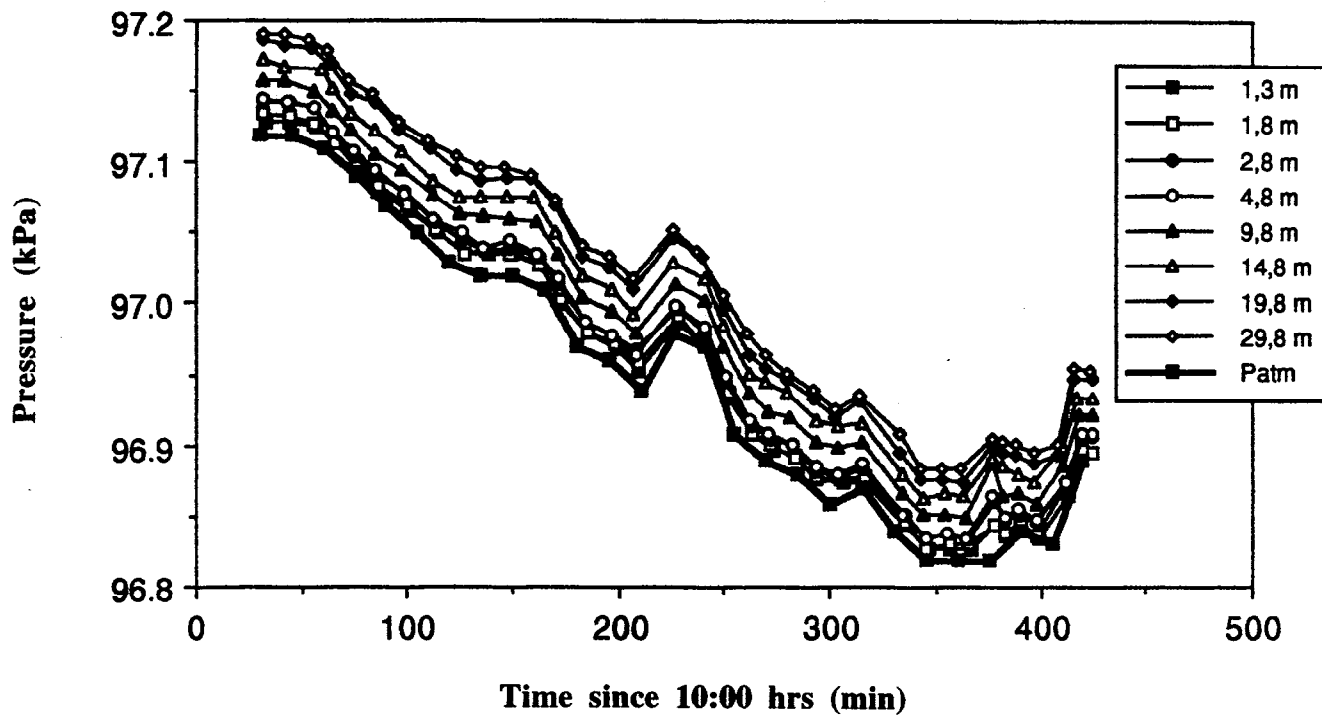
Fig. 2.9 Example of air pressure data. BH-6, 18 August 1992
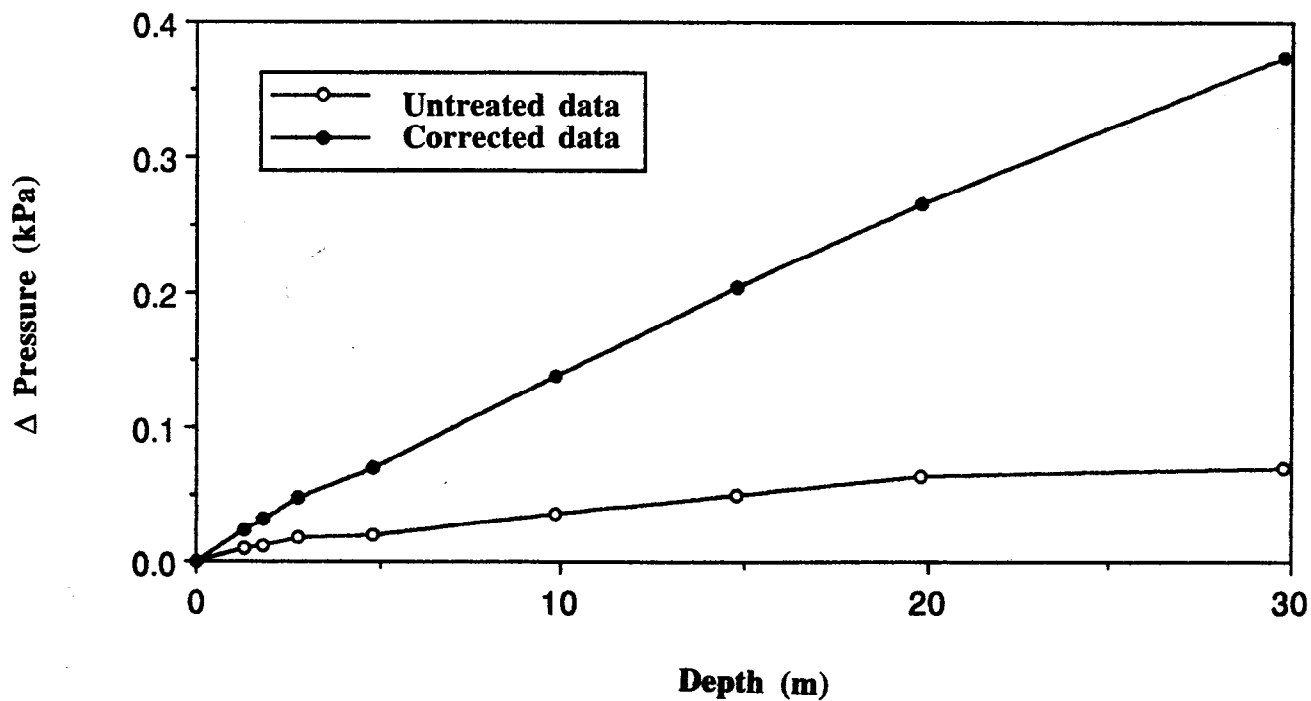
Fig. 2.10 Mean differential air pressure as a function of depth. BH-6, 18 August 1992

Large-scale temperature surveys can be obtained by infrared imagery. The thermal infrared transmission spectrum emits in the 2-5 μm and 8-14 μm frequency bands. Infrared sensors detect radiation in a given frequency band according to the emissivity of the medium. Prior field calibration procedures must be carried on to determine waste rock emissivity.

On small surfaces, temperature measurements can be done using hand-held infrared pyrometer that gives spot values of temperature at distances of a few meters. Pyrometers can be used to map small areas on the field around known heat sources.

Aerial surveys are done using an infrared thermographic camera. False colors of 128-level black and white thermal images can be obtained using a VCR to register the information. Emissivity has to be known before the survey and air temperature must be known during the flying period. If the survey is done using a helicopter, an estimate of elevation above ground must be made. The AGEMA Thermovision 400 infrared camera at a sensitivity level of 1 has a temperature span of 6°C. At sensitivity level 2, the span is 14°C. Depending on the sensitivity level, terrain emissivity, ambient air temperature and distance between the camera and the surface, accurate temperature images can be obtained.

Aerial surveys should be done during a period of the year when maximum differences exist between air and dump surface temperatures and in absence of snow cover. These conditions usually exist in May and October in most mining areas of Canada. An ideal time of the day is before sunrise or shortly after if the sky is cloudy but no precipitation occurs. Direct solar radiation interferes with the picture quality and is more representative of solar heating at surface than heat emitted by the dump.

A survey of the South waste rock dump of Mine Doyon was done on October 9, 1991 between 7 and 10 A.M. on a cloudy day with and outside temperature of 10 to 12°C. Thermal images were stored on a videorecorder 8 mm tape and selected images were extracted and digitized using a frame grabber. Two pictures in false colors are illustrated in Figure 2.16 taken on the South side of the dump, near the edge of the slope that runs SW-NE at the bottom of the picture. Two alignments of hot spots are observed, one in the lower right corner (the edge of the slope and the other some 20 meters NW of it). The bright point right near the top is due to the warm engine of a small truck that was parked there for scale. As will be shown later (Chapter 7) convection cells develop readily near the edges of the dump where colder air is entering the base of slopes to emerge near the top. Local disturbance due to placement of material, different compaction and sizes of blocks change the picture locally. On this picture, temperatures vary between 8 and 20°C.

Surface infrared temperature measurements were done to compare with airborne data. On August 18 1992, two experiments were carried on the right side of the lowermost hot spot on the left of Figure 2.16. A 20x20 m grid was marked on the ground to cover the hot and cold part of the anomaly. Temperatures were measured between 7:00 and 8:00 A.M. using and hand-held infrared pyrometer held at one meter from the surface with emissivity adjusted at 0.90. The results are presented on Figure 2.17. It shows that thermal anomalies can be mapped effectively either from surface measurements or from an airborne survey. A second experiment was performed to compare a line profile extracted from the airborne survey with surface measurements taken every meter along a 100-m line located at the same place. These results are shown on Figure 2.18. The

7 8 9 10 11 12 13 14 15 16 17 18 19 20 21 22°C
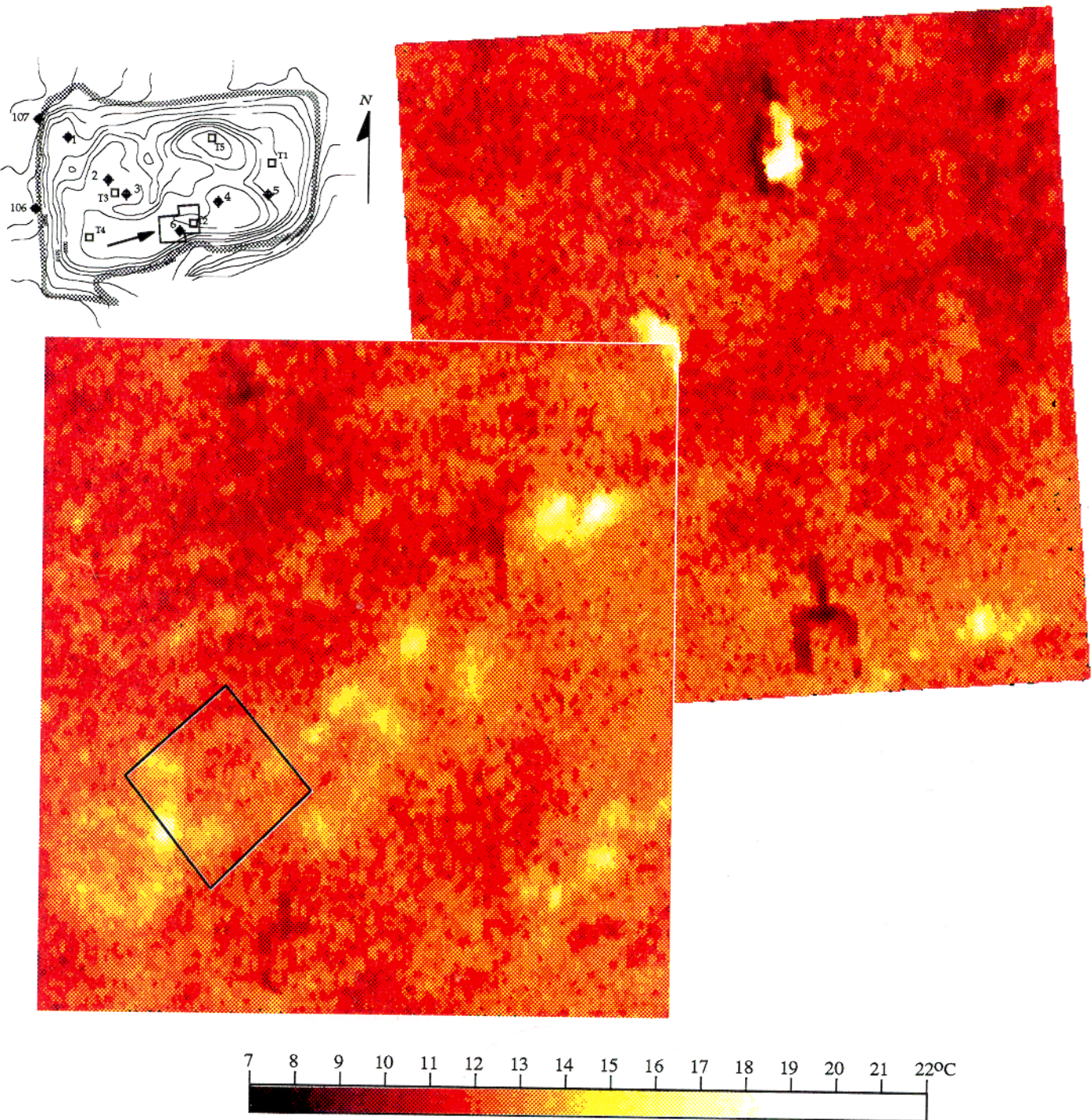
Fig. 2.11 Infrared image from the southern portion of the dump. Square area is approximate location of hand-held pyrometer mapping shown in Fig. 2.12

shaded area represents field temperature and the line profile is extracted from the air survey. There again the two profiles compare fairly well considering that 10 months separate the two periods of measurements. These results are important since they demonstrate that temperature distribution at the surface attributed to air convection patterns are stable. Distance separating maxima and minima on figure 2.20 varies from 10 to 15 m which could indicate that air convection is somewhat limited to the upper part of the dump (mainly in the first 10 m) according to data on temperature gradients and oxygen concentration.

From the data collected in the field, a conceptual model of air circulation is formulated as follows: 1) near the edges of the dump, air enters at the base and rises to the top creating a strong thermal anomaly at the surface; 2) inside the dump, air circulates in irregular convection patterns possibly controlled by material heterogeneity and anisotropy; very little oxygen reaches below 10-15 meters deep; 3) below 10-15 meters, air is more or less stagnant and oxygen-poor; locally CO_2 may be more abundant due to dissolution of carbonates as was observed in BH-6 in 1991. This conceptual model is used to simulate physico-chemical processes of acid mine drainage generation (Chapters 6 and 7).
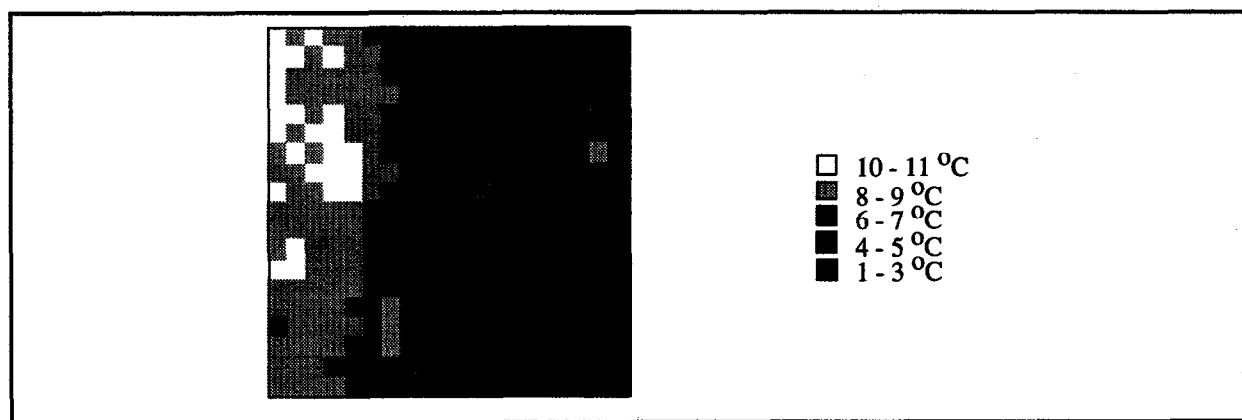
Fig.2.12 Hand-held IR pyrometer temperature mapping of a 19x19 m area near BH-6 (see Fig. 2.11 for location)
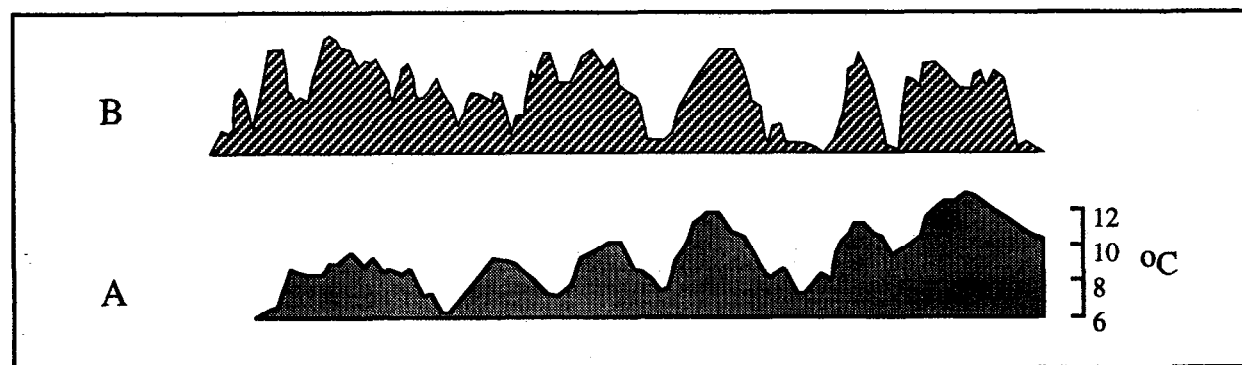
Fig. 2.13 Temperature profiles of S-N section 100 m west of BH-6. Profile A is from IR pyrometer readings and profile B is from the heliported IR image

3/ Mechanical and physical properties of Mine Doyon waste rocks

3.1 INTRODUCTION

Prediction of acid mine drainage potential relies chiefly on chemical tests either static or dynamic. Static tests are performed on finely ground material so that all particles are assumed mono-mineralic and free to react when chemicals are added. It is then possible to determine total potential for acidification and neutralization because reactions are complete. These tests have been applied successfully to tailings since they also are fine grained material.

For waste rocks, similar static tests have been applied but interpretation of data is often difficult because the size or the geometry of fragments are not taken into account. The ability of a given waste rock pile to generate acid depends of course on the net acidification and neutralization potentials but the rates at which they occur depends also on reaction surfaces where sulfides are exposed to oxidation. It is then assumed that the rate of acidification depends on the total surface area of the waste rocks, the surface area of exposed sulfides and the potential to expose new surfaces after placement in the dump.

The goal of this section is to investigate different methods to calculate the total surface area of waste rocks, to measure some of their mechanical properties as an index of their relative hardness and weathering potential, and to estimate the surface area of exposed sulfides.

Surface area is calculated from a geometric model of particles and applied to their particle size distribution. Mechanical properties are analyzed with two standard tests used to evaluate concrete aggregates, the Los Angeles abrasion test, and the Micro-Deval abrasion test. The magnesium sulfate test is used to measure susceptibility to weathering by swelling under freezing conditions or by absorption of solutes. Microfractures and other discontinuities in rock fragments are easily detected using an ultrasonic celerometer that measures the propagation of elastic waves (shear and compression) across a solid. Exposed area of sulfides is measured by a chemical method (hydrogen peroxide attack) and using image analysis of polished surfaces of rock fragments. The following is a summary of a MEND report presented by Locat *et al.*, 1994.

3.2   MATERIALS INVESTIGATED

Rock fragments representing the four major lithologies present in the Mine Doyon south waste dump include: felsic (acid) volcanoclastics, sericitic schists, mafic tuf, and intrusive rocks of the Mooshla complex (Savoie *et al.* 1991).

Sericitic schists (SC) (Unit 4b) are the most frequent rock type and form 50% of the waste rocks. They are composed quartz and muscovite with up to 30% weathered alumino-silicates. Secondary minerals are pyrite (7%), rutile and some chlorite. They do not usually contain plagioclase. This unit shows intense penetrative schistosity so that rock fragments are platy and very brittle. In this chapter, their geometry is represented by a disc with a radius of $1\,L$ and a thickness of $0.2\,L$ (coefficient of flattening of 10). Its surface area is $2.4\,\pi L^2$ and its volume is $0.2\,\pi L^3$.

Intermediate or mafic tuffs (MF) (Unit 3) account for 30% of the waste rocks. They are composed of plagioclase, quartz, chlorite (10-30%) and variable amount of carbonates (0-25%) and epidote (1-25%). Their pyrite content is low (1.8%). They show some schistosity but less developed than in the schists unit. Fragments are blocky and are represented by a cube with a surface area of $6\,L^2$ and a volume of L^3.

Felsic volcanoclastics (FV) (Unit 4a) form 15% of the waste rocks and are composed mainly of plagioclase and quartz with 5-15% muscovite. Secondary minerals include chlorite, pyrite (5,5%), rutile, apatite and carbonates. The rock shows penetrative schistosity and rock fragments are elongated and platy. A geometrical model of the fragments has a width of $1\,L$, a length of $2\,L$, and a thickness of $0.5\,L$. Its surface area is $7\,L^2$ and its volume is $1\,L^3$.

Intrusive rocks (IR) represent only 5% of the waste rocks and are represented by diorites and tonalites from the West pit. They are composed mainly of plagioclase, quartz, chlorite and may contain up to 5% pyrite. Fragments are massive blocks without schistosity nor weak planes. Their geometric figure is represented by a cube as for the mafic tuffs.

3.3   SPECIFIC SURFACE AREA

Specific surface area is the external area per unit mass of a solid. To determine its value for a sample of waste rocks or soil, a particle size analysis is done to determine the mass of material for each granulometric class. Taking L as the mean size particle in a given class and knowing the density of the solids, it is easy to calculate the number of particles present in each class since the volume and the mass of a single particle may be determined. The total surface area is the number of particles times unit surface area. The specific surface area is then computed and expressed in cm^2/g or m^2/kg. For different geometries, a graph is drawn (Figure 3.1) illustrating change in specific surface area as a function of mean particle diameter (d_{50}). For the same density of particles, the specific surface area of disc, platelet and cube are in the following ratios 1.47 (disc)::1.17 (platelet)::1.00 (cube). Specific surface area will be used to compare the results of different mechanical tests on the four lithologies described above.
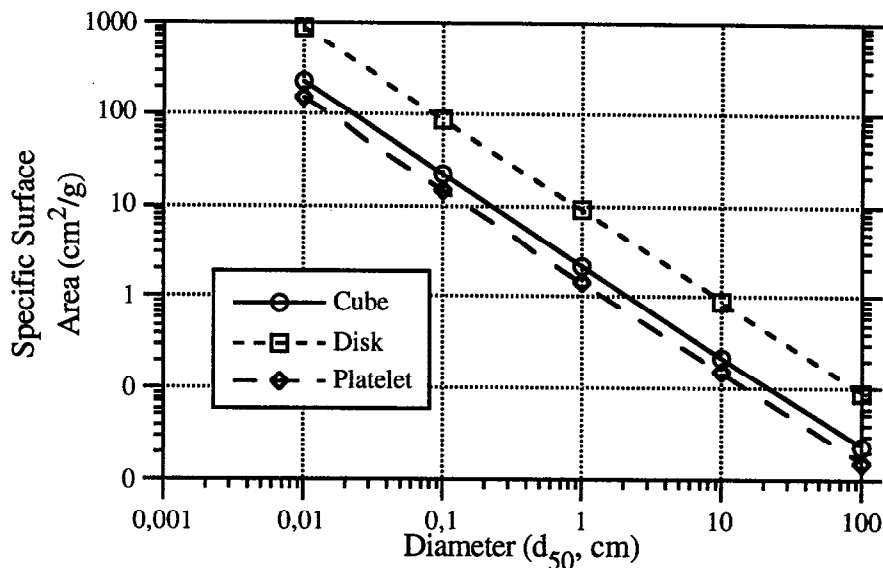
Fig. 3.1 Relationship between particle mean diameter (d_{50}) and specific surface area for different geometries

3.4 MECHANICAL TESTS

Three tests are commonly used in concrete technology to check the soundness of aggregates: the Los Angeles abrasion test, the Micro-Deval (measurement of wear by attrition), and the magnesium sulfate test, a measure of disintegration.

The Los Angeles abrasion test (BNQ 2560-400/1983) measures abrasion resistance under fragmentation by shock and wear by friction between particles and steel balls. The results are expressed as a percentage of mass that is lost to fine particles from an original mass retained between two sieves. This is expressed as a percentage of loss.

The Micro-Deval attrition test (BNQ 2560-070/1982) determines a coefficient of wear when a coarse aggregate is rotated in a cylinder in presence of water. As for the Los Angeles test, the loss to fine particles is expressed in percent.

The magnesium sulfate (MgSO$_4$) disintegration test (BNQ 2560-450/1983) consists in soaking a coarse aggregate into a saturated MgSO$_4$ solution and allowing the sample to swell and break down

under the crystallization pressure of magnesium sulfate crystals. This test simulates weathering conditions such as freeze/thaw or dry/wet cycles. It is important because it relies chiefly on existing weakness planes or microfractures present in the sample. Again the results are expressed as a loss of mass to fine particles in percent.

Table 3.1 Results of standard tests (mass loss as %)

	Los Angeles		Micro-Deval		Magnesium sulfate	
	10-40 mm	20-40 mm	10-20 mm	40-80 mm	<10 mm	10-75 mm
Sericitic schists	82.9	75.4	84.4	88.8	27.3	8.02
Mafic tuffs	21.8	20.5	16.1	17.5	6.0	0.21
Felsic volcanoclastics	28.3	30.9	25.2	26.7	4.8	0.60
Intrusive rocks	10.7	34.6	7.5	12.6	4.9	0.45

In Table 3.1, it is obvious that the schists are the most susceptible rocks to disintegrate according to each test. In order of increasing toughness we have: sericitic schists, felsic volcanoclastics, mafic tuffs, and intrusive rocks. Figure 3.2 show typical particle size curves *before* and *after* Los Angeles tests.

Another series of experiments were done using the Los Angeles test to measure specific surface area before and after tests. Three samples were taken for each lithology and a mean value was obtained for specific surface and the difference observed at the end.

Table 3.2 Changes in specific surface during Los Angeles tests (cm^2/g)

	Before test	After test	Difference
Sericitic schists	22.2	172.4	150.2
Mafic tuffs	11.9	61.8	49.9
Felsic volcanoclastics	10.5	90.5	80.0
Intrusive rocks	11.5	58.2	46.7

These results partly explain why oxidation rates for the schists are much higher than what is usually observed in waste rock dumps. Creation of new surfaces results from breaking and crushing of rocks, from dry/wet and freeze/thaw cycles and from the very process of oxidation of sulfides with precipitation of new minerals such as gypsum and jarosite that help open new planes. If sulfides distribution in rocks is assumed homogeneous, then more surface area means a greater amount of sulfides being exposed to oxygen and bacteria. The simple tests above are indicators of

the susceptibility of any rock type to disintegrate and show high oxidation rates early in the history of a waste dump. A non-destructive test is described next that has a potential to measure the same properties is less time and at lower cost.
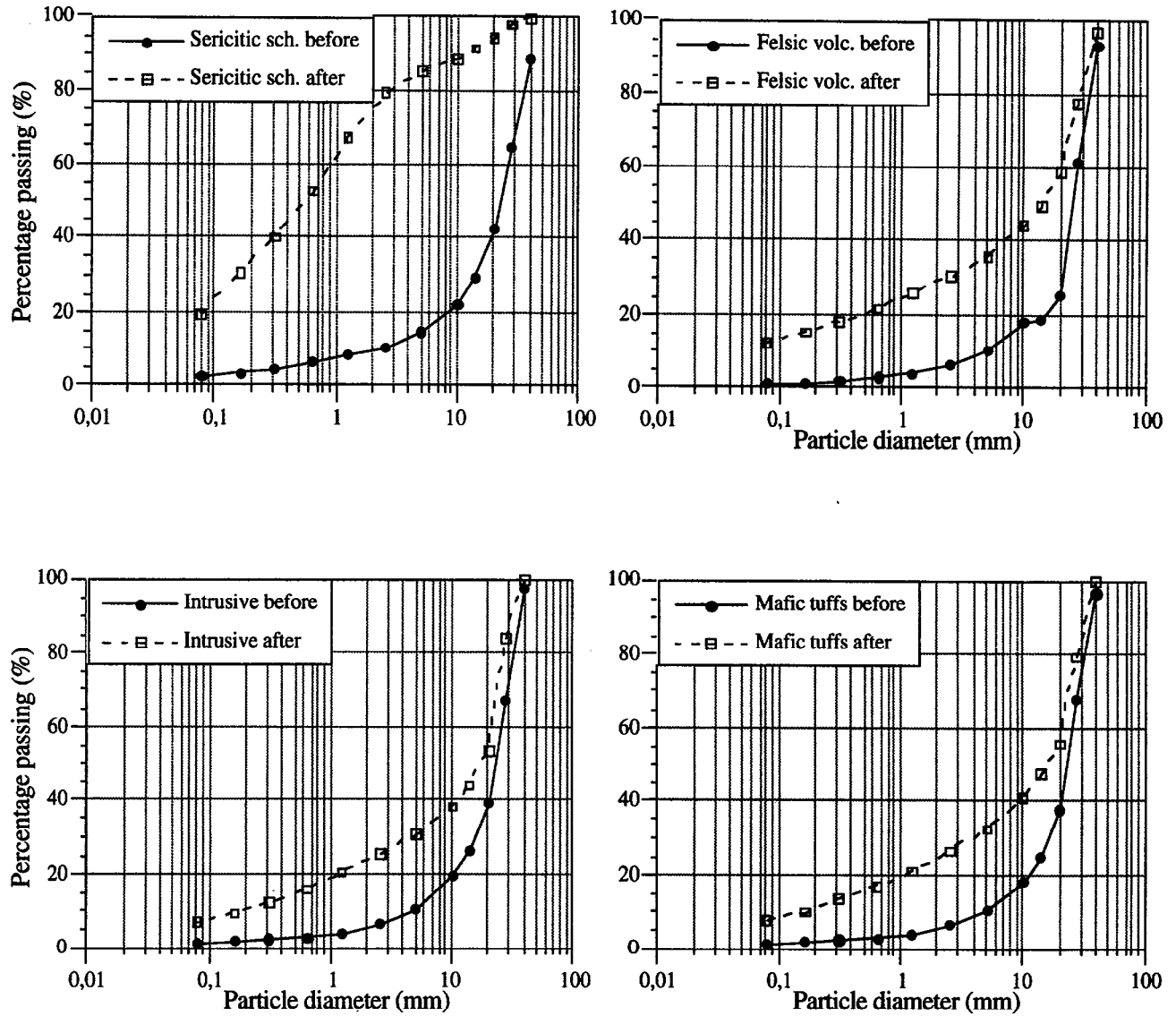
Fig. 3.2 Particle size curves before and after Los Angeles test

3.5 ACOUSTIC CELEROMETER TEST

Recent developments in acoustical methods make it possible to obtain in the laboratory rapid and reliable measurements of the speed of propagation of the compression (V_p) and shear (V_s) waves in soil and rock samples (Locat et al., 1986). The ultrasonic celerometer is an apparatus that emits and receives sonic waves in the range of 1 to 80 kHz. Resonance frequency of transducers for compressive waves is 63 kHz and 33 kHz for shear waves. Two transducers are placed at the extremities of a sample and a sonic wave is emitted. The received signal is amplified and the travel time in micro-seconds (μs) is calculated. Knowing the distance between the transducers, V_p and V_s are calculated and expressed in meters per second. Tests were done using an Oyo Corporation Model 5217A celerometer.

Samples are first trimmed in the form of blocks 5x5x10 cm and measurements are made across three axes to measure anisotropy. Ten measurements are made on each face after displacing the transducers slightly between measurements. Average values of all results are given for each plane. The same procedure is repeated to measure shear waves velocity. Detailed results are presented in a MEND report by Locat et al., 1994. A summary is given in Table 3.3.

Table 3.3 Compression and shear waves velocities in waste rocks

	Shear waves			Compression waves		
	V_s m/s	V_s ratio	Aniso.	V_p m/s	V_p ratio	Aniso.
Sericitic schists	1260	0.45	1.47	2756	0.64	2.85
Mafic tuffs	2728	0.98	1.11	4218	0.97	1.24
Felsic volcanoclastics	1400	0.50	2.72	3703	0.85	3.40
Intrusive rocks	2822	1.00	1.00	4349	1.00	1.24

In this table, V_s ratio and V_p ratio are used to compare velocities values between themselves by putting V_s and V_p ratios for intrusive rocks equal to 1.00. It can be seen that intrusive rocks and mafic tuffs are very similar in behavior as compared with volcanoclastics and schists. The sericitic schists are the weakest rocks both in shear and compression. The column labeled "Aniso." shows the ratio between the maximum velocity on a given plane to the lowest velocity measured across the weakest plane. Intrusive rocks and tuffs are more isotropic than volcanoclastics and schists which show large differences according to the direction of measurement.

The significance of these results for predicting acid generation rates for waste rocks lies in the actual oxidation potential represented by the surface area of sulfides exposed to oxygen, bacteria and water as compared with the theoretical long term potential of oxidation of all sulfides present in the waste rock. Elastic waves velocity is a good indicator of the degree of fissuration of a rock fragment so that the lower the velocity, the greater its potential to form new surfaces, absorb more water and expose more sulfides minerals to oxidation.

Mechanical conditions are not static with time; vulnerable rocks degrade more rapidly and create fine particles that are free to move in the coarse pore network. The absorption of water by disintegrated rocks increases the water content of the dump and influences water balances calculations.

3.6   EVALUATION OF PYRITE SURFACE AREA

A limited number of tests were done using chemical and physical methods to determine pyrite active surface area in different rock types. The chemical test involved hydrogen peroxide attack with monitoring of pH and temperature with time. The physical method involved image analysis of polished surfaces, measuring a large number of pyrite grain characteristics on selected surfaces of rock fragments.

3.6.1   HYDROGEN PEROXIDE (H_2O_2) TESTS

Fine-grained pyrite can be oxidized easily by a solution of hydrogen peroxide (H_2O_2). To evaluate surface area of pyrite, we tried to calibrate a test where pH and temperature were monitored with time during the reaction. A prepared sand sample containing 5% pyrite was used to calibrate the reaction. Then samples of waste rocks ground to 90-250 μm were subjected to the same oxidation procedure. The lowering of pH with time is calibrated with the sand and compared to the curves for different lithologies from the waste rocks. After equilibrium is reached, final pH values are estimated by comparison (Figure 3.3). This estimate was good for the sericitic schists with an estimated pyrite content of 5 to 6% which is close to average values of pyrite content in schists. For volcanoclastics and tuffs, the pyrite content is estimated at 3 to 4%. For intrusive rocks, the pyrite content is around 1%. Because of differences in grain size and specific area of particles, this method does not seem adequate to determine surface area of pyrite.

Figure 3.3 Hydrogen peroxide tests on four rock types: pH as a Monitoring temperature during the tests with H_2O_2 is based on heat released by pyrite oxidation. The temperature increase for the sericitic schists is very rapid as temperature soars to 80°C within 20 minutes. However a similar curve was expected for the calibrated sand and it failed to show positive results (1 to 3% extrapolated versus 5% in the sample). To be successful these methods would require considerably more testing for a variety of conditions and materials before they can be used as a predictive tool.
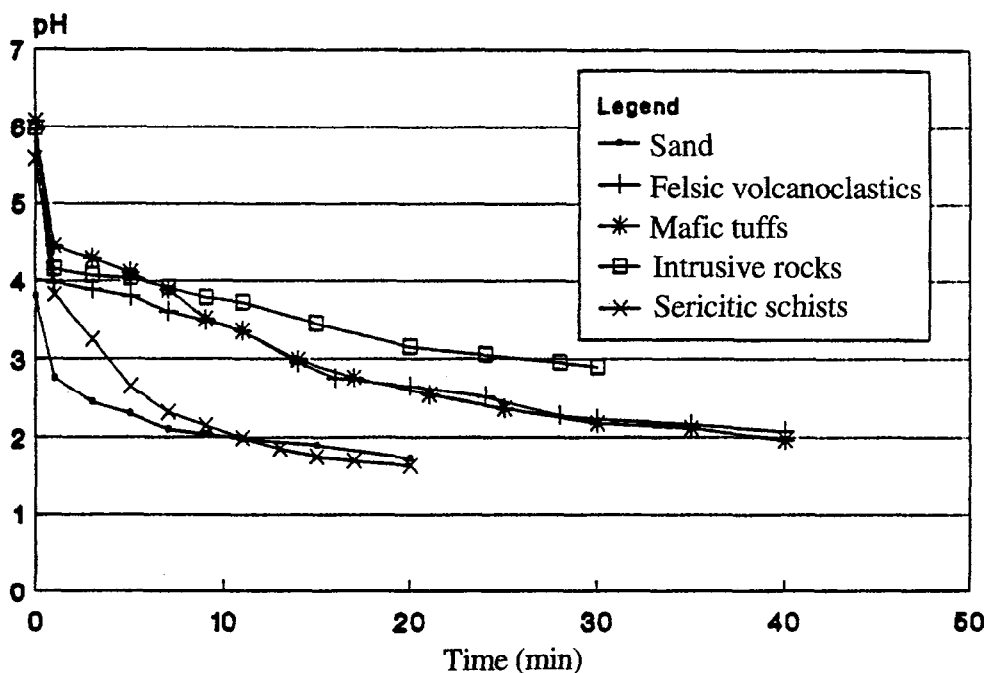
Fig. 3.3 Hydrogen peroxide tests on four rock types: pH as a function of time

3.6.2 IMAGE ANALYSIS OF PYRITE CONTENT

Selected rock fragments from the four lithologies were studied using image analysis techniques to determine mean area of pyrite grains on prepared surfaces. The purpose was to measure typical surface area of pyrite grains in different rock types and compare sizes. Three samples were used for each lithology and from 100 to 300 individual grains were measured. Area in mm^2 was measured and equivalent diameters of a circular grain were calculated for comparison (Table 3.4).

Table 3.4 Pyrite grains dimensions from image analysis

	Surface area (mm^2)	# of grains	Equivalent diameter (mm)
Sericitic schists	0.335	151	0,65
Mafic tuffs	0.040	320	0.23
Felsic volcanoclastics	0.031	242	0.20
Intrusive rocks	0.121	93	0.39

This table shows that pyrite grain area in the sericitic schists is 3-10 times larger on average with a diameter 2-3 times bigger than for other rock types. This may help explain the higher reactivity of this rock type and rapid rates of oxidation observed at Mine Doyon.

3.7   DISCUSSION

Mechanical and physical characterization of waste rocks affords new ways of understanding and predicting acid mine drainage generation since important parameters such as specific surface, physical integrity and toughness of rock fragments, as well as the degree of weathering can be assessed and compared. A geometric description is needed for all shrinking-core reaction models and it was shown that different rock types break in blocks of different shapes that can be analyzed as cubes, platelets or discs. For the same mass, the difference in external surface area can be as much as 47% for the disc-shaped particles. Internal surfaces caused by fractures, joints, or schistosity are even more important since dissolved oxygen can reach reaction sites with subsequent formation of secondary minerals with a larger volume such as gypsum and jarosite. This indeed contributes to open existing fissures still wider and to accelerate disintegration of rock fragments.

Mechanical resistance to abrasion and weathering is measured with standard tests such as the Los Angeles, Micro-Deval and $MgSO_4$ tests. The ability of different rock types to create new surfaces is clearly shown by the results. The sericitic schists are clearly the weakest rock from this point of view mainly because of their intense schistosity and their content in alumino-silicates (clay-type minerals) that are products of alteration. Other volcanic rocks (volcanoclastics and tuffs) are also fairly weak as compared with the intrusive rocks. Since half of the rock waste is composed of sericitic schists, this is a very important factor to explain unusual oxidation rates at Mine Doyon.

The most convenient measurement of rock toughness, degree of weathering and internal fissuration is given by the acoustic celerometer test. This method is simple, cost effective and yields results that compare favorably with the more involved test using aggregates such as the Los Angeles or $MgSO_4$ tests. This procedure is non-destructive and measures the physical continuity of minerals forming a rock. Chemical methods to determine surface area of pyrite on rock fragments did not yield data that can be analyzed easily and more testing of these methods should be done before using them to give realistic data. Even then, the sericitic schists show clearly different properties compared with other rock types. Pyrite surface area using image analysis makes possible the measurement of average area and size of individual grains. Only a few of these analyses were done and a much larger sample size should be used to give results that could apply to the whole dump. Sericitic schists again show larger pyrite grains and surface area than other rock types present at Mine Doyon.

The results of the physical and mechanical characterization are used to explain some geochemical results on reaction rates and to build a numerical model of acid rock drainage as will be discussed in chapter 7.

4 / Water balance for the waste rock dump

4.1 INTRODUCTION.

4.1.1 PROBLEM DEFINITION.

Acid mine drainage (AMD) generation from waste rock dumps (WRD) constitutes a challenging problem for the mineral industry of Canada. Unlike AMD generated by tailings ponds, AMD generated by WRD is more concentrated and can reach much higher flow rates. So, even if acid generating WRD are less common than acid generating tailings ponds, they constitute an important threat to the environnement and must be managed at great cost by the mineral industry.

The South waste rock dump at La Mine Doyon is one of the largest acid generating dump in Eastern Canada. Since the beginning of our research program, numerous reports describing the site and the ongoing physico-chemical processes have been released by GREGI. It is now well established that the large magnitude of the AMD production at this WRD is related to the rapid supply of air and water to the reaction sites through convection and percolation in this very permeable porous medium.

Water entering a dump from precipitation is a key element of the AMD generation processes and is the main vector of acid release into the environment. This is why a complete characterization of the AMD processes in a waste rock dump must include a comprehensive water balance.

4.1.2 OBJECTIVES.

The first objective of this section is to present the hydrologic data made available by the various characterization programs going on at La Mine Doyon. These data are growing as monitoring continues and as new registering devices are regularly added. This chapter thus presents a preliminary analysis of a developing collection of data and knowledge about hydrologic processes at the South dump of La Mine Doyon .

The measurement of hydrologic variables like rainfall, temperature and drainage flow rates is straightforward. However, other key hydrologic variables, like infiltration, are more difficult to measure and some developments of monitoring procedures or devices are included in the project. Automation of monitoring devices is also used to facilitate the task of on-site data collection and to

ensure a more continuous record of critical data. The second objective of this report is to present both classical and innovative methodologies used to monitor hydrological processes at La Mine Doyon.

The third and final objective is to present a comprehensive water balance of the South dump. This balance must be consistent with observations provided by the geochemical and mineralogical data available. This type of information was used to build a geochemical mass balance related to the water balance through concentration and volume changes.

4.1.3 METHODOLOGY.

As stated earlier, classical hydrological methods were used when applicable. These include analysis of meteorological and climatic data from close weather stations as well as the operation of an automatic weather station on site. Weir stations and piezometers are also operated on site. Some less standard instrumentation used in this project include gravity lysimeters.

During this project, we tried to measure as many hydrological variables as possible to obtain the longest and most accurate records. These data are used to calculate the water balance. Since the project has been going on for more than four years, some records are becoming more and more significant. Moreover, as the water balance picture becomes clearer, data deficiencies are identified and new monitoring devices are designed and put into operation.

The analysis of hydrological data collected is also supported with some modeling. Models are used to assess hydrologic variables that cannot be measured. Model calibration with measured data ensures realistic modeling estimates.

4.2 HYDROLOGIC DATA COLLECTION

4.2.1 REGIONAL METEOROLOGICAL DATA

Regional meteorological and climatological data come from the official provincial weather stations network. These can be obtained from "Ministère de l'Environnement et de la Faune" (MEF) which operates the network. Some stations, located at airports, are operated by Environment Canada and the data are shared with the provincial network.

Three weather stations are in operation in the region. These are the Kinojévis River station (#7086630), the Amos station (#7090120) and the Val D'Or airport station (#7098600). These stations are located at distances ranging between 25 km and 60 km from Mine Doyon. They are in different directions and their location form a triangle around the study site. A location map, Figure 4.1, illustrates this.

Various parameters related to these weather stations are summarized in Table 1. Weather data from these regional stations are used to establish a meteorological record for Mine Doyon since on-site measurements were not continuous over the period covered by this project. Complete daily data sets are available for these three stations from 1991 to 1993.

Table 4.1 Location of regional weather stations

Station	Code	East	North	Elevation	Distance from site
Val D'Or	7098600	48°03'	77°47'	338 m	59.75 km
Amos	7090120	48°34'	78°08'	310 m	49.00 km
Kinojévis	7086630	48°13'	78°52'	290 m	26.25 km

Complete daily data sets are available for these three stations from 1991 to 1993. These data, supplied in raw files by MEF, are extracted and presented in separate EXCEL files.

4.2.2   ON SITE METEOROLOGICAL INSTRUMENTATION

An automated weather station is in operation at the Mine Doyon site since March 1992. It includes a data-logger connected to temperature, relative humidity, and precipitation probes. In June 1992, a barometric probe was added. The data logger was built by Omnidata International Inc. The "Easy Logger" model is especially designed to operate an automated weather station. Relative humidity and temperature are measured by a combination sensor. Temperature is measured by a 3-wire precision thermistor to ±0.25 °C. The relative humidity sensing probe is composed of two thin-film electrodes forming a capacitor. The moisture can pass through the upper film electrode and change the capacitance of the element. Precision of relative humidity readings is ±3 %. The precipitation gage is a tipping-bucket type. It has a circular aperture of 200 mm diameter and its sensitivity is 0.25 mm. The overall precision of the system is 3 %. The precipitation gage is heated to collect and measure snow precipitations. It is protected from direct high winds by a special circular wind shield. The barometric probe is an absolute pressure sensor composed of a vacuum sealed reference space separated from atmosphere by a deformable ceramic capacitance acting as a strain gauge. The atmospheric pressure changes induce a deformation of this gauge. The system accuracy is ± 0.03 kPa.

At Mine Doyon, the logging unit and the barometric probe are installed in an office in the concentrator plant. The combination temperature/humidity probe and the precipitation gage are installed on the plant roof.
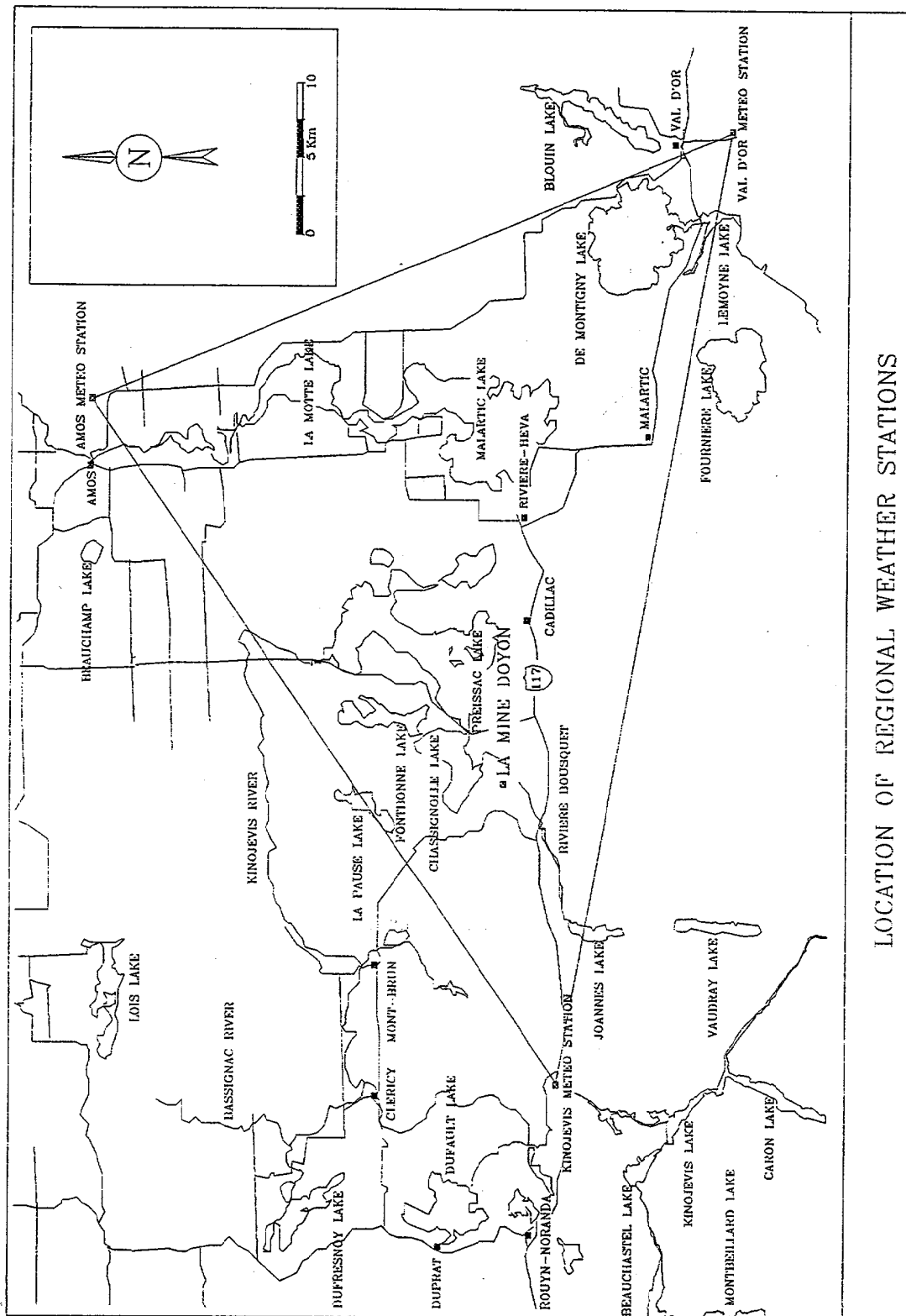
Fig. 4.1 Location map of regional weather stations

4.2.3. LOCAL METEOROLOGICAL DATA.

The data collected at the local weather station are presented in a separate report (Isabel *et al.*, 1994). These files contain meteorological records, on a 15-minute time step, going from April 1992 up to June 1993. The data set is not always complete as some monthly files are missing or are lacking some records. These missing records were noticed during the first months of operation and are due to various system testings and adjustments, as well as operational errors. The complete data set has not yet been used in any long term analysis. Only short subsets were used to perform short term hydrological or physical analysis. The accuracy of the data is good, except for the relative humidity measurements. Recalibration of the combination temperature/humidity probe was not performed on a regular basis, as suggested by the manufacturer. Since only precipitation and barometric data have been used until now, this does not cause any problem.

4.2.4. ON SITE HYDROLOGICAL INSTRUMENTATION

The local hydrological instrumentation is composed of weir stations, piezometers and lysimeters stations. The three weir stations, or runoff gauging stations, are located at the end of the ditches that circle the south dump. The exact location of the ditches and gauging stations is shown in Figure 1.3. Each station consists of a small dam with a V-notch weir. Overlooking the weir, there is a small instrument shelter containing an automatic sampler, a level detector and a flow meter. This flow meter, using data from the level meter, integrates the runoff volume and feeds a paper recorder where flowrate is graphically recorded. The flowmeter also has a display where the cumulative runoff volume is continually updated. This last information is noted each week when the station is visited by the operator responsible for the collection of samples. It should be noted that the station is not operated during part of the winter when ice formation precludes the exact determination of flowrate and impairs the operation of the automatic sampler.

Gravity lysimeters made of plastic half barrel having a capacity of about 48 liters were buried at various depths in the South dump during the summer 1992. Each station includes six (6) lysimeters. Each lysimeter is linked to the surface by a drain pipe allowing water level measurement, sampling, and purging of accumulated water. The two lysimeters stations, named T92-1 and T92-2, are located in very different environments in the dump. T92-1 is located in a low-reaction zone where less reactive rock waste is covered by very low grade ore. T92-2 is located in a highly reactive zone where strong heat losses are observed at the dump surface. These locations are shown in Figure 1.3.

A series of monitoring wells used as piezometers are operated at the south dump since 1991. The location of these is shown in Figure 1.3. Water levels are measured on a regular schedule since 1991 and complete record of the measurements up to April 1993 is included in a separate report (Isabel *et al.*, 1994).

4.2.5. HYDROLOGICAL DATA

Weir Station Data

Hydrological data, that is drainage discharge data, collected from the south dump weir stations is available on graphical support only. To obtain numerical data, one must take the paper rolls from the recorders and numerize the recorded trace. There are some problems inherent to this procedure. First, there is no specific mark to indicate the position of the true zero flow rate as well as the flowrate scale. Second, there is also a lack of a specific mark to precisely indicate the time reference on the record. The time scale is well indicated but there is no absolute time reference. Paper records are especially confusing when, following a power failure, the recorder clock is reset to 0. As those breaks in power supply are numerous, the recordings are difficult to relate to any absolute time frame. The lack of adequate time reference and flowrate reference does indicate that the complete numerization of the records would be a useless task. A small subset of the records was however numerized for the analysis of short rainfall-runoff events. This was not an easy task and results are presented in section 4.3.2. Recently, digital loggers with independent time circuits were installed.

The weekly runoff totals, hand-recorded by the stations operator, are however available. This information is transformed in constant average daily flowrate and recorded in data files. This record is completed with interpolated flowrates for the missing data during the winter period. This interpolation is based on a constant base flowrate measured sporadically during the winter period when the ice cover is broken to take a measurement. The complete data file content is presented in Isabel *et al.*, 1994, with weekly and monthly averages and totals. The resulting hydrographs for year 1991 through 1993 are presented in Figures 4.2 to 4.4.

Lysimeter Stations Data.

Hydrological data is collected in lysimeters by regularly purging them and measuring the volume of accumulated water. These measurements were taken from time to time between June 1992 and September 1993. This monitoring program is still going on but data collected after September 1993 are not included here. The resulting volumes are converted into precipitation or infiltration heights.

Graphs of cumulative height of infiltration collected in lysimeters are presented in Figures 4.5 and 4.6. Cumulative infiltration for the first 4 months of operation are not included in these graphs. It is assumed that waste rocks handling during the installation of lysimeters affected water distribution in the unsaturated zone. A period was needed to allow waste rocks to reach field capacity and dynamic equilibrium state. Complete data set and complete graphs are nonetheless included in Appendix D of Isabel *et al.*, 1994.

Fig. 4.2 Weir stations hydrographs for the year 1991
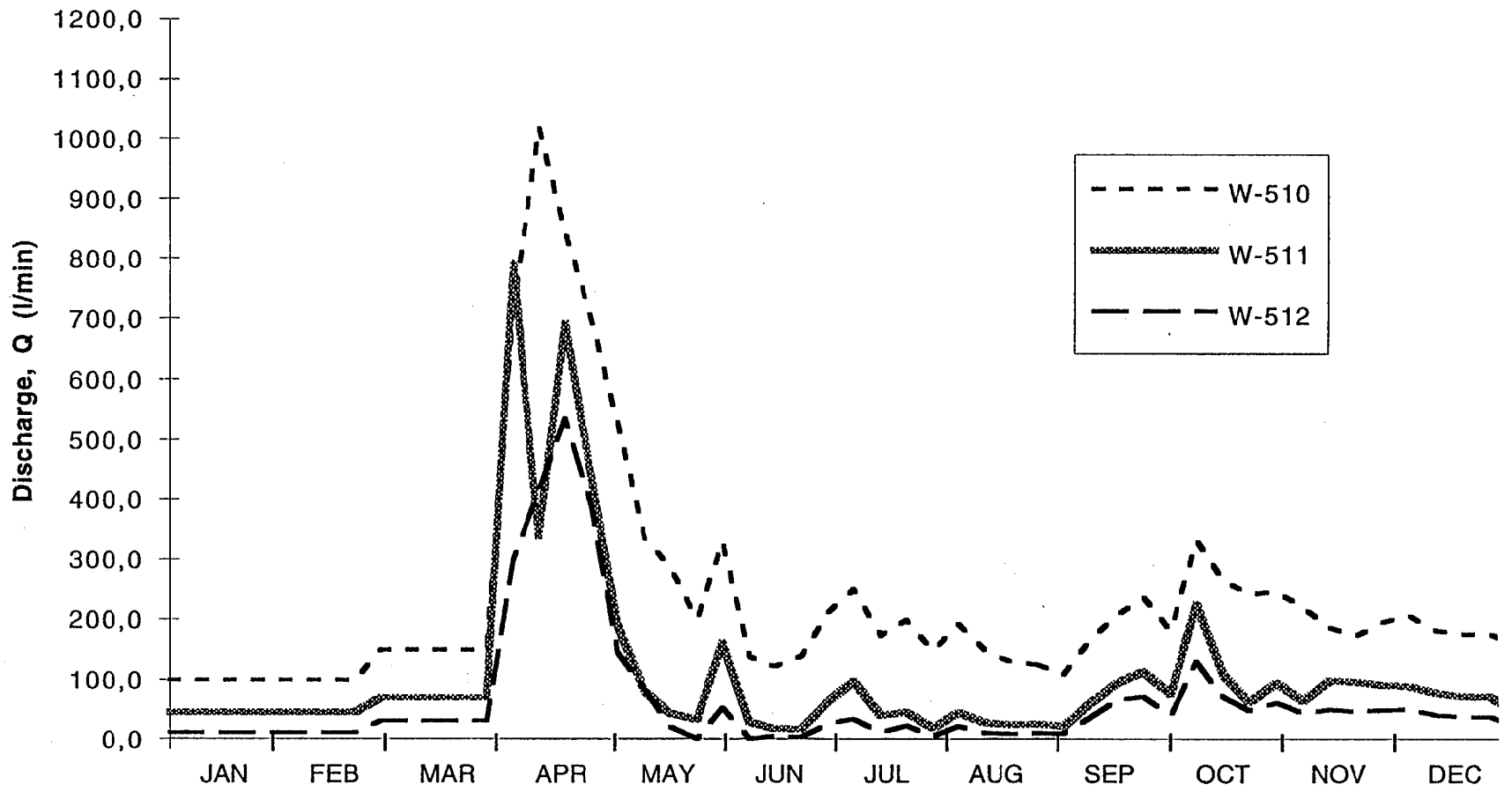
Fig. 4.3 Weir stations hydrographs for the year 1992
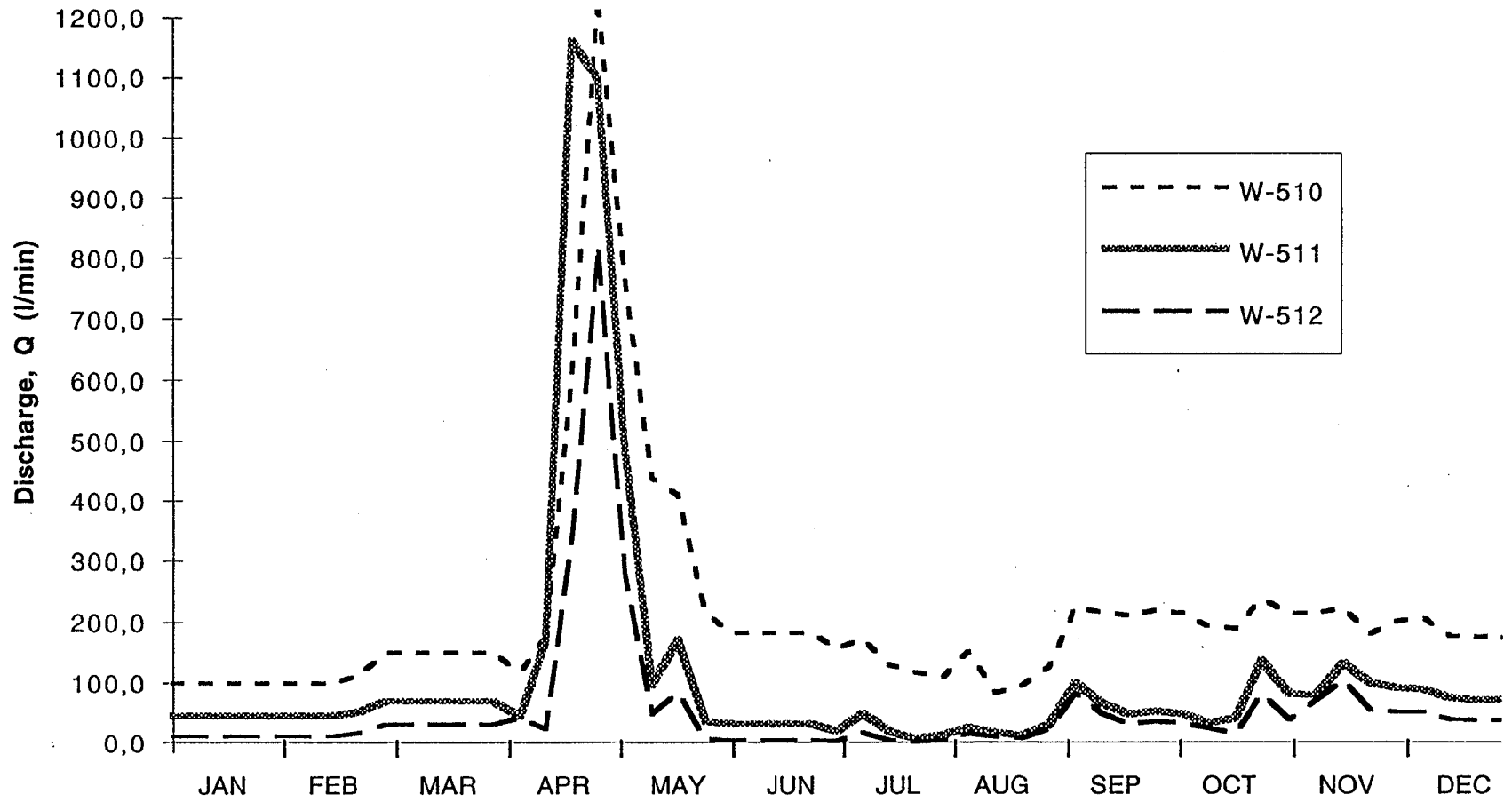
Fig. 4.4 Weir stations hydrographs for the year 1993
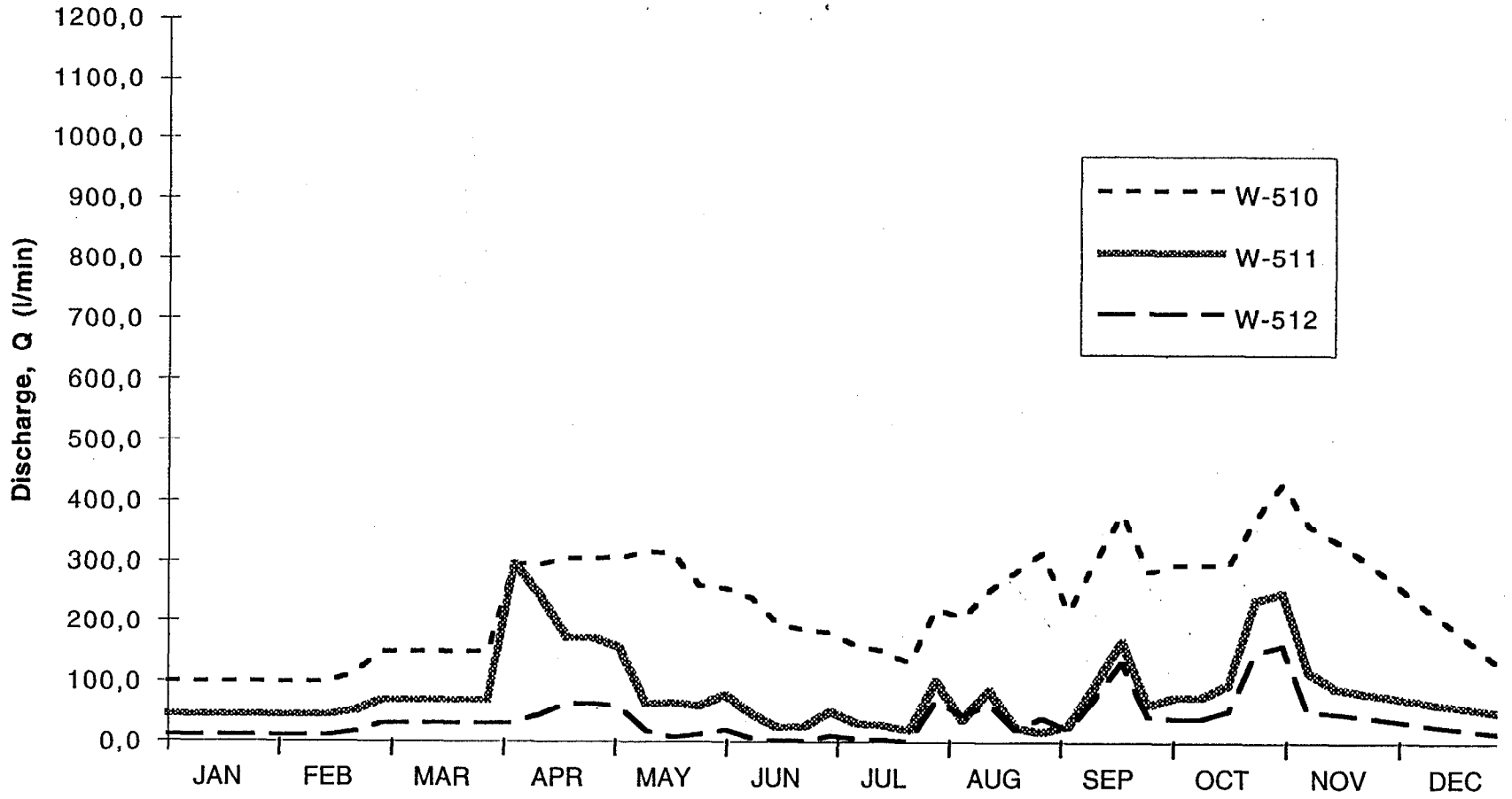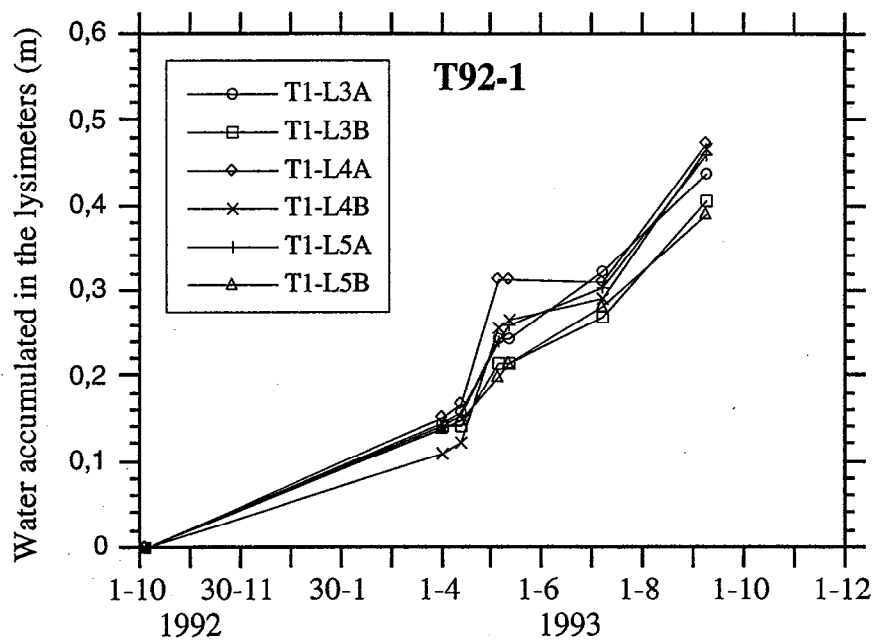
Fig. 4.5 Infiltration results from lysimeter station T92-1
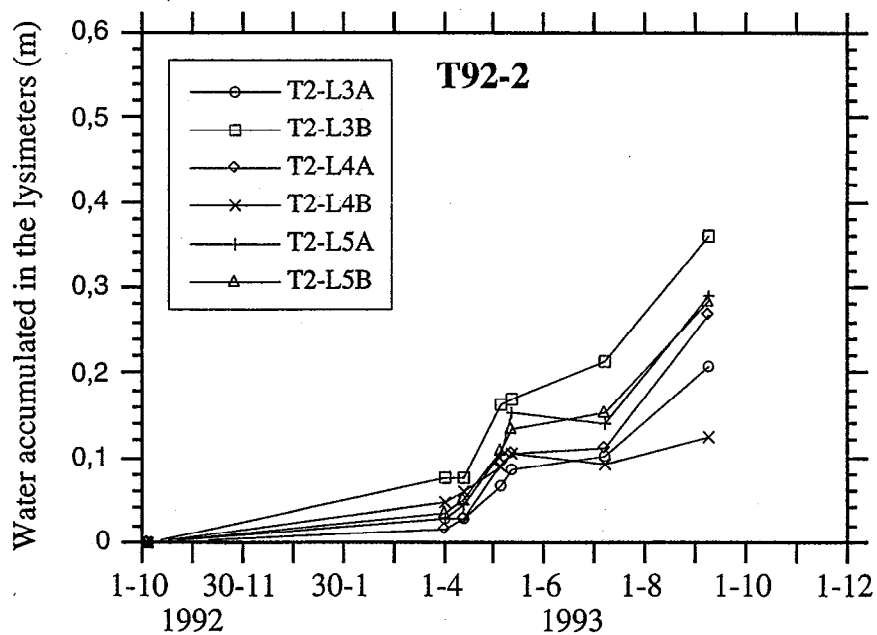
Fig. 4.6 Infiltration results from lysimeter station T92-2

4.3   DATA ANALYSIS

The collected data set is used to assess various elements of the South dump water balance. Many parts of this analysis are based on classical hydrological methods but some new or modified techniques are also proposed.

A first classical analysis is based on the preparation of annual and monthly hydrologic balances. These are calculated from meteorological data collected at existing regional weather stations and from base flow separation of recorded hydrographs at weir stations. A second classical analysis is performed on some single rainfall-runoff events of the summer 1992 using the unit hydrograph technique. A third data analysis task is to assess the groundwater flow component at the site with the help of a numerical hydrogeological model. Finally, results from all these analyses are synthesized in a overall hydrologic balance completed with other data sources.

4.3.1.   ANNUAL AND MONTHLY HYDROLOGIC BALANCES.

The complete hydrologic balance of the South waste rock dump is difficult to assess. Despite the numerous monitoring devices described in the preceding sections and the large data set gathered, the direct measurement of some elements of the water balance is not yet available or even feasible. The missing parts are thus estimated from alternate data and methods or through balance equations.

Analysis of Precipitations

Precipitations are the key element of the hydrologic balance. The regional meteorological data set is used to assess local precipitations since weather records at the site are sporadic and incomplete. Total precipitations from each of the three regional weather stations are combined, through a weighted average, to derive a local precipitation record. The weights are determined as a function of the distance between the weather stations and the mine site. These distances are shown in Table 4.1. The relative weight of each station precipitations I_i is put proportional to the inverse of the distance r_i. The weighted average I_w is thus computed. The results for 1991 and 1992 are presented in Tables 4.2 and 4.3.

Analysis of Runoff

Runoff data from weir stations are used to produce hydrographs that are in turn used to separate base flow from runoff. This separation is performed on annual hydrographs like the one presented in Figure 4.2. The separation technique is described in Llamas (1985) and involves graphical work. This method is based on the premise that base flow recession follows an exponential decline law. The hydrograph is traced on semilog paper and recession curves appear as linear slopes tangent to the lower part of the hydrograph curve. This kind of graphical presentation is included in Appendix C of Isabel *et al.*, 1994. A summary of the results of this separation is presented in Table 4.4.

Table 4.2 Monthly precipitations for 1991 (in mm)

Month	Stations			
	Kinojévis	Amos	Val d'Or	Doyon
January	52	65	69	59
February	15	23	35	22
March	62	68	72	66
April	62	55	45	56
May	66	81	47	66
June	95	71	65	82
July	63	127	50	77
August	97	86	119	99
September	118	119	83	110
October	90	93	63	85
November	56	67	61	60
December	40	54	66	50
TOTAL:	816	909	775	832

Table 4.3 Monthly precipitations for 1992 (in mm)

Month	Stations			
	Kinojévis	Amos	Val d'Or	Doyon
January	47	56	73	55
February	34	36	38	36
March	41	54	92	56
April	49	69	45	54
May	75	88	58	74
June	58	53	87	63
July	100	81	92	93
August	137	126	125	131
September	107	99	107	105
October	64	69	62	65
November	78	90	69	79
December	61	60	70	63
TOTAL:	853	882	920	875

Table 4.4 Results of base flow separation

Station	Year	Runoff (mm)	Base flow (mm)	Runoff coefficient	Surficial flow coef.
510	1991	106	226	0.13	0.40
510	1992	81	220	0.09	0.34
511	1991	112	96	0.13	0.25
511	1992	120	94	0.14	0.24
512	1991	122	61	0.15	0.22
512	1992	103	57	0.12	0.18
Total	1991	114	144	0.14	0.31
Total	1992	96	145	0.11	0.28

The analysis of runoff flowrate must take into account the area of the watersheds contributing to each station. For example, in Table 4.4 flowrates are normalized by dividing them by the respective area of each watershed. A complete analysis of flowrates therefore requires information on the watershed area and even a subdivision of this area into various types of surfaces. A complete subdivision of the South dump is presented in Figure 4.7. The subdivisions identified on the map are related to the original drainage watershed and to the nature of the soil surface. The original watershed division is obtained from the former topography of the site and is thereafter subdivided according to the soil surface as observed on aerial photographs and from visits to the site. The numbered subdivisions appearing on Figure 4.7 are listed in Table 4.5.

These subdivisions are compiled according to surface type and watershed. This gives Table 4.6 where the surface composition of each watershed has been summed. This is important since many hydrological processes are controlled by the nature of the soil surface. The term "Earth fill" represents a portion of the waste rocks that was covered with a thin layer of till, mainly at the toe of slopes.

Table 4.5 List of site subdivisions

Subdivision number	Watershed number	Type of soil surface	Area (m^2)
1	510	Vegetation	10135
2	510	Earth fill	39216
3	510	Vegetation	4880
4	512	Vegetation	4912
5	512	Earth fill	46069
6	512	Vegetation	101731
7	511	Earth fill	20347
8	511	Vegetation	23070
9	511	Bedrock outcrop	10787
10	511	Vegetation	60991
11	510	Vegetation	2376
12	510	Bedrock outcrop	1529
13	511	Bedrock outcrop	1368
14	511	Bedrock outcrop	5480
15	511	Bedrock outcrop	4301
16	511	Vegetation	23837
17	510	Vegetation	7126
18	510	Earth fill	31857
19	510	Waste rock	306084
20	512	Waste rock	22402
21	512	Waste rock	5952
22	511	Waste rock	81027
23	511	Waste rock	8842
24	511	Waste rock	25370

Fig. 4.7 Watershed Subdivisions of the South dump

MAP OF WATERSHED DIVISIONS AND SUBDIVISIONS

4.14
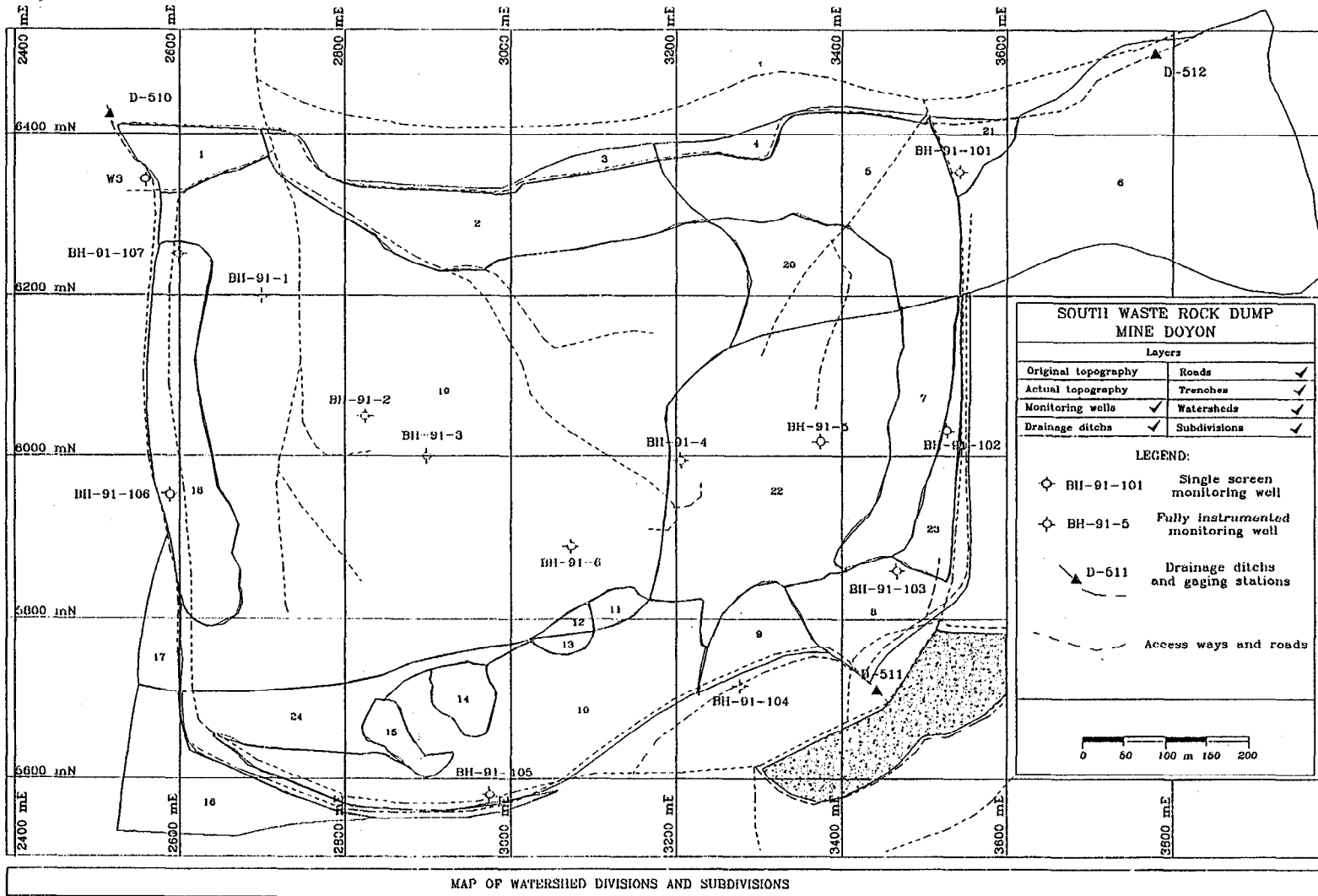
Base flow is more important in watershed number 510 (Table 4.4). This watershed has low relief, a more permeable soil surface and it includes a larger part of the dump (62%). Surface runoff is thus less important, as can be expected. The two other watersheds have steeper slopes, more bedrock outcrops and more earth fill surfaces. Their base flow component is therefore less important as compared to their runoff component.

Table 4.6 Watershed surface composition (m^2)

Watershed number	510	511	512
Vegetation	24517	107896	106643
Earth fill	39216	20347	46069
Bedrock outcrop	1529	21936	0
Waste rock	306084	115239	28354
TOTAL:	371346	265418	181067

If we assume that each type of soil surface has a typical base flow component, it can be evaluated from comparison between each watershed baseflow and surface compositions. There are three weir stations and four types of soil surface. Information is lacking to assess base flow for each sub-basin. But, if surface types are combined, it is possible to assess the dump base flow as compared to other surfaces. The following equation can be used:

$$Q_{b(total)} = (Q_{b(wrd)} \times F_{wrd}) + (Q_{b(other)} \times F_{other})$$

where Q_b is the base flow and F is the surface fraction. When applied to the results from the three weir stations, this equation gives for each year a set of three equations with two unknown. Applying to this system the least square method, the base flow of the waste rock dump and the average base flow of other surfaces are estimated. These results are presented in Table 4.7.

Table 4.7 Base flow for the WRD and other soil surfaces (mm)

	Year 1991	Year 1992
Waste Rock Dump	261	256
Other surfaces	8	6

Combination of precipitation and runoff analysis

A combined analysis of precipitation and runoff data, on a yearly basis, includes the calculation of runoff coefficient and surficial flow coefficient. The runoff coefficient is the ratio of surface runoff over total precipitations. The surficial flow coefficient is the ratio of total flowrate (base flow and runoff flow) over total precipitation. These coefficients are given in Table 4.4. Their values are related to soil surface properties for each watershed.

Runoff coefficients are quite similar for each watershed. But surficial flow coefficients are somewhat higher for watershed 510. This is explained by a smaller evaporation rate in this watershed due to a smaller vegetative cover and high rate of infiltration in the dump.

4.3.2.   SINGLE RAINFALL-RUNOFF EVENTS ANALYSIS

The following data analysis uses both meteorological and hydrological data collected on site. The goal is to assess the temporal relation between rainfall and runoff for some single rainfall-runoff events on a waste rock dump. The classical unit hydrograph analysis technique is used here.

Selection of Rainfall-Runoff Events

A detailed inspection of runoff logs obtained from the three weir stations operated on site and precipitation data from the Mine Doyon automatic weather station allowed the identification of five (5) isolated rainfall-runoff events which occured between May and June 1992. These events were selected among many others by applying the following criteria: This should be a large event, it must be recorded at each station, the data must be complete, the event must be well separated from previous and later rainfall-runoff events and it must be preceded by many days without significant precipitations.

The five selected events are listed in Table 4.8. In each case, the corresponding precipitation data are extracted from the local weather data base. Also, the corresponding graphical records of flowrate at weir stations were digitized to obtain numerical data files. The two data sets are presented in Appendix F of Isabel *et al.*, 1994.

Table 4.8 Selected rainfall-runoff events

Date	Duration (minutes)			Maxi. flowrate (m^3)		
Station	510	511	512	510	511	512
May 1 to 5 1992	7186	5745	5796	3838	7286	3610
May 11 to 14 1992	4330	4415	7286	1294	2200	1000
June 5 to 8 1992	4320	4320	4320	503	936	523
June 18 to 20 1992	2880	2880	2880	1600	2410	2200
June 21 to 22 1992	1440	1440	1440	800	560	436

The Unit Hydrograph Method

The unit hydrograph method is a classical tool used in hydrology. Its main purpose is usually to use rainfall-runoff data from a past single simple event to produce a runoff forecast from a precipitation forecast. Here it is used as a fitting method to facilitate the comparison of single-event hydrographs. The theory for this method can be found in any hydrology textbook.

The unit hydrograph is a single hydrograph corresponding to a unit precipitation height during a unit time step. It is obtained from deconvolution of a non-unit hydrograph with effective precipitation record. The preparation of the unit hydrographs from the five single events starts with the base flow separation on each recorded hydrograph. The resulting net runoff flows are then summed to obtain the total runoff volume of each event. The effective precipitation must match this volume and recorded precipitations are reduced in proportion to match this objective. The result is a set of records of net precipitation and runoff for each station and each event. Those calculations and records are included in Appendix F of Isabel *et al.*, 1994. An example of a net pluviograph and a hydrograph is given in Figure 4.8. The corresponding unit hydrograph is illustrated in Figure 4.9.

Results of the Analysis

Table 4.9 presents a summary of the various information given by this analysis of each rainfall-runoff event using this analysis. When compared with the type of soil surfaces present in each watershed (Table 4.6), it becomes evident that waste rock surfaces produce very small quantities of runoff. On the contrary, bedrock outcrop and other types of soil surfaces have higher runoff coefficients. The difference is so important that it can be concluded that runoff at weir stations comes essentially from outside the waste rock dump and that base flow is derived essentially from the waste rock dump.

Table 4.9 Results of single events analysis.

Event	Watershed	Base flow (mm)	Runoff (mm)	Runoff coefficient	Rise time (hours)	Runoff duration (hrs)
May 1	510	1.62	5.10	0.26	8.0	16.5
May 1	511	1.13	12.16	0.62	7.0	14.5
May 1	512	1.11	8.87	0.45	8.0	17.0
May 13	510	0.81	1.63	0.07	2.0	10.0
May 13	511	0.38	2.68	0.12	5.0	13.5
May 13	512	0.00	2.11	0.09	2.0	12.0
June 7	510	0.27	0.20	0.04	1.5	7.5
June 7	511	0.11	0.42	0.08	5.5	9.0
June 7	512	0.06	0.26	0.05	4.0	8.0
June 19	510	0.67	0.34	0.05	3.5	4.0
June 19	511	0.00	0.62	0.09	3.0	4.0
June 19	512	0.00	0.49	0.07	3.5	2.5
June 21	510	0.81	0.25	0.05	3.0	4.5
June 21	511	0.75	0.28	0.05	3.0	5.0
June 21	512	0.00	0.44	0.08	3.0	11.5
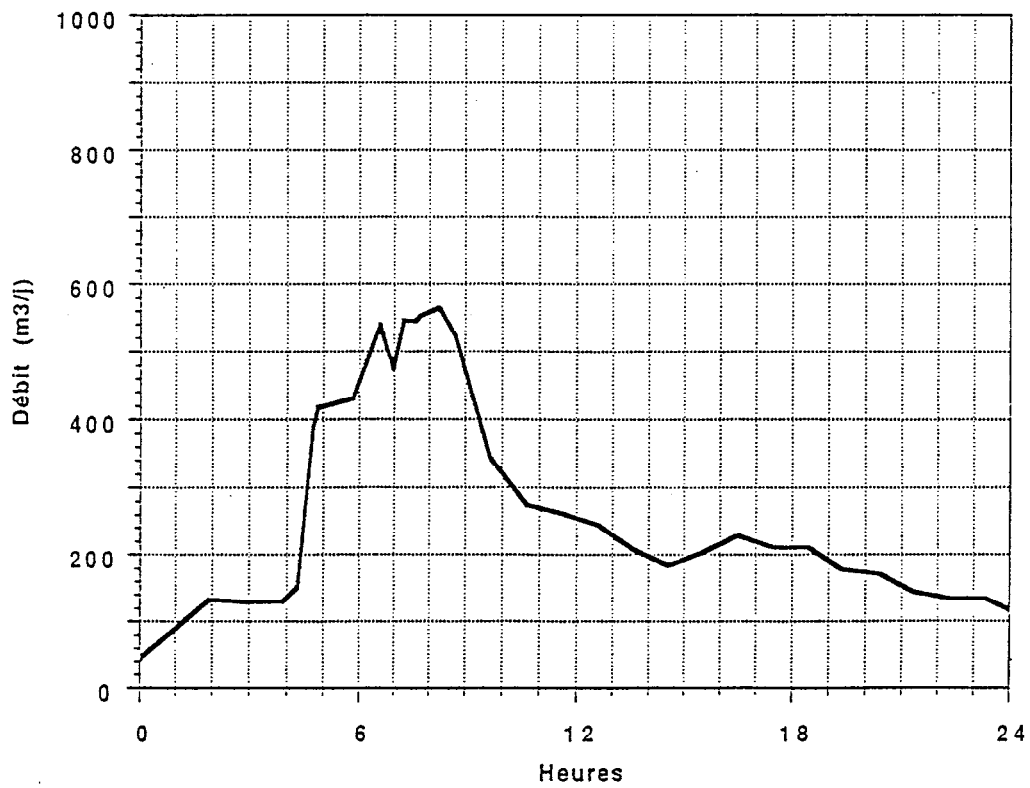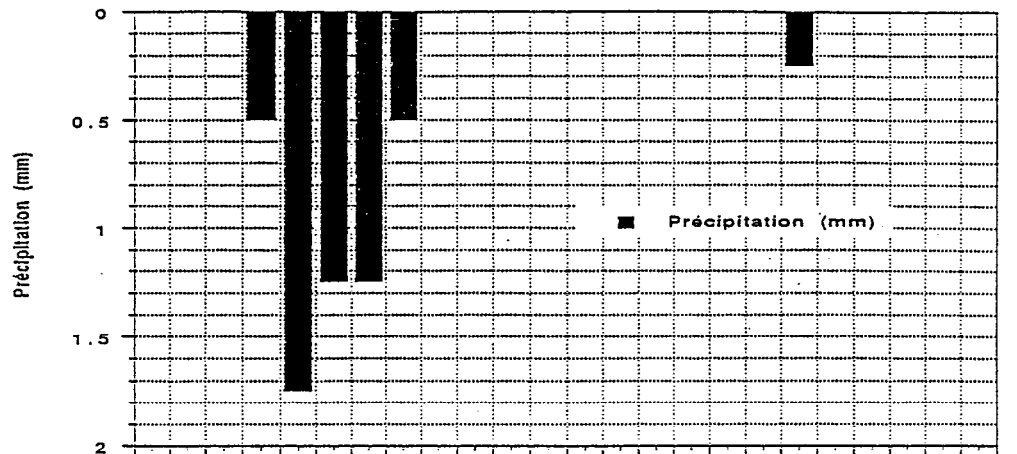
Fig. 4.8 Examples of measured net pluviograph and hydrograph
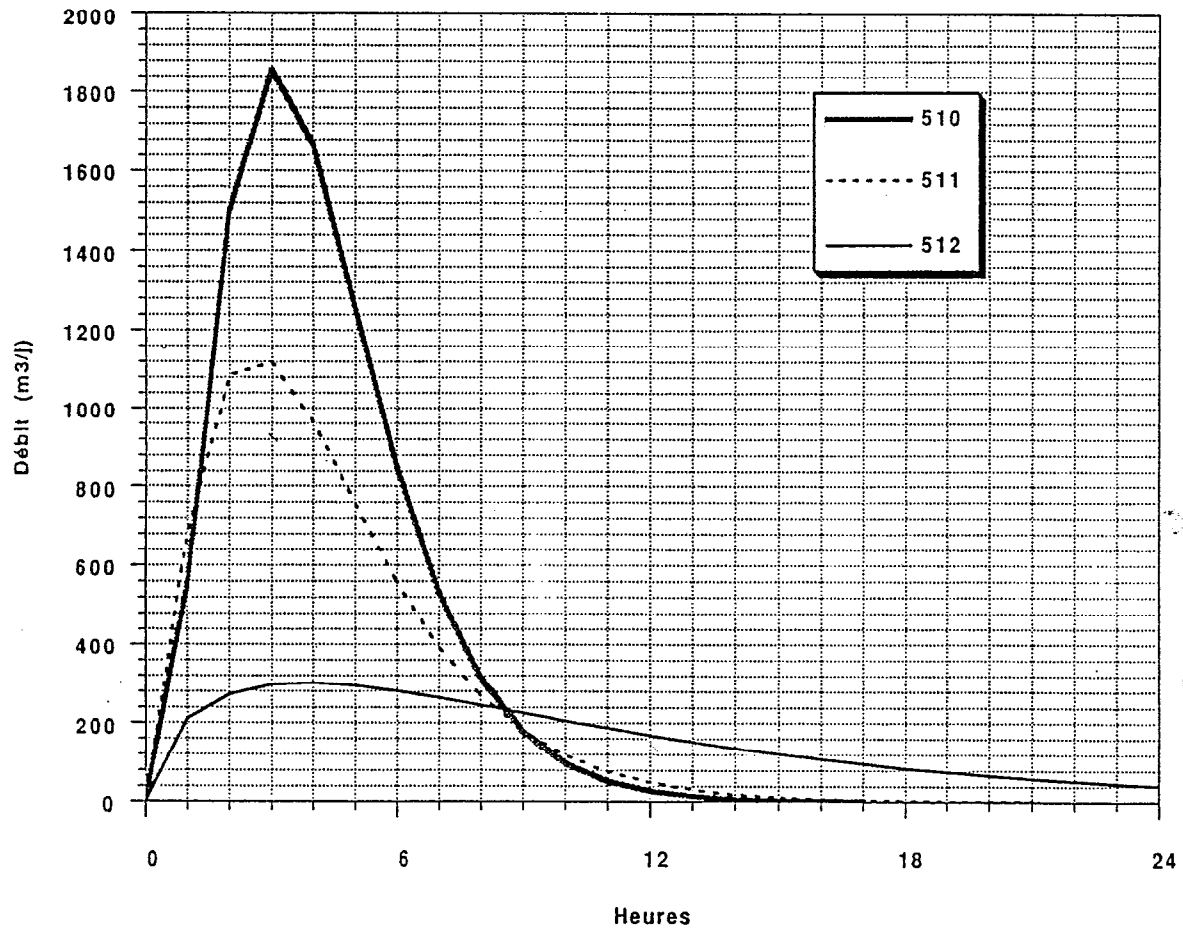
Fig. 4.9 Example of Nash Cascade unit hydrographs

4.3.3   HYDROGEOLOGIC MODELING

A major component of the water balance which has to be determined is the interaction between acid drainage and groundwater. Before discharging in the ditches around the dump, leachate reaches the base of the unsaturated rock waste and moves either laterally or infiltrates to deeper groundwater. Since boreholes and geologic mapping allow a stratigraphic section to be drawn of the site, some hydraulic properties were measured or estimated (for deep bedrock) in order to simulate groundwater flow at the base of the dump. A check with figures obtained for total discharge in the ditch system and total input from precipitation is used to validate the model. The modeling exercise is performed using the United States Geological Survey MODFLOW model. This is a two-dimensional finite difference groundwater flow model capable of modeling multi-layer systems. For the South dump, four layers were modeled with MODFLOW. These are described in Table 4.10.

Table 4.10 Geological layers definition for the MODFLOW model.

Layer	Hydraulic conductivity (m/s)	Hydraulic conductivity (m/d)	Thickness (m)	Transmissivity (m^2/d)	Vertical conductance (d^{-1})
1: Rock waste	1.00×10^{-3}	86.4	30.0	---	0.024
2: Soil	6.98×10^{-7}	0.06031	5.0	0.3015	0.0144
3: Fractured rock	1.04×10^{-6}	0.0899	5.0	0.4493	4.59×10^{-6}
4: Deep bedrock	3.45×10^{-9}	0.0003	130.0	0.0387	---

The site is discretized on a regular mesh composed of 29 rows and 46 columns of square cells. These cells have a 50 m by 50 m dimension. There are thus 1334 cells per layer for a total of 5336 cells. The cells located outside of the model domain are assumed inactive. This modelization domain is bounded like this:

- A constant head boundary to the north corresponding to the mine pit with a hydraulic head of 4891 m (using Mine Doyon arbitrary datum of 5000 m above sea level).
- A constant head boundary to the north-east corresponding to the final effluent stream with a head varying from 4961 to 4955 m.
- A constant head boundary to the south corresponding with the second reach of the final effluent stream with a head varying from 4995 to 4955 m.
- A constant head boundary to the south-east corresponding to the Bousquet river with a head of 4955 m.
- A constant head boundary to the north-west corresponding to the former process water reservoir with a head of 4975 m.
- A constant head boundary between the dump and Bousquet River corresponding to Basin D with a head of 4957 m.

Figures 4.10 to 4.13 illustrate the discretization mesh used for each layer. Layer properties are based on previous characterization studies and calibration for layer 4. The recharge rate for the dump is assumed to be 260 mm/y based on a preliminary water balance. The resulting piezometric maps for layers 2 to 4 are presented in Figures 4.14 to 4.16.

Fig. 4.10 Discretization mesh for layer 1

RAPPORT GREGI

MINE DOYON: MAILLAGE UTILISE POUR MODELISER LA COUCHE I
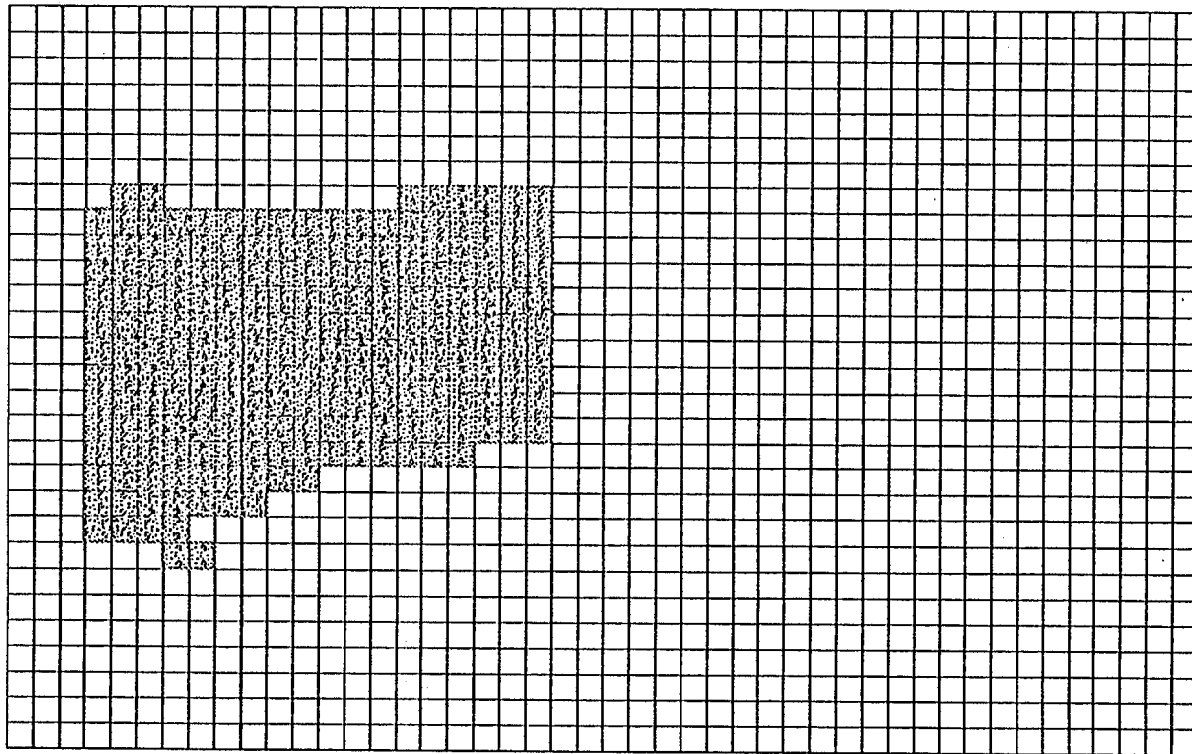
LEGENDE:

ZONE INACTIVE

LA HALDE

DRAINS

N

ECHELLE:

0   100   200   300 m

GREGI - UNIVERSITE LAVAL   juillet 1993

RAPPORT GREGI

MINE DOYON: MAILLAGE UTILISE POUR MODELISER LA COUCHE II

LEGENDE:

ZONE INACTIVE

DEPOT MEUBLE

ZONE A CHARGE IMPOSE

DRAIN

ECHELLE:

0   100   200   300 m

GREGI - UNIVERSITE LAVAL   juillet 1993
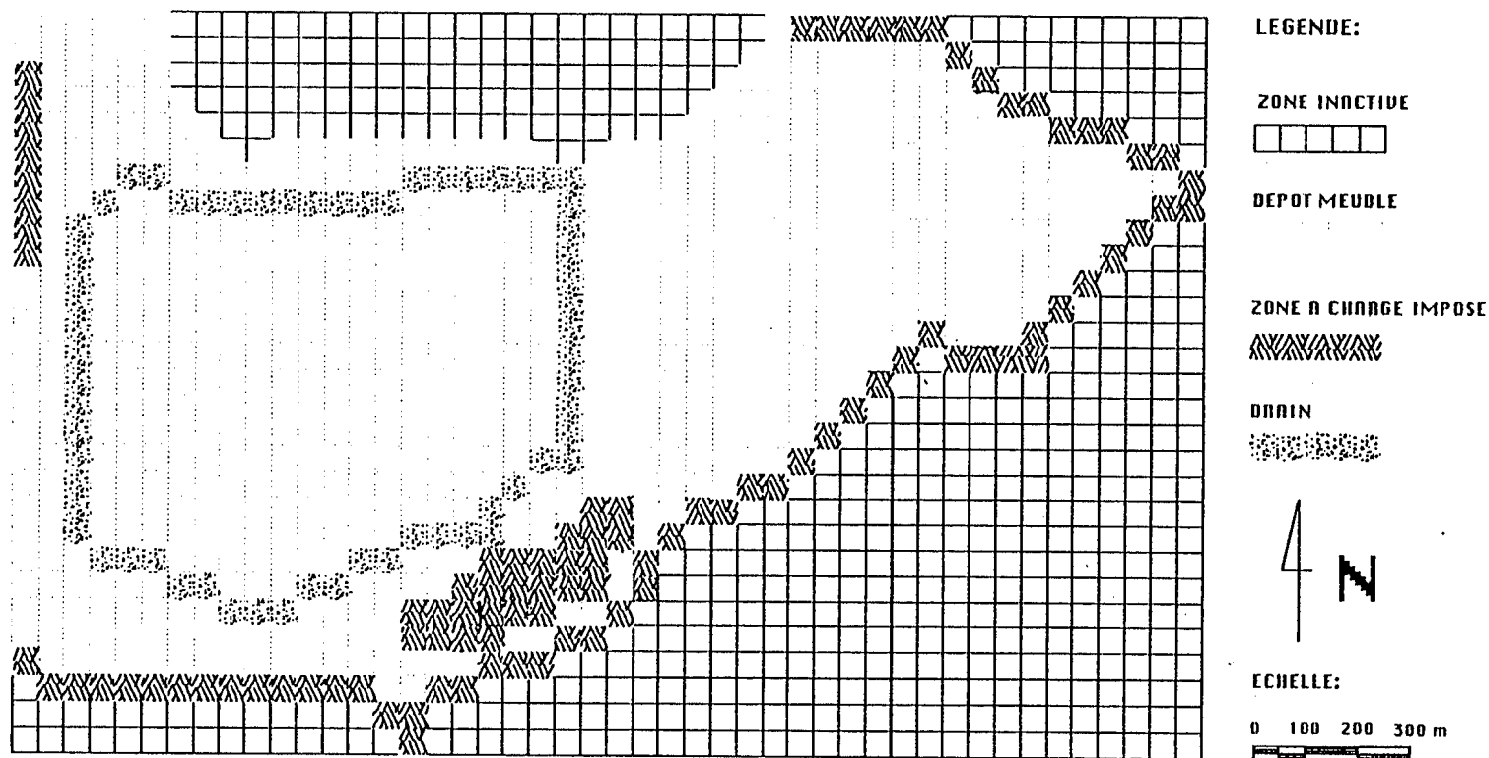
Fig. 4.11 Discretization mesh for layer 2

Fig. 4.12 Discretization mesh for layer 3

RAPPORT GREGI

MINE DOYON: MAILLAGE UTILISE POUR MODELISER LA COUCHE IV

Fig. 4.13 Discretization mesh for layer 4
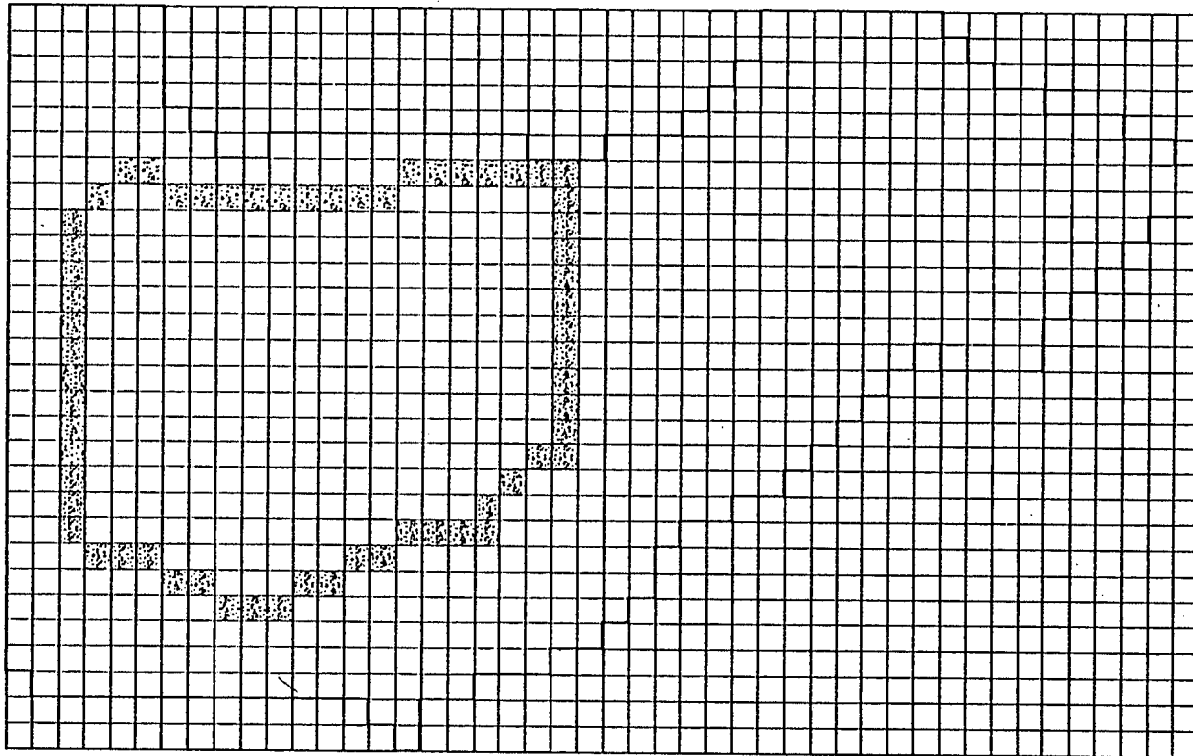
LEGENDE:

ZONE INACTIVE

ROC SOLIDE

ZONE A CHARGE IMPOSE

N

ECHELLE:

0   100 200 300 m

GREGI – UNIVERSITE LAVAL   juillet 1993

RAPPORT GREGI

MINE DOYON: CARTE PIEZOMETRIQUE DE LA COUCHE II
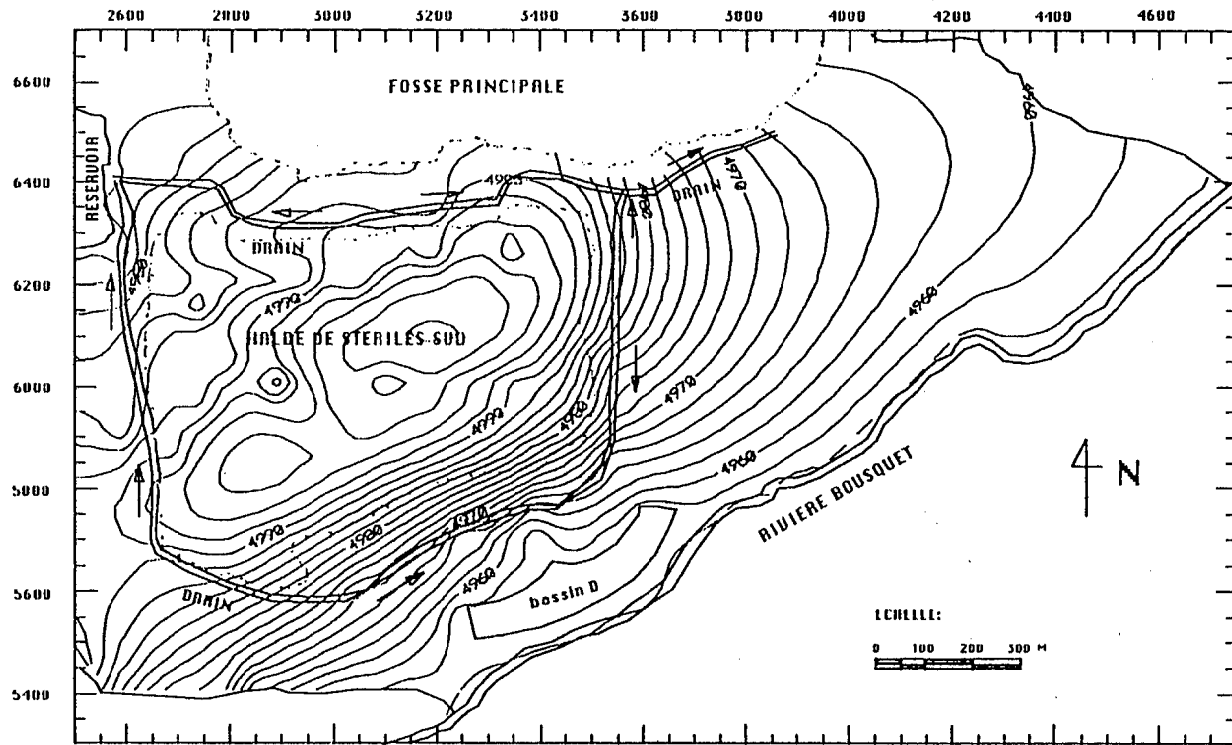
Fig. 4.14 Piezometric map for layer 2

GREGI – UNIVERSITE LAVAL   juillet 1993

4.25

RAPPORT GREGI

MINE DOYON: CARTE PIEZOMETRIQUE DA LA COUCHE III
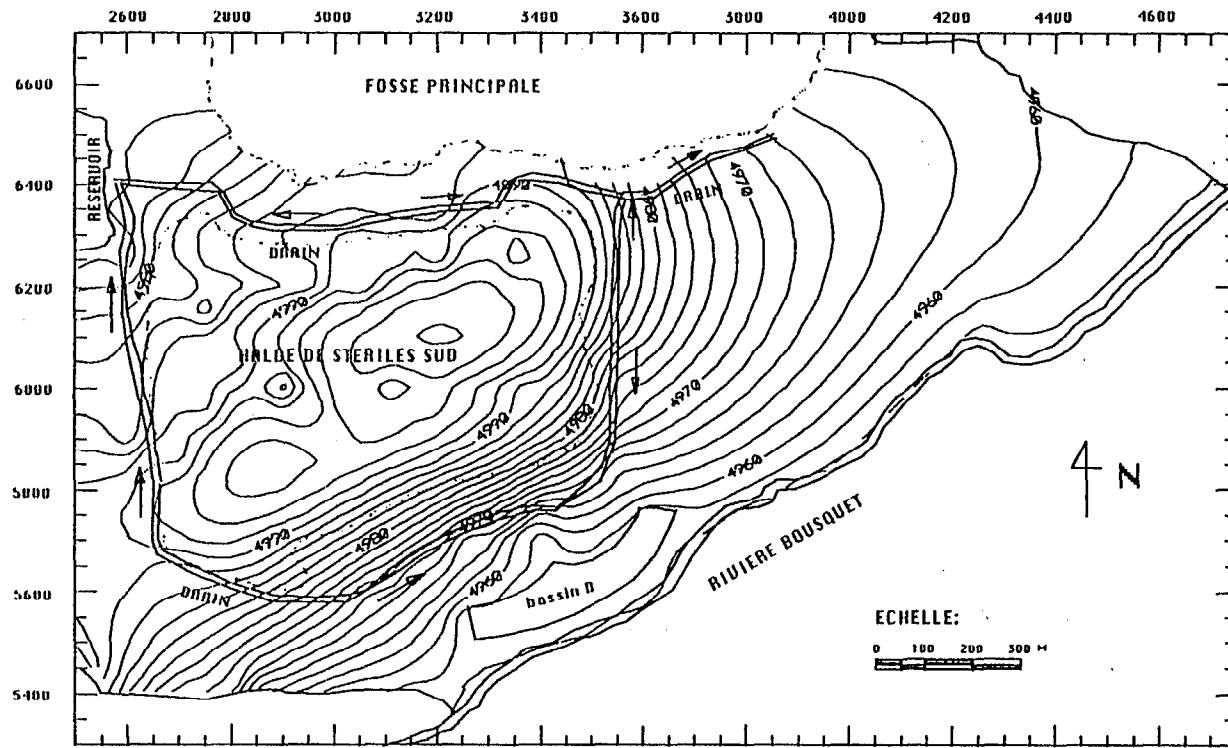
Fig. 4.15 Piezometric map for layer 3

GREGI – UNIVERSITE LAVAL   juillet 1993

Fig. 4.16 Piezometric map for layer 4
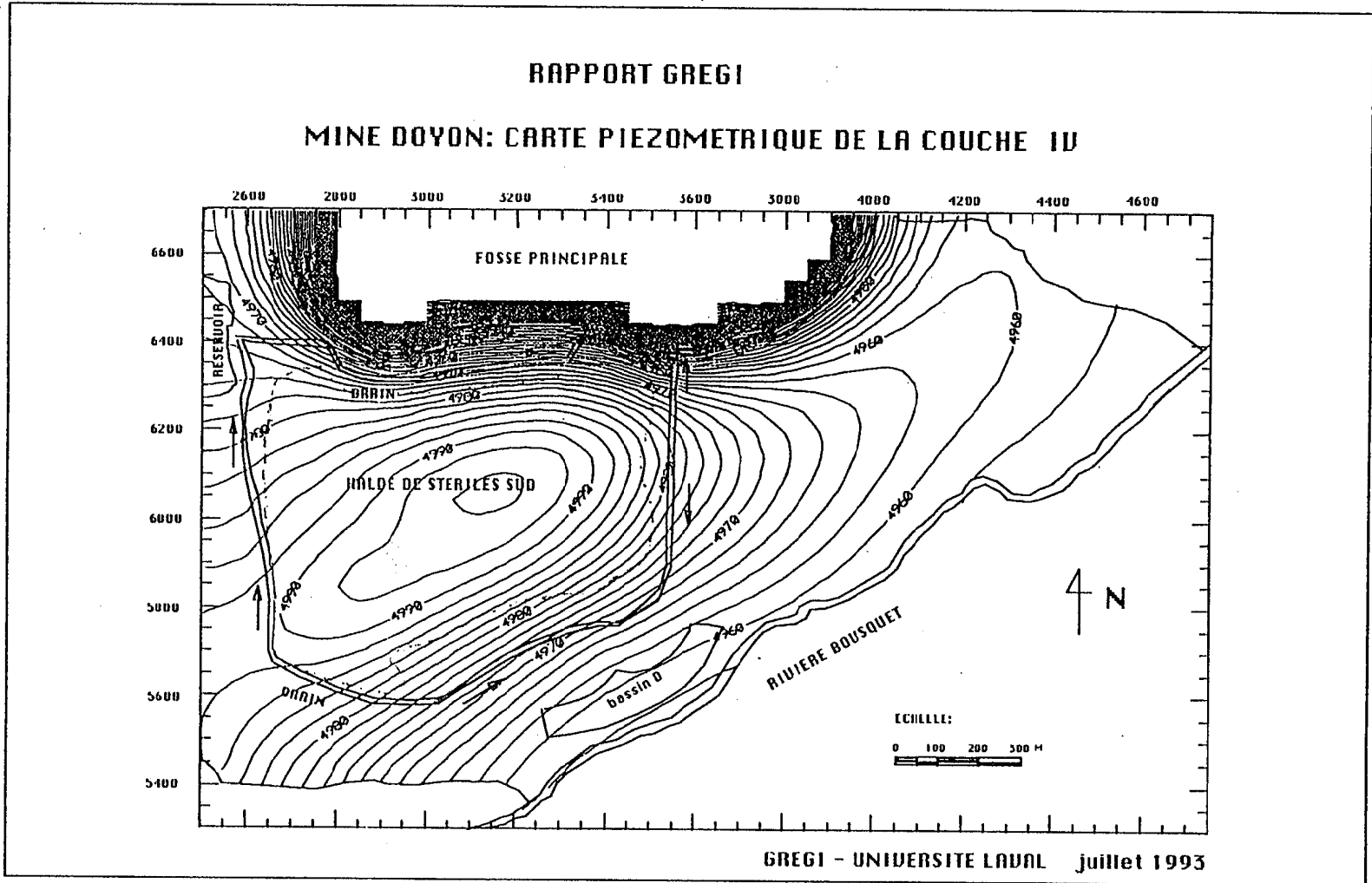
A complete hydrogeologic balance for this model is computed using a subdivision into various zones. Those zones are illustrated in Figure 4.17 and the result of these balance calculations is presented in Table 4.11.

In this table, zones 1 to 4 refer to different layers in the dump: zone 1 is the waste rock itself, zone 2 corresponds to the original soil (silty clay), zone 3 is the shallow fractured bedrock, and zone 4 is sound bedrock of very low permeability. Zones 5 to 7 refer to areas outside the dump where water fluxes in or out can occur.

In Table 4.11 the column entitled "DRAINS" is the sum of all infiltrated water that is discharged to the ditches around the dump in the form of groundwater baseflow. The total of 107 467 m^3 per year corresponds to a water depth of 199 mm of equivalent rainfall. Another estimate of that value was obtained from hydrograph separation and gives 115 000 m^3 per year or 213 mm.

Table 4.11 Hydrogeologic balance (m^3/y)

| | ZONE | TO | | | | | | | | | |
| | | DUMP (layer 1) AND BELOW | | | | OUTSIDE DUMP | | | | | |
	NO	1	2	3	4	5	6	7	CONST.CH.	DRAINS	Σ OUT
F	1	-	303	-	-	-	-	-	-	68080	68383
	2	47695	-	76249	-	2030	1595	10464	-	16218	154250
R	3	-	28074	-	7126	3030	2382	15596	-	22456	78663
O	4	-	-	334	-	1963	3608	1319	-	-	7224
	5	-	753	1118	43	-	46	-	8463	713	11136
M	6	-	104	152	5	90	-	4311	13367	-	18028
	7	-	750	1119	50	858	2721	-	43734	-	49232
	INFILT.	18902	125589	-	-	3300	7001	10601	-	-	165393
	CONST.CH.	-	-	-	-	941	676	6940	-	-	8556
	Σ IN	66596	155572	78971	7224	12212	18028	49231	65564	107467	560867

(BASE FLOW)

Net loss through the dump base layer is calculated by making the difference between fluxes from the dump to zones 5, 6 and 7 and the fluxes from zones 5, 6, and 7 in the dump. This net flux is 37 900 m^3 per year and is equivalent to a loss of 70 mm (rainfall equivalent).

RAPPORT GREGI

MINE DOYON: ZONES UTILISEES POUR REPARTITION DES ECOULEMENTS

ZONE 5

ZONE 6

ZONE 1, 2, 3 ET 4

ZONE 7

N

ECHELLE:

0   100   200   300 m

GREGI - UNIVERSITE LAVAL juillet 1993

Fig. 4.18 Zones used for hydrogeologic balance calculations

4.29
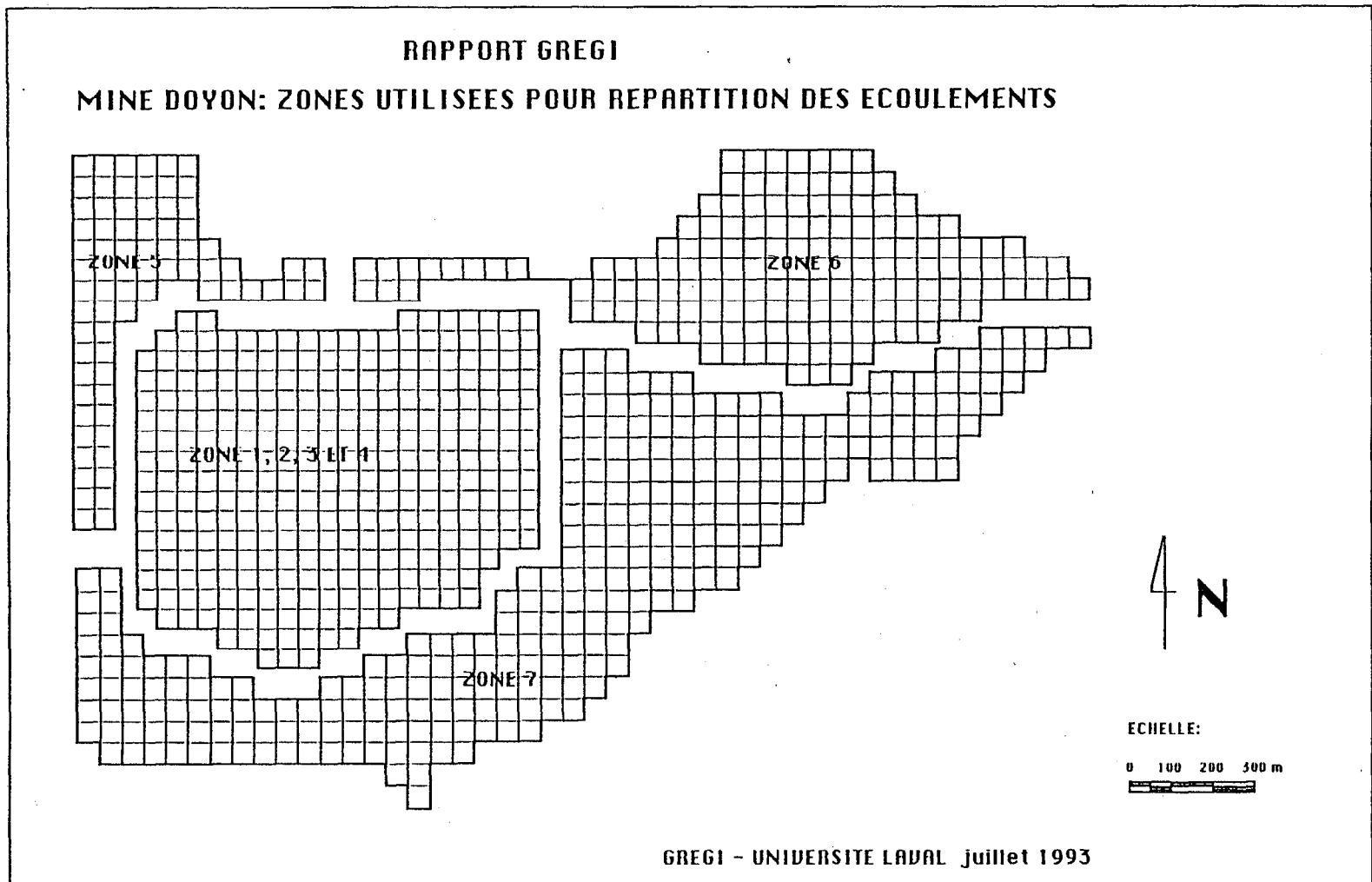
4.3.4. OVERALL HYDROLOGIC BALANCE

Computing a hydrologic balance for a major waste rock dump poses several problems because the microenvironment created by its construction does not lend itself to analysis like other natural or man-made systems. This section is a critical review of data gathered at Mine Doyon over a three-year period and suggestions are made to improve the quality of data and for new ways to establish water balances for waste rock dumps.

Precipitation Data

Short term records of precipitation are available for some time intervals at Mine Doyon but they are discontinuous and since the weather station is located on the plant roof top, precipitation data may not be representative for the waste dump. However, since instantaneous precipitation data was available on a 15-minute time interval, some of the data were used to analyze storm events.

Data on a yearly basis were calculated for Mine Doyon from three regional weather stations and a weighting factor based on distance to the mine was used to give annual and monthly mean precipitation values. Over a long period of time, this method usually gives good precipitation data for annual water balance. It is however difficult or even impossible to relate daily precipitations to daily storm events or infiltration estimates. For the two years (1991-1992) for which complete data are available, the mean annual precipitation is 855 mm.

Local distribution of precipitation must also take into consideration altitude, wind direction, and local relief especially for snow accumulation. At Mine Doyon, strong winds blowing from the west influence snow accumulation which is much deeper at the base of slopes; accumulated snow, which is from 25 to 30% of total precipitation, thus contributes more to run-off than to infiltration through the waste rocks.

Water flow

Flow data are available for three complete years (1991 to 1993). The annual volumes are 210 697 m^3 for 1991, 197 618 m^3 for 1992, and 181 012 m^3 for 1993. The last year (1993) was unusual because there was very little precipitation during winter and the spring peak flow was not larger than summer and fall peak flows. The three-year average is 196 442 m^3. Since the area of the hydrologic basin is 81,8 ha, the average flow over the total basin is 240 mm.

Flow must be evaluated for winter conditions when it is not possible to measure discharge with the equipment in place because ice is forming in the holding basins. Winter flow is mainly baseflow and it is assumed more or less steady. Discharge being low, the four-month period from December to March represents 20,5% of the annual flow. Errors associated with this period are estimated to be in the order of 5% of the annual flow.

Baseflow was evaluated by two methods: modeling infiltration through the dump and through the base materials gives 107 467 m^3; hydrograph separation gives approximately 115 000 m^3 of baseflow. Runoff from the dump can be calculated by the difference between mean flow from the

dump area (54 ha) minus baseflow. Runoff is evaluated to be between 14 000 and 22 000 m^3 per year and it is generated mainly from the slopes of the dump that are partly covered with till (a total area of 7 ha).

The ratio between total flow and precipitation (240mm/845mm) is 0,284 or 28,4%. This value is similar to figures obtained by Mine Doyon for the water balance of the entire property which is close to 30%.

The ratio of baseflow to total flow is also very high and is estimated from above to 83 to 88% of total discharge. This is consistent with the very large permeability of rock waste as compared with ordinary soils. This factor is very important for the management of acid rock drainage and steps must be taken to reduce infiltration in the waste dump.

Losses to Groundwater

One part of the water balance that cannot be measured is the loss of acid drainage to regional groundwater. Data available to estimate the magnitude of groundwater flow include: water levels for piezometers in and around the waste dump, estimates of hydraulic conductivity of various sediments and rocks, local topography, changes in storage in the system, stratigraphy and structural geology. A model presented in section 4.3.3 was used to analyze these data. A major problem in using a model is the attribution of values to hydraulic conductivities of the various layers as well as their areal distribution. Direct measurement of permeability in the saturated zone was done during the installation of piezometers. Values obtained from slug tests (Golder Associates Ltd.,1991) are typical for silty clay deposits at the base of the dump. Permeability values for bedrock are relatively high and represent local conditions (sets of fractures) but may not be representative of the bedrock formation as such. Early model simulations showed that measured rock permeabilities were too high so that the bedrock would become unsaturated very early if these values were used. Connectivity of fracture sets seems to have a major control on rock mass permeability. This parameter was adjusted by the model subjected to two external conditions: first, water discharge in the ditches must be respected for a given infiltration rate, and second, water levels measured in the dump and below it should be consistent with the model. With these controls, the model was able to estimate losses to groundwater as 37 900 m^3 which is an equivalent of 70 mm distributed over the total area of the dump.

At this point of balance calculations, total precipitation minus discharge to the ditches and to regional groundwater is equal to 545 mm. Two other processes can account for this difference: evaporation and change in storage.

Evaporation and Change in Storage

In classical hydrologic analyses, loss of water to atmosphere is in terms of evapo-transpiration, a process involving evaporation from free water surfaces and water consumption (transpiration) by plants. There is no vegetation on most major rock waste dumps, so that the evaporation in the main mechanism of returning water to the atmosphere. During the active oxidation period when strong thermal gradients exist, vapor flow may be an important factor contributing to evaporation.

Condensation of water vapor can be observed near the top of slopes during cold days when strong winds are blowing. However an important mass of water vapor condensates inside the dump due to sharp temperature gradients (up to 10 $^{\circ}$C/m) near the surface. This topic is discussed in Chapter 7. Evaporation is made easier on bare surfaces as temperature gets higher than on soils covered with vegetation.

Direct measurements of evaporation are seldom made and its value is commonly established by the water balance method:

$$E = P - Q_B - Q_R - G - \Delta S$$

where E is evaporation, P is precipitation, Q_B is baseflow, Q_R is runoff, G is groundwater loss and ΔS is the change in storage. This last parameter must be estimated in order to calculate evaporation.

The change in storage in a waste rock dump results in accumulation of water in the pore space until field capacity or residual water content is reached. Results from field measurements of gravimetric water content, microgravity measurements and modeling establish the residual water content at 10 to 12% (volumetric). Mine Doyon south dump with a volume of 11,5 million m^3 can store from 1,2 to 1,4 million m^3 of water against gravity. Water content of freshly blasted rocks from the main pit is assumed to be in the order of 1 to 2% so that during the years that followed construction, storage had to increase rapidly near its actual value. Certain rock types such as sericitic schists which form about 50% of the rocks in the dump can also swell by absorbing water in their inner structure. Fine particles, released by oxidation processes and subsequent fragmentation of rocks, increase capillary pressure which also leads to increase water storage and degree of saturation. Therefore, it is difficult to estimate the change in storage on a yearly basis and it should not exceed 5% of total precipitation or and equivalent 40-45 mm per year.

Using the water balance equation, evaporation is calculated to be about 500 mm/year, depending on the value estimated for change in storage. Seasonally, evaporation is higher during summer when precipitations are more important and temperatures higher. Other methods of estimating evaporation on waste rock dumps include the energy balance method and the mass transfer technique (turbulent transfer of water vapor by eddy motion). Special equipment not available for this project is needed to use these techniques.

Infiltration

An important parameter in ARD prediction is the amount of infiltration through waste dumps. Infiltration I can be measured directly using gravity lysimeters and calculated using the following equation (all the terms are defined above):

$$I = Q_B + G + \Delta S$$

Shallow infiltration is usually compensated by evaporation and is not considered in this equation. Using results from the preceding section, deep infiltration is estimated at 320 mm/year. This estimate is close to what was observed at lysimeter station T92-2 where waste rocks are mainly sericitic schists with a greater amount of fine particles. In lysimeter station T92-1 where volcanoclastitic rocks predominate near the surface, infiltration is higher with an annual value of 400 to 500 mm. These results are preliminary because it may take a year for the disturbed materials to reach equilibrium water content after the installation of lysimeters.

The water balance approach can yield interesting results for the hydrology of waste rock dumps by showing relationships between the different elements of the water balance (Table 4.12). However, this technique fails to estimate dynamic conditions such as rates of percolation, average residence time of water in the dump, and other parameters that are needed to model physical and geochemical processes. Field experiments should be conducted on well-instrumented areas to get more information on these processes.

Table 4.12 Water Budget Summary (in millimeters of water per year)

· Precipitation	P	855
Total flow	Q	240
Base flow	Q_B	205
Runoff	Q_R	35
Groundwater losses	G	70
Evaporation	E	500
Change in storage	ΔS	45
Infiltration	I	320

4.4 CONCLUSION

This section presents results of the hydrologic data analysis for the south waste rock dump at Mine Doyon between 1991 and 1993. Meteorological data is presented for the region and at the site itself. Flow measurements were obtained from three (3) weir stations for three complete years from 1991 to 1993. Piezometric data on monitoring wells inside and outside the dump are also presented. Preliminary data from lysimeter stations installed in 1992 and 1993 are analyzed.

Total precipitation at Mine Doyon is estimated from three regional stations with a mean value of 855 mm for 1991 and 1992. Long term averages for a station that operated for a long period in Cadillac, 10 km SE of Mine Doyon, are 863 mm/a. The snow fraction of precipitation varies from 25 to 30% over the years. More than 50% of precipitation occurs during the four months between

June and September. The most significant hydrologic event is the melting of snow which accounts for most infiltration in the dump and generates large amounts of acid drainage at the weir stations.

Total average daily flow from the dump is 538 m^3/d but wide variations occur with seasons. Winter flow is about 230 m^3/d, spring flow may reach 4300 m^3/d but most of the year, flow ranges from 200 to 1200 m^3/d with an average of 400 m^3/d. The ratio of total flow to precipitation is 28% only which indicates that other processes are important in explaining the hydrologic behavior of the Mine Doyon waste dump.

Losses to regional groundwater have been determined by modeling using hydraulic properties of the materials and the water level measured in monitoring wells inside and outside of the dump. Groundwater losses are small and represent only 8,2% of total precipitation. This is due to the fact that waste rocks lie on a deposit of silt and clay of low permeability and that bedrock fractures are poorly connected. Discharge in the peripheral ditches accounts for most of the acid drainage produced by the waste rock dump.

The stream hydrograph can be separated in two components: baseflow discharging from the original soil surface and runoff from surficial flow following storms or spring snow melt. Hydrograph analysis shows that most runoff is coming from the parts of the sub-basins that lay outside the ditches so that only a small proportion of the runoff (12 to 17%) is generated on the slopes of the waste dump. Baseflow from the dump is then estimated at 83 to 88% of the drainage generated by the waste rocks.

Two parameters account for the difference between precipitation and flow: evaporation and changes in storage inside the dump. Based on the difference between original and actual water content (from an estimated 2% to an actual 10 to 12% volumetric over a period of 10 years), storage *between* and *within* rock fragments has been an important part of the water balance. Mean absorption of water by the waste rocks during the first years may have accounted for 30% of total precipitation on the dump. However, storage has reached values close to field capacity and actual contribution to storage is probably lower, in the range of 40 to 50 mm/year. The breakdown of rock fragments due to physico-chemical processes results in the exposure of new surfaces and the release of fine particles able to adsorb capillary water in significant amounts.

Evaporation is calculated rather than measured by taking the difference between intrants (precipitation) and extrants (change in storage, groundwater losses and baseflow). It represents about 58% of total precipitation, a value that compares well with normal evapotranspiration calculated for this region (55 to 60% of precipitation).

Infiltration which is the sum of baseflow, groundwater losses and change in storage accounts for 37% of precipitation. This estimate is consistent with preliminary measurements of infiltration in gravity lysimeters installed in two locations at Mine Doyon. With time, infiltration may become less important as surface layers get clogged by fine particles thus favoring retention, evaporation, and runoff. However, baseflow may remain about the same because the storage capacity of the dump will tend to stabilize with time.

The main results of this project are the realistic estimation of all the important hydrologic parameters controling the movement of acid drainage in a large waste dump. However these estimates relate to mean values on an annual basis and merely represent mass balance. Rates of transfer or fluxes will also have to be estimated in the future. Important issues such as the seepage velocity, or the average residence time in the dump cannot be analyzed with the present data. Controled infiltration tests using simulated rainfall and field tracer tests using special sampling techniques for the unsaturated zone (neutron probes, suction lysimeters) should be designed to answer these questions. Evaporation should be evaluated using energy balance and mass transfer technique (turbulent transfer of water vapor by eddy motion).

5 / Geochemical, mineralogical, and microbiological characterization

5.1 INTRODUCTION

The purpose of this chapter is to report on geochemical, mineralogical, and microbiological studies on the generation and evolution of acid rock drainage in a major waste rock dump. Results of this work have been presented in separate MEND reports (Choquette *et al.*, 1993a, 1993b; Guay, 1993; Gélinas *et al.*, 1993; Choquette and Gélinas, 1994; Guay, 1994).

The first part will outline briefly the monitoring program and the types of analyses which were performed on ARD water samples. Chemical data are presented for samples coming from observation wells in and below the dump, piezometers around it, acid drainage at weir stations, and some leachate collected in gravity lysimeters or squeezed from moist rock in the unsaturated zone. Typical composition of ARD are presented for April 1994 and some graphs illustrates chemical evolution of acidity in the last three years of monitoring.

A second part looks at the mineralogical changes that occur during acidification resulting from pyrite oxidation and neutralization mechanisms involving carbonate dissolution, silicates transformations, and precipitation of new minerals. Geochemical profiles of leachate in contact with rocks and minerals are discussed in terms of vertical gradients in the chemical composition of the acid leachate and the resulting mineral assemblage trying to reach equilibrium with the solution. Silicates dissolution and new minerals formation are identified as major components in the geochemical evolution of ARD at Mine Doyon.

Microbial diversity is important in the generation of acid rock drainage and the evolution of ferrous iron into ferric iron as the leachate percolates to the base of the dump. Appropriate bacteria counting and identification procedures have been developed for this project. Field sampling of rock cuttings during drilling and water sampling from boreholes were used to identify strands of bacteria. A technique of *in situ* colonization of substrates immersed in acid drainage in the field gave also important insight of microbiological processes in anoxic environments. Biological activity and oxidation kinetics were measured in the lab to support a model of microbiological zoning in an active waste rock dump.

Finally, a preliminary chemical mass balance is presented that gives indications on the rate of acid generation and transport in the south waste dump of Mine Doyon. A particular point in the discussion looks at the relatively large amount of reaction products that are stored temporarily or permanently in the waste dump as compared with the leachate that is collected and treated. Long

term management options should look more closely into the natural processes of slow rate neutralization that occurs if infiltration and percolation rates can be controled in such a way that less acidity is released to the outside environment.

5.2 MONITORING AND GEOCHEMICAL EVOLUTION OF ACID ROCK DRAINAGE

5.2.1 MONITORING ARD

ARD can be sampled at different locations in and out of the dump to study its spatial variation for a given time interval. ARD also evolves in time at a given location so that a monitoring program is necessary. At Mine Doyon, there are two important sets of data for monitoring: ARD inside the dump and acid drainage collected at weir stations. A large number of rock fragments samples were also used to gain more information in the unsaturated zone where it was not possible to monitor variations in time due to the limitation in field resources and equipment.

Geochemical data on ARD is derived from sampling the following points (Figure 5.1):

- Six (6) boreholes (BH-1 to BH-6) drilled to the base of the dump and underlying soil and bedrock; BH-1 to BH-4 have two levels of piezometers for sampling, one at the interface between rock waste and soil and the other in bedrock. BH-5 does not reach the saturated zone and was not sampled.
- Eight (8) boreholes located around the waste dump in natural soils and bedrock. They are labeled BH-101 to BH-107, and BH-W3. Two boreholes have a double sampling point (BH-105 and BH-106); BH-W3 is sampling in the soil formation only.
- Three weir stations (510 to the NW, 511 to the SE, and 512 to the NE) are sampling the ARD collected by the peripheral ditch around the dump. They are sampled once a week on a routine basis.
- Twelve (12) gravity lysimeters concentrated in two stations (T-92-1 and T-92-2). Each station has three groups of two lysimeters at different depths between 1.5 and 4.5 m from the surface of the dump. They were sampled at five occasions in 1992-1993.
- Sixteen (16) samples of pore water squeezed from moist waste rock samples taken during the installation of gravity lysimeters; they witness the composition of the unsaturated zone near the surface of the dump.
- Approximately 150 samples of reconstituted ARD solutions by leaching in 50 ml of distilled water for 30 minutes, 25 g of less than 2 mm fraction of cuttings taken at 1.5 m intervals during drilling (Choquette et al., 1993). This type of data show the probable composition of ARD in the unsaturated zone at the time of drilling in 1991. Samples are dried out by air circulation during sample recovery and soluble sulfates of iron, aluminum, and magnesium are easily put back into solution with distilled water in a few minutes. The data are expressed in g/L in the solution but since water content is not known it is better to report results in g/kg or kg/t of dry rock. Other samples were also obtained from shallow trenches and surface sampling of the waste dump.

Following detailed chemical characterization of the ARD during Phase I of the project, only key parameters were used for monitoring in Phase II of the project. The following set of parameters were measured:

pH, Eh (mV), Conductivity (mMHOS), Specific gravity SG (g/cm^3), Total Dissolved Solids TDS (mg/L), Acidity (mg/L), Aluminum Al (mg/L), Fe total (mg/L), Fe^{2+}/Fe^{3+}, Magnesium Mg (mg/L), and Sulfates SO_4 (mg/L). For some samples, Mn, Ca, Na, and K were also determined.

pH was determined using a combined glass electrode, Eh was measured with a combined platinum electrode, and conductivity was determined with a YSI Conductance Meter Model 32. Specific gravity is calculated by the use of pycnometer to a precision of 0.00001 g/cm^3 or using calibrated hydrometers. Total dissolved solids are measured by evaporating a 10-ml water sample at 180°C for 24 hours. Acidity was measured by titration using AWWA Standard Methods 201 and expressed as mg/L of $CaCO_3$ equivalent. Metals were determined by atomic adsorption spectroscopy (AAS) and wet chemical methods (Fe^{2+}). Liquid ion chromatography and wet chemical method were used for determination of sulfates. Special techniques using EDXF (energy dispersive X-ray fluorescence spectroscopy analysis) were also used for extracted pore-water samples. Details of these techniques are described in Choquette *et al.*, 1993a, 1993b, and 1994. On routine monitoring, a consistent use of statistical relationships between parameters, derived from the data base accumulated in Phases I and II of the project, allowed determination of acidity, Al, Fe_{total}, and sulfates.

Chemical analyses results are presented in tables in the MEND reports of Choquette *et al.*, 1993a, 1993b, and of Choquette and Gelinas 1994.

5.2.2   ARD IN THE SATURATED ZONE OF THE WASTE ROCK DUMP

A typical chemical analysis of the leachate in the observation wells at the base of the dump is presented in Table 5.1 for samples taken in April 1994. Total dissolved solids vary from a low of 5080 mg/L in BH-4 (soil) to 196 210 mg/L in BH-6 (rock). The average value is 126 900 mg/L and if BH-4 is removed because the integrity of the piezometer is in doubt, the mean value is 142 000 mg/L. Typical values for sulfates vary between 42 700 mg/L and 126 500 mg/L. pH values are from 2.39 to 3.73 with most values between 2.5 and 3.0. Total iron can reach 20 500 mg/L, Al reaches 10 000 mg/L as well as Mg. The high concentrations is Al and Mg will be discussed in the next section as reflecting important transformations in silicate minerals. Calcium is always very low in the range of 300-800 mg/L. Acidity for this series of analysis was estimated from the TDS, sulfate content and conductance and ranges typically from 60 000 to 100 000 mg/L. Except for BH-4, there is no significant difference between samples taken at the base of waste rock and in underlying bedrock. Differences between boreholes are also small: BH-1 is clearly different from the others as it could result from the thickness of waste rock which is less important at that location.

Table 5.1 Chemical analysis of the leachate in the piezometers inside the dump (April 1994)

		BH-1 Rock	BH-1 Soil	BH-2 Rock	BH-2 Soil	BH-3 Rock
pH		3,17	2,68	2,83	2,45	2,39
EH	mV	328	345	335	390	379
Conductance	µS	26 216	39 672	42 456	32 248	43 268
SG	g/cc	1,0525	1,1045	1,12	1,0795	1,1445
TDS	mg/l	65 810	131 100	152 660	100 660	189 020
Acidity	mg/l CaCO3†	*39 310*	*78 676*	*91 756*	*60 277*	*113 905*
Al	mg/l	3 697	6 636	8 099	4 095	8 396
Ca	mg/l	489	451	417	338	363
Fe tot	mg/l	5 575	12 206	13 405	11 553	18 515
Fe ++	mg/l††	*5 032*	*10 349*	*11 831*	*6 835*	*12 371*
Fe +++	mg/l††	*543*	*1 857*	*1 574*	*4 718*	*6 144*
Mg	mg/l	2 533	5 175	5 686	3 338	7 135
SO4 =	mg/l	42 753	84 438	94 288	62 270	107 174

		BH-3 Soil	BH-4 Rock	BH-4 Soil	BH-6 Rock	
pH		2,37	3,23	3,73	3,48	
EH	mV	379	288	285	221	
Conductance	µS	43 616	38 744	4 466	46 632	
SG	g/cc	1,144	1,0915	1,0015	1,152	
TDS	mg/l	187 660	114 030	5 080	196 210	
Acidity	mg/l CaCO3†	*113 075*	*68 349*	*997*	*118 298*	
Al	mg/l	8 709	5 239	41	10 099	
Ca	mg/l	469	521	299	821	
Fe tot	mg/l	18 089	11 857	171	20 515	
Fe ++	mg/l††	*12 087*	nd	nd	nd	
Fe +++	mg/l††	*6 002*	nd	nd	nd	
Mg	mg/l	6 418	6 523	421	10 524	
SO4 =	mg/l	109 697	80 005	3 434	126 484	

†: Calculated values from TDS
††: Calculated values from EH and Fe

Variations with time are presented on Figure 5.1 for analyses taken from 1991 to present. Most stations show a slight increase in acidity with time over the three-year period but already in 1991 the conditions were very acid six or seven years after dump construction began. A sharp increase in acidity in BH-1 was observed during the last year.
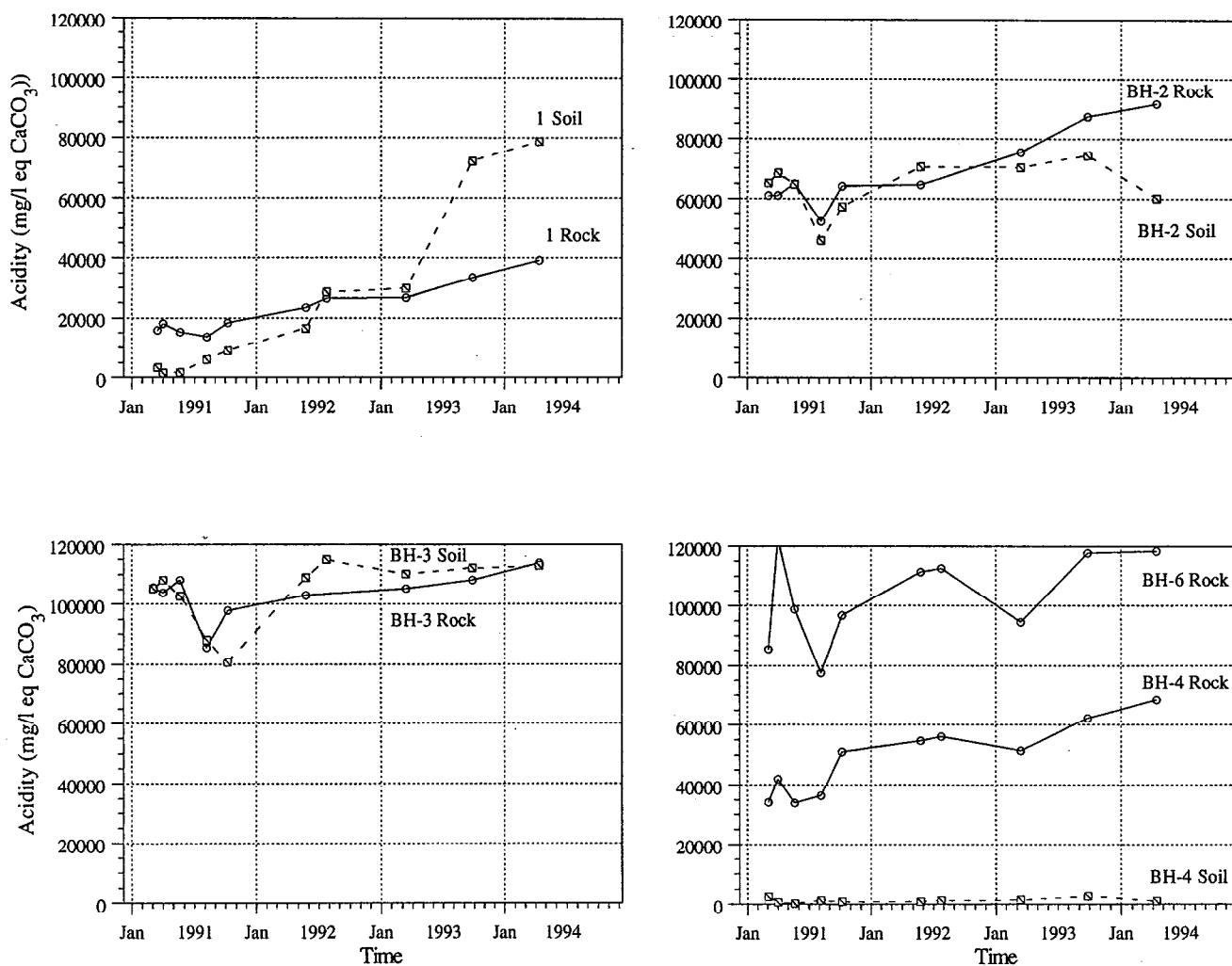
Fig. 5.1 Acidity of the leachate at the base of the South dump (soil piezometers) and in the underlying bedrock (rock piezometers)

5.2.3   GROUNDWATER SAMPLES OUTSIDE THE WASTE ROCK DUMP

Nine (9) sampling points are used to analyze groundwater outside the dump. All of them except BH-104 are located between the waste rock dump and the ditch that collects acid drainage. A typical analysis for April 1994 (the last monitoring activity) is given in Table 5.2. On the East side of the dump, groundwater is slightly acid (values below 1000 mg/L) with pH between 4.0 and 6.35. On the South side, BH-103 and BH-104 are acid whereas BH-105 is not affected. BH-103

and 104 are located on a steeper slope as compared with other monitoring points and they represent important discharge of acid leachate towards the ditch. The most strongly acid samples are on the West boundary of the dump where most of the ARD is drained due to the nature of the terrain surface before building the dump. Sulphates in BH-106 and BH-107 vary between 56 000 and 88 000 mg/L. Total iron reaches its maximum value in BH-106 together with the lowest pH at 2.17. As was expected leachate is less acid outside the dump than inside but the differences are small in the main drainage area to the West. In some samples, iron is mainly in the ferrous form Fe^{2+} (BH-106 and 107) but most of the time is has been partly oxidized to Fe^{3+} (BH-103, 104 and W3).

Table 5.2 Chemical analysis of the leachate in the peripheral piezometers (April 1994)

		BH-101 Rock	BH-102 Rock	BH-103 Rock	BH-104 Rock	BH-105 Rock
pH		3,99	6,35	2,44	2,6	5,81
EH	mV	285	191	503	414	276
Conductance	μS	2 865	4 234	10 417	26 332	59
SG	g/cc	1	1,0015	1,024	1,0645	<1
TDS	mg/l	3 660	4 630	33 620	83 340	70
Acidity	mg/l CaCO3†	605	863	20 036	49 844	6
Al	mg/l	220	<21	1 108	4 464	<21
Ca	mg/l	379	547	262	461	nd
Fe tot	mg/l	<61	<61	5 065	7 101	<61
Fe ++	mg/l††	nd	nd	238	2 939	nd
Fe +++	mg/l††	nd	nd	4 827	4 162	nd
Mg	mg/l	<40	244	359	2 456	nd
SO4 =	mg/l	2 310	2 728	18 133	48 703	<42

		BH-105 Soil	BH-106 Rock	BH-106 Soil	BH-107 Rock	BH-W3 Soil
pH		4,66	2,17	2,49	2,65	2,7
EH	mV	278	489	468	375	410
Conductance	μS	1 935	15 625	7 575	3 132	12 876
SG	g/cc	<1	1,0345	1,0065	1,075	1,0205
TDS	mg/l	120	48 820	10 850	94 930	28 130
Acidity	mg/l CaCO3†	11	29 126	3 492	56 822	16 757
Al	mg/l	nd	6 248	104	3 680	1 087
Ca	mg/l	<35	nd	342	536	480
Fe tot	mg/l	<61	20 653	767	11 773	2 683
Fe ++	mg/l††	nd	18 029	nd	8 173	1 189
Fe +++	mg/l††	nd	2 624	nd	3 600	1 494
Mg	mg/l	nd	6 104	330	2 764	811
SO4 =	mg/l	60	87 939	5 530	55 998	16 830

†: Calculated values from TDS
††: Calculated values from EH and Fe

Variations with time of chemical composition is illustrated in Figure 5.2. Except for BH-106 which shows a sharp increase in 1993, the composition of leachate has remained more or less constant in the last three years.
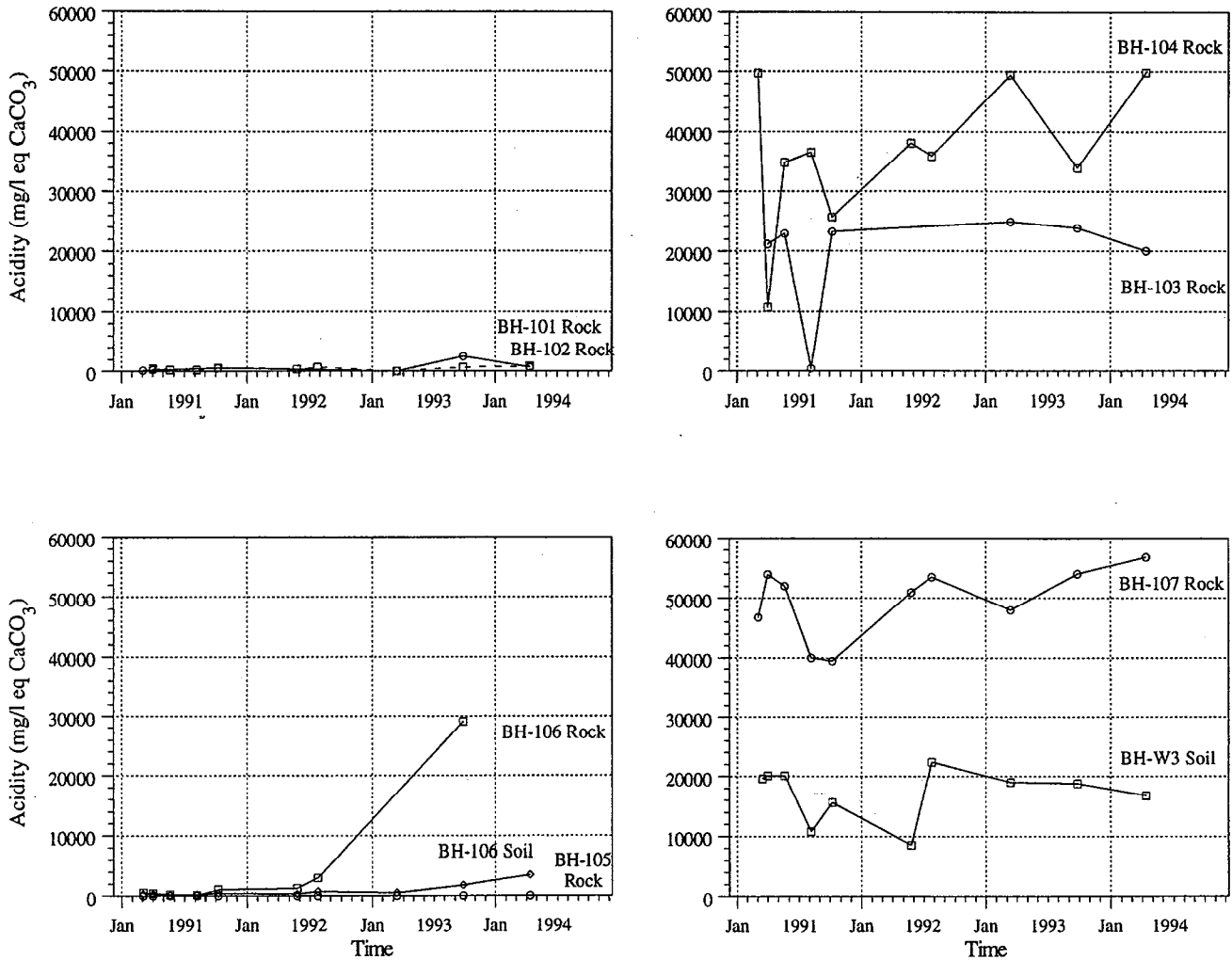
Fig. 5.2 Acidity of the leachate in the peripheral piezometers

5.2.4 ACID ROCK DRAINAGE AT WEIR STATIONS

The largest set of chemical monitoring data represents samples taken weekly at the three weir stations where flowrate is continuously measured. During winter, ice forms and it is impossible to take representative samples since ice crystallization may affect the composition of leachate. At station 510 where flowrate is more important, 131 weekly samples were analyzed from 1991 to

1993; 122 were obtained from basin 511 and only 108 samples came from station 512 where flowrates go to zero for part of the winter. Chemical analyses are reported in Choquette *et al.*, 1993a. In 1991, comprehensive analyses of ARD were conducted which included trace metals (Cd, Cu, Ni, Pb, and Zn) and some cations such as Na, K, Mn, and Si (data from Phase I as reported in Gélinas *et al.*, 1991). Table 5.3 gives examples of complete chemical analyses of each weir station, from the data in Choquette *et al.*, 1993a. From Phase II, most monitoring data from weir stations have been determined by a quick procedure based on strong correlations between TDS and conductivity with all the chemical parameters (Choquette *et al.*, 1993b).

Table 5.3 Typical chemical analysis of the leachate at the three weir stations

Weir Station		510	511	512
Date		25/3/91	25/3/91	3/4/91
Acidity	mg/l	61 957	60 484	19 963
Al	mg/l	4 074	4 328	949
Ca	mg/l	618	506	361
Cd	mg/l	1,31	1,17	na
Conductance	μS	28 532	25 631	11 473
Cu	mg/l	na	na	15
Fe tot	mg/l	17 715	15 211	6 413
Fe ++	mg/l	6 413	1 666	99
Fe +++	mg/l	11 302	13 545	6 314
K	mg/l	0,15	0,26	0,12
Tot.Diss.Sol.	mg/l	107 120	105 600	33 960
Mg	mg/l	3 737	3 611	841
Mn	mg/l	249	195	54
Na	mg/l	1,0	91,9	6,0
Ni	mg/l	12,4	12,5	3,0
Pb	mg/l	1,2	1,2	0,5
Si	mg/l	na	na	33
SO4 =	mg/l	62939	62190	15917
Zn	mg/l	26,5	20,0	6,0
pH		2,1	2,1	2,3
Eh	mV	435	474	520

Monitoring concentrates on evolution of acidity and mass balances are established for three parameters: acidity, SO_4 and Fe. Table 5.4 gives a summary of acidity values for the three weir stations from 1991 to 1993. The mean values of 58 810 mg/L (Station 510), 44 857 mg/L (Station 511), and 23 905 mg/L (Station 512) are significantly different from one another but much of the difference is related to the proportion of baseflow coming from the dump in the total flow

measured at the weir (see for instance Table 4.4). For each station, the trend over a three-year period is not easy to establish: there is a slight increase in acidity at Station 510, a decrease at Station 511, and a rise and fall at Station 512. Variation in precipitation, especially during winter, may provoke different responses in different sub-basins since the proportion of the basin covered with waste rock varies considerably.

Table 5.4 Ditches acidity. Statistical data 1991-1993.

Station - Year	Number of Measures	Mean Value	Min. Value	Max. Value	Std. Dev.
510 - 1991	49	56 888	25 000	120 144	13 730
510 - 1992	43	59 149	13 100	78 070	10 409
510 - 1993	44	60 618	28 036	79 998	12 751
510- 91-93	**136**	**58 810**	**13 100**	**120 144**	**12 449**
511 - 1991	48	48 000	14 617	120 143	21 805
511 - 1992	41	44 319	6 544	78 010	16 058
511 - 1993	33	40 957	9 050	74982	17 242
511- 91-93	**122**	**44 857**	**6 544**	**120 143**	**18 887**
512 - 1991	34	22 913	9 500	39 411	7 109
512 - 1992	38	26 441	7 140	52 046	9 758
512 - 1993	31	21 886	7 775	34 327	7 318
512- 91-93	**103**	**23 905**	**7 140**	**52 046**	**8 402**

Figures 5.3 to 5.6 present acidity data in a different format. Weekly values for acidity in mg/L are given for each station as calculated or extrapolated (for the winter months). Higher acidity corresponds usually to periods of low flow and lower values are observed during periods of high flow. Weekly acid mass production takes into account the mass of waste rock that is involved in each sub-basin and the results are expressed as kg of $CaCO_3$ equivalent per tonne of waste rock. This type of graph shows that acid release is fairly constant except during spring melt when a larger quantity of baseflow reaches the collection ditches. Cumulative acid mass production curves show nearly linear increase with time with an offset corresponding to spring conditions. On Figure 5.6 the weekly acid mass release for 1993 does not show any anomaly during spring due to very low winter precipitation.

Release of acidity, sulfates, and iron through the collecting ditches can be computed from monitoring data. Table 5.5 present the data as kg/year of acidity, SO_4, and Fe_{total} for each station

and each year. Normalized data is expressed as kg/tonne/year and takes into account the mass of waste rock contributing to acidity, sulfate or iron release in surface drainage. It can be seen that basin 512 produces more acidity per tonne of rock than the two other basins. One reason for this is the fact that the oldest part of the waste rock dump is located on the East and Southeast and that the dominant rock type in that area is unit 4B (sericitic schist). In this table, the total mass of sulfates released in surface drainage will be used later to compare with sulfate production as evidenced from thermal data (chapter 6). Sulfate production is about three times larger than what is released outside the dump. This will be discussed in Section 5.3 of the report.

South Dump
(Weirs 510, 511 and 512 combined)
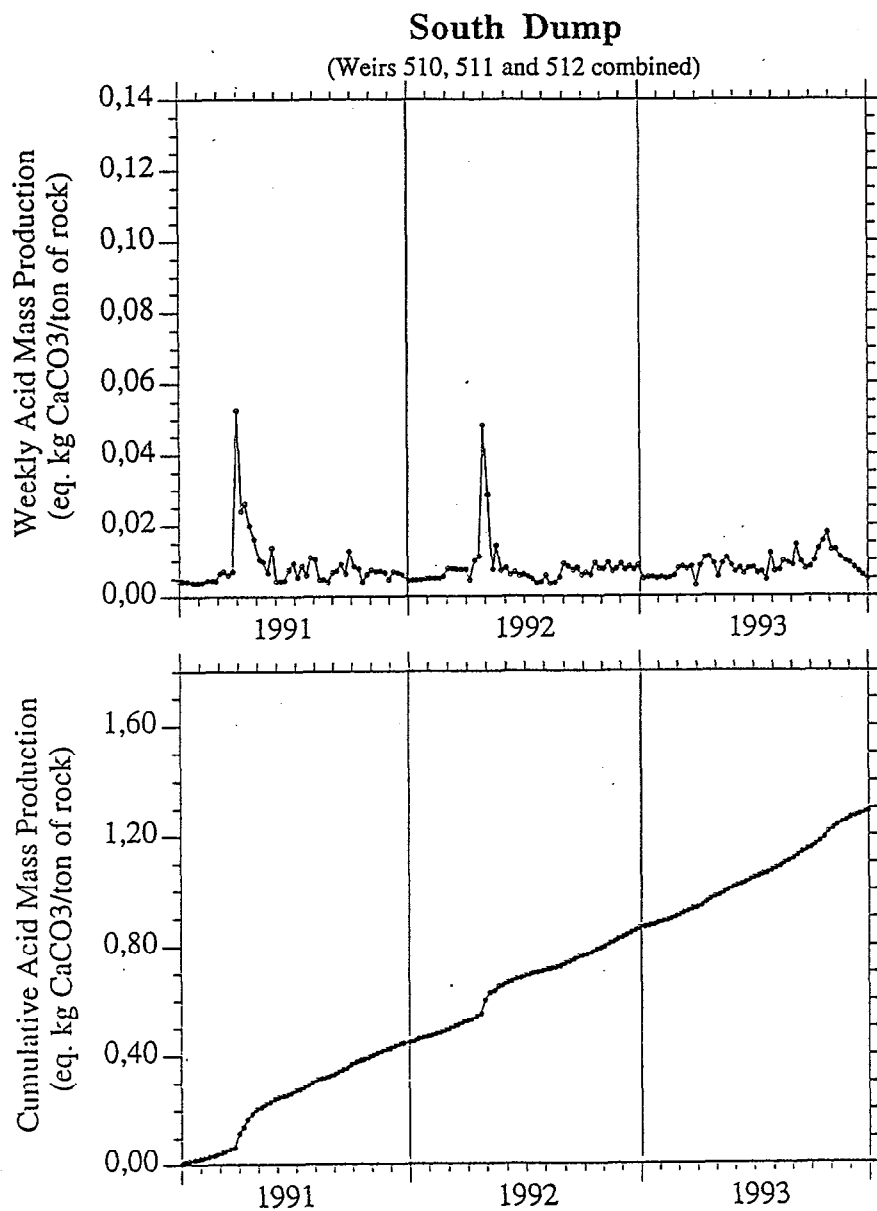
Fig. 5.3 Acid production 1991 to 1993. Entire South dump.
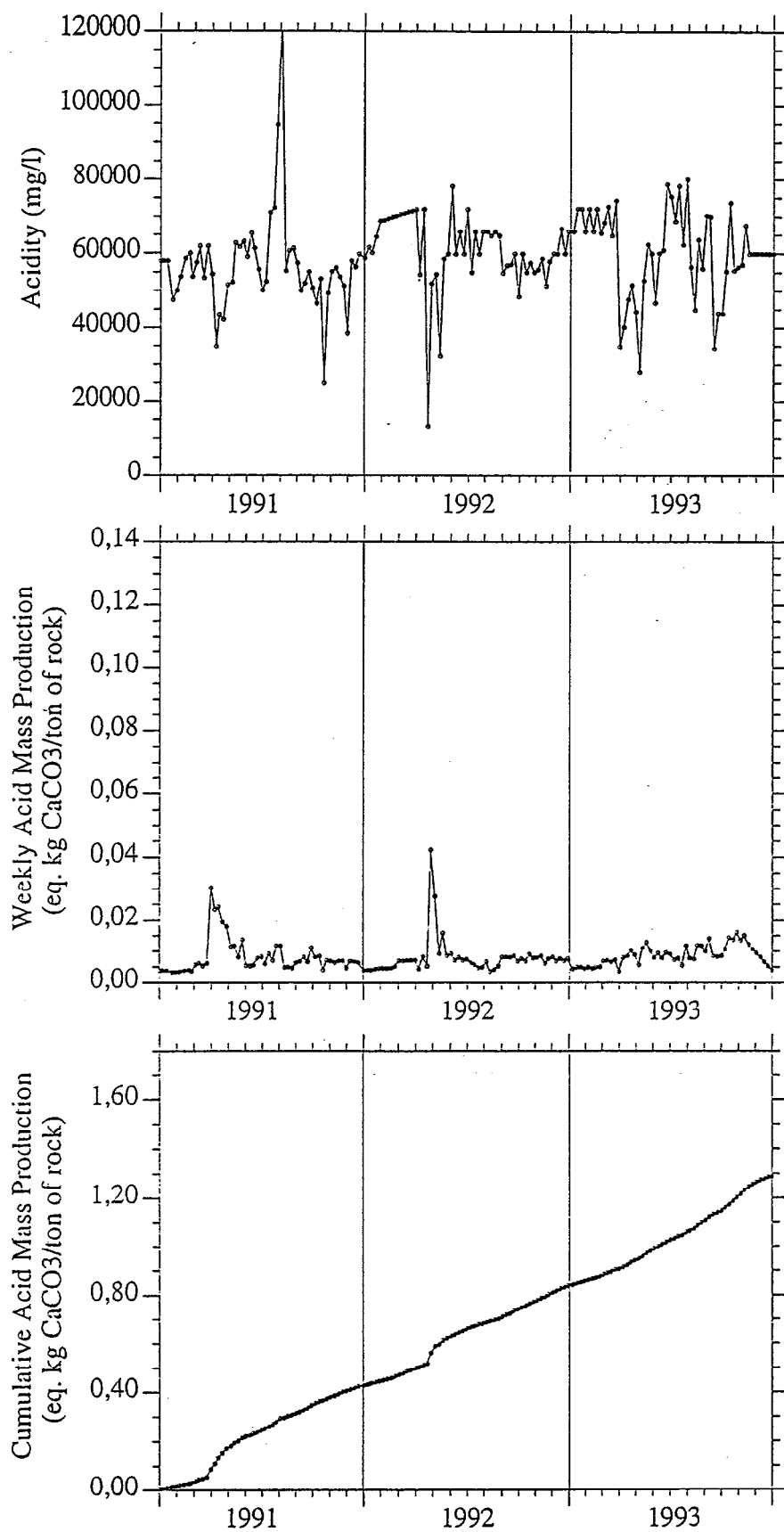
Fig. 5.4 Acid production 1991 to 1993. Weir station 510
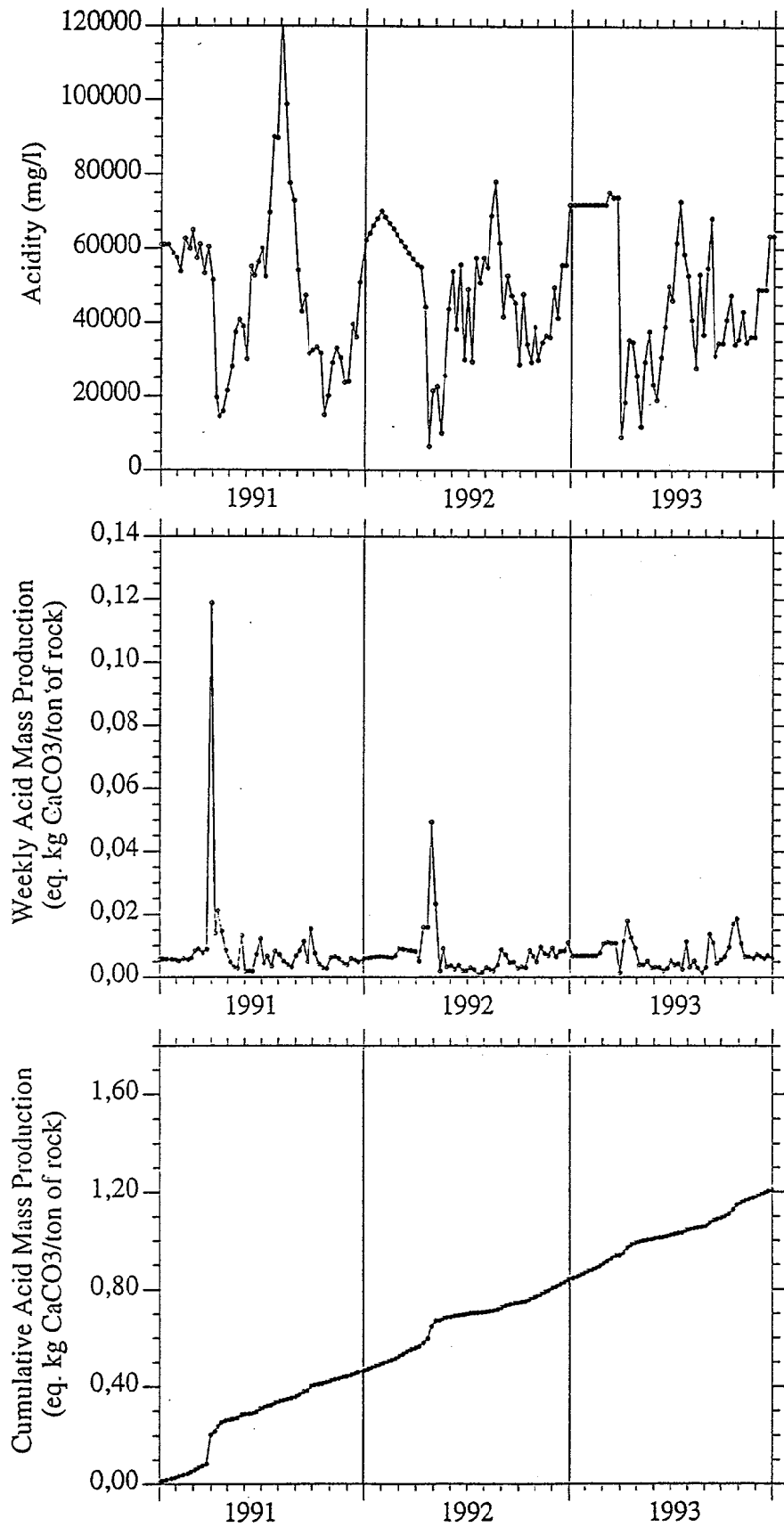
Fig. 5.5 Acid production 1991 to 1993. Weir station 511
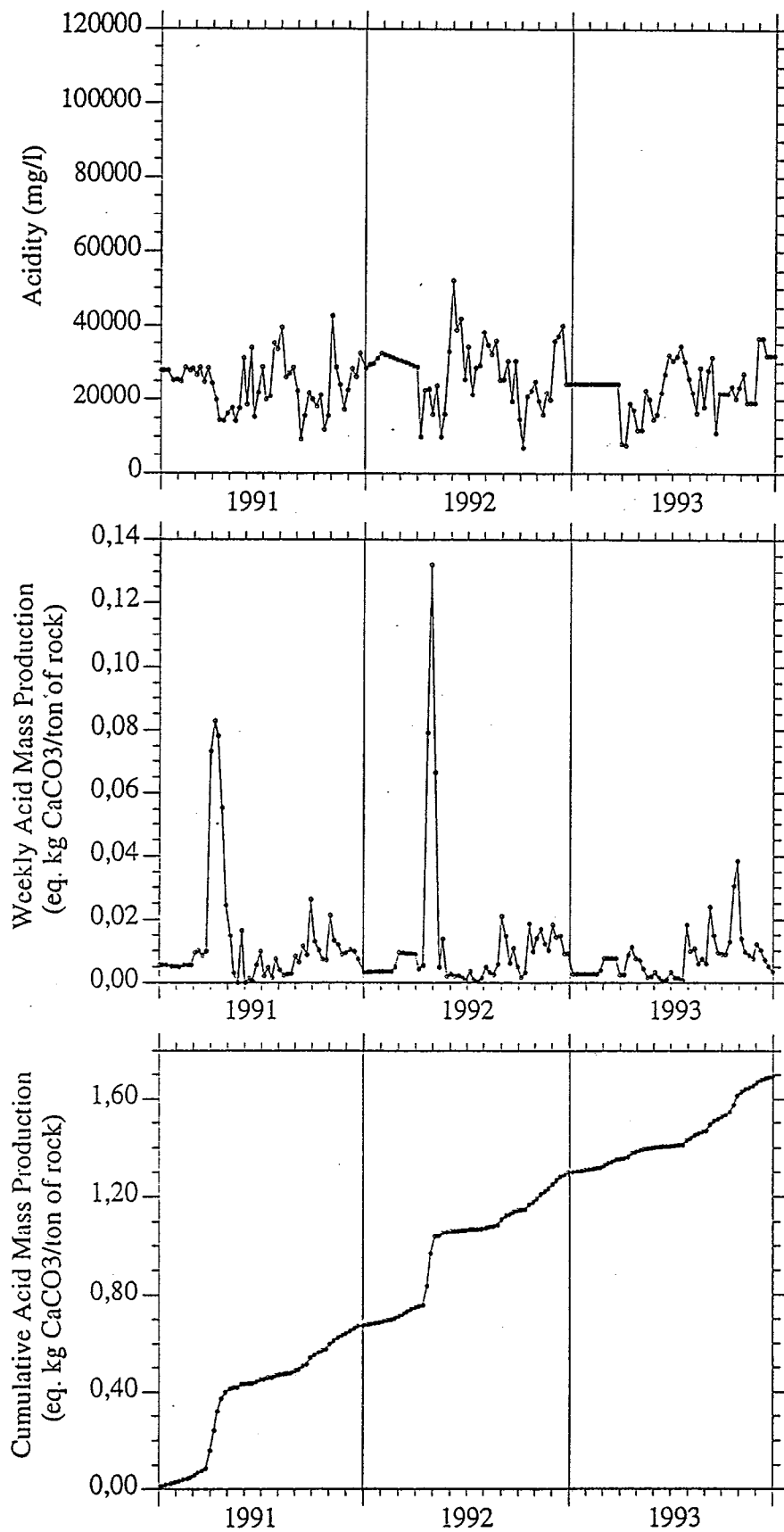
Fig. 5.6 Acid production 1991 to 1993. Weir station 512

Table 5.5 Acid Production Summary from the South Dump (1991-1993)

	Year	Acidity (kg*)	SO4 (kg)	Fe (kg)	Normalized** Acidity (kg/t)	Normalized** SO4 (kg/t)	Normalized** Fe (kg/t)
Weir 510	1991	6 541 835	6 808 716	1 745 080	0,4265	0,4439	0,1138
	1992	6 347 900	6 185 940	1 546 475	0,4139	0,4033	0,1008
	1993	6 860 978	6 722 497	1 678 039	0,4474	0,4383	0,1094
	Tot. 91-93	19 750 713	19 717 153	4 969 594	1,2878	1,2856	0,3240
Weir 511	1991	2 215 436	2 234 399	549 638	0,4603	0,4642	0,1142
	1992	1 822 863	1 741 915	424 287	0,3787	0,3619	0,0882
	1993	1 779 578	1 709 943	397 451	0,3697	0,3553	0,0826
	Tot. 91-93	5 817 877	5 686 257	1 371 376	1,2087	1,1814	0,2849
Weir 512	1991	676 546	576 731	195 123	0,6709	0,5719	0,1935
	1992	631 420	581 441	173 818	0,6262	0,5766	0,1724
	1993	400 368	365 602	115 069	0,3970	0,3626	0,1141
	Tot. 91-93	1 708 334	1 523 774	484 010	1,6941	1,5111	0,4800
Combined Stations	1991	9 433 817	9 619 846	2 489 841	0,4459	0,4547	0,1177
	1992	8 802 183	8 509 296	2 144 580	0,4160	0,4022	0,1014
	1993	9 040 924	8 798 042	2 190 559	0,4273	0,4158	0,1035
	Tot. 91-93	**27 276 924**	**26 927 184**	**6 824 980**	**1,2892**	**1,2727**	**0,3226**

* Values in eq. CaCO3
**Mass of rock supplying weir 510 (t):   15 336 694 (72.5%)
**Mass of rock supplying weir 511 (t):   4 813 182 (22.7%)
**Mass of rock supplying weir 512 (t):   1 008 410 (4.8%)
Total dump mass (t):   **21 158 286

5.2.5   ACID LEACHATE IN THE GRAVITY LYSIMETERS

The next three sections address the problem of characterization of acid leachate in the unsaturated zone where oxidation occurs and acid conditions are developing. Direct measurement of leachate composition has been done on 60 samples coming from 12 lysimeters sampled five times. Tables 5.6 to 5.9 (from Choquette et al., 1993a) show the detailed analyses for lysimeter samples. There are still some questions about the representativity of these samples because rock waste was disturbed during installation of lysimeters. Later analyses are probably more reliable since more than a year has elapsed since lysimeter installation.

Lysimeter station T-92-1 shows low acid production near surface as typical values for acidity are less than 500 mg/L with a small increase with depth. It is located on a pile of very low grade ore with massive volcanoclastic rocks near surface. Lysimeter station T-92-2 is located in a very active area where sericitic schists dominate. At that location acidity soars to 61 500 mg/L in one very shallow sample (1,67 m) showing that oxidation rates can be very high near the surface. The limited data obtained from these lysimeters is also influenced by weather conditions and seasonal events such as strong rainfall, snow melt or ice condition at surface. Further sampling is required to analyze these effects. Another problem is caused by the sampling procedure itself. Since acid leachate accumulates in lysimeters, the samples may represent infiltration over more than a month before the lysimeters are purged. Controlled artificial rain experiments should be carried on to derive data on acid generation near surface.

One set of parameters that is most important to evaluate is the oxidation conditions as evaluated from Eh measurements and the ratio Fe^{2+}/Fe^{3+} in each sample. Actual data are not coherent because at the same location either Fe^{2+} or Fe^{3+} may dominate over a short time period. This data will now be compared with two other types of data for the unsaturated zone: extracted pore water, and reconstituted acid solutions.

5.2.6   EXTRACTED PORE WATER SAMPLES

During excavation for lysimeters installation, several moist samples were collected every 0.5 m to a depth of 4 meters. Pore water samples were extracted with a hydraulic press. A few milliliters of liquid were obtained by this procedure and the samples were analyzed by EDXRF (Choquette et al., 1994). Table 5.10 show the results of these analyses. For the reasons given in the preceding section, the two sets of values are very different in terms of degree of acidification.

Samples from Station T-92-1 show very low sulfate content of barely 3 g/L and almost non-detectable metals. At Station T-92-2, sulfate content reaches 145 g/L at 3.0 meters below surface and iron soars to 40 g/L. A common feature however is the very low activity in the first meter. Being in contact with the atmosphere may keeps the top layer too cold for bacteria to develop. Because of a strong thermal gradient, temperature of nearly 50°C are recorded within 5 meters near Station T-92-2. Because of the limited data available, one observation that can be made is that oxidation processes can develop very near the surface with a composition which is not entirely different from what is found at depth in the saturated zone. A better perspective is given by the leaching procedure described next.

Table 5.6 Composition of the leachate in lysimeters T92-1 (3A, 3B and 4A)

T92-1 L3A (1,67m)		11/8/92	29/9/92	5/1/93	4/4/93	7/7/93
Acidity	mg/l CaCO3	_386_	6	9	8	_131_
Al	mg/l	_10_	2,13	1,49		_2_
Conduct.	µS	1820	1990	1960	1242	2157
Fe tot	mg/l	_98_	3,28	1,97	0	_32_
Fe ++	mg/l		0,32	1,5	0	
Fe +++	mg/l		2,96	0,47	0	
TDS	mg/l	2680	2500	2200	1060	1180
Mg	mg/l		21,5	11,7	4,9	
SO4 =	mg/l	_1168_	1400	1479	629	_514_
pH		6,91			6,81	7,06
EH	mV	351			249	315
SG	g/cc	1,003			1,001	1

T92-1 L3B (1,66m)		11/8/92	29/9/92	5/1/93	4/4/93	7/7/93
Acidity	mg/l CaCO3	_274_	6	8	9	_111_
Al	mg/l	_7_	1,92	0,43		_2_
Conduct.	µS	1820	1940	2040	1470	2304
Fe tot	mg/l	_69_	3,78	0,63	0	_27_
Fe ++	mg/l		0,38	0,4	0	
Fe +++	mg/l		3,42	0,23	0	
TDS	mg/l	2090	2600	2400	1690	1030
Mg	mg/l		26,4	18,1	9,1	
SO4 =	mg/l	_911_	1300	1525	827	_449_
pH		6,93			6,94	7,32
EH	mV	344			240	294
SG	g/cc	1,002			1,001	1

T92-1 L4A (2,42m)		11/8/92	29/9/92	5/1/93	4/4/93	7/7/93
Acidity	mg/l CaCO3	_380_	8	7	7	_207_
Al	mg/l	_10_	1,95	0,75		_4_
Conduct.	µS	1820	1890	1960	1625	2951
Fe tot	mg/l	_96_	4,79	1,16	0	_52_
Fe ++	mg/l		0,42	0,6	0	
Fe +++	mg/l		4,37	0,56	0	
TDS	mg/l	2650	2600	2100	1550	1690
Mg	mg/l		29	18,2	11,1	
SO4 =	mg/l	_1155_	1400	1433	994	_736_
pH		6,89			6,81	7,02
EH	mV	359			250	288
SG	g/cc	1,002			1,001	1

Note: underlined values are calculated.

Table 5.7 Composition of the leachate in lysimeters T92-1 (4B, 5A and 5B)

T92-1 L4B (2,55m)		11/8/92	29/9/92	5/1/93	4/4/93	7/7/93
Acidity	mg/l CaCO3	_382_	8	7	9	_246_
Al	mg/l	_10_	0,89	3,41		_6_
Conduct.	µS	1820	2020	2200	1708	2815
Fe tot	mg/l	_97_	1,52	5,21	0	_62_
Fe ++	mg/l		0,22	3	0	
Fe +++	mg/l		1,3	2,21	0	
TDS	mg/l	2660	2800	2400	1700	1930
Mg	mg/l		32,3	20,4	8,1	
SO4 =	mg/l	_1159_	1400	1602	946	_841_
pH		6,95			7,08	7,31
EH	mV	355			237	297
SG	g/cc	1,002			1,001	1

T92-1 L5A (4,05m)		11/8/92	29/9/92	5/1/93	4/4/93	7/7/93
Acidity	mg/l CaCO3	_446_	7	7	11	_348_
Al	mg/l	_12_	5,69	0,35		_9_
Conduct.	µS	2070	2020	2390	2315	3916
Fe tot	mg/l	_113_	8,99	0,58	0	_88_
Fe ++	mg/l		1,3	0,3	0	
Fe +++	mg/l		7,69	0,28	0	
TDS	mg/l	2970	2800	3100	2400	2490
Mg	mg/l		36,3	50,9	35,3	
SO4 =	mg/l	_1294_	1400	1740	1495	_1085_
pH		6,6			6,97	6,98
EH	mV	368			226	277
SG	g/cc	1,002			1,002	1

T92-1 L5B (3,75m)		11/8/92	29/9/92	5/1/93	4/4/93	7/7/93
Acidity	mg/l CaCO3	_483_	6	8	7	_362_
Al	mg/l	_14_	0,91	1,09		_9_
Conduct.	µS	2230	2340	2490	2401	3383
Fe tot	mg/l	_123_	3,75	1,66	0	_91_
Fe ++	mg/l		0,34	0,8	0	
Fe +++	mg/l		3,41	0,86	0	
TDS	mg/l	3140	3200	3200	2510	2560
Mg	mg/l		97,3	78,9	55,5	
SO4 =	mg/l	_1368_	1500	1847	1535	_1115_
pH		6,63			7,13	7,18
EH	mV	363			252	301
SG	g/cc	1,004			1,002	1

Note: underlined values are calculated.

Table 5.8 Composition of the leachate in lysimeters T92-2 (3A, 3B and 4A)

T92-2 L3A (1,67m)		11/8/92	29/9/92	5/1/93	4/4/93	7/7/93
Acidity	mg/l CaCO3	*1346*		35030	61459	*41151*
Al	mg/l	*49*		1430	2324	*2498*
Conduct.	μS	15880		32000	21185	18616
Fe tot	mg/l	*351*		12100	16614	*9965*
Fe ++	mg/l			700	11400	
Fe +++	mg/l			11400	5214	
TDS	mg/l	6140		65000	96290	66070
Mg	mg/l			1130	1677	
SO4 =	mg/l	*2675*		45000	63029	*37507*
pH		2,02			1,77	2,09
EH	mV	458			514	480
SG	g/cc	1,049			1,076	1,0505

T92-2 L3B (1,21m)		11/8/92	29/9/92	5/1/93	4/4/93	7/7/93
Acidity	mg/l CaCO3	*242*	8624	7718	8766	*4126*
Al	mg/l	*6*	600	520	557	*179*
Conduct.	μS	7610	11000	16000	8998	8547
Fe tot	mg/l	*61*	1950	1760	1454	*1097*
Fe ++	mg/l		280	180	900	
Fe +++	mg/l		1670	1580	554	
TDS	mg/l	1906	20000	22000	18450	11940
Mg	mg/l		610	530	485	
SO4 =	mg/l	*830*	12000	14325	10875	*5202*
pH		2,25			2,11	2,27
EH	mV	560			662	554
SG	g/cc	1,015			1,016	1,007

T92-2 L4A (2,54m)		11/8/92	29/9/92	5/1/93	4/4/93	7/7/93
Acidity	mg/l CaCO3	*627*	24400	22850	29220	*26799*
Al	mg/l	*19*	2690	2170	2412	*1589*
Conduct.	μS	12410	24000	43000	17588	16380
Fe tot	mg/l	*161*	4780	4670	2878	*6699*
Fe ++	mg/l		2200	2650	1933	
Fe +++	mg/l		2380	2020	945	
TDS	mg/l	3750	54000	48000	43210	43700
Mg	mg/l		1840	1530	1555	
SO4 =	mg/l	*1634*	23000	31500	28832	*24346*
pH		2,17			2,03	2,18
EH	mV	425			484	499
SG	g/cc	1,031			1,037	1,033

Note: underlined values are calculated.

Table 5.9 Composition of the leachate in lysimeters T92-2 (4B, 5A and 5B)

T92-2 L4B (2,36m)		11/8/92	29/9/92	5/1/93	4/4/93	7/7/93
Acidity	mg/l CaCO3	*2974*	45100	40170	58440	*53746*
Al	mg/l	*124*	2480	1600	2501	*3327*
Conduct.	µS	19350	30000	36000	22334	24405
Fe tot	mg/l	*787*	14200	12900	14342	*12667*
Fe ++	mg/l		4700	2000	11400	
Fe +++	mg/l		9500	10900	2942	
TDS	mg/l	9886	91000	75000	91670	85170
Mg	mg/l		2600	1550	2096	
SO4 =	mg/l	*4307*	42000	50000	59004	*49118*
pH		1,93			1,73	2,06
EH	mV	462			499	465
SG	g/cc	1,077			1,074	1,065

T92-2 L5A (4,07m)		11/8/92	29/9/92	5/1/93	4/4/93	7/7/93
Acidity	mg/l CaCO3	*3194*	33500	29740	36525	*43423*
Al	mg/l	*134*	3530	2450	2634	*2646*
Conduct.	µS	22160	30000	35000	22532	26789
Fe tot	mg/l	*846*	6910	7590	7888	*10464*
Fe ++	mg/l		4300	5000	4800	
Fe +++	mg/l		2610	2590	3088	
TDS	mg/l	10306	78000	59000	64210	69550
Mg	mg/l		3500	2130	1868	
SO4 =	mg/l	*4490*	39000	40000	40750	*39597*
pH		2,15			1,9	2,03
EH	mV	413			432	426
SG	g/cc	1,031			1,053	1,0545

T92-2 L5B (3,93m)		11/8/92	29/9/92	5/1/93	4/4/93	7/7/93
Acidity	mg/l CaCO3	*1182*	21800	16968	17288	*14743*
Al	mg/l	*42*	1790	1260	1079	*855*
Conduct.	µS	16950	25000	32000	17588	15018
Fe tot	mg/l	*307*	5480	4370	3151	*3788*
Fe ++	mg/l		5000	3800	2733	
Fe +++	mg/l		480	570	418	
TDS	mg/l	5660	51000	36000	32050	24370
Mg	mg/l		1880	1200	727	
SO4 =	mg/l	*2466*	28000	24272	19800	*13355*
pH		1,84			1,67	2,2
EH	mV	433			438	434
SG	g/cc	1,046			1,026	1,0185

Note: underlined values are calculated.

Table 5.10 Chemical data T-92. Chemical analysis of extracted pore-water and characteristics of leach solutions.

T92-1

Sample	Depth (m)	Extracted pore-water analysis by EDXRF					Parameters measured on the leach solution			
		Fe (g/l)	Ca (g/l)	SO4 (g/l)	Al (g/l)	Mg (g/l)	pH	Eh (mV)	Conductance (μS)	TDS (mg/l)
T92-1 00	0,0	na	na	na	na	na	6,85	566	662	490
T92-1 05	0,5	nd	0,840	2,412	nd	nd	6,90	537	796	620
T92-1 10	1,0	nd	1,117	3,402	nd	nd	6,85	518	1 096	910
T92-1 15	1,5	nd	0,714	2,152	nd	nd	6,62	515	1 452	1 240
T92-1 20	2,0	nd	0,746	1,809	nd	nd	6,59	451	1 643	1 850
T92-1 25	2,5	nd	0,724	2,261	nd	nd	6,86	444	1 879	1 750
T92-1 30	3,0	nd	0,684	1,904	nd	nd	6,92	436	1 932	1 800
T92-1 35	3,5	nd	0,744	2,223	nd	nd	6,87	430	2 069	1 920
T92-1 40	4,0	nd	0,626	1,922	nd	nd	6,65	441	1 963	1 850

T92-2

Sample	Depth (m)	Extracted pore-water analysis by EDXRF					Parameters measured on the leach solution			
		Fe (g/l)	Ca (g/l)	SO4 (g/l)	Al (g/l)	Mg (g/l)	pH	Eh (mV)	Conductance (uS)	TDS (mg/l)
T92-2 00	0,0	na	na	na	na	na	6,84	446	1 214	1 000
T92-2 05	0,5	nd	0,554	2,130	nd	0,092	6,76	430	1 782	1 660
T92-2 10	1,0	nd	0,645	1,997	nd	0,072	6,80	433	1 895	1 680
T92-2 15	1,5	7,425	0,780	28,506	0,470	0,725	2,12	863	5 834	9 460
T92-2 20	2,0	6,406	0,515	21,219	0,360	0,270	2,04	791	6 724	13 150
T92-2 25	2,5	19,070	0,552	80,737	3,576	3,060	2,14	820	6 736	14 520
T92-2 30	3,0	36,982	0,780	145,280	5,172	4,428	2,25	799	7 181	14 840
T92-2 35	3,5	6,018	0,696	44,625	3,360	1,920	2,16	793	6 229	10 910
T92-2 40	4,0	19,358	1,164	131,140	8,196	6,576	2,16	772	8 195	17 040

na: not available
nd: not detected

5.2.7 CHEMICAL CHARACTERIZATION USING A LEACHING TECHNIQUE

One important tool to investigate acidification in the unsaturated zone of large waste rock piles is to analyze rock fragments obtained during drilling. Air drilling using an eccentric bit and a full casing brings to surface broken rock that can be easily sampled. Moisture that was present at different depths is dried out during the process because of intense air circulation. Dissolved solids that were present are precipitated mostly as complex soluble sulfates which can be readily dissolved in distilled water. Controlled lab experiments that consisted in rapidly drying small quantities of acid leachate produced solid crystals and an amorphous gel. Very small amounts of gypsum was also formed but it was limited by the low concentration of calcium in the leachate. Upon adding distilled water, more than 95% of the dried leachate went back in solution. Assuming that leachate that has dried on rock fragments can also be put back into solution, a large number of drill cuttings have been leached to gain information on the distribution of soluble oxidation products with depth in the dump.

Samples from seven (7) boreholes were taken at 1.5 meters intervals and sieved to extract the smaller than 2 mm fraction. Since most of the surface area is concentrated in the fine fraction, this is a good approximation of the total surface area present at a given depth in the dump. Sub-samples weighing 25 grams were mixed with 50 ml of distilled water and agitated for 30 minutes. Early experiments show that after 15 minutes, most of the soluble salts have dissolved. The supernatant solution was separated by centrifugation and analyzed. Results can be expressed as mg/L in the solution, but since the original water content at a given depth is not known for sure, results are best expressed in mg/kg of solids. This is obtained by multiplying the result in mg/L by 0.002 to obtain mg/kg. It is then possible to calculate equivalent ARD composition provided water content and porosity are known.

More than 150 samples coming from boreholes (132) and trenches have been analyzed using that technique. Results are presented in Choquette *et al.*, 1993a and 1994. A detailed profile coming from BH-7 (drilled in November 1993) is discussed in the next section.

5.3 MINERALOGICAL TRANSFORMATIONS ASSOCIATED WITH ARD

Sulfide oxidation being a strong exothermic reaction, high temperatures can be developed and induce density-driven air convection (Lefebvre et al., 1993). These currents supply oxygen deep in the pile for further sulfide oxidation. Pyrite oxidation generates low-pH waters that contain high concentrations of SO_4, Fe^{2+} and other metals and often with high levels of aluminium and magnesium. In the presence of iron oxidizing bacteria, Fe(II) is rapidly oxidized to Fe(III) which in turn can oxidize more pyrite.

In a waste rock pile affected by ARD, the acid that is produced may be rapidly flushed away by storm events or snow melt, but more often in large piles, the leachate accumulates and interacts with the waste rock as it moves slowly downwards. When the acid waters contact an acid consuming mineral phase, neutralization occurs and a portion of the acidity is removed. Fast neutralizing minerals such as calcite consumes H^+ from the solution and releases HCO_3^- or

$H_2CO_3^0$ and Ca^{2+}. If the sulfate concentration is high enough, saturation with respect to gypsum is reached, and the calcium is reprecipitated. Neutralization by carbonate minerals will usually buffer the pH of the leachate at a value between 5.5 and 6.9 (Morin 1988). Hydroxides also react with a low pH solution, but buffering occurs at a lower pH value than with carbonates, typically between 3 and 5. Many silicate minerals are unstable in such an acidic solution. However, the study of interactions between silicate minerals and AMD has been neglected in most research papers on AMD. Aluminosilicates weathering should be investigated when high concentrations of aluminium and magnesium are measured in a dump leachate, in the absence of primary Al and Mg hydroxides in the waste rock. At the Mine Doyon site, Al and Mg concentrations of 5,000 mg/l are common in the leachate from the South waste rock dump, indicating extensive reaction between aluminosilicates and the acid water inside the dump.

The main objective of this section is to describe mineralogical transformations associated with acid generation in a waste rock pile. We present here a compilation of mineralogical observations and analyses performed on samples collected in the South waste rock dump at la Mine Doyon. These minerals transformations from the top to the bottom of the waste pile are the basis to define a mineralogical index of acid production and neutralization in waste dumps.

Waste rock samples from two exploration pits dug in 1992 and from borehole BH-7 drilled in 1993 (see Figure 5.1) were used for the study. All samples were analyzed by X-ray diffraction with emphasis on phyllosilicates. Several samples were examined by scanning electron microscopy (SEM-EDX). Due to the coarse nature of the material, pore water could not be extracted but its chemistry was determined using a leaching procedure and the results are reported on a dry basis. For samples collected in trenches, a few drops of pore-water were obtained by pressure extraction and analyzed by X-ray fluorescence spectroscopy (EDXRF).

Heat is generated within the dump due to the pyrite oxidation, which is an exothermic reaction. The average year-round temperature within the dump is 40°C. The maximum measured value was over 65°C in borehole #6. High temperature favors potential reactions between the acid leachate and other minerals. High concentrations of Al and Mg (typically 5,000 mg/l or more) in the leachate indicate extensive reaction of the leachate with aluminosilicate minerals.

5.3.1   OXIDATION PROCESSES

Overall oxidation reactions of sulfides, pyrite in particular, are well understood and summarized by Hiskey and Schlitt (1981). The first important reaction is the direct oxidation of pyrite with oxygen and water:

$$FeS_2 + 3.5\ O_2 + H_2O \dashrightarrow Fe^{2+} + 2\ SO_4^{2-} + 2H^+ \qquad (1)$$
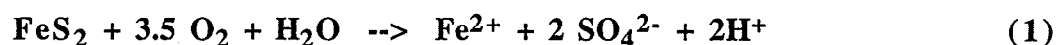
The second oxidation reaction of pyrite is by ferric iron:

$$FeS_2 + 14\ Fe^{3+} + 8\ H_2O \dashrightarrow 15\ Fe^{2+} + 2\ SO_4^{2-} + 16\ H^+ \qquad (2)$$
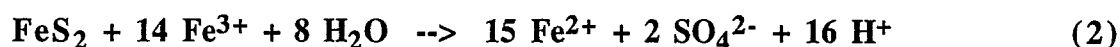
In order for the second reaction to take place, Fe(II) produced in reaction (1) must be oxidized to the Fe(III) state by dissolved oxygen. At the pH characteristic of AMD, the chemical oxidation reaction is very slow. However, in the presence of chemolithotrophic bacteria, such as *Thiobacillus ferrooxidans*, the following reaction is catalyzed:

$$Fe^{2+} + H^+ + 0.25\ O_2\ \textit{(+bacteria)} \rightarrow Fe^{3+} + 1/2H_2O \qquad (3)$$
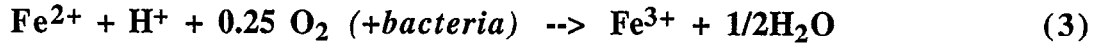
In reaction (3) there is a net H^+ consumption. If, locally, the pH of the solution is above 3, $Fe(OH)_3$ will likely precipitate:

$$Fe^{3+} + 3\ H_2O \longleftrightarrow Fe(OH)_{3\ solid} + 3\ H^+ \qquad (4)$$

For each mole of Fe^{3+} precipitated, 3 moles of H^+ are produced. If the pH falls below 3, the reaction will be reversed and more Fe^{3+} will be made available. The sum of reaction (2) and (3) gives reaction (1) so, whatever the mechanism, 2 moles of H^+ are produced for every mole of pyrite consumed.

5.3.2 PROCESSES OF NEUTRALIZATION

From one point of view, reaction (4) is a neutralization reaction, buffering the system at a pH around 3. However, the most effective and common acid consuming mineral is the calcium carbonate calcite ($CaCO_3$). Its buffering capacity will maintain the pH of the leachate to a value near 7. Dissolution of calcite releases Ca^{2+} ions that will precipitate with SO_4^{2-} to form gypsum, if saturation conditions are met. Possible encapsulation of calcite particles by gypsum will likely affect the neutralization reaction by preventing the leachate to come in contact with the carbonate. In the absence of carbonates or hydroxides, the pH of the acid leachate is likely to fall under 3.

Silicates are generally unstable in acid conditions. However, the rate at which they dissolve to neutralize acidity is much slower than for carbonates or hydroxides. Aluminosilicates dissolution under acidic conditions is held responsible for the high concentration of Al in tailings pore water (Blowes and Jambor, 1990). Example of such a neutralization reaction by complete dissolution of a potassium feldspar at a pH under 4 is given below:

Potassium feldspar dissolution

$$KAlSi_3O_8 + 4\ H^+ + 4\ H_2O \rightarrow K^+ + Al^{3+} + 3\ H_4SiO_4 \qquad (5)$$
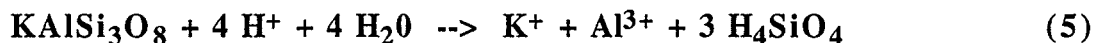
In an acid solution, silicic acid ($H_4SiO_4^0$)will be the dominant silica species. A typical Mg-Chlorite will dissolve in an acid solution (pH < 4) according to:

Chlorite dissolution

$$(Al_1Mg_4Fe_1)\ (Si_3Al)\ O_{10}\ (OH)_8 + 16\ H^+ \rightarrow$$
$$2\ Al^{3+} + Fe^{2+} + 4\ Mg^{2+} + 3\ H_4SiO_4 + 6\ H_2O \qquad (6)$$
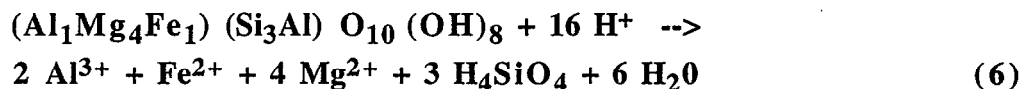
Acid dissolution of chlorite will generally proceed without preferential attack on tetrahedral or octahedral sheets (Ross 1969). The final end-product of acid dissolution of chlorite is an amorphous silica residue. In reaction (6), 16 moles of H+ are needed to dissolve 1 mole of chlorite. So, without taking into account the kinetics of this reaction, chlorite is efficient at removing H^+ ions. It has also been shown that transformation of chlorite into a vermiculite-like mineral by specific acid removal of the interlayer sheet requires that the latter be structurally disturbed and ferrous iron be oxidized to the ferric state (Ross and Kodama 1974).

Mica dissolution and transformations

Weathering of micas has been studied for many years by soil scientists. It has been shown that micas, and particularly trioctahedral species (e.g., biotite), are less resistant to weathering than dioctahedral micas (e.g., muscovite). In many situations, through weathering, micas will be transformed to expansible 2:1 minerals by replacement of the interlayer K. Under acid conditions, the 2:1 layer of micas may disintegrate as rapidly as micas interlayer cations are exchanged (Fanning et al. 1989). Transformation of a 2:1 micas to an expansible micas (smectite or vermiculite) is generally accompanied by a reduction in layer charge. There are several possible mechanisms to reduce the layer charge of 2:1 micas. One that is often mentioned is the oxidation of structural Fe(II) to Fe(III) during the opening of the interlayer. Combining of H^+ with apical oxygens of the tetrahedral layers to form OH may also reduce layer charge. The formation of expansible minerals will generally modify the whole rock texture and particularly its mechanical properties. Schistosity planes are likely to be opened by the swelling of these minerals, exposing more pyrite to the acid solution. In a laboratory experiment of bacterial leaching of a black-schist ore material containing the trioctahedral Mg micas phlogopite, Bhatti et al. (1992) found that the latter was transformed into a vermiculite-like mineral by the acid weathering.

To summarize, the interaction between an acid leachate and silicate minerals and in particular phyllosilicates is two-fold. First, while being very effective to remove H^+, the neutralization reaction (dissolution) is accompanied by the release of structural cations (e.g., Al, Mg, Fe) and interlayer cations (e.g., K) to the solution. Second, possible transformations of phyllosilicates to expansible mineral phases during the acid attack may contribute to expose more pyrite for further oxidation. Crystallization of gypsum, following calcite dissolution, has such an effect as will be seen in later sections.

5.3.3   SAMPLE COLLECTION AND METHODS OF INVESTIGATION

Sample collection

Samples of waste rock for detailed mineralogical profiles were collected in the two exploration pits T92-1 and T92-2 (see Fig. 5.1) at 0,5m interval, down to a depth of 4 m. Particle size analyses were partly conducted in the field. Samples of about 550 kg were collected and seived on a 7cm screen. The fraction of material smaller than 7cm was divided in sub-samples that were brought back to the laboratory for particle size analyses. Samples for mineralogical analyses were collected as the trench was dug. Particles larger than about 5cm were discarded by hand. T92-1 is located in the central western part of the dump in a separate sub-pile identified as the "very low grade" ore

pile. The dominant rock type in this zone of the dump is the felsic volcanoclastics. T92-2 is located in the southern section of the dump, where sericitic schists are the dominant rock type, and where an intense AMD generation has been observed.

Samples from borehole #7 (BH-7, see Fig. 5.1) were also used for mineralogical analyses. It is situated in the southern part of the dump, roughly 250 m west of T92-2, in a zone where all three types of rock are present. The boreholes inside the dump were drilled using a down-the-hole hammer with an eccentric head (15cm Ø). Drill cuttings were recovered by a stream of compressed air. A casing of the same diameter was forced down right behind the drill head. A composite sample was recovered at each 1,5 m interval. Since the drilling method is destructive, all particles recovered were less than 1,5 cm in size. The advantage of this type of drilling is that no water is used, and therefore the chemical characteristics of the sample are partially preserved by the drying process. In BH-7, twenty samples were collected through the entire thickness of the dump, two in the soft material on the original soil surface, and one in the bedrock below the soil.

Analytical methods

X-ray diffraction analyses were done using a Siemens D-5000 diffractometer (Cu target, graphite monochromator) or a Philips PW1050 unit (Cu target, graphite monochromator). Two methods of preparation were used for X-ray diffraction analysis. First, powder mounts were prepared for a general overview of the mineralogical composition, and second, oriented mounts were prepared for the specific analysis of phyllosilicates. Original samples were splitted and sieved to 2 mm. For powder mounts, a two gram sub-sample was recuperated and grind 5 minutes using an impact grinder (Spex 8000 mixer/mill). Powder mounts were prepared using the back-loaded method. For oriented mounts, 25 g sub-samples (< 2 mm fraction) were disintegration using an industrial blender. Three washings using distilled water and centrifugation were then performed to remove soluble salts. Separation of the < 2 μm was then accomplished using standard centrifugation methods. Oriented slides were prepared according to the paste method of Theisen and Harward (1962). Oriented mounts were analyzed in the natural state (sodium saturated) and glycerolated.

SEM observations were done using a JEOL 840 microscope with an EDX attachment (Ge crystal, Norvar window) for qualitative chemical analyses on hand picked fragments less than 5 mm in diameter. Some samples were observed just as they were, and polished thin sections were prepared for some other. On polished sections, fragments were oriented with the schistosity plane perpendicular to the observation plane. Polished sections could be observed in the backscattered electron mode (BSE) or secondary electron mode (SE) and irregular surfaces are observed only in the SE mode. The polished sections could also be used for observation under the standard petrographic microscope or the reflected light microscope.

The leachate quality from samples collected in the borehole was evaluated using a leaching procedure in which precipitated sulfate salts were put back into solution under standardized conditions. For this test, sample preparation was kept to a minimum, involving separation of a representative <2 mm fraction. To recover 100 g of <2 mm, the whole sample (appr. 2kg) was seived to 2 mm, and a sample splitter was used to recover the weight fraction needed. Leaching was done by mixing a 25 g sub-sample (<2mm) with 50 ml of distilled water under constant

agitation for 30 min on a wrist-action agitator, at a rate of approximately 250 strokes/min. Preliminary tests showed that consistent results could be obtained with 15 min. of agitation. Settling of the particles was then allowed prior to the recovery of the supernatant leachate. The leachate was then filtrated with a 0.45 mm membrane filter. Parameters such as pH, conductivity, Eh, and total dissolved solids where then measured. Sulfate was determined by ion chromatography and concentrations of Fe, Al, Mg, Ca, K and Na were determined by atomic absorption spectroscopy (AAS). All chemical analyses results are reported on a air dry basis , usually in g of element or species per kg of rock.

Samples collected in the exploration pits T92-1 and T92-2 were also subjected to the leaching procedure. In addition, a few drops of interstitial water were obtained by pressure extraction using a stainless steel die and a high pressure press that is used to extract water from mortar samples (Duchesne 1993). Each sample, a few microliters each, was analyzed by EDXRF (Choquette et al. 1993a). In this method, a precise fixed volume of solution (usually 20μl) is put in the center of a membrane filter and allowed to dry. The filter is then analyzed by EDXRF and values obtained are compared to standard calibration curves. This method allows the quantification of S, Fe, Mg, Al and Ca.

5.3.4   RESULTS

X-ray diffractometry

The general mineralogical composition of each sample is given by the powder mount analysis. In BH-7, in all samples, quartz is the dominant mineral. Muscovite is also a major mineral in most samples. Qualitatively, the third most abundant mineral is chlorite. Pyrite is present and sometimes abundant in all samples. Plagioclase feldspar is found only in a few samples from the waste material. It is however abundant in samples from the soil and the bedrock underneath the dump. A trace amount of calcite was observed in the first sample (0,75 m) from the surface, it is absent throughout the rest of the waste material, and becomes a major constituent in the bedrock. Rutile is also found as an accessory mineral in many samples. The powder mount also revealed the presence, in many samples, of paragonite (Na-muscovite) and pyrophyllite in some samples. Secondary minerals like jarosite ($KFe_3(SO_4)_2OH_6$) and gypsum were also observed in many samples. Figure 5.7 shows a typical powder diffractogram (see Choquette *et al.* 1994, Appendix A for all powder diffractograms). Due to the many variables involved and the impossibility to prepare adequate standard mixtures (with the same mineralogical, physical and chemical characteristics) , reliable quantitative information could not be obtained by XRD. From that, mineralogical trends with depth in BH-7, were evaluated in a crude qualitative way by using intensities of key reflections, most often reflections with the less interference. Taking quartz as an example, the surface area of the (112) reflection at 1.82Å was measured in all samples and starting from the highest measured value down to zero, categories ranging from abundant to not-detected were divided. Table 5.11 presents the results.

Fig. 5.7 Typical XRD powder diffractogram from BH-7 18.25m.

BH-7 18.75m

9.9 Muscovite

Gypsum
7.6

Chlorite
7.1

Jarosite
5.1

1.82 Quartz

Pyrite
1.63

2-Theta
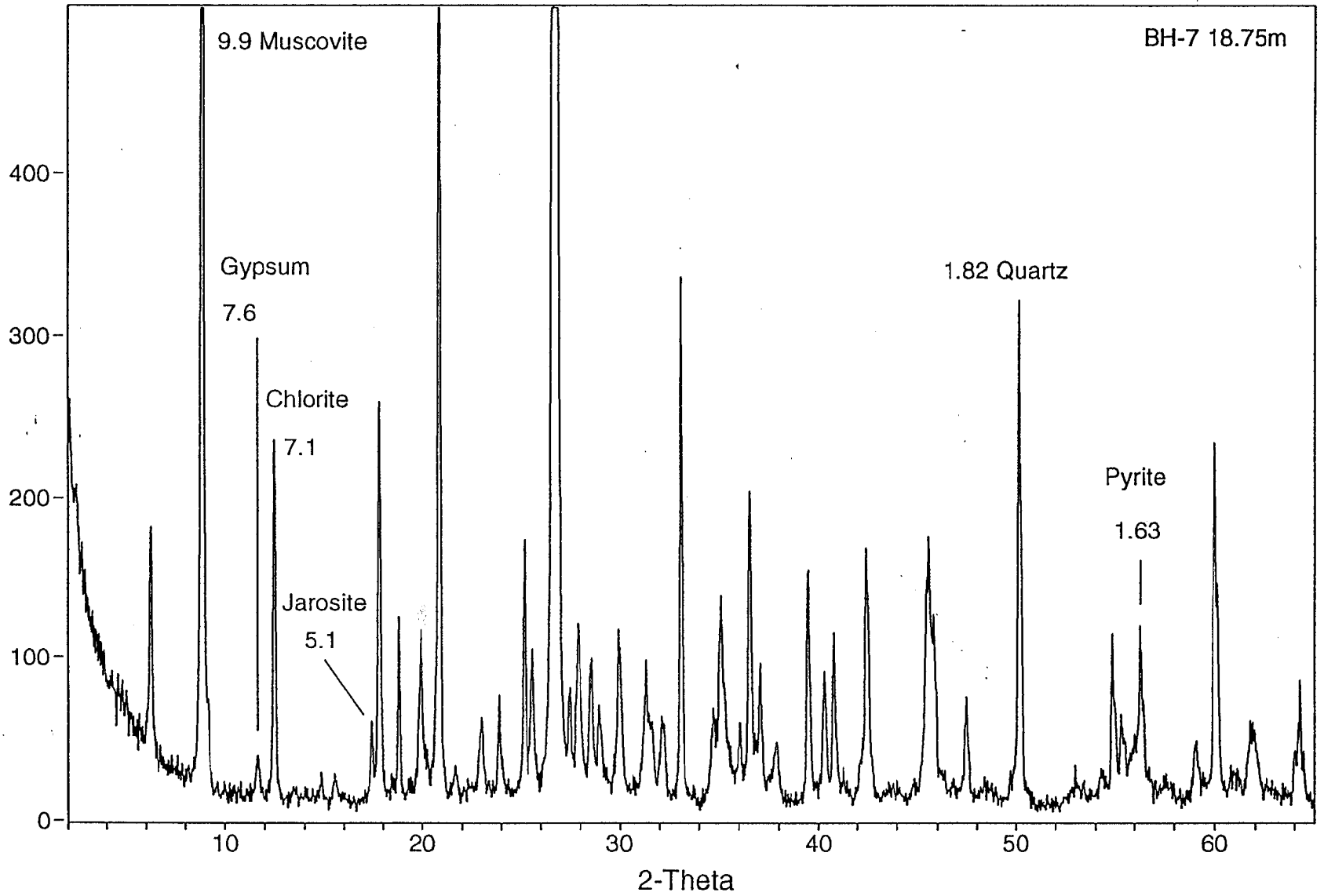
The presence of gypsum through the whole column of waste material and in the first soil sample indicates that, at some time, a sulfate rich solution flowed through it. We cannot tell however if the calcium necessary for its precipitation came from in-situ dissolution of calcite, or if the solution was already saturated with respect to gypsum in the upper part of the dump. The total absence of calcite, except in the uppermost sample, suggests that it was depleted following neutralization of the acid leachate. The presence of jarosite is a good indication of very acid conditions within the dump. Jarosite is first detected at 8,25 m and is present down to 27,75 m. Jarosite being a Fe(III) sulfate, indicates oxidizing conditions. The source of potassium necessary for the precipitation of jarosite must necessarily be muscovite, since it is the only K-bearing mineral. This implies that muscovite is undergoing some form of alteration.

X-ray powder analysis of samples from T92-1 and T92-2 are also presented in Table 5.11. T92-1 shows an uniform mineralogical composition with quartz, chlorite and muscovite being the most abundant species. Calcite is always present and gypsum appears at a depth of 2 meters.

In T92-2 some important mineralogical trends are observed. Gypsum is present in all samples and particularly abundant from 1,5 to 3,0 m. Jarosite appears at 1,5 m which coincides with the loss of calcite. The maximum content of jarosite is found at 3,0 m. Pyrite shows also a significant decrease between 1,5 and 4,0 m. There is a possible relationship between the decrease in muscovite between 2,0 and 3,0 m and the increase of jarosite but it is most probably due to a change in rock type since a positive correlation is also observed with the plagioclase feldspar.

A typical oriented diffractogram in the natural state and glycerolated is presented in Figure 5.8. Results from oriented mounts analysis revealed some new data not detected by the powder method. In most samples, it was found that paragonite is a much more abundant mineral phase than was initially estimated (001 reflection at 9.7, 4.8 and 3.21Å). The presence of pyrophyllite is also confirmed by the 9.2Å reflection and its harmonics at 4.6 and 3.07Å. In some samples, kaolinite is also observed. This identification is possible because of the good separation between the (002) of kaolinite at 3,57Å and the (004) of chlorite at 3,54Å.

Jarosite is also visible in the oriented mounts. Its reflection at 5.7Å (003), usually a 45% intensity reflection, is now the most intense. This is evidence of preferential orientation, the c axis of jarosite oriented perpendicular to the glass slide. Since jarosite has a granular crystal habit and does not usually show prefered orientation, it is assumed that this orientation is imposed by another mineral, muscovite. In orienting muscovite on the glass slide, a prefered orientation is also acquired by jarosite. It is postulated that jarosite crystalized epitaxially on muscovite, the K plane in each phase bridging them together. It is not ruled out that the interlayer, or K plane, in muscovite could act as a nucleation place for jarosite since each phase has a hexagonal symmetry at this level. This would however involve shifts in K positions to accommodate each phase. Evidences for this mode of formation were collected from SEM observations of jarosite grains between muscovite crystallites.

Table 5.11 Qualitative mineralogical composition of BH-7, T92-1 and T92-2

| Depth (m) | Quartz 1,82Å | Muscov. 10,0Å | Feldspar 4,03Å | Chlorite 7,1Å | Gypsum 7,56Å | Jarosite 5,09Å | Pyrite 1,63Å | Calcite 3,03Å |

BH-7 — Waste — Soil — Bedrock

Depths: 0,75; 2,25; 3,75; 5,25; 6,75; 8,25; 9,75; 11,25; 12,75; 14,25; 15,75; 17,25; 18,75; 20,25; 21,75; 23,25; 24,75; 26,25; 27,75; 29,25; 30,75; 32,50; 34,00

T92-1 — Depths: 0,0 na; 0,5; 1,0; 1,5; 2,0; 2,5; 3,0; 3,5; 4,0

T92-2 — Depths: 0,0; 0,5; 1,0; 1,5; 2,0; 2,5; 3,0; 3,5; 4,0
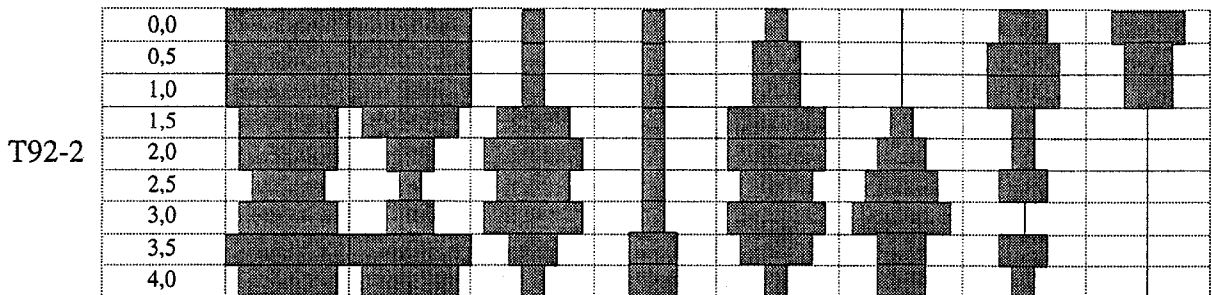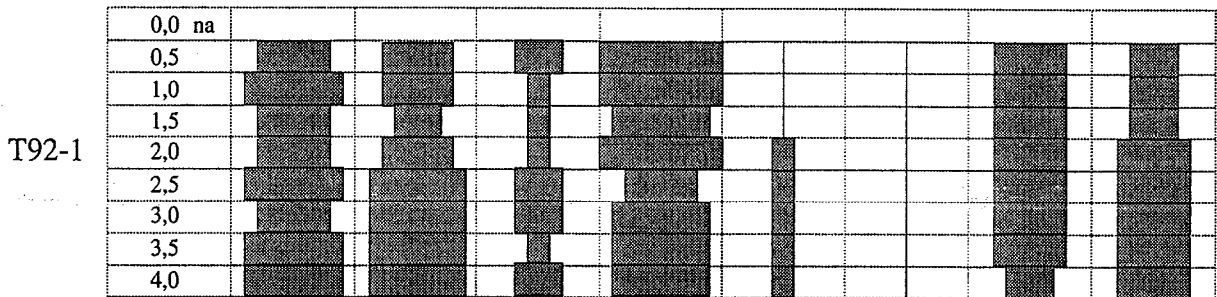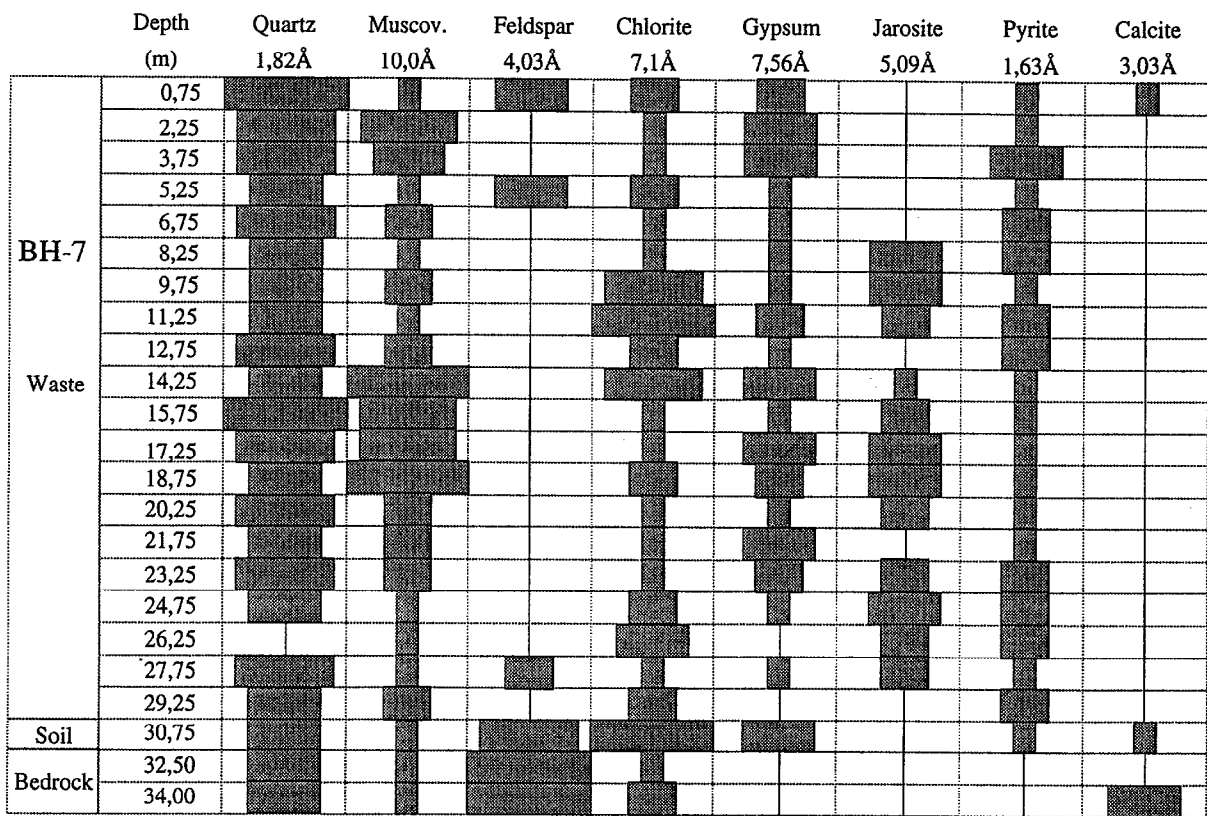
Major phase ———————————→ Not detected

Fig 5.8 Typical XRD oriented mount diffractograms from BH-7 18.25m

Glycerol

Smectite
17.9

Chlorite
14.2

9.9 Muscovite

Paragonite
9.7

7.1 Chl

5.7 Jarosite

Jar
5.08

4.99 Mus

4.81 Parag

4.73 Chl

3.54 Chl

BH-7 18.75m

3.32 Musc

Parag
3.2

Jaro
2.84

12.3

Natural

2-Theta
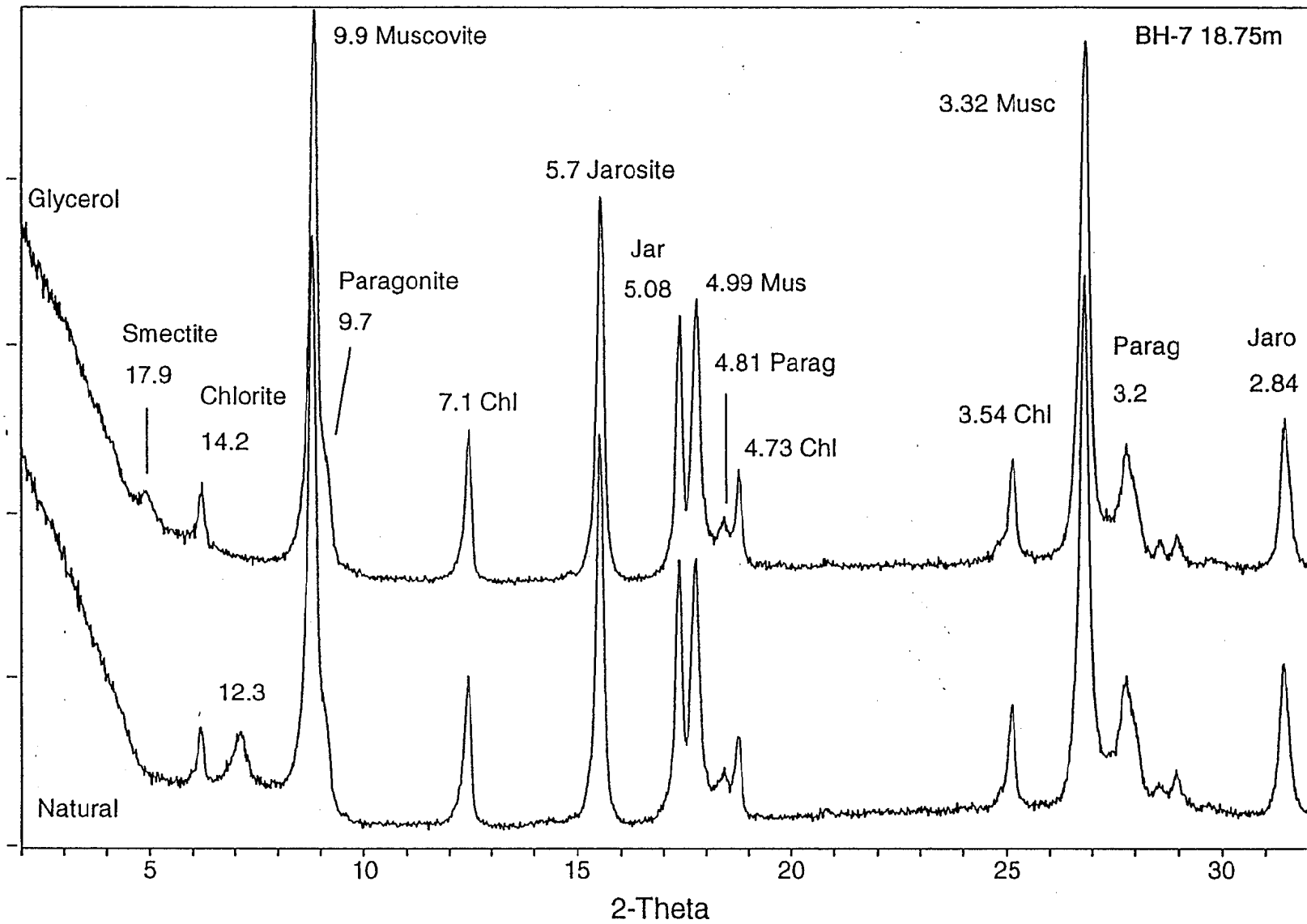
Oriented mounts were instrumental in the detection of a swelling mineral phase that has all the characteristics of a smectite. Upon sodium saturation, a characteristic reflection at 12,3Å, swelling to 17,9Å after glycerolation, is observed. In BH-7, the "smectite type" phase is visible in acidic horizons. The presence of smectite in the waste rock pile, not reported before from the rocks at la Mine Doyon, is evidence that micas can undergo transformation into a swelling phase by the action of an acid oxidizing solution. XRD is not providing evidence however of which mineral (i.e. muscovite, paragonite or pyrophyllite) is transforming. An indication that paragonite probably undergoes this transformation comes from two samples (8,25 m and 21,75 m) in which the presence of a regular mixed-layered structure showing a reflection at 27.5Å (glycerolated) is observed (Fig. 5.9). For a regular mixed-layered species, the d-spacing of its basal (001) reflection is equal to the sum of the basal d(001) of each layer type. Obviously, the two types of layers involved are micas and smectite. More precisely, paragonite is the favored micas type since its basal reflection is 9.66Å, which summed to the 17.9Å of smectite gives 27.56Å. The presence of a rational series of (001) reflections, characteristic of a regular stacking, was not possible to confirm, since there is interference from chlorite (at 14Å) and pyrophyllite (9,2Å).

In each sample following the one containing the regularly interstratified phase, at 9,75m and 23,25m, the broadening of the 17,9Å reflection towards lower d-spacings suggests the presence of irregular stackings with a dominance of the smectite layer type. Rimmer and Eberl (1982) interpreted the presence of regular and irregular illite/smectite mixed-layers in an underclay beneath a bed of coal in Illinois by a more or less pronounced acid leaching originating from pyrite oxidation in coal bed. Regular interstratification is believed to represent a first step of alteration that is done under gentler acid conditions than irregular interstratification.

Finally, an other behavior is observed in samples at 17,25 m and 26,25 m. Upon glycerolation, the 12,3Å reflexion is swelling only to 14.2Å. This incomplete swelling is typical of a "low charge" vermiculite behavior and could correspond to an intermediate alteration development between micas and smectite.

Diffractograms of samples (oriented mounts) from T92-1 and T92-2 are also presented in Appendix B of Choquette and Gélinas (1994). In all samples from T92-1, the same smectite type phase is present as a minor component. However, comparing to samples from BH-7, there are almost no traces of paragonite. This could mean that, at least in this zone of the dump, smectite is derived from muscovite. The absence of regular interlayering could also indicate that muscovite alters directly to smectite without or with very rapid intermediate stages of interstratification. In T92-2, where the acidification process is much more pronounced, smectite is a dominant phase in many samples. Again, in the absence of paragonite, all that is detected is a single smectite type phase. There is also an overall decrease of intensity from all phyllosilicates with depth, that could be caused by surface coating of particles. Jarosite is detected from 1,5m down, again its (003) reflection being amplified by prefered orientation. The maximum jarosite intensity is found at 2,5m, corresponding with a minimum intensity from phyllosilicates.
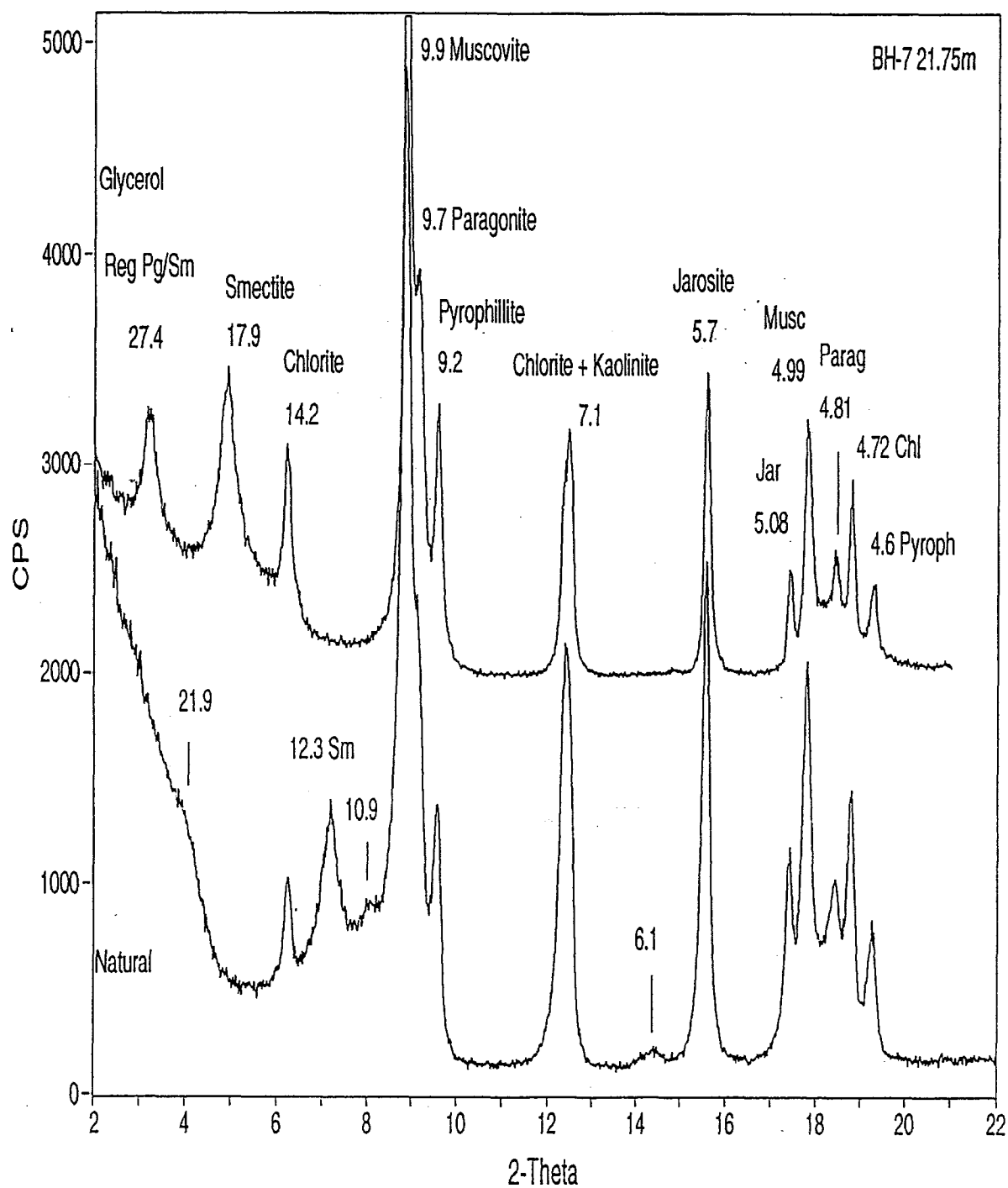
Fig 5.9 XRD oriented mount from BH-7 21.75m

SEM observations

Most samples observed under the SEM came from T92-2 and observations were made in the backscattered electron mode. This permits identification of mineral phases on the basis of mean atomic weight (minerals with high mean atomic weight appears white and those with low Z appears black).

Figures 5.10a and 5.10b shows a typical texture encountered in the surface sample from T92-2 (0,0 m). In this micrograph, pyrite grains are white, calcite is light grey, phyllosilicates are medium grey, quartz is dark grey and the impregnating material is black. It is clearly shown here that in this grain, approximatively 50% of the calcite has been dissolved. The newly created porosity has not been filled with gypsum. Free pyrite grains, or those that were in contact with the pore water are covered with an alteration rim approximately $1\mu m$ thick (Figs. 5.10c,d). EDX analysis of these rims showed that they are composed of Fe and O, probably goethite (FeO(OH)), ferrihydrite ($Fe_5HO_8 \cdot 4H_2O$), or amorphous $Fe(OH)_3$ since none of the first two phases were detected by X-ray diffraction. Alteration rims of this type were also reported by Jambor and Blowes (1991) surrounding pyrite and other sulfides in high carbonate tailings. The presence of such rims indicate that surface oxidation of pyrite has occured, sulfates were leached in the pore water and the iron (or part of it) precipitated as an iron crust. The dissolved iron must remain in the near-environment of pyrite or else an iron coating would be observed on other minerals. The effects that such alteration rims can have on further oxidation of pyrite are unknown. Absence of jarosite also characterizes this sample.

Transformation of micas into a smectite type phase is best illustrated by Figure 5.11a,b. In these micrographs from T92-2 (3,0 m), muscovite grains are gradually transformed into smectite. In Fig. 5.11a, EDX analysis of the unaltered, partially altered and totally altered parts of the grain shows that alteration is accompanied by a loss of K, loss of Al and probably a gain of Mg. Figure 5.11b is showing the same trend with the exception that the central part of the micas is already potassium depleted. Figure 5.12a shows paragonite from BH-7 being transformed into smectite. There is no microscopic evidence however for interstratification. In Figure 5.12b, the last stage of phyllosilicates alteration, residual amorphous silica, is depicted. In the left central part of the micrograph, a light grey mass of amorphous silica is seen as a pseudomorph of smectite.

The weathering of micas as the source of K for the precipitation of jarosite has already been mentioned by Bhatti et al. (1992) in a laboratory experiment. The same association is also observed in this study. X-ray diffraction analysis results described in the preceding section suggested that jarosite could crystallize epitaxially on muscovite. Figures 5.12c and d show this process clearly . Crystals of jarosite tend to precipitate directly near the source of potassium, inside muscovite grains. In the lower left part of micrograph 5.12c, a jarosite rhombohedron is clearly seen with its c axis oriented parallel to the c axis of muscovite. In that same micrograph, the muscovite grain has already been transformed into a sub-micron interstratification of smectite (dark bands) an muscovite (clear bands). Opening and disintegration of muscovite results from this process as shown in Figure 5.12d. In acidic samples, chlorite aggregates were thoroughly corroded without any associated secondary phases. Again, the end product of chlorite alteration would be amorphous silica, as suggested by the EDX analysis of the intact and altered zones in Figure 5.13c, which shows loss of Mg, Al and Fe.
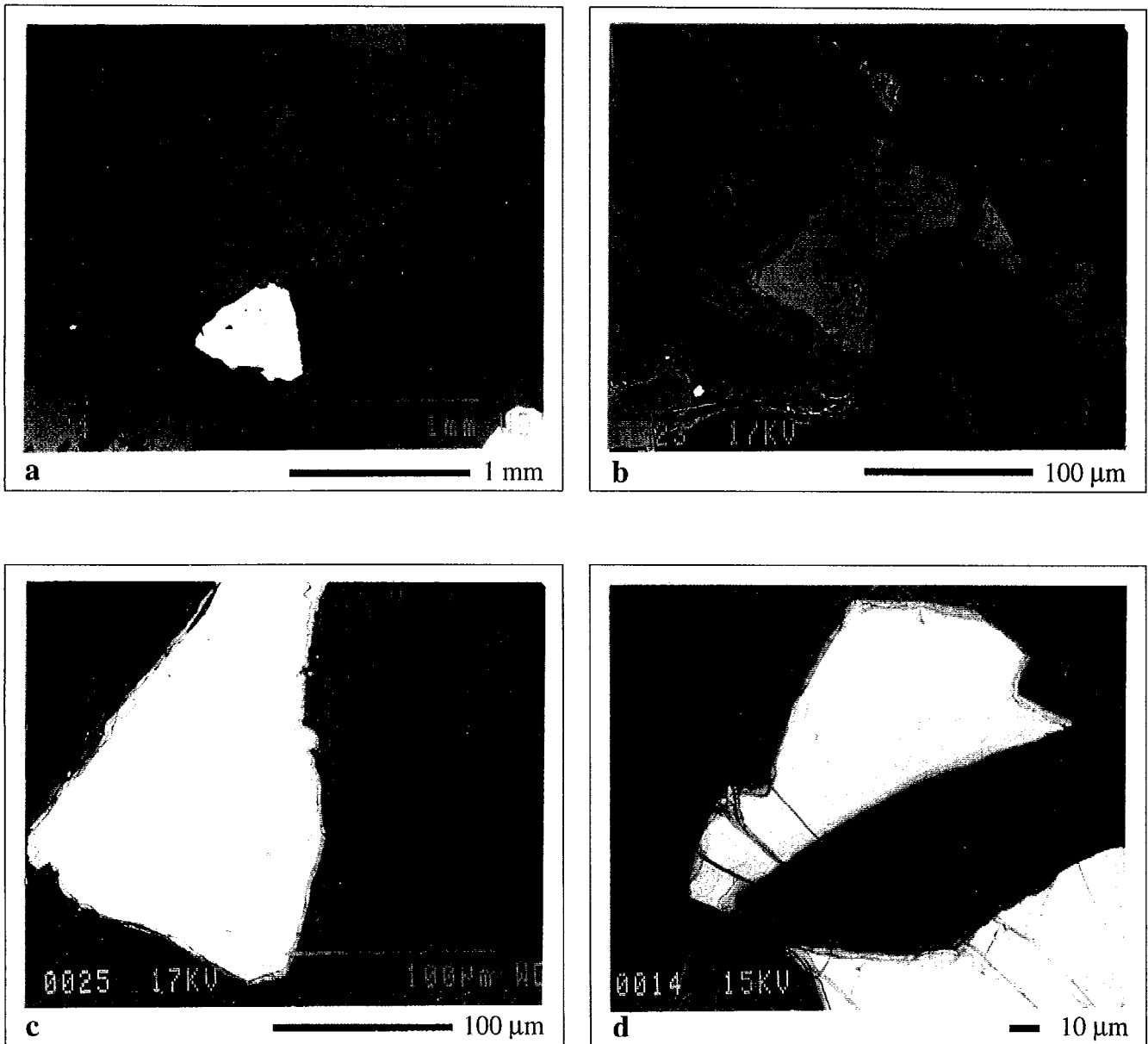
Fig. 5.10 SEM micrographs from T92-2, 0,0 m.

a) Calcite dissolution resulting from acid neutralization. Calcite is light grey, pyrite is white, phyllosilicates are medium grey and quartz is dark grey. Note that the newly created porosity is not filled with gypsum. *b)* Other example of calcite dissolution. *c)* Iron hydroxide coating on a free pyrite grain. *d)* Iron hydroxide coating on partly exposed pyrite grains.
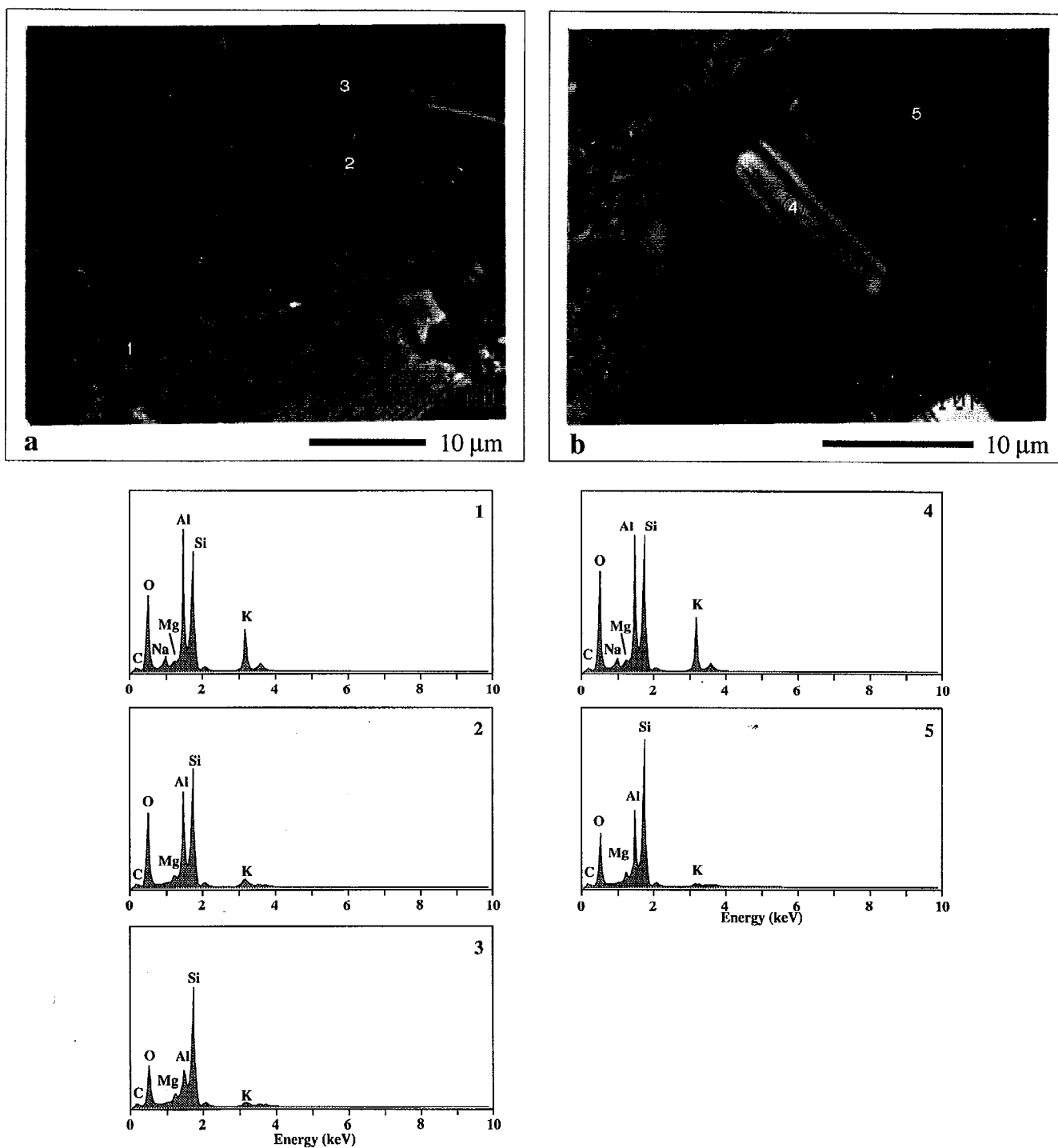
Fig. 5.11. SEM micrographs from T92-2, 3,0 m.

a) *Muscovite grain being transformed into smectite. EDX analysis of intact part is shown in (1), intermediate alteration is shown in (2) and complete transformation is in 3.* **b)** *Other example of the same transformation. (4) is intact muscovite and (5) is complete transformation.*
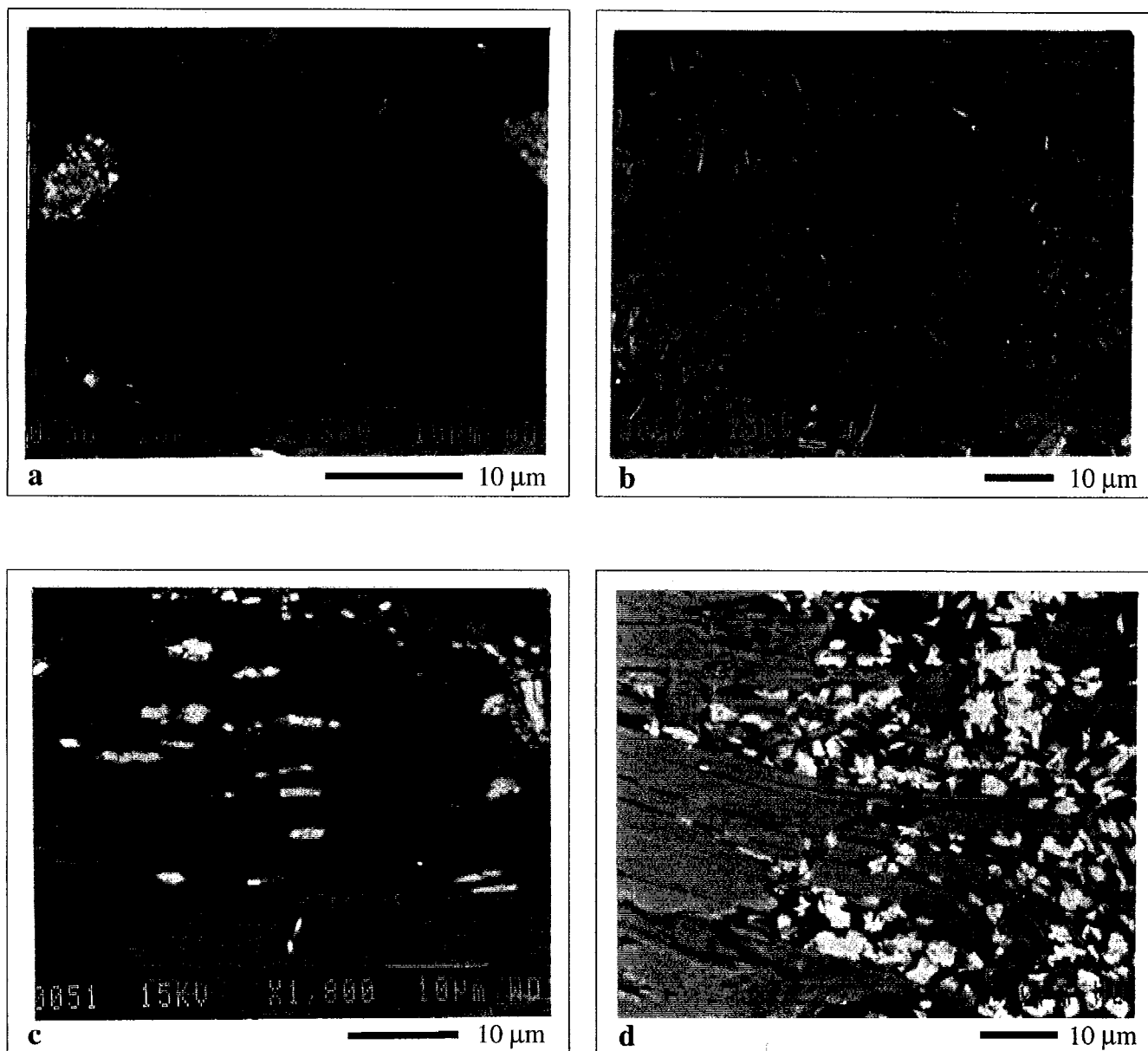
Fig. 5.12. SEM micrographs from BH-7 11.25m and T92-2 3,0 m.

a) Paragonite grain being transformed into smectite (BH-7, 11,25m). b) Intense smectite formation resulting from muscovite alteration. The lighter zone in the left part of the micrograph is amorphous silica. c) Epitaxial growth of jarosite (white) in the interlayer region of muscovite. Note the sub-micron interstratification of smectite (dark bands) with muscovite (lighter bands) (BH-7, 11.25m) d) Growth of jarosite in a muscovite grain and the resulting reduction in muscovite crystal size (T92-2,3,0m).
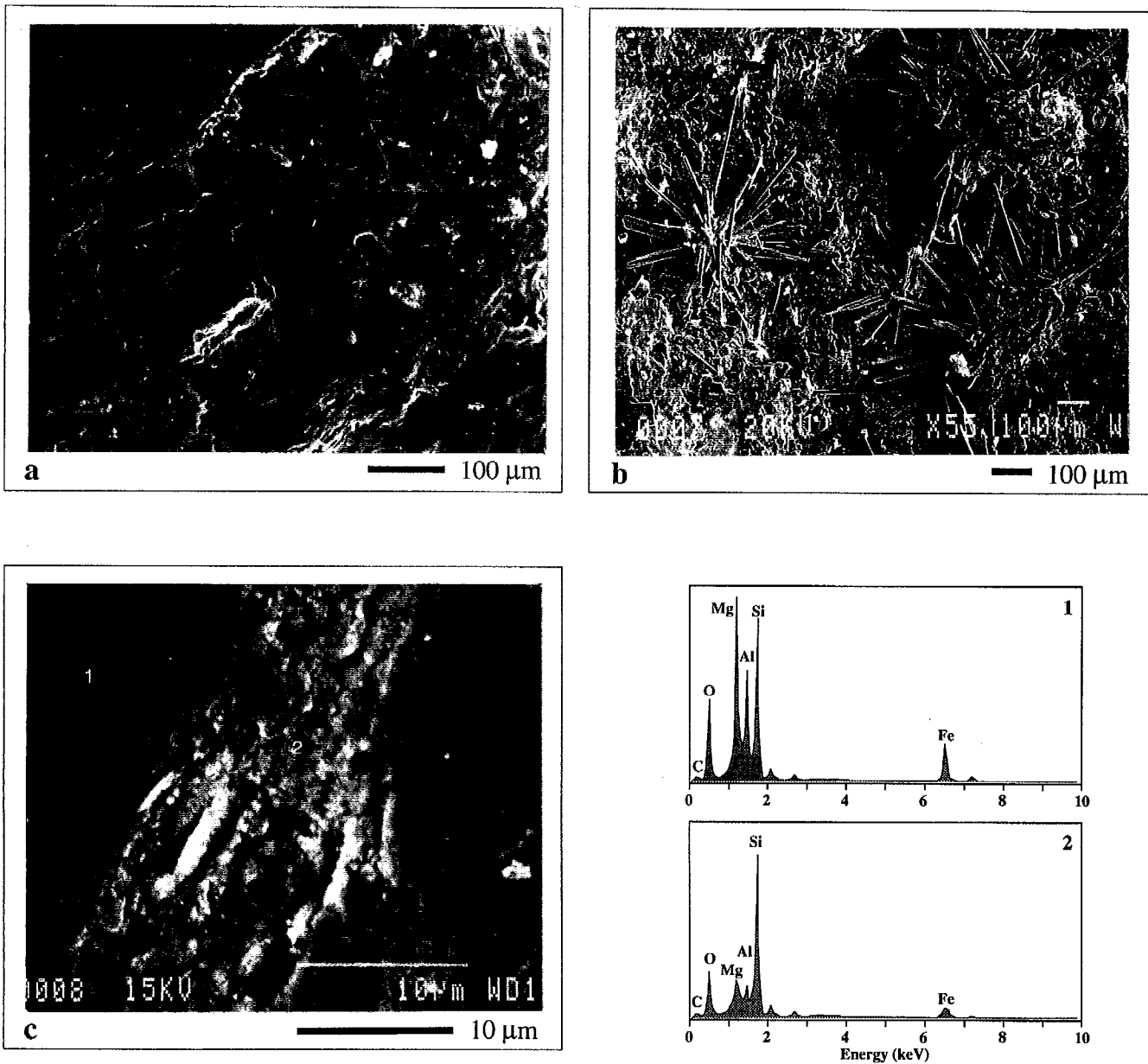
Fig. 5.13. SEM micrographs from T92-2.

e) Dissolution channels and etch pits in a pyrite crystal. f) "Star like" gypsum crystal opening a schistosity plane in the sericitic schist. g) Chlorite grain partially dissolved. EDX analysis of (1) intact chlorite and (2) altered zone (T92-2, 3,0 m).

Pyrite crystals are usually subhedral with an aspect ratio (maximum projection/width) over 1,5. The grain size of pyrite varies from less than 0,01 mm up to 5 mm in all rock types. In the intermediate tuffs (unit 3) and the felsic volcanoclastics (unit 4A), the mean grain size is approximately 0,1 to 0,2 mm and in the sericitic schists is 0,6 mm. These data come from image analysis of at least 150 pyrite grains in each rock type. Pyrite grains are often corroded, broken apart by dissolution channels, or covered with etch pits. All these features are visible in Figure 5.13a. The partial oxidation and subsequent loosening of pyrite grains will often leave voids that will be filled with sulfates minerals, especially gypsum. As gypsum crystallizes, it will develop pressure on the surrounding matrix and will generally force opening along schistosity planes. This mechanism is seen in Figure 5.13b where star shaped aggregates of gypsum are seen forming in a plane parallel to the schistosity.

Pore-water quality evaluation

Pore-water quality evaluation was made using the leaching method described earlier. Analytical results are presented in Figure 5.14. The leachate pH shows a very rapid drop to a value just over 2 within the first 3,5 m. Deeper, a constant but slow rise to pH 3,6 is measured. In the surface sample, leachate Eh is 575 mV and rapidly increases to 775 mV at 3,75 m. A constant slow drop is then measured with depth. Conductance and total dissolved solids (TDS) are extremely well correlated. These two parameters are also perfectly correlated to $SO_4^=$ (measured by ion chromatography). In the first two sub-surface samples, Al, Fe and Mg are almost absent while $SO_4^=$ concentrations reaches 1500 mg/l and Ca is at its highest level (near 600 mg/l). K and Na are also present. Further down, Al, Mg and $SO4^=$ concentrations are rising, Fe reaches a maximum value at 5,25 m and then drops gradually, K and Na are almost absent while Ca shows a slow drop down to 12 m and then stabilizes at approximately 460 mg/l deeper. The concentration curves of Al and Mg are very similar both in shape and values, which suggests a common source, most likely chlorite. Acidity values were calculated from TDS according to the relationship developed from the database of chemical analysis from numerous leachate samples from the south dump (Choquette et al., 1993b):

$$\text{Acidity (mg/l eq. } CaCO_3) = (0,0856 \text{ TDS}) + (2,177 * 10^{-5} \text{ TDS}^2)$$

In the absence of porosity and saturation data for these samples, we can only speculate on the absolute element concentrations in the pore water. However, since the leaching procedure was standardized, it is possible to calculate concentrations on a dry basis. Results can then be represented in % or, more visually, in g/kg. Values in mg/l in the leachate are converted to g/kg by:

$$\text{Element (g/kg of rock)} = \text{El.(mg/L)} * 0,05(L) / 25(g) = \text{El. (mg/L)} * 0,002$$

> *given 0,05 L : volume of water used in the leaching procedure.*
>
> *25 g: dry sample mass.*

The curves obtained after this conversion are exactly identical to the concentrations curves since each value is multiplied by a constant, however, this conversion allows a better representation of

the situation in the dump. On this basis, the measured acidity in BH-7 ranges from 0,5 g/kg (surface samples) to over 9,5 g/kg in the middle of the column.
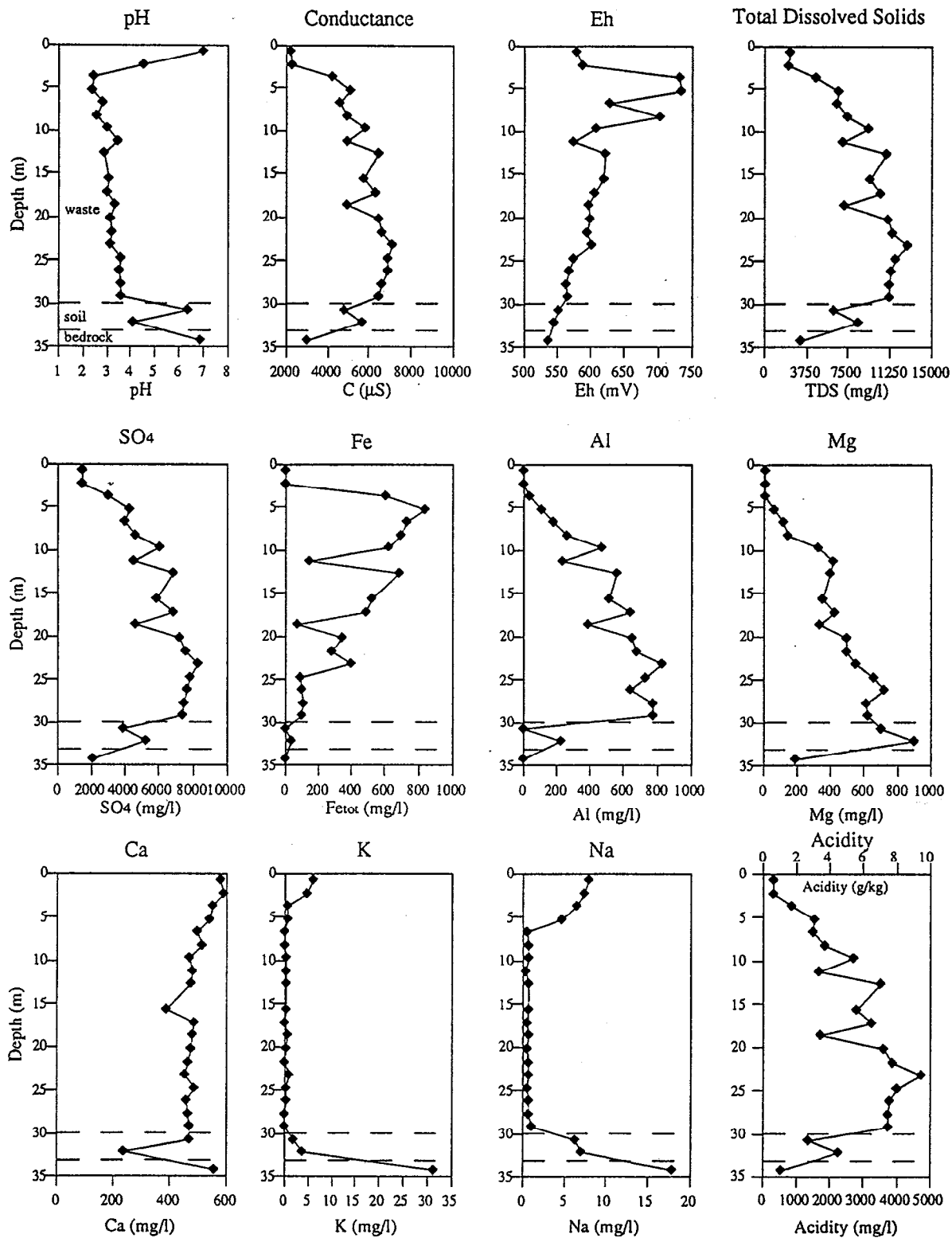
Fig 5.14 Chemical characteristics of the leachate from BH-7

Data collected from the leaching of samples from T92-1 and T92-2 are presented in Figure 5.15 (elemental analyses were not performed on these leachate samples). T92-1 does not show any pronounced trend with depth. T92-2 however is showing an important change between 1,0 and 1,5 m. At this depth, the pH drops from 7 to 2, Eh increase from 400 mV to approximately 800 mV. There is also a sudden increase in conductance and TDS. If these results are compared to the mineralogical composition (see Table 5.11), the beginning of acidic conditions is correlated to the depletion of calcite and the precipitation of jarosite. The pore-water obtained by a pressure extraction method was analyzed by EDXRF for S (expressed as SO_4), Fe, Mg, Ca and Al. Results are presented in Figure 5.16. In T92-1, even if the pH is near 7, SO_4 concentrations of approximately 2000 mg/l are measured. All other elements, to the exception of Ca are below 100 mg/l. In T92-2, the SO_4 concentration reaches 110 000 mg/l at a depth of 3,0 m. Fe, Mg and Al are all following the same general trend as SO_4.

T92-1
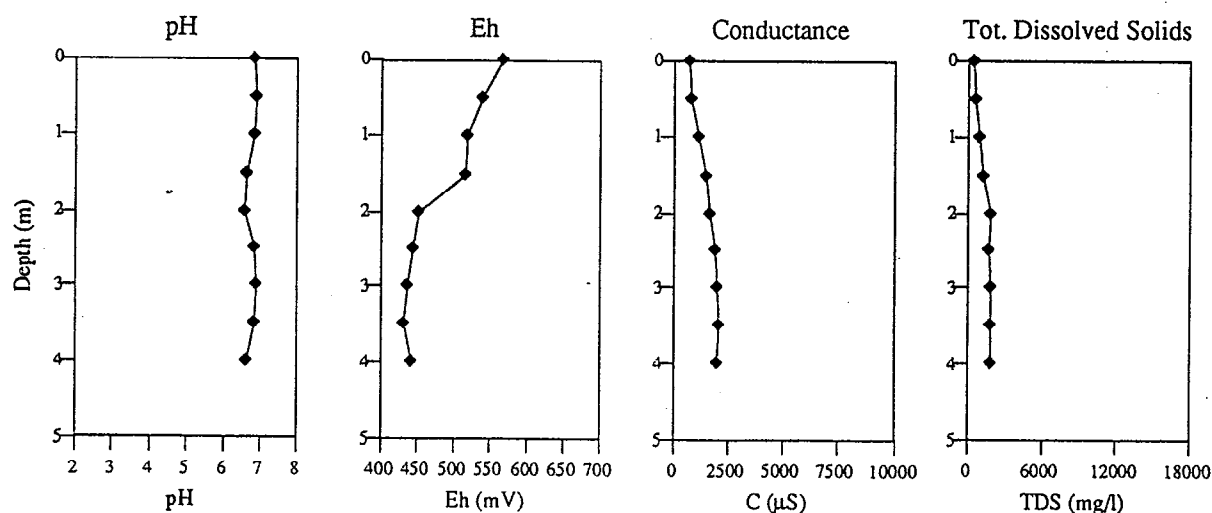
T92-2
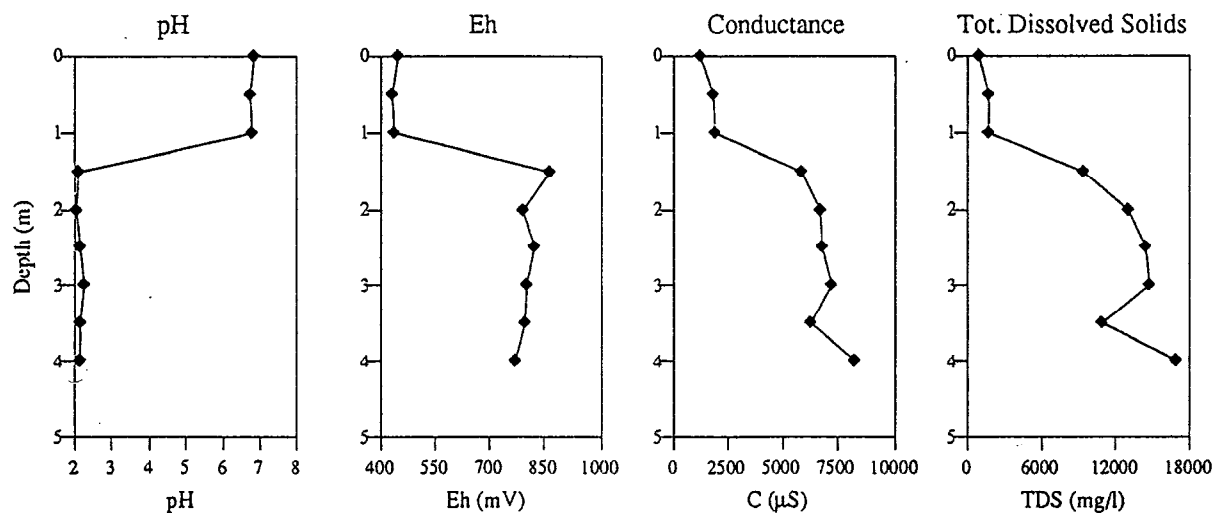
Fig. 5.15 Chemical characteristics of the leachate from T92-1 and T92-2
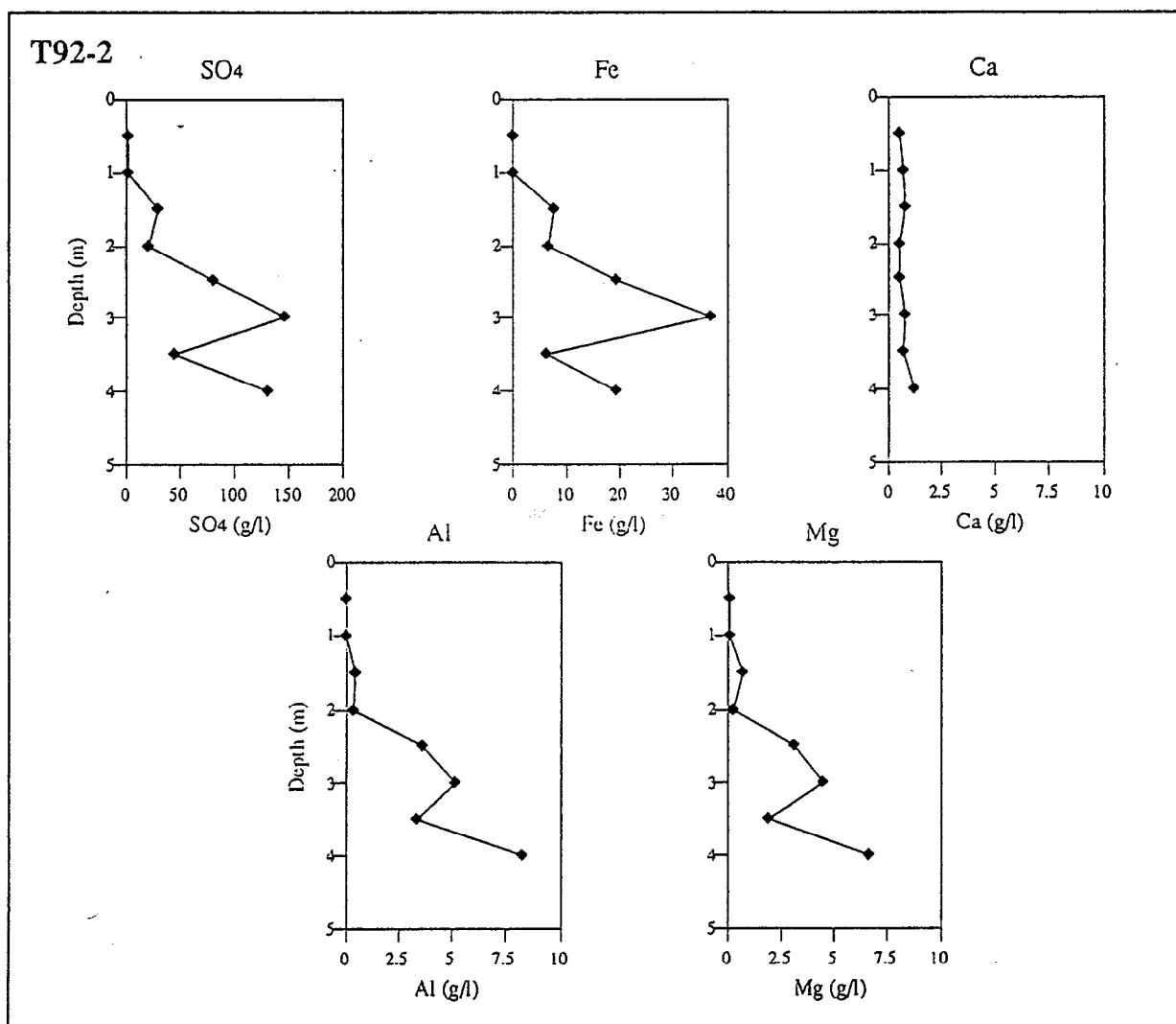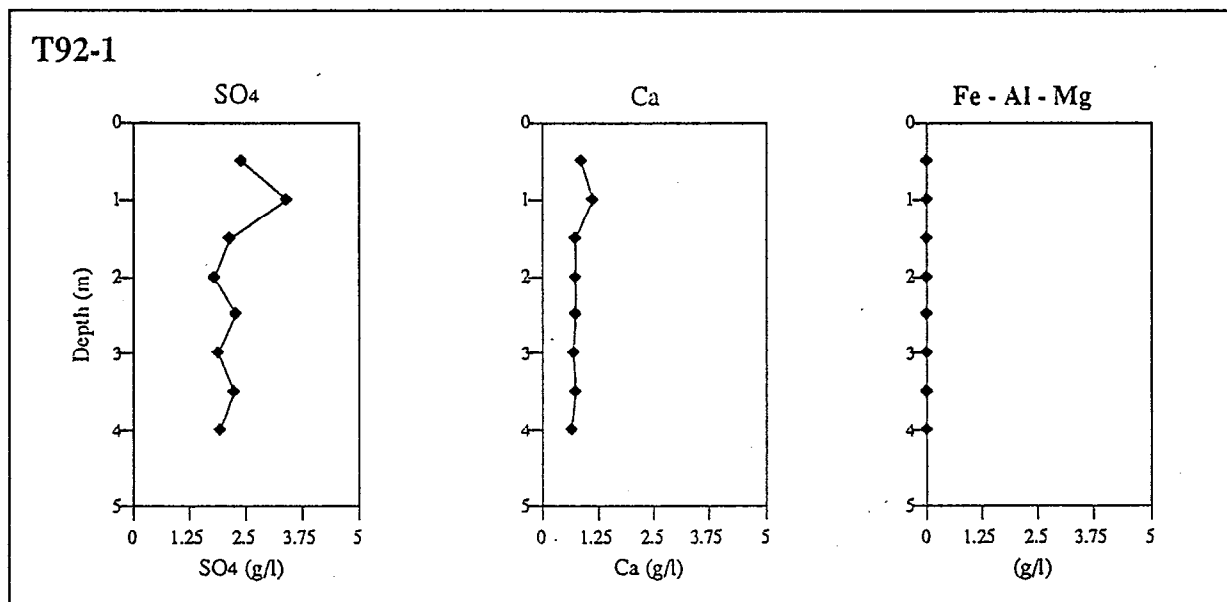
Fig. 5.16 EDXRF analysis of the pore-water extracted from T92-1 and T92-2

5.3.5 DISCUSSION

Mineralogical transformations

Acidic conditions are well developed in the south dump and the mineralogical assemblages found provide evidence of these conditions. In all samples analyzed, pyrite is present. Where the pH is still over 3, free or exposed pyrite grains are coated with an iron hydroxide layer. The role of this layer is not well defined but it possibly acts as a barrier, limiting pyrite oxidation. In BH-7, calcite is present in the first surface sample and absent or depleted downwards. As in T92-2, its depletion corresponds to the appearance of acidic conditions. Gypsum is not an indicator of such acid conditions since it is present in many samples with a near-neutral pH (i.e. the precipitation of gypsum is not pH dependent). However, in such samples, it indicates that pyrite oxidation and calcite dissolution likely occured, saturating the pore-water with respect to gypsum, but leaving the overall pH of the solution near-neutral.

With continuous pyrite oxidation and in the absence of calcite or other neutralizing minerals such as hydroxides, pH conditions will drop to values near 2. Phyllosilicates minerals will then interact strongly with the acid solution. Evidence from XRD and SEM observations suggests that micas are transformed into swelling minerals which have all the characteristics of a smectite. Figure 5.17 shows schematically the alteration sequence of the main phyllosilicate minerals.
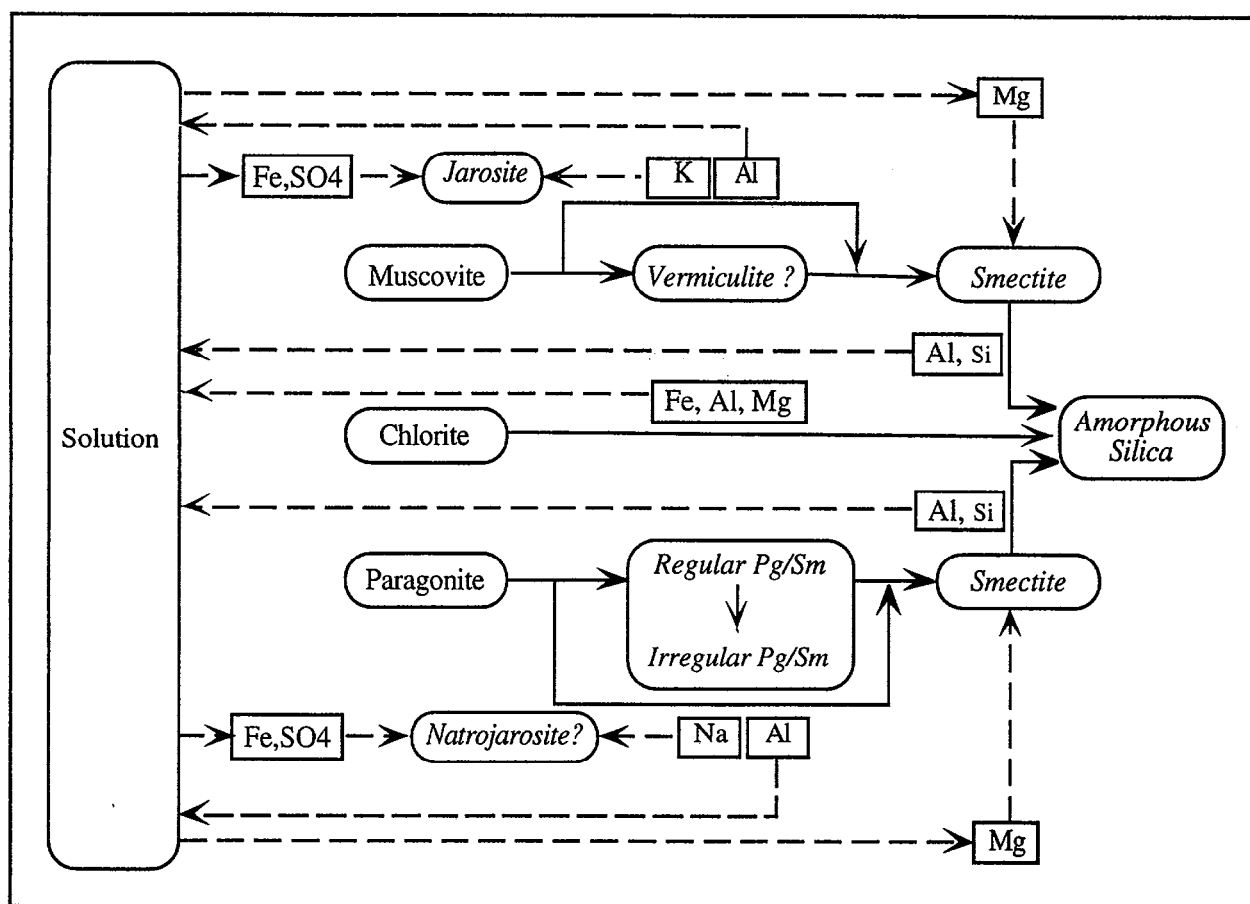
Fig. 5.17 Schematic phyllosilicates alteration sequence

Starting with paragonite, the alteration sequence through interstratification was observed in some samples. Evidence of direct alteration into smectite were also collected. Both paths must then be considered possible. During this first alteration step, Na is lost from paragonite and will likely precipitate as natrojarosite, even if the presence of this phase was not confirmed. Part of structural Al is being lost to the solution during transformation into smectite. The alteration sequence of muscovite into smectite has a possible intermediate stage of "vermiculite-like" formation, as observed in two samples from BH-7. In acid conditions, the K loss to the solution during this alteration will be precipitated as jarosite. For both paragonite and muscovite, evidences from SEM suggest that the transformation into smectite is accompanied by a gain in Mg. The source of Mg for smectite formation is the dissolution of chlorite. The final product of smectite dissolution is amorphous silica. Since the solubility of silica at low pH is not very high (approx. 2 millimoles/liter at pH 2), residual amorphous silica is an expected end product of the alteration of phyllosilicates.

SEM observations revealed that chlorite undergoes extensive alteration and that amorphous silica is the end-product. Chlorite being the only important Mg-bearing mineral, the high magnesium concentrations measured in the ditches around the dump (see Choquette et al., 1993b) and in samples from the leaching test indicate that extensive chlorite dissolution is occuring. If chlorite is dissolved in a nonpreferential way (tetrahedral and octahedral cations are removed at the same rate), Al should enter solution at the same rate. In the absence of extensive Mg or Al sulfate precipitation, which is the case, Al concentration in the leachate should be at least high enough to satisfy the Al/Mg ratio in chlorite. The muscovite transformation to smectite will also contribute to the total Al concentration. The ratio of Al/Mg should be higher than that for chlorite stochiometry. In the sericitic schists, chlorite has approximately 16% Mg and 12% Al (Savoie et al. 1991), i.e. a Al/Mg ratio of 0,75. In the leachate from BH-7, the mean Al/Mg ratio is 1,25, which is in line with the hypothesis of complete chlorite dissolution with Al contribution from muscovite. Chlorite dissolution will contribute in neutralizing the pH of the solution as seen in equation (6). However, if the pH remains low, Al will likely remain in solution and contribute to the acidity.

Potassium jarosite is an important mineralogical phase in the waste dump. The source of potassium for its formation is muscovite. Jarosite can precipitate from solution, or directly at the source of potassium, epitaxially on muscovite. Physically, this will alter the structure of the muscovite grains and will contribute to the overall physical destruction of the rock. Jarosite will precipitate according to the reaction:

$$K^+ + 3\ Fe^{3+} + 2\ SO_4^= + 6\ H_2O \ \longrightarrow \ KFe_3(SO_4)_2(OH)_6 + 6\ H^+ \qquad (7.1)$$

Precipitation of jarosite from solution will contribute to lowering the pH by producing 6 moles of H^+ for each mole of jarosite precipitated. However, in some circumstances, a net decrease in acidity will result, mainly by reducing the Fe(III) concentration of the solution (Choquette, 1994 unpublished report). Also, after $SO_4^=$ levels decrease as acid production (oxidation) slows, jarosite will dissolve and remobilize K^+ and $SO_4^=$. In addition, jarosite dissolution can result in precipitation of $Fe(OH)_3$ as in the following reaction where acidity is released:

$$KFe_3(SO_4)_2(OH)_6 + 3\ H_2O \ \longrightarrow \ K^+ + 2\ SO_4^= + 3\ Fe(OH)_3 + 3\ H^+ \qquad (7.2)$$
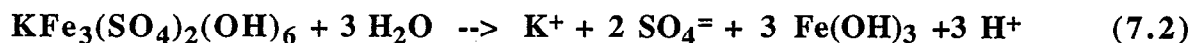
Mineralogical mass-transfer in BH-7

From the chemical data collected in the leaching procedure of BH-7, we can evaluate, on a dry basis, the mass transfer of minerals between 2 sampling points. Even if this calculation is subject to many sources or error, the highest being caused by the non-uniform chemical composition of many phases, it allows us to visualize active zones in BH-7 at the time of sampling. For example, chlorite dissolution can be evaluated using the increase in Mg concentration between two consecutive samples, or ΔMg. With a known mass of chlorite dissolving, excess Al can be attributed to muscovite dissolution (including paragonite). Dissolution or precipitation of other mineral can be evaluated by the relationships given in Table 5.13.

Table 5.12. Base equations used to calculate mass transfer in BH-7

$$\Delta Mg = Chl*Mg_{Chl} \tag{8.1}$$

$$\Delta Al = Chl*Al_{Chl} + Mus*Al_{Mus} \tag{8.2}$$

$$\Delta Fe = Py*Fe_{Py} + Chl*Fe_{Chl} + Jar*Fe_{Jar} + Goe*Fe_{Goe} \tag{8.3}$$

$$\Delta SO_4 = Py*SO_{4Py} + Jar*SO_{4Jar} + Gy*SO_{4Gy} \tag{8.4}$$

$$\Delta Ca = Cal*Ca_{Cal} + Gy*Ca_{Gy} \tag{8.5}$$

where ΔSp = difference in species or element content on a dry basis from two consecutive samples.
Mx = Mass of mineral dissolved or precipitated.
Sp_{Mx} = Species or element content of mineral Mx.

List of abbreviations used:

| Chl:Chlorite | Mus:Muscovite | Py:Pyrite | Gy:Gypsum | Jar:Jarosite |

Cal:Calcite   Goe:Goethite

Convention: A positive phase indicate dissolution and a negative phase indicates precipitation.

Equations (8.3) to (8.5) cannot be solved directly and have to be simplified. We can use a simplified set of equations for the first surface sample in which a neutral pH is measured. From eq. (8.3) we remove the jarosite and the chlorite terms because jarosite precipitation and chlorite dissolution is highly unlikely. We can also remove jarosite from eq. (8.4). We will also assume that all the Ca in solution comes from calcite dissolution and that no gypsum is precipitated, so that the gypsum term can be removed from eq. (8.4) and (8.5). In all other samples, gypsum, chlorite and jarosite terms are reintroduced and the calcite and the goethite terms are removed since calcite was not detected by XRD and SEM and pH conditions do not allow the presence of goethite (or amorphous $Fe(OH)_3$). This lead to the relationships presented in Table 5.13.

In equations (8.9) to (8.11), gypsum is first calculated and values are fitted in eq. (8.10). Chlorite is then calculated using eq. (8.1) and fitted in eq. (8.9). Equations (8.9) and (8.10) are then resolved simultaneously for pyrite and jarosite. The concentration values used for these

calculations were first smoothed using a gaussian filter. The chemical composition of minerals is presented in Table 5.14. Results are presented in Table 5.15 and Figure 5.18.

Table 5.13 Specific equations used to calculate mass transfer in BH-7 (exclusive of chlorite and muscovite).

First surface sample

$$\Delta Fe \quad = Py^*Fe_{Py} + Goe^*Fe_{Goe} \tag{8.6}$$

$$\Delta SO_4 = Py^*SO_{4Py} \tag{8.7}$$

$$\Delta Ca \quad = Cal^*Ca_{Cal} \tag{8.8}$$

All other samples

$$\Delta Fe \quad = Py^*Fe_{Py} + Jar^*Fe_{Jar} + Chl^*Fe_{Chl} \tag{8.9}$$

$$\Delta SO_4 = Py^*SO_{4Py} + Jar^*SO_{4Jar} + Gy^*SO_{4Gy} \tag{8.10}$$

$$\Delta Ca \quad = Gy^*Ca_{Gy} \tag{8.11}$$

Table 5.14 Chemical composition of minerals used in the mass transfer calculations.

*Chlorite**	$(Mg_{3.90}Fe_{0.71}Al_{1.39})\ (Al_{1.21}Si_{2.79})\ O_{10}\ (OH)_8$
*Muscovite**	$(Na_{0.20}K_{0.80})\ Al_2\ (Al_{0.90}Si_{3.10})\ O_{10}\ (OH)_2$
Pyrite	FeS_2
Jarosite	$KFe_3(SO_4)_2\ (OH)_6$
Gypsum	$CaSO_4 \cdot 2H_2O$
Goethite	$FeO(OH)$
Calcite	$CaCO_3$

*: chemical composition from Savoie et al. (1991).

A specific trend that was barely visible in the elemental concentration curves emerges from these calculations. First, we can observe a high level of pyrite dissolution in the first surface sample. This accounts for the SO_4 concentration of 1400 mg/l measured in that sample. The absence of Fe in that sample is a result of iron hydroxide precipitation, in the near-neutral environment provided by calcite dissolution. Further down, two active zones are detected, one at a depth of 8 m and the other at a depth of 22 m. These zones are characterized by jarosite precipitation, chlorite dissolution and pyrite dissolution. Muscovite does not follow this trend.

Table 5.15 Calculated mineral mass transfer in BH-7

Depth	Differential concentrations*				
	ΔCa	ΔMg	ΔAl	ΔFe	ΔSO4
0,75	1,5604	0,0293	0,0000	0,0000	3,7947
2,25	-0,0209	0,0000	0,0152	0,2283	0,6389
3,75	-0,0209	0,0301	0,0619	0,3973	1,2885
5,25	-0,0209	0,0424	0,0768	0,2473	1,0170
6,75	-0,0209	0,0741	0,1130	0,0906	0,8759
8,25	-0,0209	0,1018	0,0938	-0,1047	0,5874
9,75	-0,0209	0,1217	0,1053	-0,1201	0,6939
11,25	-0,0162	0,0860	0,0582	-0,1061	0,3751
12,75	-0,0011	0,0438	0,1122	0,0367	0,6613
15,75	-0,0011	-0,0020	0,0205	-0,0278	-0,0112
17,25	-0,0011	0,0151	0,0540	-0,0655	0,2210
18,75	-0,0011	0,0235	-0,0011	-0,1489	-0,0195
20,25	-0,0011	0,0654	0,0918	-0,0081	0,8782
21,75	-0,0011	0,0664	0,0827	-0,0211	0,7516
23,25	-0,0011	0,0888	0,0717	-0,0174	0,6364
24,75	-0,0011	0,0668	-0,0021	-0,1088	-0,0327
26,25	-0,0011	0,0372	-0,0057	-0,0686	-0,1861
27,75	-0,0011	-0,0103	0,0181	-0,0387	-0,2582
29,25	-0,0011	-0,0305	0,0546	-0,0019	-0,1279

Depth	Mineral dissolution or precipitation *†						
	ΔChlor	ΔMusc.	ΔCalcite	ΔGyps.	ΔPyrite	ΔGoet.	ΔJarosite
0,75	0,1792	-0,1097	2,9229	0,0000	2,3697	-1,7552	0,0000
2,25	0,0000	0,0767	0,0000	-0,0898	0,3990	-0,2955	0,0000
3,75	0,1840	0,2000	0,0000	-0,0898	0,2323	0,0000	0,8267
5,25	0,2593	0,2292	0,0000	-0,0898	1,0073	0,0000	-0,7155
6,75	0,4525	0,2937	0,0000	-0,0898	0,9355	0,0000	-1,1236
8,25	0,6221	0,0930	0,0000	-0,0898	1,0256	0,0000	-1,8677
9,75	0,7437	0,0766	0,0000	-0,0898	0,7808	0,0000	-1,5978
11,25	0,5255	-0,0279	0,0000	-0,0695	0,8389	0,0000	-1,5922
12,75	0,2676	0,4029	0,0000	-0,0046	0,3340	0,0000	-0,4100
15,75	-0,0120	0,1108	0,0000	-0,0046	0,6509	0,0000	-0,9866
17,25	0,0922	0,2162	0,0000	-0,0046	0,0691	0,0000	-0,3111
18,75	0,1437	-0,0936	0,0000	-0,0046	0,3800	0,0000	-1,0034
20,25	0,3995	0,2192	0,0000	-0,0046	0,0223	0,0000	-0,1370
21,75	0,4059	0,1690	0,0000	-0,0046	0,8775	0,0000	-1,3674
23,25	0,5425	0,0301	0,0000	-0,0046	0,7650	0,0000	-1,2276
24,75	0,4080	-0,2603	0,0000	-0,0046	0,7455	0,0000	-1,4464
26,25	0,2272	-0,1680	0,0000	-0,0046	0,0622	0,0000	-0,3383
27,75	-0,0629	0,1298	0,0000	-0,0046	-0,1350	0,0000	0,0853
29,25	-0,1861	0,3898	0,0000	-0,0046	-0,2510	0,0000	0,3817

*: Values in g (of element or mineral) per kg (of rock) per meter: ((g/kg)/m)
†: Negative value indicates precipitation, positive value indicates dissolution
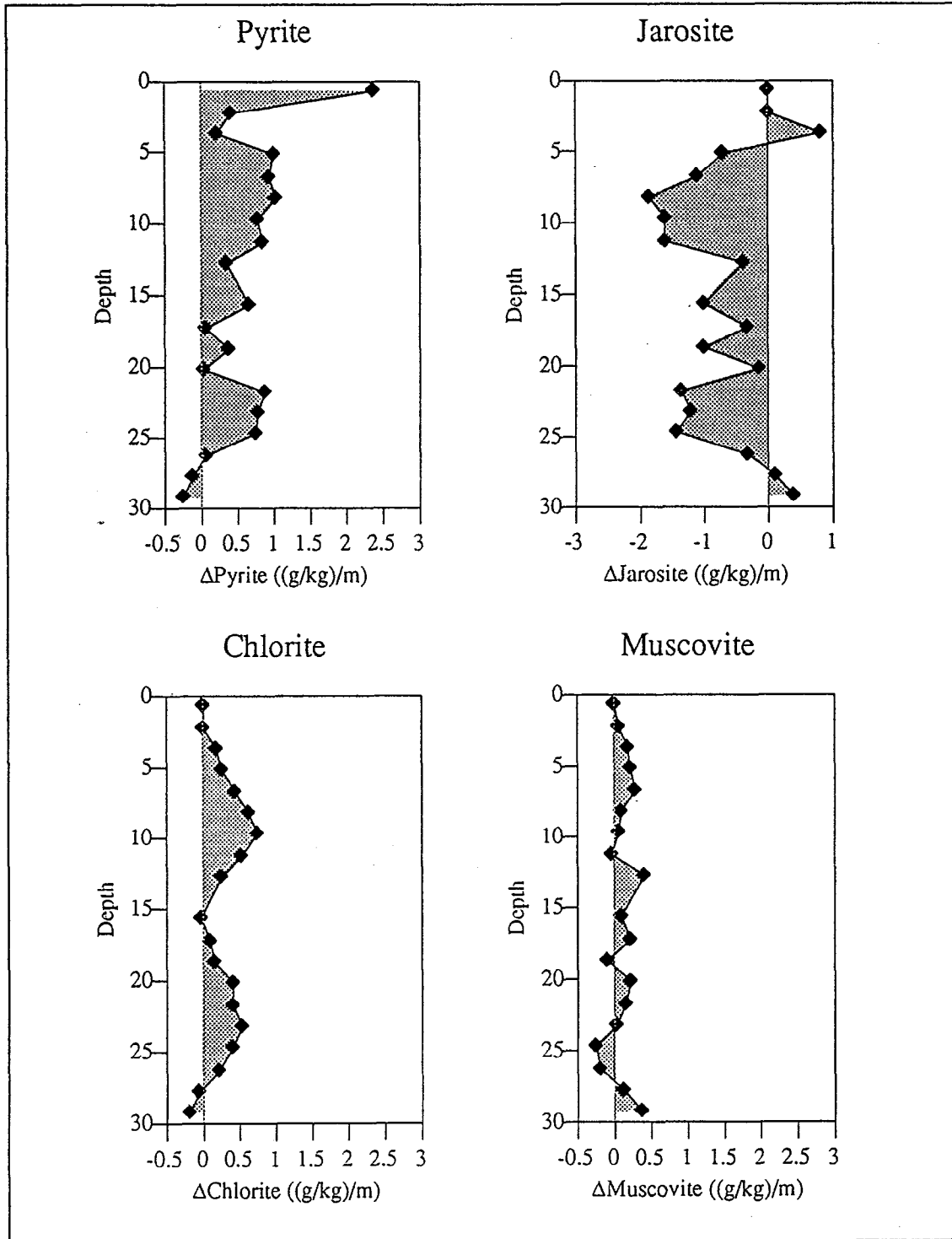
Fig 5.18 Calculated mineralogical mass transfer in BH-7. A positive value indicates dissolution and a negative value indicates precipitation

By examining the Eh values of the leachate (see Fig. 5.14), it is noticed that the first active zone corresponds to a highly oxidizing area in the column. The second zone is also marked by a small but noticeable break in the Eh curve. From these observations, we can postulate on the mechanisms leading to pyrite oxidation. At surface, pyrite oxidation is controlled by oxygen availability (reaction (**1**)). Between 4 m and 10 m, high Eh values suggests that Fe(III) has become the dominant iron species and may oxidizes pyrite following reaction (**3**). Between 10 m and 20 m, Fe(III) is gradually depleted as it oxidizes more pyrite and precipitates as jarosite.

For the second active zone, we can tentatively explain its presence by the topographical configuration of this area of the dump. BH-7 is located on the south plateau, just south of the canyon-like feature (see Fig. 1.3) which is approximately 20 m deep. It is possible that at this level, pyrite oxidation is caused by air being drawn into the pile by convection. In BH-1, at the base of the dump, near atmospheric oxygen levels have already been measured (Gélinas et al. 1991). Gas sampling ports were installed in BH-7 and oxygen measurements will be carried out by the summer of 1994. This hypothesis may then be verified.

5.3.6   CONCLUSION FROM MINERALOGICAL OBSERVATIONS

Mineralogical examination of waste rock samples collected in a borehole and two trenches of a dump producing acid mine drainage was accomplished. Results indicates that after more than 10 years of intense acid water production:

- The source of acidity, pyrite, is not depleted.
- Fast acting neutralizing minerals like carbonates are almost completely depleted.
- Typical secondary phases are goethite (of amorphous $Fe(OH)_3$) in near neutral pH, jarosite in low pH, and gypsum which is not pH dependent.
- Aluminosilicate dissolution plays an important role in the neutralization process, chlorite dissolution being the main source of Mg and Al in solution.
- Muscovite and paragonite are being transformed into a swelling smectite-like mineral phase by loss of structural Al and gain of Mg, before complete acid digestion.
- The breaking-up of the rock and the acceleration of pyrite oxidation is aided by the crystallization of jarosite inside muscovite crystals and gypsum along schistosity planes. Every new opening created this way can give access of the oxidizing solution to previously protected pyrite crystals.

The main weak point of this study was the lack of water quality data. This prevented us from doing geochemical modelling of the interactions between the mineral phases and the pore-water. Collecting pore-water inside such a rock pile, where 2 m diameter blocks are in contact with silt-size particles, is a difficult task and this problem should be getting more attention. The importance of aluminosilicates, or more precisely phyllosilicates, in such an acidic system has been clearly demonstrated. Phyllosilicates transformations and dissolution has an impact on the pore-water quality and on the structural integrity of the rock. On this basis, future work should include evaluation of such minerals for neutralization potential and water quality impact.

5.4   MICROBIOLOGICAL DIVERSITY AND ARD PRODUCTION

5.4.1   BIOLOGICAL OXIDATION PROCESSES

The biological oxidation of metal sulfides is significant in AMD production. Numerous bacterial species are known to participate in this process, these are the acidophilic bacteria *Thiobacillus ferrooxidans* , *Leptospirillum ferrooxidans* , *Thiobacillus thiooxidans* , *Thiobacillus acidophilus* and neutrophilic species such as *Thiobacillus thioparus, Thiobacillus intermedius* . Some synergistic effects have been observed with the acidophiles and a nitrogen-fixing bacterium, *Beijerinckia lacticogenes* , which increased the efficiency of *T. ferrooxidans* in the leaching of metals from metal sulfides.

Pyrite oxidation by microorganisms can be described by the following equations:

$$FeS_2 + 7.5\ O_2 + H_2O \ \text{-----}\!\!> \ Fe_2(SO_4)_3 + H_2SO_4 \qquad (9)$$

$$FeS_2 \ \text{-----}\!\!> \ Fe^{2+} + 2\ S^{\circ} + 2\ e^- \qquad (10)$$

$$Fe^{2+} + H^+ + 1/4\ O_2 \ \text{-----}\!\!> \ Fe^{3+} + 1/2\ H_2O \qquad (11)$$

$$S^{\circ} + 3/2\ O_2 + H_2O \ \text{-----}\!\!> \ H_2SO_4 \qquad (12)$$
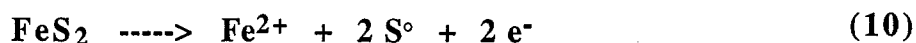
The biological iron- and sulfide-oxidizing activity is maximal at pH 2,5, in the case of the acidophilic species, their activity is also optimal at temperatures varying from 25 to 35°C during aerobic growth (Guay et al., 1977, 1989). Neutrophilic microorganisms can oxidize sulfides and elemental sulfur at pH near 7,0, they rapidly cause the pH to decrease to levels that authorize growth and activity of the more acidophilic bacteria. Moderate (35°C - 55°C) to extreme thermophilic (55°C - 90°C) microorganisms oxidize iron and sulfur (sulfides) at very low pH.

The overall production of acid mine drainage in mine waste rock and tailings most probably starts with the weak acid biological producers slowly paving the way to the strong iron and sulfide-oxidizers.

5.4.2   SAMPLES COLLECTION AND METHODS OF INVESTIGATION

Sample collection

Two types of samples were collected for microbiological analysis: drill cuttings obtained from various dephts and underground water specimens in different local physico-chemical conditions. The drill cuttings were recovered at every 1,5 m when borehole #1 was drilled. The mineral samples were placed in strerile prefilled bottles with growth medium, placed on ice and shipped within 24 h to the laboratory.

Underground water was sampled in devices especially designed to recover water samples and to evaluate bacterial adhesion to any prefered mineral surfaces (see Figure 5.21a). These "bacteria traps" were filled with chunks of local pyrite, sphalerite, chalcopyrite et sulfur pellets and immersed for a period of 40 days in underground water at BH-1, BH-2, BH-4 and BH-6. Each set of four traps was brought back to the surface and two samples of each mineral type was briefly and gently rinced with sterilized distilled water and put in a solution of glutaraldehyde 2% in phosphate buffered saline (PBS) 0,01M, pH 7,0. Other chunks of sulfur and sulfides were placed in sterile containers prefilled with sterile culture medium, kept at 0°C until microbiological analyses were performed.

Analytical methods

Mineral samples recovered from bacteria traps were prepared for scanning electron microscopy as follows: the specimens left in the buffered glutaraldehyde solution were rinced three times with PBS solution and treated with osmium tetroxide 1% solution in PBS for two hours and further rinced 5 times with PBS. Samples were dehydrated sequentialy in a ethanol gradient (30, 50, 70, 90, 95, 99, 99, 99%) and dryed at critical point before mounting on aluminium studs using Ag paint. The specimens were then coated with gold-palladium (400-500 Angström) and examined in a JEOL (JSM-T330A) scanning electron microscope at 30°angle.

Microbiological methods

Microorganisms were isolated from different samples collected on the site using standard microbiological procedures: 5,0 ml of liquid samples were inoculated in 100ml of 9K growth medium and incubated at various temperatures (25°C - 45°C) in a gyrotory incubator shaker (150 rpm) for periods of two weeks. Positive growth was evaluated by microscopic observation, visual observation of the oxidation of ferrous sulfate used as the energetc substrate which turned red after oxidation. 9K medium contained per liter 44,7 g $FeSO_4$; 3,0 g $(NH_4)_2SO_4$; 0,5 g KH_2PO_4: 0,5 g $MgSO_4$; 0,1 g KCl; 0,0125 g $Ca(NO_3)_2$ (Silverman & Lundgren, 1959), the pH was adjusted at 2,5 with sulfuric acid. The presumptive identification was performed after three pure culture transfers on FeTSB solid medium.

In order to evaluate the positive growth of iron-oxidizing bacteria isolated from underground water, the following experiment was initiated: 2,0 L of underground water pumped from BH-4 were centrifuged at 25,000 x g and further sterilized by filtration through a 0,22µm porosity filter. Ammonium sulfate was added to this liquid culture medium at a concentration of 3,0 g/L; the initial pH was 3,36. This medium was inoculated with a aliquot of the original untreated water sample to evaluate the anaerobic growth of the microorganisms.

In another series of experiments, the same basic liquid medium was enriched with $FeSO_4$ to an initial concentration of 60,0 g/L and with $(NH_4)_2SO_4$ at 3,0 g/L. 300ml flasks containing 100 ml of this growth medium were inoculated with an active culture of *Thiobacillus ferrooxidans* ATCC 13661 or with an iron-oxidizing isolate from BH-4 and incubated aerobically at 30°C under constant agitation; sterile controls were run simultaneously under the same conditions until all the ferrous iron was oxidized. When this was attained, the flasks were removed from the incubator

and 0,5 g of tyndallized sulfur/ 0,5 g of sterile pyrite was added to the growth medium and the flasks were introduced in an anaerobic chamber (the gaz composition in the chamber was as follows: 10% H_2, 10% CO_2 and 80% N_2) and incubated at 27°C without agitation for 2 weeks. Periodically, samples were withdrawn from the flasks aseptically and without any gaseous atmosphere perturbation, for iron analysis, pH measurements and bacterial enumeration.

Bacterial enumeration was done using a modified Most Probable Number (MPN) methodology (Lafleur et al., 1993). This procedure is based on the microbiological oxidation of a very low concentration of ferrous iron as a growth indicator. Correlation curve was obtained between bacteria numbers and colorimetrically determined remaining ferrous iron as a function of time. Bacteriological iron oxidation rates were determined using whole bacterial active cultures growing on ferrous sulfate used as an energy source as a function of time during exponential phase of growth. Ferrous iron concentrations were estimated volumetrically using a 0,01N potassium dichromate titrating solution.

5.4.3 RESULTS

Microbiological diversity in drill cuttings

La Mine Doyon south dump is heavily contaminated in terms of microorganisms; bacterial isolates of *Thiobacillus ferrooxidans* , *Leptospirillum ferrooxidans* , *Thiobacillus thiooxidans and Thiobacillus acidophilus* were formerly identified from drill cuttings samples collected at different horizons at BH-1. These bacteria are acidophilic isolates growing best at pH varying from 0,9 to 3,5 in the presence of oxygen, their presence throughout BH-1 indicates that oxygen concentration was not a limiting factor to their activity; in fact, it has been shown that along this borehole, there is a chimney effect bringing fresh air at the base of the dump at this location. *L. ferrooxidans* was more or less confined to a temperate level (10°C - 30°C), it has been demonstrated elsewhere that this microorganism is somehow susceptible to low temperatures but it is very active in terms of pyrite oxidation. The other bacterial strains were distributed from top to bottom of BH-1. Special care was exercised to isolate and characterize moderate thermophiles because of the presence of a strong temperature gradient inside the waste rock dump; in some areas, temperature as high as 65°C were measured. There was no evidence in this present microbiological study of the presence and activity of thermophilic microorganisms but it does not mean that they are absent.

Bacterial iron oxidation activity seems to be maximal where local temperatures appoached optimal growth temperatures. In the case of the mesophilic iron oxidizers, it is near 30°C; above 40°C, *T.ferrooxidans* and other *thiobacilli* are no longer active, there is a shift towards the natural selection of moderate thermophilic microorganisms which can take over the mesophiles.

Microbiological diversity in underground water

As expected, numerous bacteria were isolated from underground water from BH-1, BH-2, BH-4 and BH-6. Figures 5.19 and 5.20 present evidence of the activity of many microorganisms even in BH-6 where underground water temperature was near 40°C. Bacteria thrived in local environments where oxygen concentration is minimal (0,05% at saturation). They seemed to show preference for
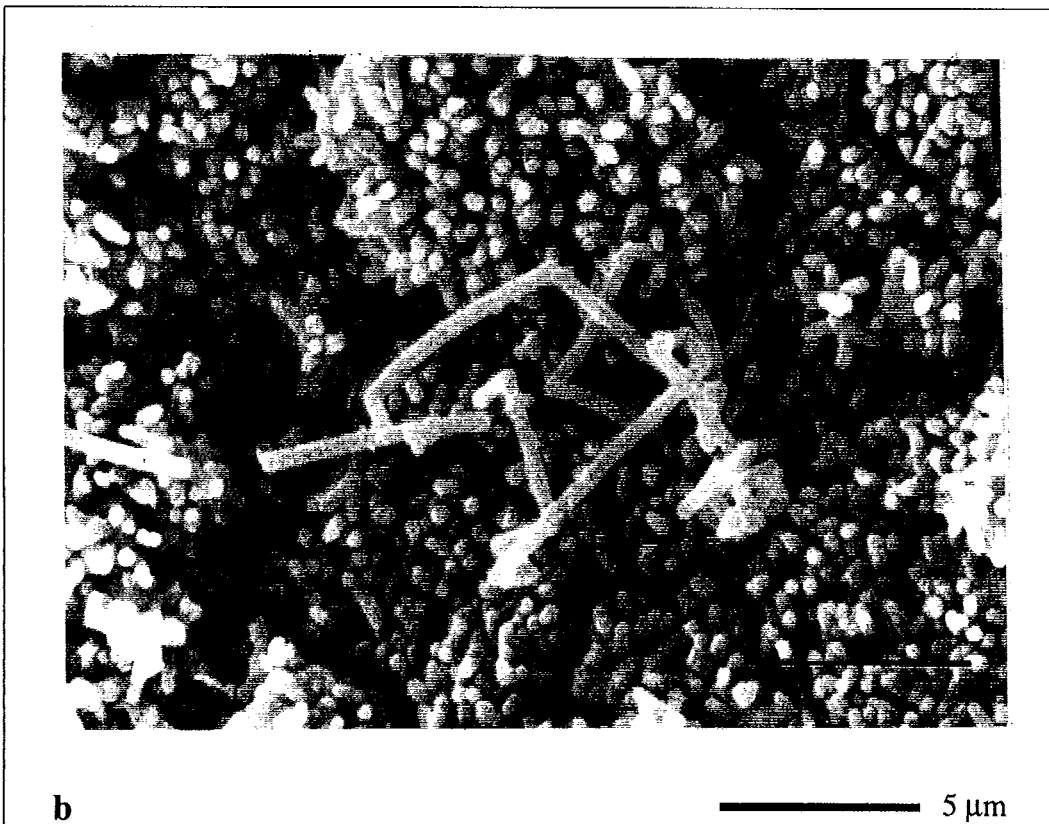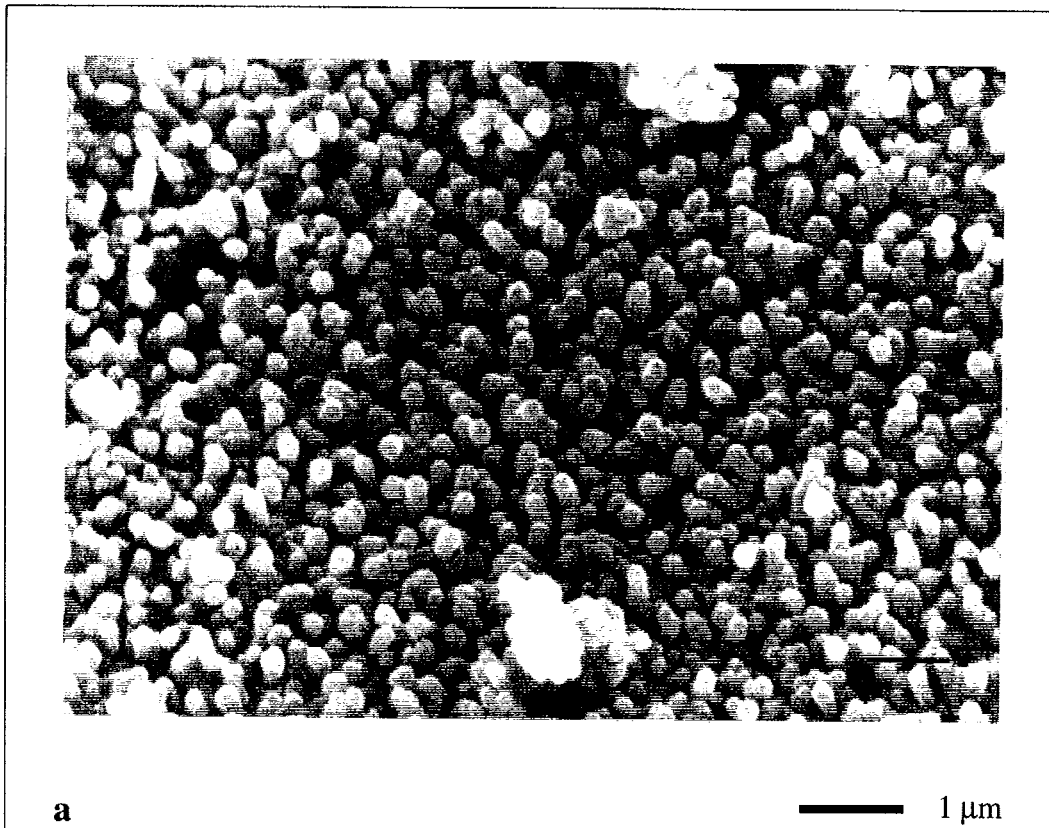
*Fig. 5.19 Isolated bacteria from **a**: BH-1, pyrite grain and **b**: BH-2, chalcopyrite grain*
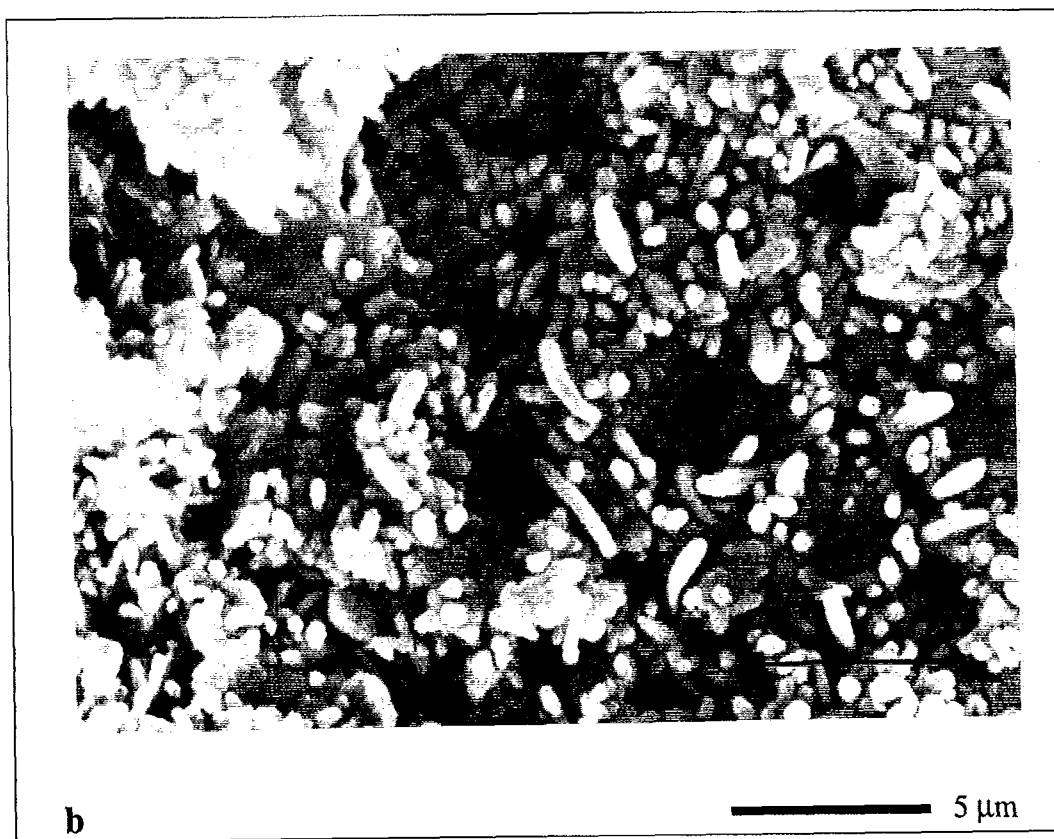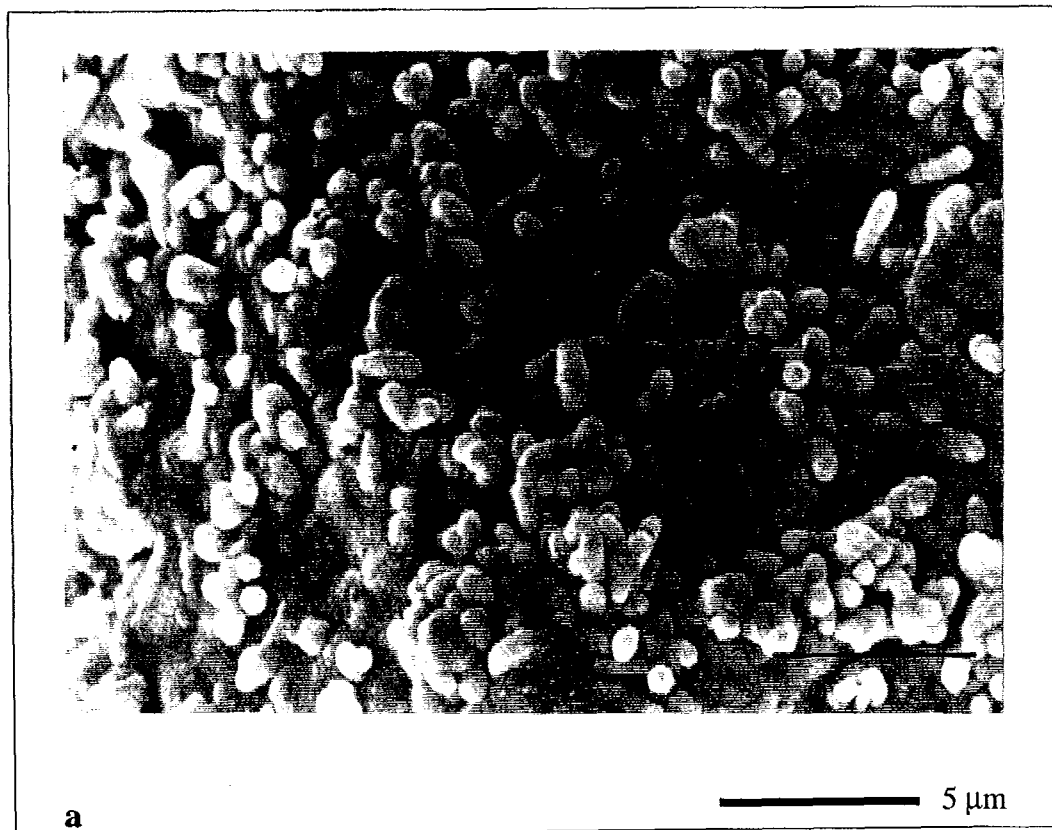
Fig. 5.20 Isolated bacteria from a: BH-4, sulfur (S^o) grain and b: BH-6, sulfur (S^o) grain
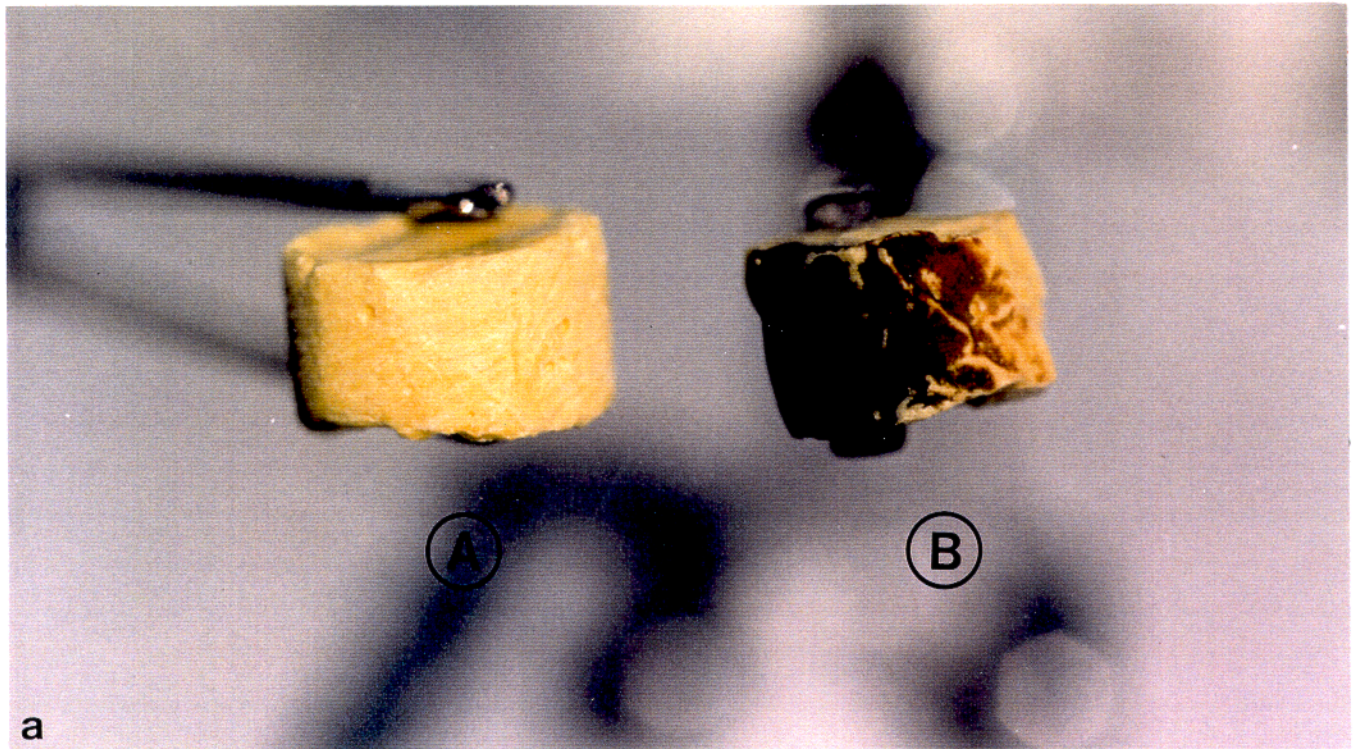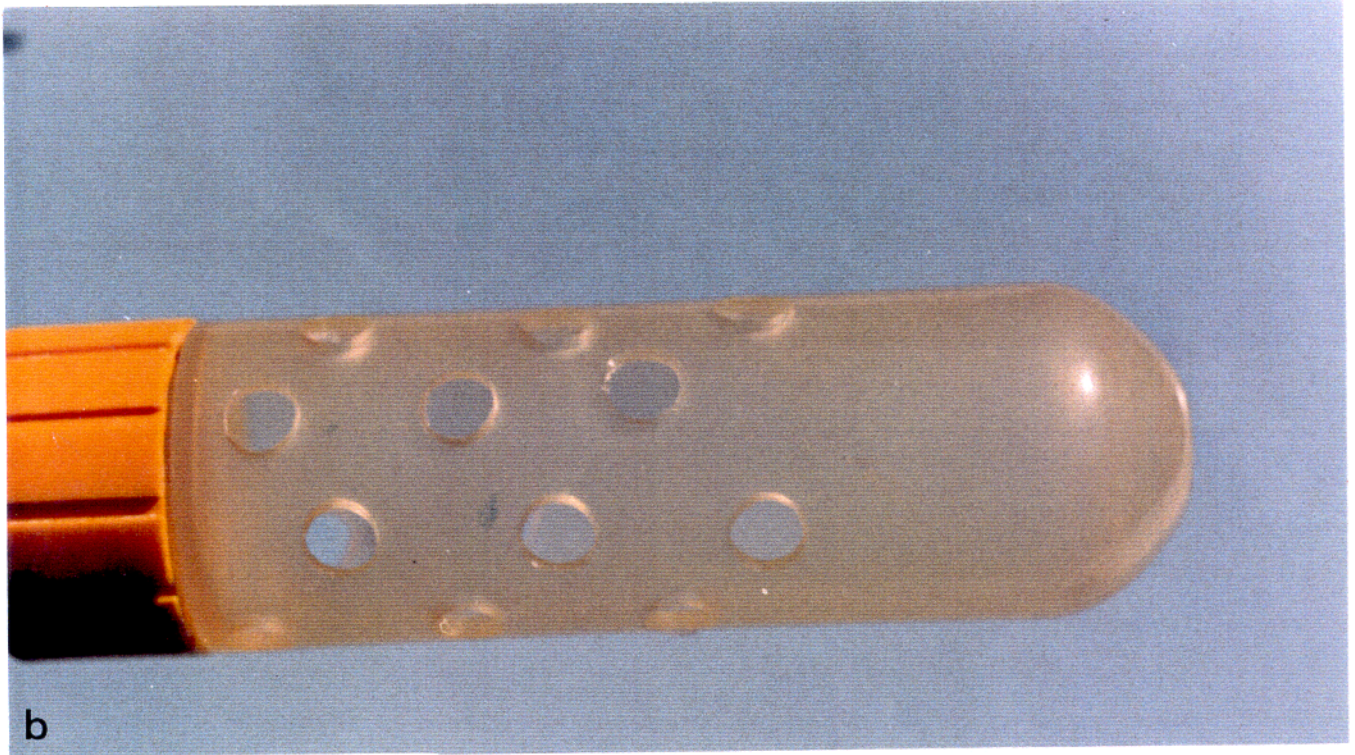
Fig. 5.21 a: Bacteria trap (diameter of trap is 3 cm). b: Secondary iron sulfide precipitation on sulfur pellet immersed in BH-4 during 40 days.

elemental sulfur; all of the tested samples of sulfur pellets revealed heavy colonization of their surface, their oxidative activity on this substrate was so strong that most of the observed bacteria were covered with $CaSO_4$. Pyrite was well colonized in BH-1 while in BH-2 and BH-4, sphalerite and chalcopyrite were respectively much more colonized than pyrite even after forty days immersion in water. In BH-4, it was noted that secondary precipitation of iron sulfide occured on the sulfur pellets (Figure 5.21b), we do not have at this moment any strong evidence that sulfate reducing bacteria are active under the waste rock dump.

However, the observation of the high diversity of microorganisms growing deep under millions of tons of waste rock led us to speculate about their anaerobic activity. We demonstrated in the laboratory that bacteria indigenous to La Mine Doyon site oxidize elemental sulfur at low pH, in complete absence of oxygen, at temperatures varying from 25°C to 30°C, and using available ferric ions as the electron acceptor; during this microbiological process, sulfuric acid was produced (Figure 5.22). The same results were obtained with a strain purchased from American Type Culture Collection, *T. ferrooxidans* ATCC13660 when grown in the same conditions (Figure 5.23). Sterile controls were run simultaneously where no acidification, and no ferric ion reduction was shown during the same period of time; it confirmed the participation of microorganisms in this anaerobic process. These results confirm the previous observations (Pronk et al, 1991; Suzuki et al., 1990)
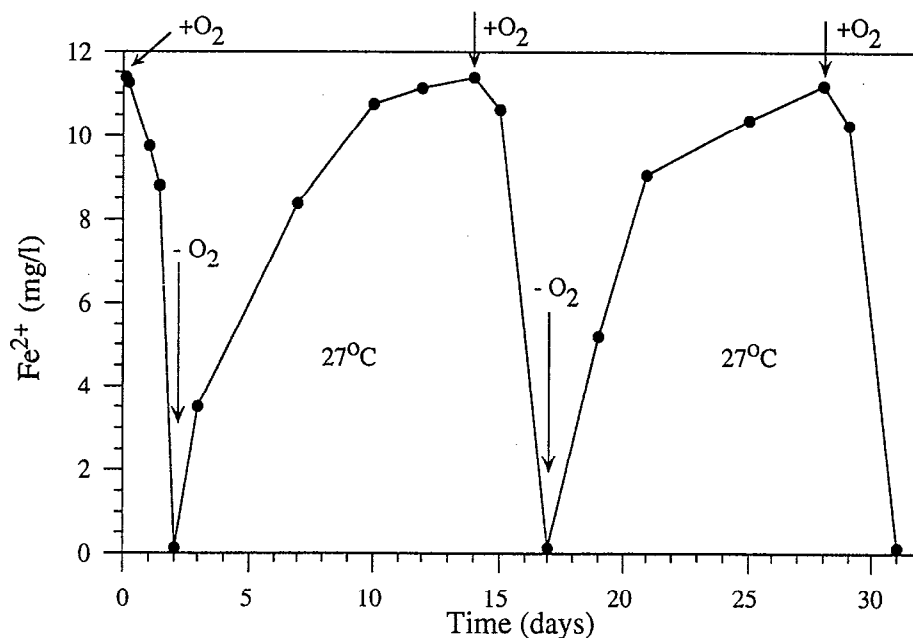
Fig. 5.22 Fe2+ oxidation and Fe3+ reduction cycles during anaerobic respiration on sulfur and aerobic growth on ferrous sulfate of South dump field bacterial isolate (BH-4)
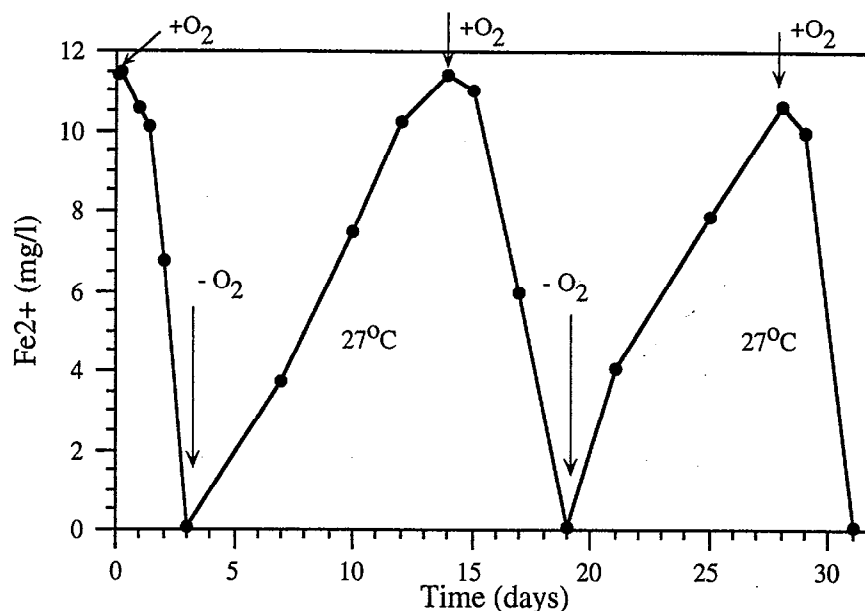
Fig. 5.23 Fe2+ oxidation and Fe3+ reduction cycles during anaerobic respiration on sulfur and aerobic growth on ferrous sulfate of T.ferrooxidans ATCC 13661

5.4.4   CONCLUSIONS FROM MICROBIOLOGICAL OBSERVATIONS

Based on experimental results obtained for the microbiological analysis of boreholes cuttings from well BH-1 and from scanning electron microscope SEM examination of mineral substrates immersed in groundwater at wells BH-1, 2, 4, and 6, we can propose a dynamic reaction model for pyrite and elemental sulfur oxidation in Mine Doyon south dump. Figure 5.24 is a schematic representation of the proposed model. Four zones are observed:

Zone 1:   aerated zone in a waste rock dump where microbiological oxidation of pyrite and elemental sulfur produced during the chemical oxidation of pyrite by ferric ions is most active; species such as *T. ferrooxidans, T. thiooxidans, L. ferrooxidans* should be typical as well as possible other unidentified acidifying or acidophilic bacteria. Microbiological activity is intense as observed on rock fragments from borehole BH-1 drilled in a zone of very active air circulation.

The figure shows a schematic cross-section with four zones. Arrows at the top right indicate H_2SO_4 and $Fe_2(SO_4)_3$. Arrows at lower left indicate CO_2, H_2O, and O_2.

Zone (1):

Oxydation microbiologique

Thiobacillus ferrooxidans Thiobacillus thiooxidans

$$2FeS_2 + 7\ 1/2O_2 + H_2O \longrightarrow Fe_2(SO_4)_3 + H_2SO_4$$

$$S^0 + 1\ 1/2\ O_2 + H_2O \longrightarrow H_2SO_4$$

$$4Fe^{2+} + O_2 + 4H^+ \longrightarrow 4Fe^{3+} + 2H_2O$$

Zone (2):

Oxydation de la pyrite
Altération chimique

$$FeS_2 + 2H^+ + 1/2O_2 \longrightarrow Fe^{2+} + H_2O + 2S$$
$$pH<2.0,\ T:70^oC$$

$$FeS_2 + H_2O + 3\ 1/2O_2 \longrightarrow Fe^{2+} + 2H^+ + 2SO_4^{2-}$$
$$pH>2.5,\ T:70^oC$$

$$FeS_2 + 2Fe^{3+} \longrightarrow 3Fe^{2+} + 2S^0$$
$$pH<2.0,\ T:25^oC$$

Zone (3):

Thiobacillus ferrooxidans

$$S^0 + 6Fe^{3+} + 4H_2O \longrightarrow SO_4^{2-} + 6Fe^{2+} + 8H^+$$

$$HCOOH + 2Fe^{3+} \longrightarrow CO_2 + 2Fe^{2+} + 2H^+$$

Zone (1): Aeration zone with moderate temperatures (0-35 ºC).

Zone (2): Restricted aeration zone at high temperature (40-65 ºC).

Zone (3): Anoxic zone at moderate temperature (15-40 ºC).

Zone (4): Groundwater (saturated zone).

Fig. 5.24 Schematic representation of a microbiological model of acid production

Zone 2: region where oxygen supply is less and less important and where ambient temperature may reach higher temperatures up to 65°C. In this zone, chemical oxidation by oxygen and ferric iron would be more important than microbiological reactions. It is believed that the production of elemental sulfur should occur in that zone. Even if temperatures in the range of 30-65°C are somewhat limiting, microbiological oxidation is possible and should be optimal at 70°C. It could be carried by strands of *Sulfolobus acidocaldarius* and *Acidianus brierleyi* for which optimal pH for growth are respectively 2.0 and 4.0. However these species could not be isolated during this project.

Zone 3: anoxic zone where partial pressure of oxygen is low and where ambient temperature is quite stable between 25 and 35°C. Microbiological activity in that zone is probably high and is due to oxidation of elemental sulfur coupleed with ferric iron reduction in acid conditions. These metabolic reactions have already been characterized (Pronk *et al.*, 1991; Suzuki *et al.*,1990; Brock and Gustafsson, 1976; Sugio *et al.*, 1992).

Zone 4: Groundwater where dissolved oxygen is fed to microorganisms in very limited amounts but where ferric ions are very abundant. Microbiological activity that we have observed can be explained by metabolic reactions based on sulfur and sulfides oxidation since among the minerals that were immersed in groundwater at four wells, only elemental sulfur was densely colonized.

Bacterial oxidation of pyrite requires oxygen and water to proceed. Oxygen is available to bacteria only in its dissolved form in water and its solubility is a function of temperature and its partial pressure. It has been demonstrated that a significant portion of oxygen in sulfates is from water (isotopic measurements). It is then in the higher part of the dump and in natural convection chimneys in the waste rock that we could find *T. ferrooxidans* and *Leptospirillum ferrooxidans* and other species of bacteria that are also acidifying and acidophilic with growth properties similar to *T. ferrooxidans*. Observation well BH-1 was drilled in an area where there is a strong upward air current. Observations on the whole stratigraphic column and in groundwater confirm the model proposed. Oxidation by bacterial activity is very intense and the variety of microorganisms is an index of the metabolic capacities of the microbial world in this environment.

Microbial activity was studied by looking at the influence of temperature and oxygen concentrations on acidophilic strands of ferro- and thio-oxidizing bacteria from Mine Doyon. Partial conclusions from the work to date are:

- High temperature in the dump and groundwater do not prevent microbiological oxidation activity. When temperature is above 40°C the growth of *T. ferrooxidans and L. ferrooxidans* is affected and also oxidation of ferrous iron but other species remain active and oxidation proceeds from sulfides and elemental sulfur. We have been able on two occasions to identify what seems to be *Sulfobacillus thermosulfidooxidans* which grows in temperatures between 20 and 60°C.

- Availability of oxygen is a limiting factor for microbiological pyrite oxidation and covering the dump with an impervious surface may limit drastically the circulation of oxygen. However, we have demonstrated experimentally that thio-oxidant activity of bacteria such as *T. ferrooxidans*

and other bacterial strands from the site can continue when oxygen is totally absent as ferric iron is becoming the electron acceptor. From this point of view, an impervious cover would not prevent microbial activity as long as ferric iron is present in the solution. This last reaction will produce enough elemental sulfur and other sulfides to maintain microbial activity. Conditions observed in well BH-4 seem to confirm that hypothesis.

• Water supplied to the reaction is constant and it is essential to maintain chemical and microbiological activity in the waste rock dumps.

The most unusual microbiological observation ever made on a site is the anaerobic respiration of *T.ferrooxidans* and possibly some other bacterial strains, their questionnable role in the production of sulfuric acid need to be fully assessed *in situ* even if laboratory experiments have shown that this phenomenon could be measured. We do not have evidence of the transient presence of elemental sulfur during the chemical oxidation of pyrite by ferric ions, it could be that this element is too rapidly oxidized by bacteria to be observed under SEM among the alteration minerals in the dump. The impact of these results is significant in the prediction of the acid rock drainage production potential in waste rock.

6/ Thermal processes during AMD production

6.1 - INTRODUCTION

AMD production in waste rocks differs significantly from that in tailings. Waste rock piles generally have a thick unsaturated zone (several meters) and are very permeable due to the coarse nature of the material. The great thickness of waste rock piles allows them to reach high temperatures caused by the exothermic pyrite oxidation beyond the zone influenced by surface temperature. When the wastes are permeable enough, these high temperatures induce density-driven air convection curents within the piles thus providing oxygen for pyrite oxidation.

Very few complete monitoring programs have been done in waste rock dumps. This is why one of the objectives of the project undertaken at the Doyon mine is to provide data on the physico-chemical conditions prevailing in waste rock dumps undergoing AMD production. We are especially concerned with obtaining data which could be used to determine water (hydrology), energy (heat transfer) and mass (geochemistry) balances for the dump. These data are used to characterize the dump and model the physical and geochemical processes responsible for AMD production. Once validated and calibrated, those models could be used to predict the long term behavior of the dump if it is subjected or not to AMD control measures.

This chapter is a summary of a previous MEND report on the analysis of thermal data from La Mine Doyon (Lefebvre et al., 1993). This analysis focuses on the temperature data acquired during almost two years of monitoring (from March 1991 until December 1992). These data are interpreted to determine the thermal properties of the wastes, evaluate the importance of the different heat transfer mechanisms, calculate the heat production rate and relate it to the AMD production rate, and asses the impact of heat transfer on oxygen supply.

We first present the interpretation of the cyclic temperature variations from which the thermal properties of the waste rocks are derived. This analysis also provides information on the magnitude of heat transfer by advection and on the amount of heat stored within the dump. The next section presents an estimate of heat generation rates from temperature profiles. These rates are related to the pyrite oxidation rates and the oxygen supply required. Finally, the relationship between heat generation and air flow is discussed. The analysis presented here is based on analytical solutions and was meant as a guide for numerical modeling. However, this study is necessary because it provides information on material properties and indications of the important physical mechanisms involved in AMD production which have to be modelled numerically.

6.2 - INTERPRETATION OF CYCLIC TEMPERATURE VARIATIONS

6.2.1 - DESCRIPTION OF CYCLIC TEMPERATURE VARIATIONS

Waste rock dumps are submitted to cyclic annual or diurnal temperature variations at their surface. These cyclic variations undergo a reduction in amplitude and a shift in phase as they propagate through the wastes. The magnitude of the amplitude and phase changes depends on the thermal properties of the wastes. Consequently, measurements of the phase and amplitude allow the computation of the thermal properties of the wastes.

At the Doyon mine site, weekly temperature measurements were made with thermistors in six (6) wells at 11 different levels. Figure 6.1 shows selected temperature profiles for each month during the first monitoring year. The profiles show major temperature increases (up to 65°C) above the mean surface air temperature, 2°C in this area. Temperature increases from the surface to reach a maximum value in the upper half or middle of the waste pile and then decreases toward the base. The temperature profiles show important fluctuations near the surface which are induced by cyclic seasonal surface temperature variations. These cyclic temperature changes do not have much influence beyond 10 m depth.
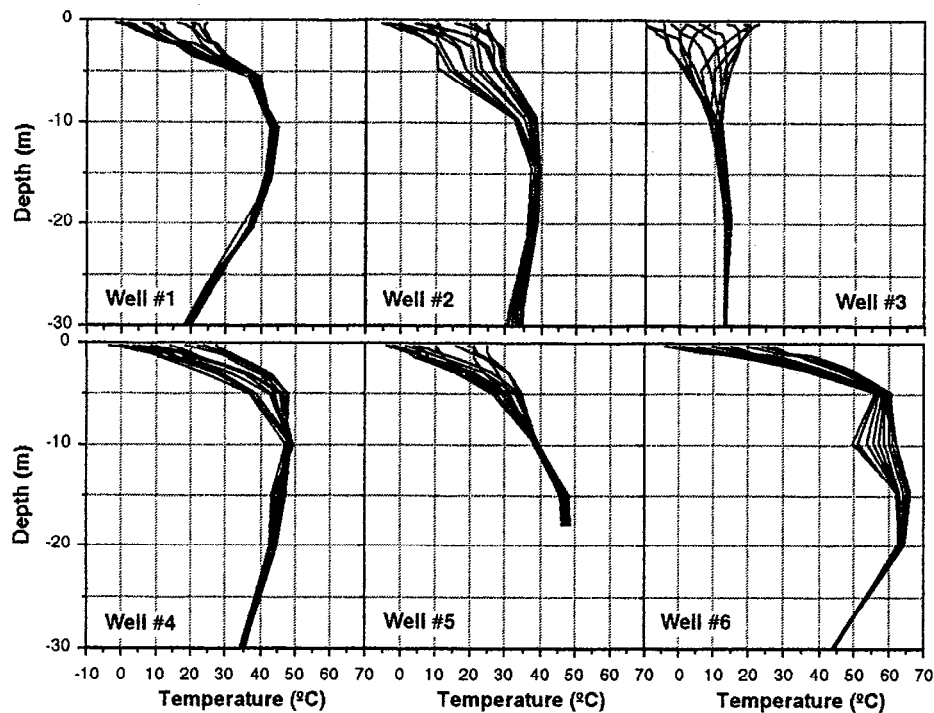
Fig. 6.1 Mid-month temperature profiles for the first monitoring year.

Figure 6.2 provides another view of the temperature data which emphasizes the time variations of this parameter: it shows, against time, all the weekly temperature measurements made during the first monitoring year at each measure point in well #5. The points are the measurements whereas the lines are best fit sinusoidal curves adjusted to the data. This figure shows one annual cycle of temperature changes within the waste dump. Seasonal surface temperature variations have a high amplitude (about ±15 °C) and influence the temperature within the wastes down to at least 10 m. The mean temperature increases from the surface to the center of the waste (this well does not have temperature measurements in the lower half of the dump).

The near surface measurements show more variability because they are influenced by daily cycles and short term weather changes. However, those short term temperature changes do not seem to affect measurements beyond 2 m depth. The amplitude of the temperature changes is reduced as we get deeper within the wastes. Also, there is a shift in the phase of the cyclic variations as it penetrates the dump: the temperature maxima and minima occur at a later time at depth than at the surface. For example, at 0,3 m the temperature change has a 15 °C amplitude and the maximum is recorded in July whereas at a depth of 5 m the amplitude is reduced to less than 5 °C and the maximum occurs in September. As we will show, the change in amplitude and phase with depth of the temperature variations may be used to derive the thermal properties of the waste rocks as well as indicate the magnitude and direction of advection within the dump. The first step, discussed in the next section, is to evaluate the amplitude and phase of the temperature changes at each measure point.
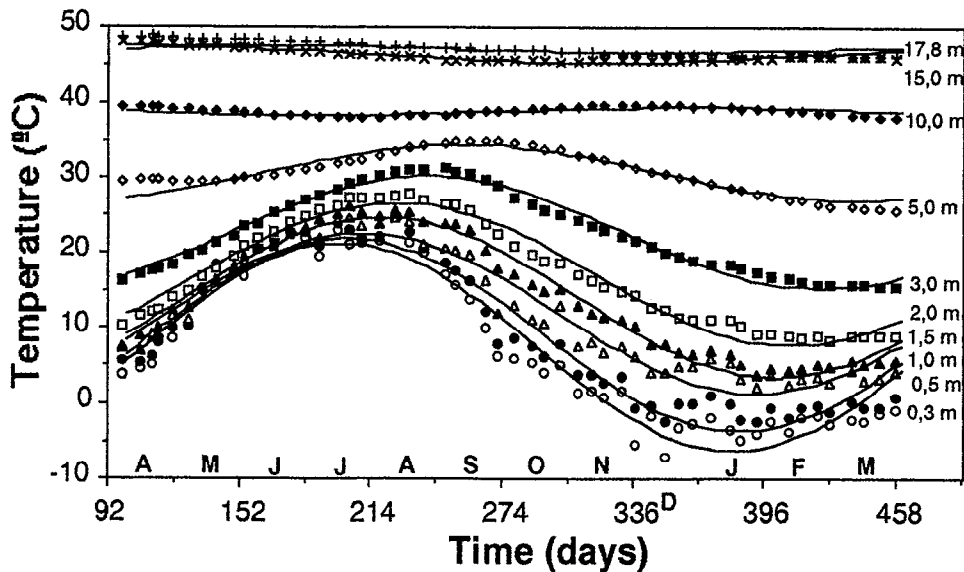
Fig. 6.2 Cyclic temperature variations for monitoring well #5.

6.2.2 - FOURIER ANALYSIS OF CYCLIC TEMPERATURE VARIATIONS

The cyclic nature of the temperature measurements has to be characterized in order to reduce the results of two years of monitoring to a few parameters. Figure 6.3 provides a representative example of the temperature data collected during two years at each measure point. It is apparent that temperature measurements show a cyclic variation but also exhibit a reduction in mean value during the monitoring period. Fourier analysis is then used to translate temperature measurements in terms of a linear trend added to a cyclic sinusoidal variation. As seen in figure 6.3, this type of model allows a good representation of the data. The problem is then to find the parameters which allow the best fit of the data with this model.
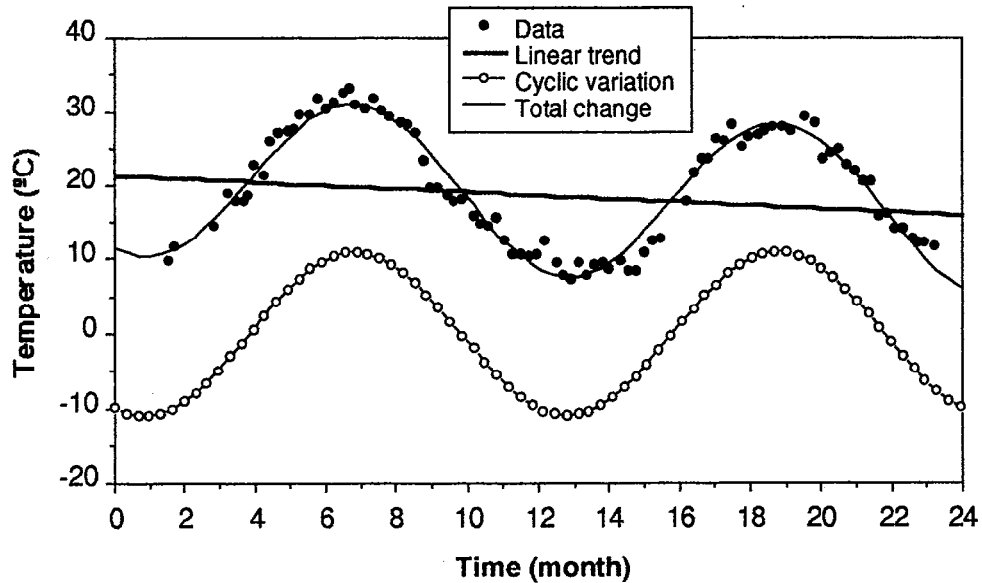
Fig. 6.3 Cyclic temperature variations analysis for Well #6 (1.0 m).

Mathematically, the two components of the model, the linear trend and the cyclic change, are expressed as follows. The linear trend in average temperature $T_a(t)$ (°C) is represented by an initial temperature value T_0 (°C) at time t (day) zero and the slope of the linear change m (°C/d):

$$T_a = T_0 + m t . \qquad (6.1)$$

The cyclic temperature variation with time $\Delta T(t)$ may be expressed as the first harmonic of the Fourier serie, with a one year period, representing this variation:

$$\Delta T(t) = \alpha \cos\frac{2\pi t}{\tau} + \beta \sin\frac{2\pi t}{\tau} = \alpha\, C + \beta\, S, \qquad (6.2)$$

where,

t:	time (days),		α:	cosine coefficient,
β:	sine coefficient,		τ:	variation period (365 days),
C:	$\cos(2\pi t/\tau)$,		S:	$\sin(2\pi t/\tau)$.

The change in temperature with time $T(t)$ will then be the sum of the contributions of the linear trend $T_a(t)$ added to the cyclic trend $\Delta T(t)$:

$$T(t) = T_a(t) + \Delta T(t) = T_0 + m\,t + \alpha\,C + \beta\,S . \qquad (6.3)$$

The four parameters T_0, m, α and β defining the change in temperature with time may be computed from temperature measurements as a function of time at different depths. The method of least squares is used to determine the parameters which allow the best description of the observed temperature as equation 6.3. Once coefficients T_0, m, α and β are determined, cyclic temperature variations may also be expressed in terms of the amplitude ΔT and phase P of a sinusoidal wave using the following transformation:

$$\Delta T(t) = \alpha\,\cos x + \beta\,\sin x = \Delta T\,\sin(x - P) , \qquad (6.4)$$

where,

$$\Delta T = \sqrt{\alpha^2 + \beta^2} \quad \text{and} \quad \tan P = -\frac{\alpha}{\beta} . \qquad (6.5)$$
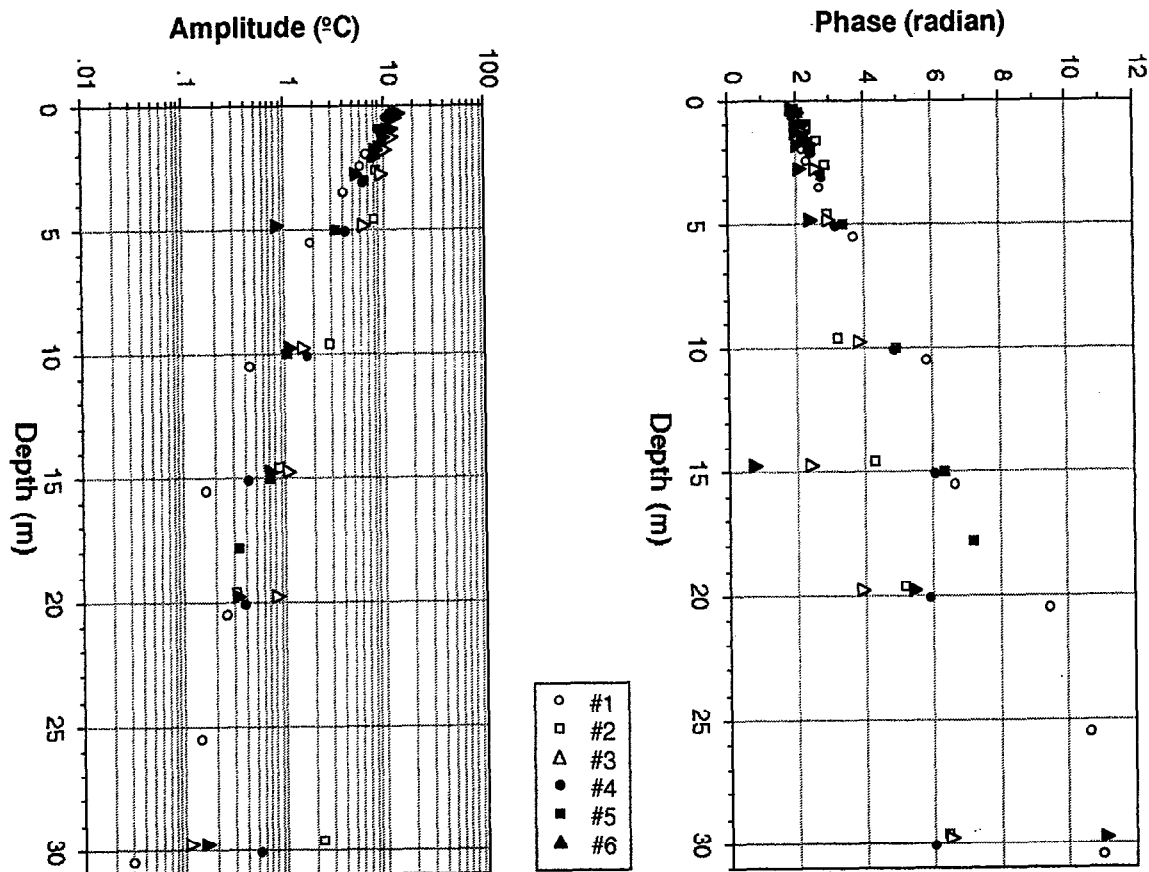
Fig. 6.4 Amplitude and phase as a function of depth for all wells.

Figures 6.4a and 6.4b show respectively the amplitude and phase derived from the Fourier analysis for all temperature measure points as a function of depth. There is an exponential decline in amplitude with depth whereas the phase increases linearly with depth. This behavior is expected from theory and allows an evaluation of the thermal properties of the waste rocks. However, the data below 5-10 meters show much more variability and follow a different trend in amplitude and phase with depth. This behavior may partly be attributed to the larger relative error in the measurements at these level. Also, the fact that temperature does not follow a cyclic variation pattern at these levels but instead may increase or decrease steadily accounts for the erratic behavior of the amplitude and phase estimates. A different air convection regime in the lower half of the dump could also be responsible for the different trends. Consequently, only the near surface measurements will be used to derive the thermal properties of the wastes using the analytical method presented later.

Fourier analysis provides us with the linear trend in average temperature $T_a(t)$ within the dump during the monitoring period. This trend is expressed as an initial temperature value T_0 at time t zero (January 1, 1991) and the slope of the linear change m which may be used to calculate the mean T_m (at February 1, 1992) and final average temperature T_f (at January 1, 1993). Figure 6.5 shows the mean temperature profiles for all wells. The near surface temperature tends toward the mean air temperature which is 2 °C in that area. Temperature increases rapidly in the top five meters to reach between 25 and 60 °C except for well #3 which exhibits a much smaller temperature increase and only reaches about 14 °C. Maximum temperature is located between 10 and 20 m and varies between 40 and 65 °C (except again for #3). Temperature slowly decreases from the maximum to values between 20 and 45 °C at the base of the dump. Temperature measurements in the saturated zone at the base of the piezometers have shown that temperature gradients remain about constant below the unsaturated zone (not presented in this report). Temperature close to the surface is different for each well. The wells with the highest temperature within the dump tend to also have the highest temperature at the surface.
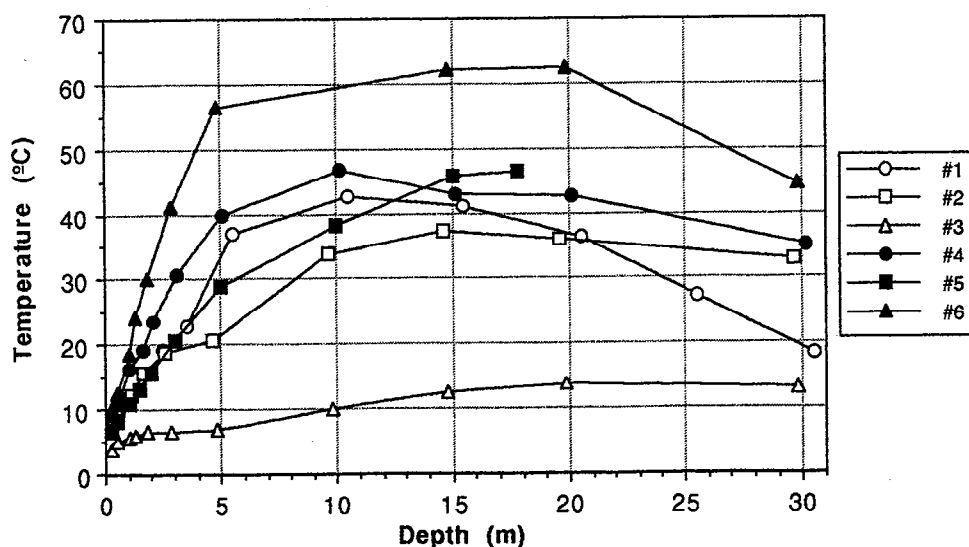
Fig. 6.5 Mean temperature profiles for all wells.
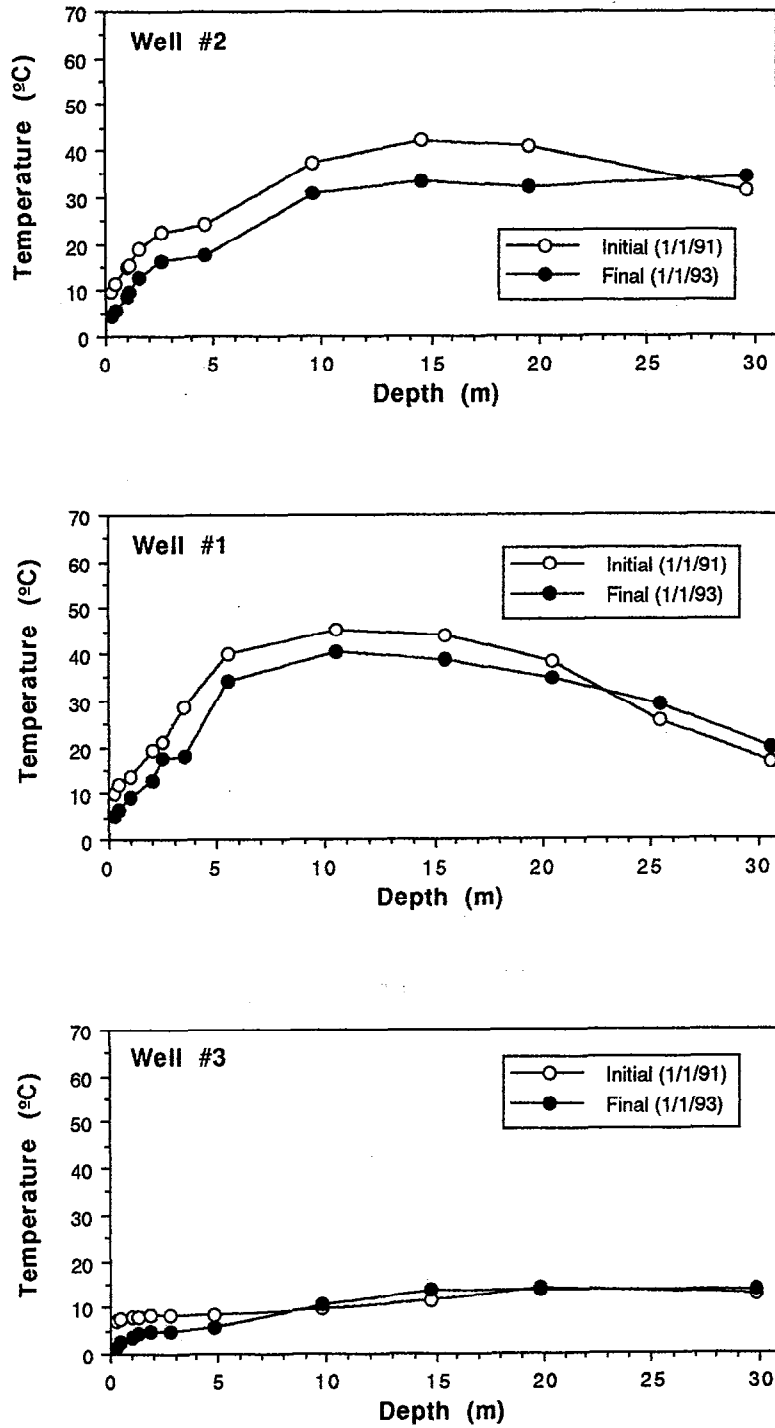
Fig. 6.6 Initial and final temperature profiles.
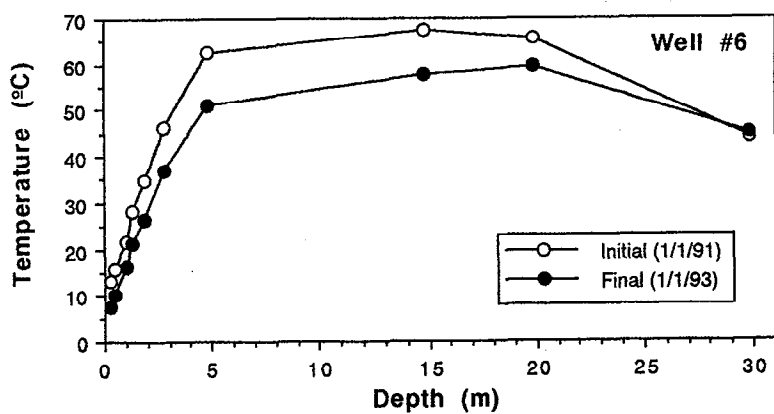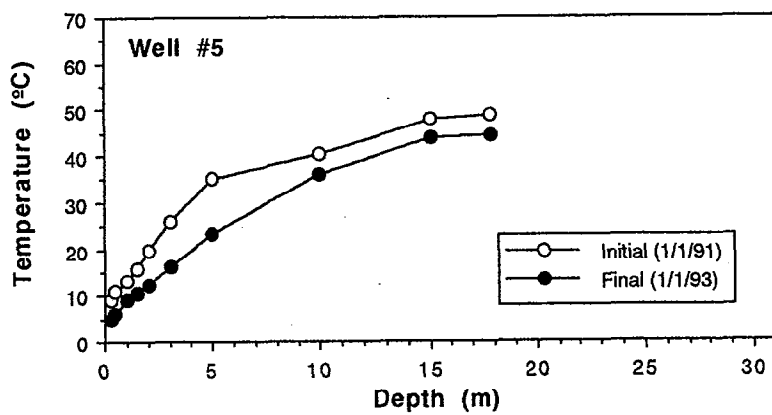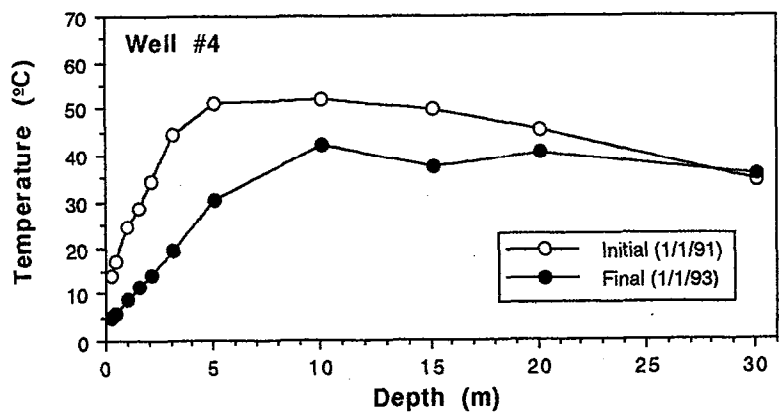
Fig. 6.6 (continued) Initial and final temperature profiles.

Figure 6.6 shows a comparison between average initial and final temperature profiles for all wells. All wells but #3 show a significant decrease in average temperature during the monitoring period. The larger temperature decrease in well #4 can be explained by the about 10 m deep excavation of waste rocks only 15 m north of the well. These operations were done in the spring and summer of 1992 to obtain backfill material for the mine. By comparing the temperature data before and after the excavation, we determined that this new exposed vertical face near well #4 not only caused heat loss but also changed the air circulation pattern in this area (compare results with Lefebvre et al., 1992). These average temperature profiles may be used to calculate the average heat stored within the dump at the beginning and end of the monitoring period.

6.2.3 - EVALUATION OF THE THERMAL PROPERTIES OF WASTE ROCKS

The problem of heat transfer by conduction and advection in one dimension in a system subjected to a cyclic surface temperature was solved analytically by Stallman (1965). Heat transfer by conduction and advection is described by the following differential equation:

$$k_t \frac{\partial^2 T}{\partial z^2} - q c_o \rho_o \frac{\partial T}{\partial z} = c\rho \frac{\partial T}{\partial t}, \qquad (6.6)$$

where: k_t: medium thermal conductivity (solid and water) (W/m °C),
   T: temperature (°C), z: positive downward depth (m),
   q: fluid flux (m/s), c_o: fluid heat capacity (J/kg°C)
   ρ_o: fluid density (kg/m³), c: medium heat capacity (J/kg°C)
   ρ: medium density (kg/m³), t: time (s).

To solve equation 6.6, we take as a first boundary condition that the surface is undergoing a cyclic temperature variation of period τ (s). The second boundary condition is that, as depth tend toward infinity, the temperature reaches the mean temperature at that level T_{mz}. The solution for the temperature variation $T(t,z)$ (°C) as a function of time t (s) for a depth z (m) is given by:

$$T(t,z) = T_{mz} + \Delta T\, e^{-az}\, \sin(2\pi t/\tau - bz) , \qquad (6.7)$$

where, T_{mz}: mean temperature at depth z (°C), τ: variation period (s),
   ΔT: surface temperature variation amplitude (°C).

Parameters **a** and **b** are defined as follows:

$$a = [(K^2 + V^4/4)^{1/2} + V^2/2]^{1/2} - V , \qquad (6.8)$$

$$b = [(K^2 + V^4/4)^{1/2} - V^2/2]^{1/2} , \qquad (6.9)$$

where,

$$K = \frac{\pi c\rho}{k_t \tau} \quad \text{and} \quad V = \frac{q c_o \rho_o}{2k_t}. \qquad (6.10)$$

These two relationships define a system with two unknowns K and V. Stallman (1965) presents a solution method using the ratio of parameters a and b. However, this method is cumbersome and does not allow the determination of V in the case where fluid advection is upward (q is negative). The system may be solved more simply by defining the unknowns K and V directly as functions of parameters a and b (see Lefebvre et al., 1993):

$$V = \frac{b^2 - a^2}{2a},$$ (6.11)

and

$$K = ab + bV,$$ (6.12a)

or, in terms of a and b:

$$K = ab + b\frac{b^2 - a^2}{2a}.$$ (6.12b)

The solution method then consists in determining parameters a and b graphically from the temperature data, evaluating V and K from relationships 6.11 and 6.12, and, finally, calculating k_t and q by transforming relationship 6.10:

$$k_t = \frac{\pi c \rho}{K \tau} \quad \text{and} \quad q = \frac{V 2 k_t}{c_o \rho_o}.$$ (6.13)

Parameters a and b are derived respectively from plots of attenuation A and phase difference ΔP with depth z. Regressions of amplitude and phase with depth for the near-surface data were made for each individual well. Table 6.1 presents the values of parameters a and b derived from those plots and the computed values of thermal conductivity k_t and advective fluid flux if the fluid considered is water or air.

Table 6.1 Thermal conductivity and fluid flux from Stallman's solution

Well	a (m^{-1})	b (m^{-1})	k_t (W/m °C)	q_{air} (m/d)	q_{water} (m/y)
1	0.336	0.255	2.92	-7.2	-3.1
2	0.168	0.385	0.97	12.0	5.3
3	0.163	0.260	2.62	11.4	5.0
4	0.221	0.287	2.31	6.1	2.6
5	0.239	0.295	2.22	4.8	2.1
6	0.364	0.095	10.67	-62.6	-27.3

The net advective heat flux results from the simultaneous flow of water and air. Water infiltration in the unsaturated zone is always vertically downward whereas air flow is driven by density gradients generated by temperature differences in the waste rock pile. Air flow is also controlled

by the creation of convection cells. In the upper half of the dump, temperature increases rapidly with depth and air flow is generally upward. The advective heat flux ($q\ c_o\rho_o$, J/m^2 s) will then be the sum of the water advective flux $q_w c_w \rho_w$ and the air advective flux $q_g c_g \rho_g$ which may have opposite directions (q positive downward):

$$q\ c_o\rho_o = q_w\ c_w\rho_w + q_g\ c_g\rho_g\ . \tag{6.14}$$

Fluid fluxes in table 6.1 were calculated for water and air if either fluid were the only one contributing to advective heat transfer. Negative signs indicate upward fluxes. Water infiltration cannot explain upward advective heat transfer. Also, the magnitude of water fluxes required to explain advective heat transfer is an order of magnitude higher than the infiltration values expected. Annual precipitations are in the order of 0.8 m in the area, so infiltration is not expected to exceed 0.5 m. Hydrographs from weir stations and the lysimeter data provide us with estimates of infiltration lower than this value. It follows that water flow cannot be the main contribution to advective heat transfer. Advective heat transfer, especially upward, may thus only be explained by air convection at a rate of a few meters per day.

The thermal conductivity k_t computed using Stallman's solution are generally in a normal range and close to the values used by Cathles and Apps (1975). However, the values obtained for wells #2 and #6 which have higher advection rates are very different and may not represent the true medium properties. If we exclude these two wells, the average thermal conductivity obtained is 2.52 W/m °C. This value will be used in the following section to calculate the heat production rate.

We can get more information from tha amplitude and phase data. The difference between the values of parameters **a** and **b** is an indication of the magnitude and direction of advective heat transfer. Figure 6.7 shows that the relationship between attenuation and phase for near-surface data is different for each well and is indicative of advection direction. The direction of advective heat transfer can be determined from the ratio of parameters **a** and **b**. A ratio **a/b** of one indicates no significant advective heat transfer whereas a ratio above one indicates an upward net advective heat transfer and a ratio below one indicates a downward net advective heat transfer.

Advection direction also affects the shape of temperature profiles. Wells where advective heat transfer is upward (#1 and #6) have steeper near surface temperature gradients and reach their maximum temperature values at shallower depths than wells in which advective heat transfer is downward (#2, #3 and #5). Well #3 does not have high temperature gradients to generate important air flow. Well #5 has a fine grained overburden material within the waste rock which may prevent upward air movements. Well #2 may be within a downward circulating convection current. These conclusions generally agree with infrared thermographic surveys even though more work could be done to explain the behavior of each individual well. This is further discussed later.
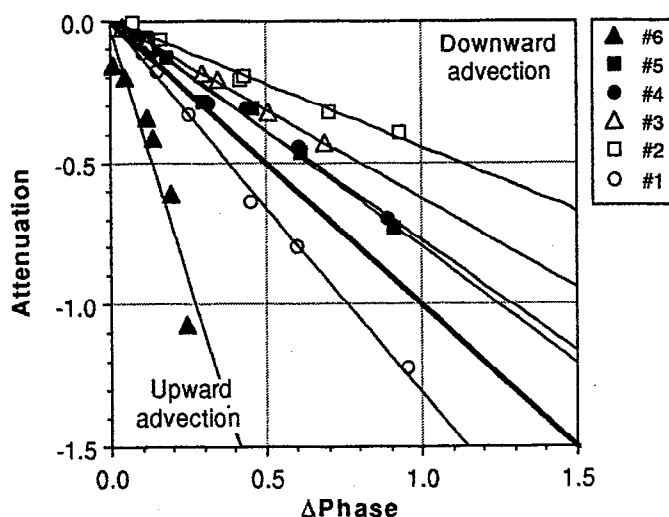
Fig. 6.7 Relationship between attenuation and phase for all wells.

It is important to note that thermal conductivities and fluid fluxes derived form this analysis are effective properties affected by the near-surface temperature gradients. In wells where high temperature gradients prevail, the effective thermal conductivity will be higher than would be the case in an isothermal system. Numerical modeling is needed to better evaluate the effect of upward heat conduction and advection when the system is submitted to cyclic temperature variations and to asses the effect of water evaporation and condensation. However, the analysis does show the importance of advection in the transfer of heat in the system.

6.3 - HEAT PRODUCTION IN WASTE ROCKS

As mentioned before, heat production in waste rocks undergoing AMD production may be related directly to pyrite (or another sulfide) oxidation. If heat production rates can be evaluated, the rate of pyrite oxidation can be derived as well as the rate of oxygen consumption. Two methods were used to derive the heat production rate from the mean temperature profiles. A simple conduction model is first used, followed next by an analytical solution also taking into account advection and oxygen supply. Neither model can fully describe all the mechanisms of heat transfer in a waste rock dump but they do provide simple means of estimating the heat production rate.

6.3.1 - SIMPLE CONDUCTION MODEL

In a steady state system in which conduction is the dominant heat transfer mechanism, the heat production rate may be calculated simply from the relationship:

$$Q(x) = -k_t \frac{d^2T}{dx^2}. \qquad (6.15)$$

This relationship requires the knowledge of thermal conductivity k_t and the temperature gradient variation d^2T/dx^2. k_t was derived in the previous section and we may use a value of 2.5 W/m°C as representative of the waste rocks. d^2T/dx^2 may be derived from a correlation of temperature measurements with depth. Wells #1, #2, #4, and #5 have a similar temperature profile and are judged representative of the general thermal regime in the waste dump. Figure 6.8a shows a third order polynomial regression of the mean temperatures with depth for these wells.

The heat flux by conduction q (W/m^2) is given by Fourier's law. Figure 6.8b shows the heat flux q and the heat production rate Q derived from the correlation in figure 6.8a. Negative values of q indicate an upward flux whereas positive values are for downward flux. The use of a third order polynomial implies a linear decrease of heat production Q with depth since the second derivative of temperature with depth will be linear. The correlation would also indicate that no more heat production occurs below 22 m depth. The total heat production per unit area in the dump is then obtained from the difference in heat fluxes at the top of the pile and at 22 m depth. The value so derived is 20 W/m^2 and represents a pyrite oxidation rate of 55 kg/year for every m^2 of dump surface and thus represents a very important mass of pyrite oxidized.

6.3.2 - CONDUCTION AND ADVECTION MODEL

An analytical model of steady state heat transfer by conduction and advection in a medium where heat is being generated has been derived (Lefebvre et al., 1993). The solution provides the temperature as a function of depth $T(x)$ (°C) above the normal temperature of the medium T_m (°C):

$$T(x) - T_m = \left[\frac{T'_b}{Ae^{Ab}} - \frac{B}{EA + A^2} e^{-(E+A)b} \right](e^{Ax} - 1) + \frac{B}{E^2 + AE}(1 - e^{-Ex}), \quad (6.16)$$

where,

$$A = \frac{qc_0\rho_0}{k_t} \quad B = \frac{FC_0K_{Ox}}{k_t} \quad E = \sqrt{\frac{K_{Ox}}{D_e}}.$$

F: conversion factor (0,4 MJ/mol), K_{Ox}: kinetic rate constant (s^{-1}),
D_e: effective diffusion coefficient (m^2/s), C_0: surface oxygen conc. (9,4 mol/m^3).
T'_b: temperature gradient at the base of the dump (°C/m).

The model supposes pyrite oxidation has first order kinetics with respect to oxygen concentration and that oxygen supply is by diffusion. These assumptions are equivalent to supposing an exponential decline in heat production from the surface. So, even though air convection is an important mean of oxygen supply, the model can still be used to represent heat production and transfer. One further limitation of the model is the use of a unique value for fluid flux. Since air flow is actually dependent on temperature gradients it would not necessarily be constant throughout the dump.

The model was applied to all wells and the mean temperature profiles were used to identify representative parameters to fit the model to the data. Since the model still requires a few parameters as input, most of these were kept the same for all wells. Only the ease of oxygen supply through the wastes (represented by D_e) and the magnitude and direction of advection (represented by the fluid flux) were modified from one well to the next. The magnitude of advection as indicated by table 1 could not be used directly since the model does not represent the same phenomena as the analytical solution. However, the direction of advection was respected for all wells but #4. In that case, the advection direction was recently changed by excavation near the well so that, in the middle of the monitoring period, advection was still upward for that well.
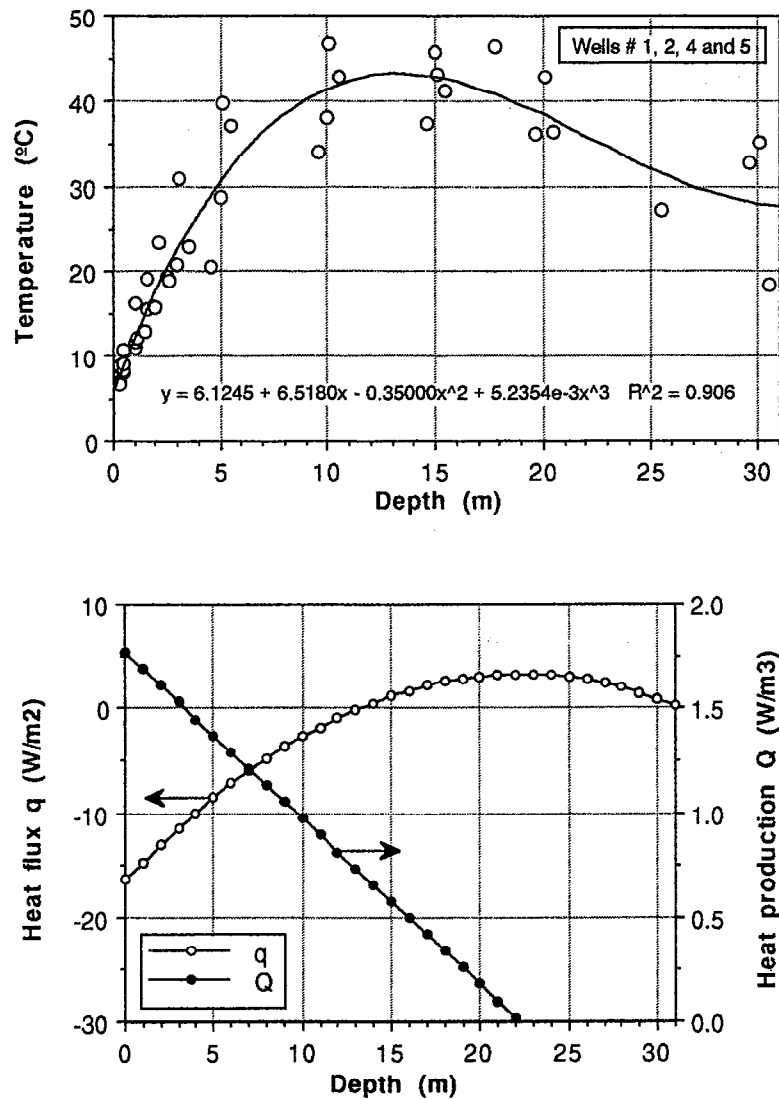
Fig. 6.8 a) Polynomial temperature correlation with depth.
b) Heat flux and production from the conduction model.

We will present the results of the model for two wells with opposite advection direction to illustrate how it affects the shape of the temperature profiles. Figure 6.9 shows the temperature profile, heat flux and heat production for well #1 derived using an upward advective flux. These results do not necessarily represent an optimal solution but one representative of the measured temperature. Figure 6.10 shows the same parameters derived for well #5 where downward heat transfer by convection is considered. For similar heat production profiles, the temperature distribution is very different.
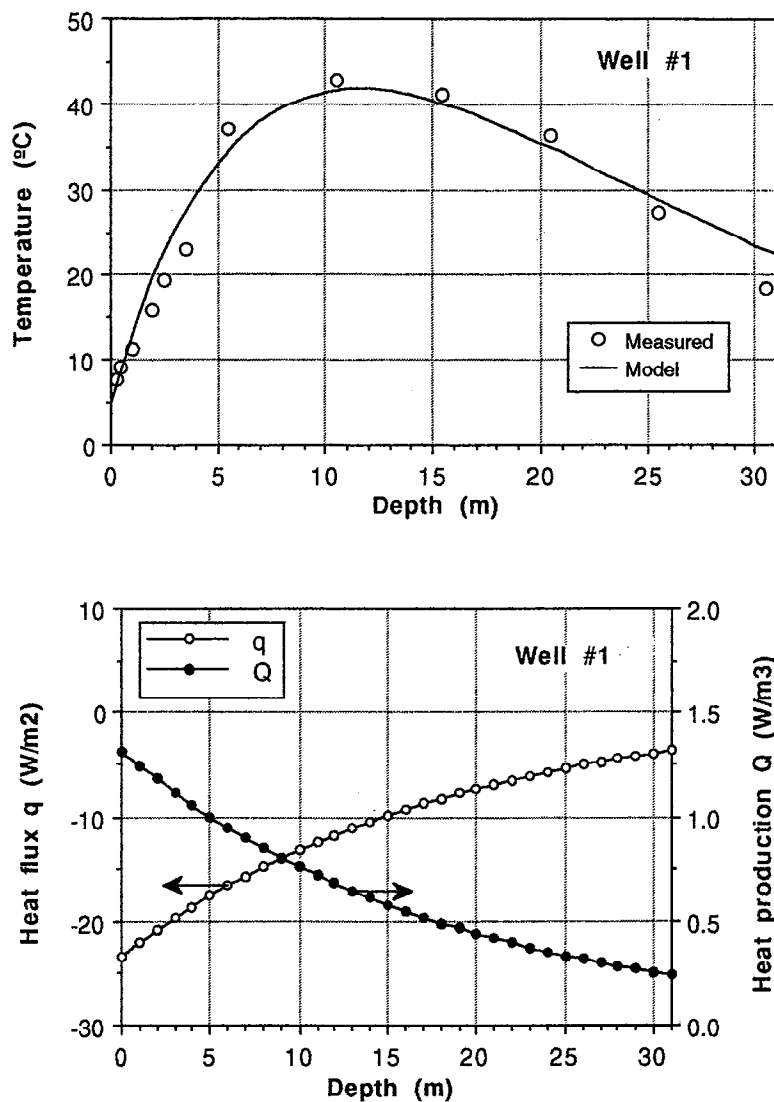
Fig. 6.9 a) Temperature computed from the advection model (well #1),
b) Heat flux and production from the advection model (well #1).

The wells for which the cyclic temperature data indicated significant upward advective heat transfer (wells #1, #6 and #4 for the mean profile) are the ones showing steep near surface temperature gradients and a maximum temperature in the upper half of the dump. The other wells (#2, #3, #5 and the final temperature for #4), which did not have indications of upward advective heat transfer, show more gradual temperature increases and reach a maximum temperature in the lower half of the dump.
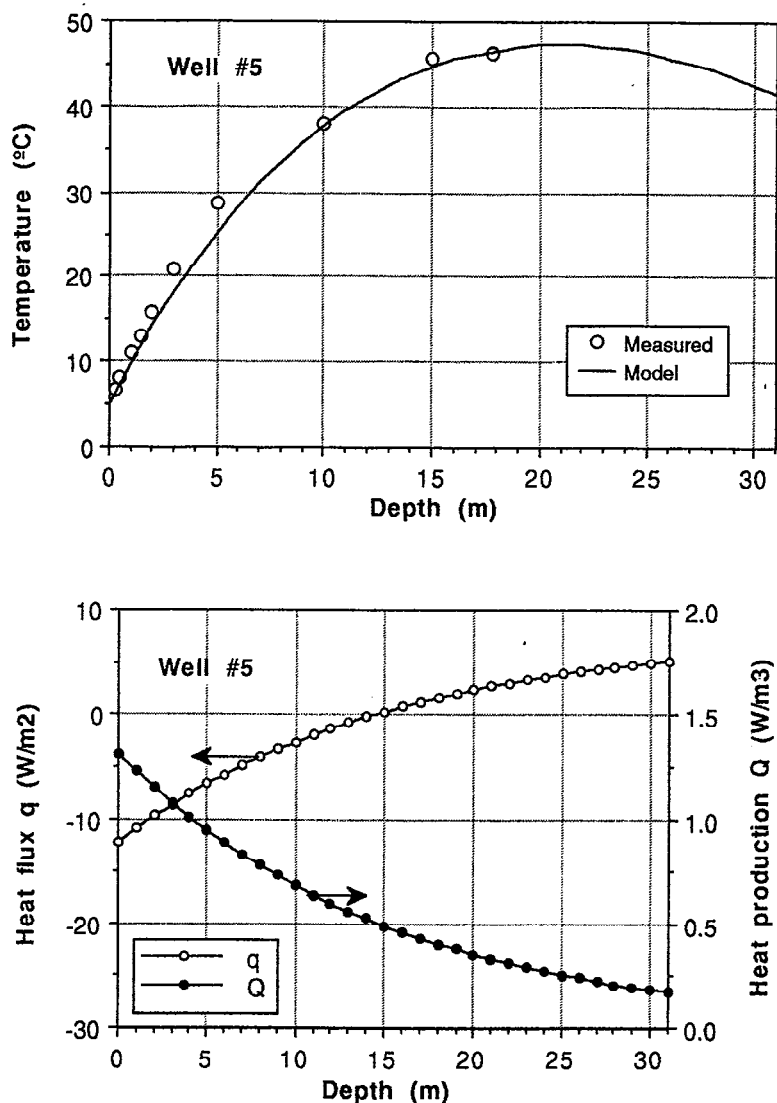
Fig. 6.10 a) Temperature computed from the advection model (well #5),
b) Heat flux and production from the advection model (well #5).

The total heat production per unit dump surface area Q_t (W/m^2) is obtained by integration of the heat production curve generated from the model. If we except well #3 with 7.6 W/m^2, the other wells have total heat production ranging from 15.4 to 20.9 W/m^2. These values are in the same

range as the results from the simple conduction model. It is interesting to compare this production rate with the heat stored in the dump (Lefebvre et al. 1993). The total heat production rate calculated would generate between about 490 and 660 MJ of heat per year. This means there is an amount of heat stored in the dump equivalent to between 2.5 and 4 years of heat production at the present rate.

This estimate has very practical importance, especially when compared with similar evaluations on water and acidity stored within the dump which come out with about the same magnitude of accumulation relative to the annual production (not discussed in this report). This stored "potential" implies that whatever is done to control AMD production in the dump, it will take some time before the results are felt because of the high "inertia" of the system.

6.3.3 - AIR CONVECTION CONCEPTUAL MODEL

Several lines of evidence indicate the importance of air convection in the South Dump. These evidences are the visual observations on the dump surface, the temperature profiles, the air composition within the dump, the oxygen requirements to sustain the observed heat production rate, and especially the thermographic surveys of the dump surface. These evidences allow the development of a conceptual model on the patterns of air convection within the dump.

Quantitative evidences of air convection are provided by the temperature profiles. The relationship between attenuation and phase derived from the cyclic temperature variations indicate the presence of important upward and downward air flow in different parts of the dump. The air movement also affects the shape of the temperature profiles which are also diagnostic of the advection direction. The analytical advection model developed confirmed the effect of air advection direction on the shape of the temperature profiles. The two types of temperature profiles illustrated in figures 6.9 and 6.10 would be generated by convection cells in which regions of upward and downward air movement would be present.

The best evidences of air convection were provided by infrared thermographic surveys of the dump surface. These surveys will not be discussed in details here but the main conclusions drawn from these measurements will be mentioned. These surveys allow the identification of relatively hot or cold surfaces on the dump. These are interpreted as representing respectively areas of hot air exit from the dump and areas of cold atmospheric air entry in the dump. The airborne survey indicated that important air entry occurs at the base of the dump and hot air exits at the upper rim all around the dump. Within the dump, irregular patterns emerge indicating the presence of areas of air entry and air exit arranged in irregular convection cells. These features are interpreted as evidences for the general size of convection cells within the dump.

If convection cells are supposed having about the same dimensions vertically as the ones observed horizontally, they would then indicate that the convection cells are restricted to the upper half of the dump. Actually, there are other evidences for the presence of two sets of convection cells in the upper and lower half of the dump. First, air convection is driven by differences in air density controlled by temperature gradients. Since temperature reaches a maximum at about the center of the dump, air could have opposite advection direction in the upper and lower half of the dump.

Furthermore, the observed air composition in the dump shows relatively high oxygen concentration in the upper half of the dump whereas the lower half is depleted in oxygen.

These evidences would indicate that two different convection regimes exist in the dump: 1) rapid convection in the upper half driven by steep temperature gradients bringing in oxygen from the surface and 2) slow air movement (or even stagnant air) in the lower half of the dump due to the slowly upward increasing temperature gradients. The air in the lower half of the dump is not in contact with atmospheric oxygen and could actually be trapped thus explaining the very low oxygen concentration in this zone. Trapping is further supported by the high CO_2 buildup (to more than 5% in places) in the lower half of the dump which is likely the result of partial leachate neutralization by carbonates. Also, the convection patterns seem to be quite stable in time as shown by thermographic surveys done in the last three years. The stability of the patterns is also indicated by gas composition within the dump which shows little variation in time for a given well.

Figure 6.11 schematically summarizes our present view of the air convection patterns within the dump based on the monitoring data presently available. The dump is believed to have two convection zones: a fast convection zone at the edge and the upper half of the dump and a slow convection (or stagnant air) zone in the lower half of the dump. Zones of upward and downward air movement show different temperature and oxygen concentration profiles. In zones of downward air movement, the temperature profiles have a relatively low near surface temperature gradient and maximum temperature is reached in the lower half of the dump. In these zones, oxygen concentration is near atmospheric values in the upper half of the dump but remains near 5% below the middle of the dump. In zones of upward air movement, temperature profiles show steep near surface temperature gradients and reach a maximum value in the upper half of the dump. In these zones, the oxygen concentration in the upper half of the dump is lower than atmospheric values probably because some oxygen is consumed as air circulates down through the dump before moving back up.

An important aspect to mention is that heat production, and thus AMD production, is higher near the surface of the dump than below despite the fact that temperature reaches a maximum value in the middle of the dump. The reason why temperature is not also at its highest value where heat production is at its peak is simply that more heat is loss near the surface of the dump than in the middle which is far from heat loss surfaces. Trenches and lysimeters provide evidence for high oxidation rates near the surface. High concentration leachate is recovered from the lysimeters even near the surface. Also, new minerals (mainly gypsum and jarosite) are seen forming just a few meters below the surface thus indicating that leachate oversaturation with respect to these minerals is reached at these shallow depths.

Advection plays a large role in heat transfer but it has a great impact as well on the AMD production rate since it is the main source of oxygen supply for pyrite oxidation. Actually, the pyrite oxidation rates indicated by this study would require unrealistic oxygen diffusion rates if advection were not controlling oxygen supply. The conceptual model for air circulation in the dump is based on the monitoring data available. However, numerical models developed by Cathles and Schlitt (1980), Pantellis and Ritchie (1991) as well as our own results also predicted the formation of convection currents in waste rock piles. The measurements, observations, and data analysis done for this project actually confirm the importance of advection for heat transfer in

waste rock dumps. The next step is to model these processes numerically in order first to further characterize the properties of the dump and then to better describe the mechanisms responsible for AMD production in waste rock dumps.
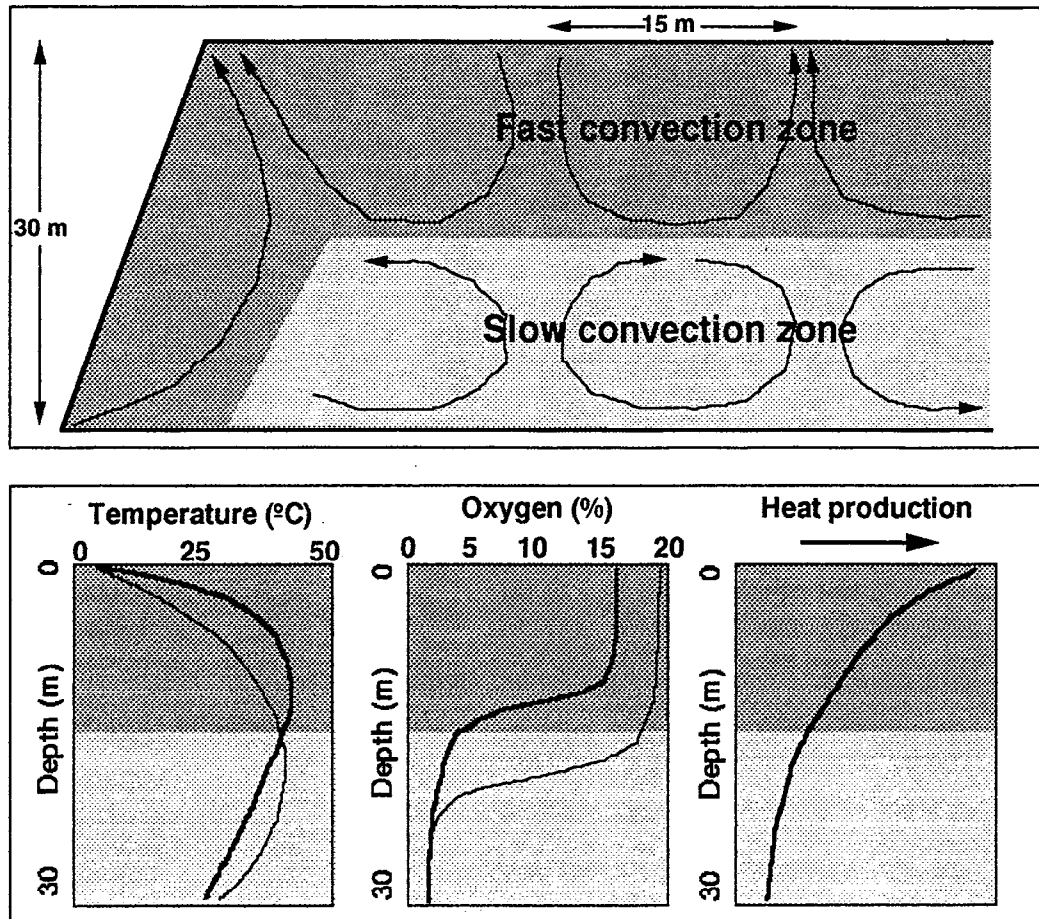
Fig. 6.11 Schematic diagram of air convection patterns.

7 - Numerical modeling of AMD production in waste rocks

7.1 INTRODUCTION

7.1.1 NUMERICAL MODELING OBJECTIVES

Our objectives for AMD numerical modeling are 1) to provide a better understanding of the physical processes involved in AMD, 2) to allow the integration of available waste rock characterization data, 3) to indicate which new data or studies are required to fill the gaps in our quantitative understanding of AMD processes, and 4) to supply a tool for the prediction of the evolution of AMD production with time taking into account the impact of control methods. Each of these objectives is further explained.

Numerous physical and geochemical processes are involved in AMD production. Most of these processes are coupled: they influence each other so that it is difficult to study them independently. It is thus difficult to understand these interactions without numerical modeling which allows the simultaneous quantitative representation of most of the coupled processes involved. For example, modeling allows the determination of the conditions required for the onset of air convection which changes drastically the behavior of AMD producing waste rock dumps. It follows that numerical modeling gives us a better fundamental understanding of AMD production.

The characterization and monitoring program put in place at La Mine Doyon allows the determination of most physical properties of the material and the knowledge of the physico-chemical conditions prevailing within the dump. Only numerical modeling provides a way to integrate this wealth of data within a single framework and the capability to evaluate the impact of these properties on the overall behavior of the system. Modeling also allows the testing of the likelihood that a given estimated parameter is realistic based on the results that it produces. In turn, the acquired data allow the validation of the model and indicate its limitations.

Modeling provides a way to identify the parameters having the greatest influence on AMD production and thus requiring the most careful evaluation. The results of modeling also indicate data which should be acquired to confirm certain model predictions. There is a necessary feedback between modeling and monitoring: characterization provides the conditions which must be replicated by modeling and models make predictions which must be verified by characterization. Those research activities are thus better carried jointly. Numerical models elaborated without field data risk being unrealistic whereas characterization and monitoring data may just be an unstructured collection of facts without the quantitative integration capability of modeling.

Considering the still limited state of our knowledge on AMD production, especially in waste rock dumps, numerical modeling is first meant as a research tool allowing a better fundamental understanding of the processes involved in AMD. However, it is also applicable to the prediction of long term AMD production behavior. The quality and precision of these predictions will keep improving as we develop a better quantitative understanding of the processes involved in AMD and ways to characterize in the field or lab the properties controlling these processes. Following these developments, modeling will become more applicable to the solution of practical field problems and will allow the prediction of the impact of AMD control methods. Such capabilities are necessary to guide the future design of waste rock dumps in which AMD production will be minimized and also to optimize the impact of control measures required at existing sites in operation or being decommissioned. The high cost involved in the implementation of any AMD control method requires ways to predict their impact and numerical modeling is one of the ways needing to be developed.

These objectives can only be met following sustained research efforts. It is our hope that our own research may be a useful step in that process and may help guide future studies. In the following section, we define the characteristics required by numerical models to properly represent AMD production.

7.1.2   REQUIRED MODEL CHARACTERISTICS

We would like here to define the general characteristics required from numerical models to properly represent AMD production. We describe 1) the type of system required and its components, 2) the physical processes needing to be represented, and 3) the conceptual model which may be used for the oxidation process.

AMD production takes place in partially saturated porous media and requires the physical proximity of gaseous oxygen and pyrite. A gas phase must then be part of the system. Reaction products (sulfate, acidity, metals) are released and transported in solution so a liquid phase is also required. Finally, since pyrite is contained in a solid phase, the properties of solids affecting the system must also be represented.

If we suppose that properties of the solids may be treated globally, it is not necessary to include specifically a solid phase and its components in the system. It would also be possible to simplify the representation of the liquid and gas phases by neglecting the exchange of components between these phases as it is done in certain models (Cathles and Schlitt, 1980; Pantellis and Ritchie, 1991). However, a more realistic representation has to take into account the dissolution of air and oxygen in the liquid phase in which the oxidation reaction takes place. Also, the exchange of water between the liquid and gas phases may have important implications on heat transfer and water saturation distribution in this system having important spatial temperature variations.

It follows that, ideally, the numerical model should have a system with liquid and gas phases (besides the solid phase) in which the components are 1) water, 2) oxygen, and 3) the other atmospheric gases grouped in one term. Since temperature and oxygen concentration change

slowly within waste rock dumps, thermodynamic equilibrium conditions are assumed locally. The distribution of components between fluid phases and the water vapor pressure are then supposed in equilibrium locally based on temperature and oxygen concentration.

Many physical processes are involved in this multiphase and multicomponent system. The first process to include is mass transfer by advection. Multiphase gas and liquid flow may be represented by the generalized Darcy's law using capillary and relative permeability properties of porous media (Dake, 1978; de Marsily, 1986; Pruess, 1987 and 1991; Parker, 1989). This representation takes into account water infiltration and gas convection under pressure or temperature gradients. Mass transfer of components in the gas phase may also take place by diffusion under concentration gradients and must also be represented. Finally, heat transfer must also be taken into account since sulfides oxidation reactions are strongly exothermic and may produce high temperatures. In such a system, the processes contributing to heat transfer are conduction, fluid advection (liquid and gas) and diffusion. The effect of water phase change on heat transfer must also be taken into account. This may be done by using the specific enthalpies of the fluid phases to represent their heat content and the effect of phase changes.

Pyrite oxidation influences the system by heat and mass (sulfate, acidity and iron) production and the consumption of pyrite and oxygen (water consumption may usually be neglected). The magnitude of these sources and sinks depends on the volumetric oxidation rate which may be estimated by a reaction core model. These models take into account the reduction in oxidation rate resulting from a decrease in the proportion of pyrite available. The release of mass (sulfate, acidity, metals) outside the dump is dependant on the release and transport of mass in solution. Mass transport by liquid advection must then be represented to properly account for the accumulation and release of mass in waste rock dumps. The assumption made in some models that mass is released outside a dump as soon as it is produced within a waste rock dump just does not properly represent the behavior of these systems.

7.1.3   DESCRIPTION OF THE APPROACH TAKEN

In order to rapidly and efficiently develop AMD modeling capabilities, a search was made to identify an existing general purpose numerical model which already allowed the representation of the most important physical processes involved in AMD production. Besides a reduction in development time, this approach allows us to benefit from the experience acquired by other researchers on the numerical representation of multiphase non isothermal processes. The literature review by Mangold and Tsang (1991) indicates programs having the required capabilities and adaptable to AMD modeling.

The numerical model TOUGH2 (Pruess, 1991) appeared to be the most suitable to represent AMD since this program already represents all the physical processes involved in AMD. TOUGH2 is a general model, using a proven numerical scheme, written in standard FORTRAN and portable on any computing platform. SUN workstations have been used for the numerical modeling. Despite its already wide capabilities, TOUGH2 required important modifications to allow it to model AMD. First, one component had to be added to the system since TOUGH2 only considered air and water. Oxygen must be explicitly specified as a component since it controls the oxidation rate and is

consumed in that reaction. Adding a new component meant also adding a new primary variable to keep the system determined.

New subroutines also had to be written 1) to represent the reaction core model and compute the sources and sinks resulting from pyrite oxidation, 2) to evaluate sulfate mass production and transport, and 3) to make mass balances after pyrite consumption. Other new subroutines were required to output results of interest to AMD and allow the graphical representation of results. The public domain UNIX geophysical graphics system GMT (Wessel and Smith, 1991) was used for two dimensional representation of the fluxes and scalar properties in the dump and to show the evolution of conditions with time. The model developed is further described after a presentation of the reaction core model derived to represent the oxidation process in waste rocks.

7.2   REACTION CORE MODEL

7.2.1   GENERAL CONCEPTS

In waste rock dumps, pyrite is contained in rock blocks and surrounded by other minerals contrary to mine tailings in which pyrite grains are mostly free. Pyrite oxidation proceeds from the surface of waste rock blocks. As pyrite near the surface is oxidized, the oxidant must penetrate within the blocks to reach unreacted pyrite. A zonation appears within waste rock blocks with an external zone in which pyrite is completely oxidized and an internal core where pyrite is unreacted (figure 7.1). The whole of pyrite within a block is not oxidized simultaneously because the rate of oxygen consumption generally exceeds the rate of oxygen diffusion in the blocks. Cathles and Schlitt (1980) mention that the general validity of the reaction core models is supported by the field observation of waste rock blocks in which pyrite has disappeared in their external portion but is unreacted within their core. The same observation is made at La Mine Doyon where cubic holes at the surface of waste rock blocks indicate that pyrite has been oxidized whereas pyrite is still present inside the blocks and shows no signs of oxidation.

Reaction core models provide a link between the pyrite oxidation surface reaction kinetics and the volumetric oxidation rate in waste rocks. They must account for the concentration and surface of pyrite exposed within waste rocks and consider the supply of oxidant within the blocks by diffusion. These models also establish a relationship between the reduction of pyrite fraction and its impact on the volumetric oxidation rate. That relationship allows a determination of the time required to oxidize a given mass fraction of the pyrite initially present within the waste rocks.

Several reaction core models have been proposed to represent the processes acting during AMD production in coarse materials. We tried to synthesize the most interesting characteristics of existing reaction core models which have been used for the numerical modeling of AMD. The model of Cathles and Schlitt (1980) is used as the main basis for the derivation of a new model with some features retained from the models of Jaynes (1983) and Pantellis and Ritchie (1991). The mathematical derivation follows the theoretical guidelines provided by Levenspiel (1972). Lefebvre (1994) presents the details of the reaction core model derivation and describes its main features. We will briefly mention here the main characteristics of this model.
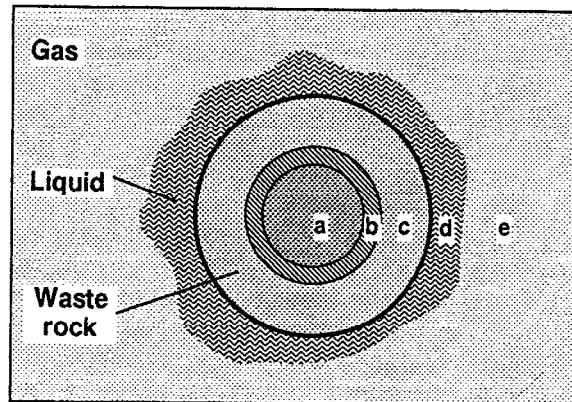
a) Internal zone with unreacted pyrite.

b) Layer in which pyrite oxidation takes place and where oxygen is consumed.

c) External zone in which pyrite is oxidized and through which oxygen diffuses to the oxidation layer.

d) Liquid phase surrounding and saturating the waste rocks and in which oxygen concentration is in equilibrium with the gas phase.

e) Gas phase between the waste rocks. Oxygen supply takes place in that phase by diffusion and advection.

Fig. 7.1 Reaction core model of pyrite oxidation in waste rocks.

Like Pantellis and Ritchie (1991), our reaction core model uses only oxygen as the effective pyrite oxidant thus making a direct link between oxygen concentration in the gas phase and the oxidation rate. This characteristic also avoids the need for leachate speciation which would have to be made if ferric iron were also directly considered as an oxidant. The model considers the effects of both the surface reaction kinetics and the rate of oxygen diffusion as controls on the volumetric oxidation rate. This characteristic was used by Cathles and Schlitt (1990), Jaynes (1983) and Levenspiel (1972). Pantellis and Ritchie (1991) who used only diffusion as a control on volumetric oxidation obtained a formulation predicting an infinite oxidation rate at initial conditions. The volumetric oxidation rate is also supposed independent of the geochemical conditions within the leachate, such as pH, Eh and ions concentrations. This same supposition was made by Cathles and Schlitt (1980) as well as Pantellis and Ritchie (1991) to avoid having to perform speciation calculations as for the model developed by Jaynes (1983).

Certain parameters limiting the oxidation rate were included in kinetic factors formulated in a way similar to Jaynes (1983). High temperatures were supposed limiting bacterial activity and the oxidation rate. Otwinowski (1993) mentions that this effect could be accounted for by the reduction in oxygen solubility at high temperatures. So, even though oxygen solubility is

supposed constant in the numerical model, the temperature kinetic factor indirectly accounts for this effect. A minimal oxygen concentration was also prescribed as done by Jaynes (1983) to account for the minimal oxygen content required for bacterial activity.

7.2.2   FORMULATION OF THE REACTION CORE MODEL

The first order kinetic constant k_{Ox} (m/s) represents the rate of oxygen consumption during the surface oxidation reaction of pyrite and has a relatively constant and well determined value (Otwinowski, 1993). However, one has to distinguish between the surface oxidation rate and the volumetric oxidation rate Q_{Ox} (kg/m^3 s) observed in a unit volume of waste rocks. This last rate is related not only to surface oxidation but is also controlled by the oxygen diffusion rate in waste rock blocks. The reaction core model provides a relationship to determine this rate:

$$Q_{Ox} = -K_{Ox}\, X_T\, X_{WO}\, \rho_{Ox}^{air}\, f(X),\qquad\qquad (7.1)$$

where:

K_{Ox}:   Global volumetric kinetic constant (s^{-1}),

X_T: Temperature kinetic factor (0 to 1),

X_{WO}:   Oxygen partial density in the liquid phase kinetic factor (0 to 1),

$\rho_{air,Ox}$:   Oxygen partial density in the air (kg/m^3),

$f(X)$:   Geometric factor of the proportion of pyrite remaining X (0 to 1).

The kinetic constant K_{Ox} is here a global parameter related to the volumetric oxidation rate in a unit volume of waste rocks having a porosity n. This parameter takes into account the surface kinetic constant k_{Ox} (m/s), the surface area of pyrite per unit volume of rock $a_{rock,Py}$ (m^{-1}), the conversion factor between the partial densities of oxygen in the gas and liquid phases γ (-), the thickness of the layer in which pyrite oxidation takes place δ (m) and the radius of waste rock blocks R (m):

$$K_{Ox} = \frac{3(1-n)k_{Ox}a_{Py}^{rock}\gamma\delta}{R},\qquad\qquad (7.2)$$

The geometric factor $f(X)$ takes into account the kinetic effect of the reduction in the proportion of unreacted pyrite X in waste rock blocks. The larger the proportion of reacted, the further has oxygen to diffuse within the blocks to reach the reaction layer, causing a reduction in the volumetric oxidation rate. This factor thus takes into account the relative effect of surface oxidation and oxygen diffusion on the reaction kinetics. These effects are represented respectively by the total time required to fully oxidize the pyrite in waste rock blocks if only surface oxidation is considered τ_c (s) or if only oxygen diffusion is considered τ_d (s):

$$f(X) = \frac{X^{2/3}}{6\tau_d / \tau_c X^{1/3}(1-X^{1/3})+1},$$

(7.3)

where

$$\tau_c = \frac{\rho_{Py}^{rock}R}{bk_{Ox}a_{Py}^{rock}\delta\gamma\rho_{Ox}^{air}},$$

(7.4)

and

$$\tau_d = \frac{\rho_{Py}^{rock}R^2}{6bD_e\gamma\rho_{Ox}^{air}},$$

(7.5)

where ρ_{Py}^{rock} is the oxygen partial density in the rocks (kg/m^3), **b** is a conversion factor between the masses of oxygen and pyrite consumed (-), and $\mathbf{D_e}$ is the effective diffusion coefficient of oxygen in the blocks (m^2/s).

Figure 7.2 shows the geometric factor **f(X)** as a function of the fraction of unreacted pyrite **X** for different values of the ratio between the total reaction times by diffusion and surface reaction τ_d/τ_c. The more diffusion limits the oxidation rate (τ_d higher), the faster is the reduction of **f(X)**, and thus of the reaction rate, with the decrease of **X** because it becomes harder to diffuse oxygen through the reacted layer.
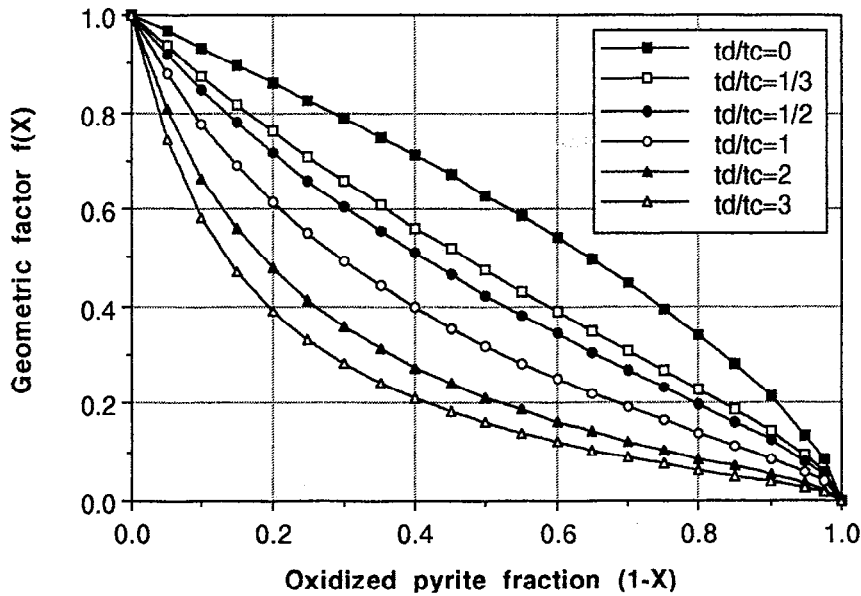
Fig. 7.2 Geometric factor as a function of unreacted pyrite.

Figures 7.3a and 7.3b illustrate the kinetic factors X_T and X_{WO} used to respectively take into account the effects of temperature and oxygen concentration on the kinetics. Parabola are used to define these factors to obtain a continuous curve tangent to the threshold value and perpendicular to the limit value of the parameter. For temperature, a threshold value of 65 °C and a limit value of 80 °C are used whereas for oxygen partial density in the liquid phase, the threshold value is 0.02 kg/m³ and the limit value is zero.
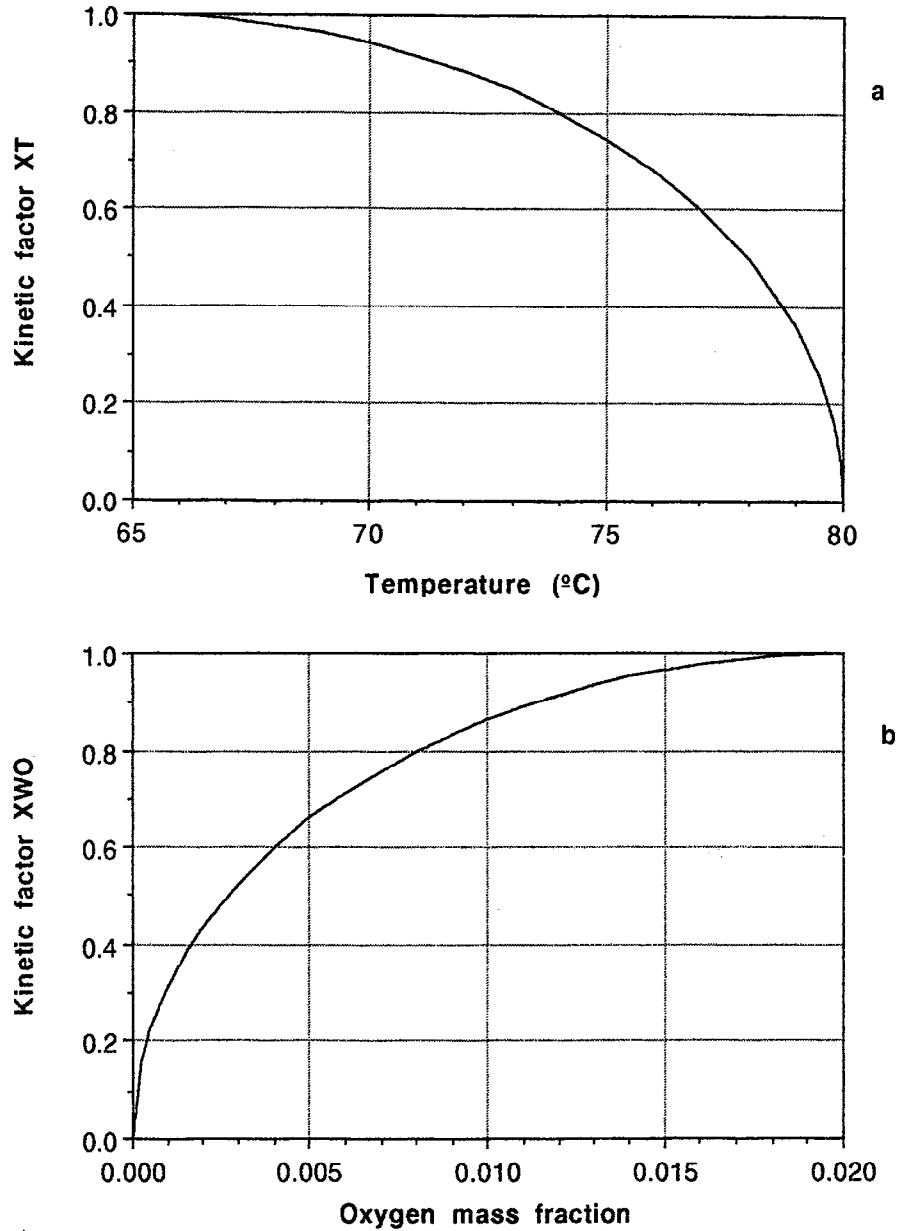
Fig. 7.3 Kinetic factors for a) temperature and b) oxygen mass fraction in air.

The reaction core model allows the derivation of relationships to determine the proportion of the total oxidation time (ratio t/τ_c) required to reach a given proportion of unreacted pyrite X. When only the surface reaction is considered, the following relationship is obtained:

$$\frac{t_c}{\tau_c} = 1 - X^{1/3},$$
(7.6)

whereas when only diffusion is considered, we have:

$$\frac{t_d}{\tau_d} = 1 - 3X^{2/3} + 2X.$$
(7.7)

Since we may add in series the resistances of the processes controlling the reaction rate (surface kinetics and diffusion), the total time necessary to reach a certain proportion of unreacted pyrite is obtained from the sum of the times required through each process, t_c (chemical reaction kinetics) and t_d (diffusion):

$$t_{total} = t_c + t_d ,$$
(7.8)

and

$$\tau_{total} = \tau_c + \tau_d .$$
(7.9)
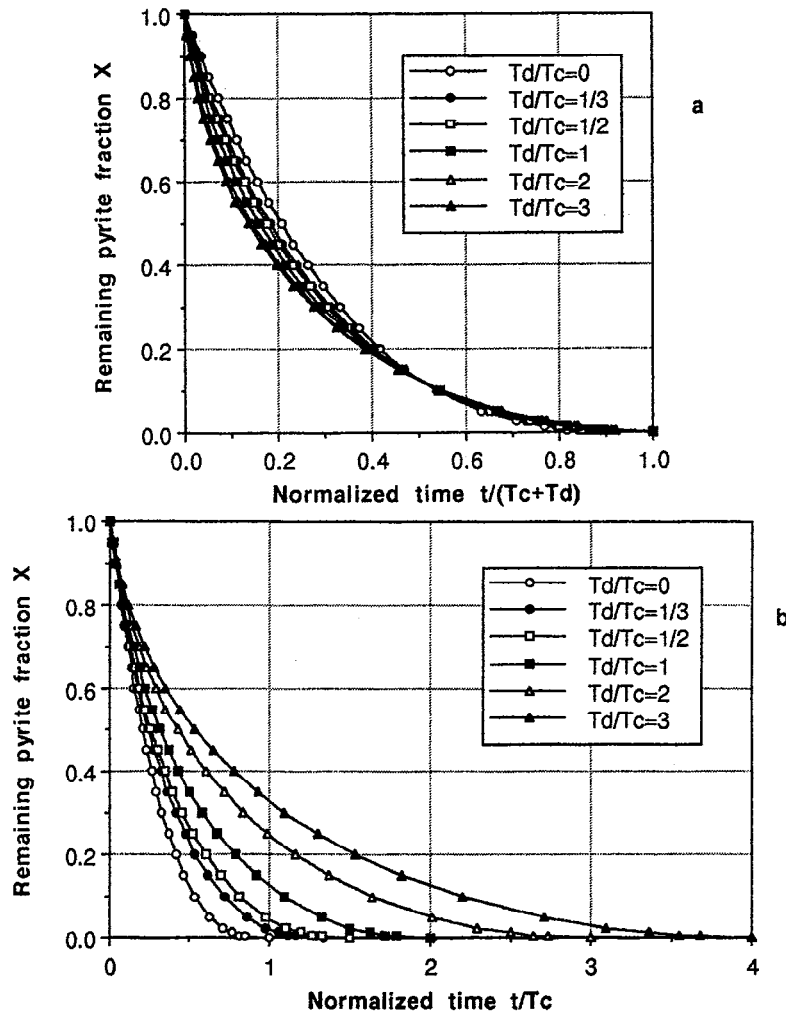
Fig. 7.4 Evolution of the unreacted pyrite fraction with time a) as a function of the total oxidation time and b) with respect to the time required if only the chemical kinetics limits the rate.

Combining the previous relationships, we get an expression giving the relative time required to reach a certain value of **X**:

$$\frac{t_{total}}{\tau_c + \tau_d} = \frac{(1 - 3X^{2/3} + 2X)\tau_d + (1 - X^{1/3})\tau_c}{\tau_c + \tau_d}, \tag{7.10}$$

or

$$\frac{t_{total}}{\tau_c} = (1 - 3X^{2/3} + 2X)\tau_d / \tau_c + (1 - X^{1/3}). \tag{7.11}$$

Figures 7.4a and 7.4b presents the evolution of unreacted pyrite with time. The first figure shows results with respect to total time, chemical and diffusive ($\tau_c + \tau_d$), whereas the second figure uses total chemical time (τ_c). The slower the diffusion, the more total time is required to reach complete oxidation. Note that about half of the total time is required to oxidize about 90% of the original pyrite present. This results from the sharp reduction in oxidation rate as pyrite becomes depleted in the waste rocks. Now that the reaction core model has been presented, we will discuss its implementation in the numerical model and the methods used to solve this system.

7.3   NUMERICAL METHODS USED IN TOUGH AMD

7.3.1   PHYSICAL PROCESSES AND EQUATION SYSTEM

This theoretical development is based on the ones by Pruess (1987 and 1991) describing the formulation used in TOUGH and TOUGH2. However, the modifications required to develop TOUGH AMD are included here, mainly the addition of a new component (oxygen) and a new primary thermodynamic variable (oxygen mass fraction in air).

Continuity equations express the principle of conservation of mass and energy. In TOUGH AMD, these equations are written in integral form for an arbitrary flow domain V_n in which mass and energy must be balanced for the four components κ of the system. There are three mass components (κ=1: water **w**, κ=2: gases other than oxygen in air **a** and κ=3: oxygen **o**) and one energy component (κ=4: heat **h**). The following relationship expresses that the changes in time of the accumulation M^κ of component κ in the volume **v** considered has to be equal to the sum of fluxes of the component F^κ in the direction **n** perpendicular to the domain surface Γ and the sources of that component q^κ in the volume considered:

$$\frac{d}{dt} \int_{V_n} M^\kappa dv = \int_{\Gamma_n} F^\kappa n d\Gamma + \int_{V_n} q^\kappa dv. \tag{7.12}$$

Four equations, one for each component, thus have to be satisfied simultaneously to solve the system. Each term of those relations will be briefly discussed.

The accumulation terms M^κ represent the storage capacity for mass (kg/m^3) or energy (J/m^3) in the fluids of the system. In the case of mass (κ=1,2,3), the quantity of a component accumulated is related to porosity n, the mass fraction of that component $w_\kappa{}^\beta$ in gas (g) or liquid (l) phases β, and the phase saturation S_β and density ρ_β (kg/m^3):

$$M^\kappa = n\ (\ S_l\ \rho_l\ w_\kappa{}^l + S_g\ \rho_g\ w_\kappa{}^g\ )\quad \text{where }\kappa\text{=1,2 or 3.} \qquad (7.13)$$

In the case of energy accumulation (κ=4), one has to consider not only the energy accumulation in the fluid phases but the accumulation in the solid phase as well. For specified pressure and temperature conditions, the energy content of fluid phases is expressed by their internal energy u_β (J/kg). For the solid phase, the heat content depends on their heat capacity c_{ps} (J/kg °C), temperature T (°C) and the amount of solid mass present. That mass depends not only on solid density ρ_s (kg/m^3) but also on porosity n:

$$M^h = (1\text{-}n)\ \rho_s\ c_{ps}\ T + n\ (\ S_l\ \rho_l\ u_l + S_g\ \rho_g\ u_g\ )\ . \qquad (7.14)$$

The mass flux of fluid components and of energy depends on the advection and diffusion transfer processes. The mass flux F_κ (kg/s m^2) of component κ depends on the mass flux of fluid phases β (liquid l and gas g), the mass fraction of the component in the fluid phase w_κ^β and on the diffusive flux of that component in the gas phase f_κ^g:

$$F_\kappa = w_\kappa^g F_g + w_\kappa^l F_l + f_\kappa^g . \qquad (7.15)$$

Similarly, the heat flux F_h (κ=4) (W/m^2) depends on the advective mass flux for each phases, the specific enthalpies of the phases h_β (J/kg), the diffusive mass flux of components in the gas phase f_κ^g and the specific enthalpies of these component in the gas h_κ^g. However, in the case of heat flux, we must add conduction which is dependent on the heat conductivity of the porous media λ (W/m °C) and the thermal gradient ∇T (°C/m) as described by Fourier's law :

$$F_h = -\lambda T + h_g F_g + h_l F_l + \sum_{\kappa=1}^{3} h_\kappa^g f_\kappa^g . \qquad (7.16)$$

The advective mass flux of phase β (liquid or gas) is determined by the general form of Darcy's law for multiphase flow multiplied by the phase density:

$$F_\beta = k\frac{k_{r\beta}}{\mu_\beta}\rho_\beta(P_\beta - \rho_\beta g), \qquad\qquad (7.17)$$

where k: permeability (m²), $k_{r\beta}$:   relative permeability of phase β (-),

μ_β: phase β viscosity (Pa s) g: gravitational acceleration vector (m/s²),

∇P: pressure gradient of phase β ($P_\beta = P_{reference} + P_{c\beta}$) (Pa).

Mass transfer of a component in the gas phase by diffusion is determined by Fick's law in which, for unsaturated porous media, the binary diffusion coefficient $D_{\kappa\kappa'}$ (m²/s) is corrected by taking into account the proportion of gas saturated pores ($n\,S_g$) and the tortuosity of the porous media τ. The diffusive mass flux is proportional to the gradient in partial density of the component in the gas phase ρ_κ^g (kg/m³). That last parameter may be replaced by the product of the gas density ρ_g (kg/m³) and the mass fraction of the component in the gas phase w_κ^β :

$$f_\kappa^g = -nS_g\tau D_{\kappa\kappa'}\rho_g w_\kappa^g. \qquad\qquad (7.18)$$

The pyrite oxidation reaction produces sinks and sources of certain components. It produces heat and consumes oxygen which are component of the system. Furthermore, that reaction consumes pyrite and produces sulfate, iron and acidity. The pyrite remaining has to be taken into account since it affects the reaction rate. The production, accumulation and transport of sulfate is also followed to represent AMD production outside the dump.

The reaction core model is used to calculate the global volumetric oxygen consumption rate Q_{Ox} (kg/m³ s) in a unit volume of waste rocks. The following relationships define the oxygen sink and heat source resulting from that consumption:

$$\int_{V_n} q^o dv = \int_{V_n} Q_{Ox} dv, \qquad\qquad (7.19a)$$

$$\int_{V_n} q^h dv = \int_{V_n} F_h Q_{Ox} dv, \qquad\qquad (7.19b)$$

where F_h (-12.58 MJ/kg O_2) is the conversion factor between heat production and oxygen consumption. Similar factors are used to relate oxygen consumption to the pyrite loss (1.071 kg Py/kg O_2) and sulfate production (-1.714 kg SO_4^{2-}/kg O_2).

The relationships presented are for continuous systems and need to be discretized to allow their numerical solution. In TOUGH2, these equations are discretized in space by the method of integral finite differences (Narasimhan et Witherspoon, 1976; de Marsily, 1986).

7.3.2   PRIMARY AND SECONDARY THERMODYNAMIC VARIABLES

Table 7.1 describes the phases and components of the system. Besides solids, whose properties do not affect the state of the system, two fluid phases are considered. Components include water and air which may be found in liquid or gas form. Air is subdivided in two components, oxygen and the other atmospheric gases. That subdivision is necessary since oxygen is consumed in the oxidation reaction and oxygen concentration affects the kinetics. Heat is also a component since conditions are non isothermal. The assumption is made that local thermodynamic equilibrium is attained between all fluid and solid phases.

In TOUGH2, different thermodynamic variables are used for single phase and two phase conditions. This choice allows the use of more "natural" variables easing the computation of the thermophysical fluid properties (Pruess, 1991). TOUGH AMD uses the following primary thermodynamic variables: for single phase (liquid or gas): 1) phase pressure p (Pa), 2) air mass fraction in the phase w_{air}, 3) oxygen mass fraction in air w_{Ox}^{air}, and 4) temperature T (°C) whereas for two phases (liquid and gas) the second primary variable is replaced by gas saturation plus ten S_g+10. The variable S_g+10 is used to allow the recognition of the number of phases present simply from the numerical value of the second primary variable.

Table 7.1 Phases and components of the system.

Phases	Components		
	Water	Air	
Gas	Water vapor	Oxygen in air	Other atmospheric gases
Liquid	Liquid water	Oxygen in solution	Other gases in solution

All water properties follow the standard steam table representation (International Formulation Committee, 1967). Air is supposed being an ideal gas with additive partial pressure of its components. The viscosity of air and water vapor mixtures is computed following the formulation of Hirschfelder et al. (1954). The solubility of air components in the liquid phase is represented by Henry's law. For each phase (gas and liquid), the following properties, the secondary variables, are determined 1) saturation, 2) relative permeability, 3) viscosity, 4) density, 5) specific enthalpy and 6) capillary pressure.

7.4   TOUGH AMD DESCRIPTION

TOUGH AMD is derived from the program TOUGH2 developed by Karsten Pruess at Lawrence Berkely Laboratory (Pruess, 1991) which is itself an improved version of TOUGH (Pruess, 1987). Before describing the changes made to TOUGH2 to make it suitable for AMD modeling, the main features of this program will be described.

7.4.1   TOUGH2 FEATURES

TOUGH2 is a general program for the numerical modeling of the coupled transport of liquid water, water vapor, air and heat in porous or fractured media. TOUGH2 considers two fluid phases (gas and liquid) besides the solid phase and two components (water and air). Liquid and gas advective fluxes are computed with the generalized Darcy's law for multiphase systems. The diffusive mass fluxes of components in the gas phase are computed with Ficks' law using an effective diffusion coefficient. Heat fluxes are the sum of conduction, advection and diffusion. The specific enthalpies of fluid phases are used to take into account both sensible and latent heat effects (resulting from phase changes). Sources and sinks of mass and heat components may be specified directly or computed with a multilayer well model.

The primary variables used depend on the number of phases. In single phase conditions, pressure, air mass fraction and temperature are used whereas in two phase cases gas saturation is used as the second variable. Fluid properties are secondary parameters depending on the primary variables. For each phase, the following parameters are computed in an equation of state module: saturation, relative permeability, viscosity, density, specific enthalpy and capillary pressure.

Integral finite differences are used to discretize the flow domain and allow the specification of irregular elements. The non linear coupled equation system is solved iteratively by the Newton-Raphson method. A module allows automatic grid generation and the definition of double permeability media. Standard FORTRAN77 is used and the program may be compiled on any 64 bit word computer.

7.4.2   CHANGES REQUIRED TO CREATE TOUGH AMD

The modified TOUGH2 version representing physical AMD processes in waste rock dumps is called TOUGH AMD. The main changes made to TOUGH2 are as follows. Three components are considered in TOUGH AMD: water and air subdivided in two components (oxygen and the other air gases). Oxygen has to be considered as a separate component because it is consumed by the oxidation reaction and its concentration affects the kinetics. To define a system with three components and heat, four primary variables are required. The mass fraction of oxygen in air was thus added to the primary variables. As in TOUGH2, those variables differ depending on the number of phases present.

Modeling with TOUGH AMD may be performed in three different modes according to the number of primary variables kept constant. 1) The full use of the model capabilities is made with non isothermal modeling with variable oxygen concentration in air. 2) Keeping temperature constant, isothermal modeling may be done but still with a variable oxygen concentration. 3) At last, isothermal modeling with constant oxygen concentration is obtained by keeping both temperature and the mass fraction of oxygen in air constant.

An existing subroutine **qloss** was adapted to allow the semi-analytical calculation of heat loss to confining beds. Usually, insulating conditions at the base of dumps are supposed in numerical AMD models because otherwise the computation grid would have to be extended at the base of dumps and would require too much computing capabilities. However, this subroutine offers a precise and very efficient way to take into account heat losses at the base of dumps.

A new subroutine **qox** represents the reaction core model and computes the oxygen loss and heat production resulting from pyrite oxidation for different conditions of temperature, oxygen concentration and pyrite mass fraction. Optionally, an Arrhenius relationship may be use to account for the effect of temperature on the oxidation rate. Another new subroutine **so4** performs sulfate mass balances and advective transport calculations in the liquid phase. This module accounts for the production, transport and accumulation of sulfate in waste rock dumps. The new subroutine **cpy** calculates the remaining pyrite mass fraction in an element. Three other new subroutines **amdbal, trace** and **plot** generate reports or disk files in a format suitable for graphics generation. The public domain system GMT (Wessel and Smith, 1991) for graphics generation in UNIX environments is used to create graphic outputs from these files.

7.4.3   TOUGH AMD GENERAL CAPABILITIES

TOUGH AMD is adapted to the modeling of AMD and allows the representation of the main processes involved:

- <u>Hydrology</u>: Takes into account variable infiltration with time from the surface and represents unsaturated and saturated liquid flow within the dump.
- <u>Gas transfer</u>: Represents gas convection under pressure or temperature gradients as well as the diffusion of gas components under concentration gradients.
- <u>Heat transfer</u>: Includes the processes of conduction, fluid advection and gas diffusion. Takes into account the effect of phase changes on heat transfer. Allows the calculation of heat losses to confining beds.
- <u>Geochemistry</u>: Uses a reaction core model including the effects of surface reaction and diffusion on the volumetric oxidation rate. Computes the rates of consumption of pyrite and oxygen and the rates of heat and sulfate production.
- <u>Mass transport</u>: Uses sulfate to represent AMD production. Computes the production and the advective transport of sulfate. Computes the rates of mass accumulation within the dump as well as its release outside the dump.

7.5   APPLICATION OF AMD NUMERICAL MODELING

The first objective of numerical modeling is here to better understand the physical processes involved in AMD production in waste rocks. A general case is then modeled to study the interaction of the processes and identify the parameters having the greatest impact on the behavior of the system. The parameters and conditions used in the base case are still representative of the South Dump at La Mine Doyon so that results may be compared to observations at this site. We are presenting here some of the findings of the modeling work for the base case and will illustrate the effect of a change in permeability on the behavior of the system. The application of the model to the evaluation of a control method, here a border membrane, will be illustrated. A more detailled account of the modeling work is presented in Lefebvre (1994).

7.5.1   MODEL PARAMETERS AND CONDITIONS

The base case is modeled for 15 years and as such includes the period during which the dump has been in place (about 9 years) and provides a potential outlook of the future evolution of AMD production. It would be unrealistic to model the behavior of the dump for a longer period given the uncertainty in our knowledge of the site and in particular the absence of data on the evolution of physical properties in time which could affect significantly the behavior of the dump. This model actually supposes that physical properties remain constant even though we know from field observations that the material evolves and new minerals are formed and could alter the physical properties. Further studies are required to quantify the impact of this change in physical properties. The extensive characterization and monitoring program at La Mine Doyon allowed an evaluation of many physical properties of the waste rocks. Table 7.2 summarizes the physical parameters used in the model.
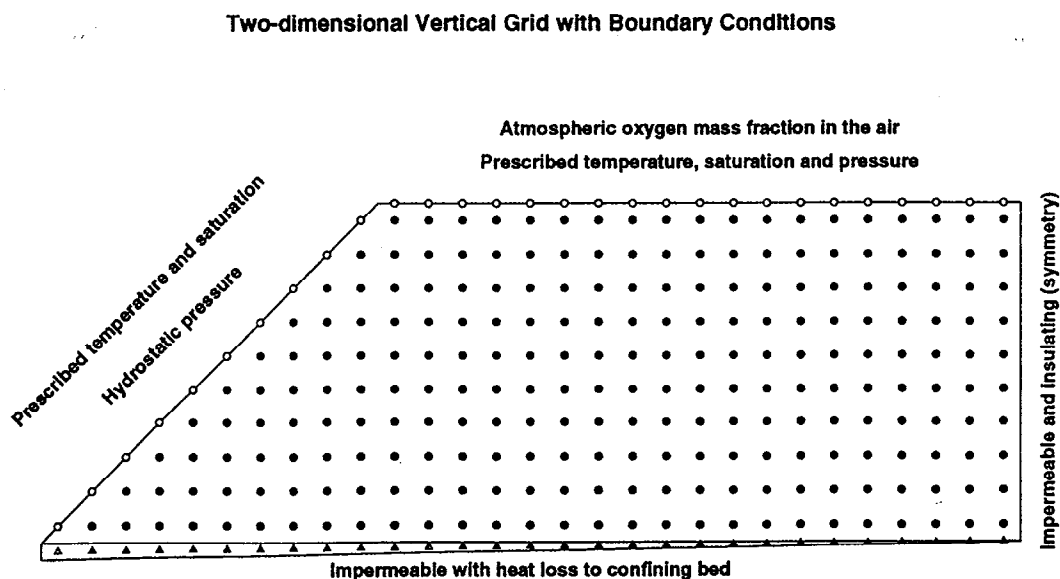

Fig. 7.5 Computation grid and limit conditions for the base case.

Table 7.2 Physical properties of the base case

Property	Symbol, value and units
Volumetric oxidation constant	$K_{ox} = 0.75 \times 10^{-6}$ s^{-1}
Diffusive / Chemical total times	$t_d/t_c = 2.5$
Pyrite mass fraction in solids	$w_{py} = 0.07$
Horizontal permeability	$k_h = 2.5 \times 10^{-9}$ m^2
Vertical permeability	$k_v = 1.0 \times 10^{-9}$ m^2
Porosity	$n = 0.33$
Solids density	$\rho_s = 2740$ kg/m^3
Dry thermal conductivity	$\lambda_d = 0.9$ W/m °C
Saturated thermal conductivity	$\lambda_w = 3.7$ W/m °C
Heat capacity of solids	$c_{ps} = 837$ J/kg °C
Thermal conductivity of the base	$\lambda = 1.55$ W/m °C
Global density of the base	$\rho_b = 2008.6$ kg/m^3
Heat capacity of the base	$c_p = 1504$ J/kg °C
Standard diffusion coefficient	$D_o = 2.13 \times 10^{-5}$ m^2/s
Temperature diffusion coef.	$\theta = 1.80$
Tortuosity factor	$\tau = 0.7$
van Genuchten "m" factor	$m = 0.23$
van Genuchten "α" factor	$\alpha = 0.504$ Pa^{-1}
Residual water saturation	$S_{wr} = 0.14$

The computation grid and limit conditions used in the base case are presented in figure 7.5. That grid represents a vertical half section within the dump and uses cartesian coordinates. The model has an unsaturated zone 30 m thick and a thin wedge-shaped saturated zone from zero to 1.5 m thick. Lateral dimensions are 87 m at the base and 57 m at the surface. The slope at the border is necessary to obtain representative air convection patterns as shown by Pantellis and Ritchie (1992). Since the internal limit is a symmetry limit, the grid represents a system twice as wide. Those dimensions are representative of the south part of the main zone at the South Dump.

The limit conditions used are a water saturation of 0.42 generating an infiltration of about 35 cm per year, a temperature of 5 °C and atmospheric oxygen mass fraction (0.2315). Atmospheric pressure is set at 100 kPa at the surface whereas a hydrostatic pressure profile is used at the border. The system is supposed to be homogeneous. These conditions are also used as initial conditions within the dump at time zero. The following sections summarize the main conclusions of the modeling runs using these conditions.

7.5.2 PHYSICAL CONDITIONS WITHIN THE DUMP

Figure 7.6 shows the conditions prevailing in the dump after 9 years of AMD production: a) gas velocity and temperature, b) oxygen mass flux and relative concentration, and c) oxidation rate and remaining pyrite mass fraction. The key process in AMD production is oxygen supply to oxidation sites. Convection may provide oxygen in a much more efficient way than diffusion.

Figure 7.6a shows that air convection is controlled by temperature gradients. An increase in temperature reduces density and causes gas movement. Since temperature is higher within the dump than outside, the gas column is lighter in the dump and the gas pressure will be smaller thus forcing the air entry inside the dump at the border. Within the dump, this light gas has a tendency to move upward and emerges at the top surface of the dump. A convection movement is thus initiated which is responsible for the supply of oxygen within the dump. Gas convection at the border generates an auxiliary convection patterns from the inner surface of the dump to the base and then upward through the zone of highest temperature.

Figure 7.6b illustrates the oxygen mass flux and the relative oxygen concentration in the dump (with respect to atmospheric oxygen concentration) after 9 years of AMD production. The most important source of oxygen supply is through the border and is related to air convection which provides oxygen from the outside of the dump. The oxygen flux is reduced along a given convection path within the dump because it is gradually consumed by the oxidation reaction. The oxygen concentration is thus maximum near air entry points and is gradually reduced within the dump. The slower convection path from the surface of the dump does not supply oxygen fast enough so it is totally consumed before reaching the base of the dump. The central core of the dump is thus deprived of oxygen and does not produce much AMD. The effect of diffusion is only apparent at the central surface of the dump where gas flow is horizontal and contains little oxygen provided from the surface of the dump by diffusion.

Since pyrite oxidation follows first order kinetics with respect to oxygen, its distribution has a direct impact on the oxidation rate. Figure 7.6c shows, after 9 years of AMD production, the remaining pyrite mass fraction (contours) and the oxidation rate (circles). Of course, the highest oxidation rates are observed in areas of maximum oxygen concentration at the border of the dump and near its surface. The remaining pyrite mass fraction follows similar patterns which are generally perpendicular to the direction of oxygen supply. There is a sharp decrease in pyrite at the border of the dump whereas the reduction is not as important at the surface of the dump. In the central part of the dump, very little pyrite is oxidized.

7.5.3 PHYSICAL TRANSFER PROCESSES

Transfer processes play an important role in AMD production. We will discuss here numerical modeling results providing more insights on the processes of heat transfer, water circulation and sulfate transport in waste rock dumps.
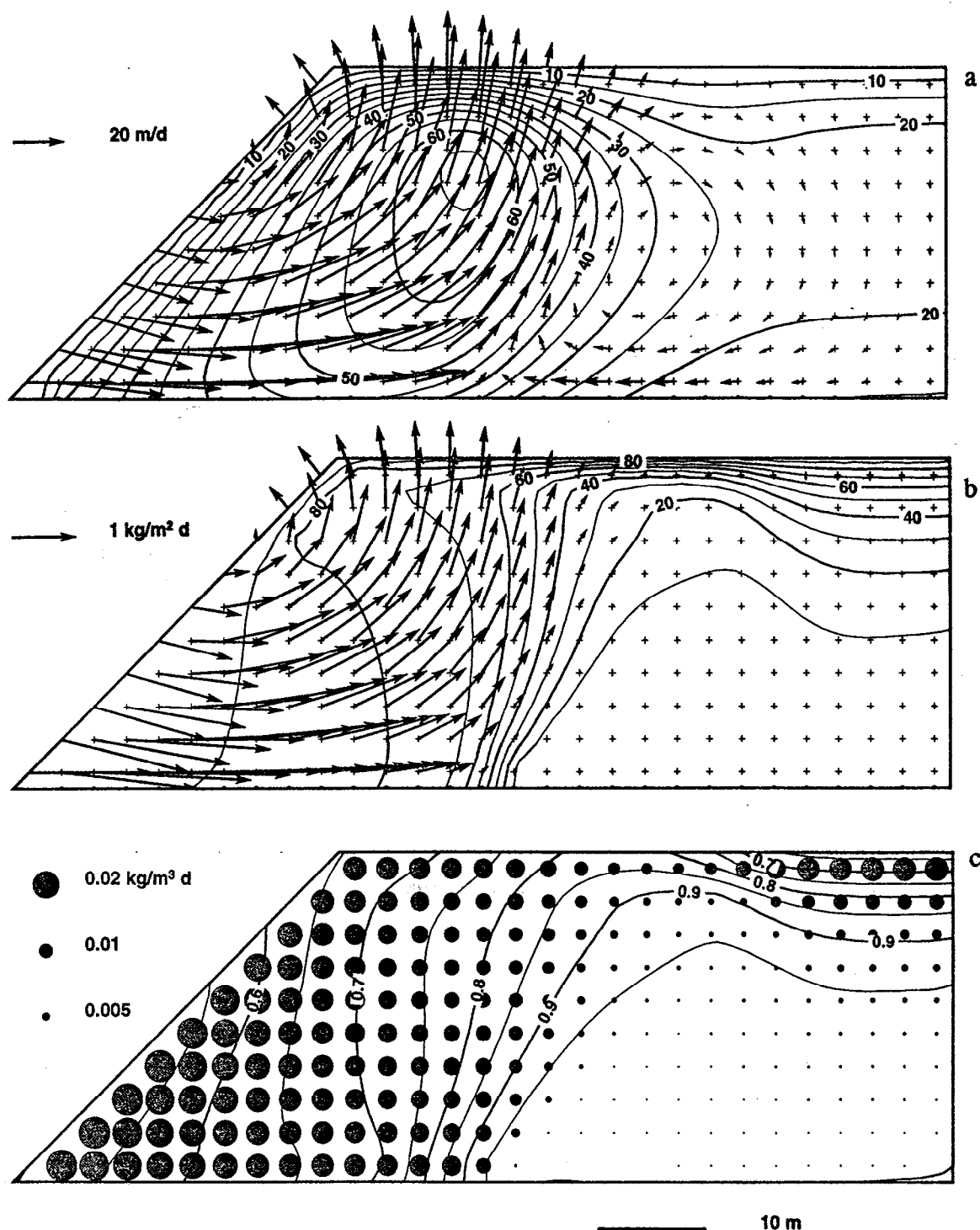
Fig. 7.6 Conditions for the base case after 9 years of AMD production. a) Gas velocity (m/d) and temperature (°C). b) Oxygen mass flux (kg/m² d) and oxygen mass fraction in air with respect to atmospheric value (%). c) Unreacted pyrite mass fraction and oxidation rate (kg O₂/m³ d).

Heat transfer in waste rock dumps occurs through the mechanisms of 1) conduction in the bulk of the material resulting from temperature gradients, 2) advection of fluid (liquid and gas) carrying heat with them, and 3) diffusion of components in the gas phase. Figure 7.7a shows, after 9 years of AMD production, the temperature distribution and the components of heat transfer. Three families of arrows represent respectively 1) the total heat flux, 2) the conductive heat flux (perpendicular to temperature contours) and 3) the diffusive heat flux. The difference between the total flux and the other components is the advective heat flux.

At the outer limits of the dump, heat conduction is generally the dominant heat transfer mechanism. Conduction is also responsible for heating the center of the dump by carrying heat away from the zone of maximum temperature. Heat transfer by gas advection is dominant in the central hot zone where the gas phase contains more water vapor and carries a lot of heat. Water advection and its effect on heat transfer is very small in this case because of the low infiltration rate. However, this process can be significant in other circumstances. Heat transfer by diffusion in the gas phase is negligible because it is a binary process with diffusion and counterdiffusion of components with nearly equal heat capacity.

It is important to understand the modes of water circulation in the dump since the mass produced during AMD (sulfate, acidity, metals) is carried in solution. Figure 7.7b shows, after 9 years of AMD production, the distribution of water saturation and the mass fluxes of water in the liquid (downward pointing gray arrows) and vapor phase (black arrows). Liquid water moves downward from the surface during infiltration in the unsaturated zone. Water is also transfered in the vapor phase by gas advection. Water transfer in the vapor phase is actually responsible for the redistribution of water within the dump. Relatively dry cold air entering the dump, mainly at the toe of the slope, acquires more and more water as it first moves horizontally and heats up. The gas phase carries the most water, as much as the liquid phase, as it moves upward through the hottest zone. Beyond that zone, in cooler areas near the surface, water vapor condenses and contributes to more infiltration. That process induces water saturation variations within the dump from 37.5% to 41.5%. The zone most influenced is near the toe of the slope at the base where water is withdrawn. Although important, the process of water vapor transfer by advection does not lead to important water losses from the dump because most of the water withdrawn from the base recondenses near the top before leaving the dump.

AMD production is followed in the model by sulfate production, transport and release. Figure 7.7c shows the distribution of sulfate concentration (contours) and the net sulfate flux in the elements. These net fluxes represent the difference in mass of sulfate entering and leaving an element. Net negative fluxes (dark circles) indicate that more mass exits the element than enters it whereas positive net fluxes (light circles) have an opposite meaning. Negative net fluxes occur in zones of high oxidation rate and consequently of high sulfate production. In these areas, more mass leaves the elements because internal production adds to the sulfate mass flux. Positive fluxes occur mainly at the core of the dump where sulfate mass production is low: in these areas, leachate of high concentration mixes with the leachate contained in the elements and comes out with less mass. This type of mass transport representation in the unsaturated zone supposes mixing of fluids instead of piston displacement and accounts for the limited leaching caused by small infiltration rates compared with the large volume of leachate stored in the unsaturated zone. This results in an increase in concentration and sulfate mass storage within the dump as more mass is
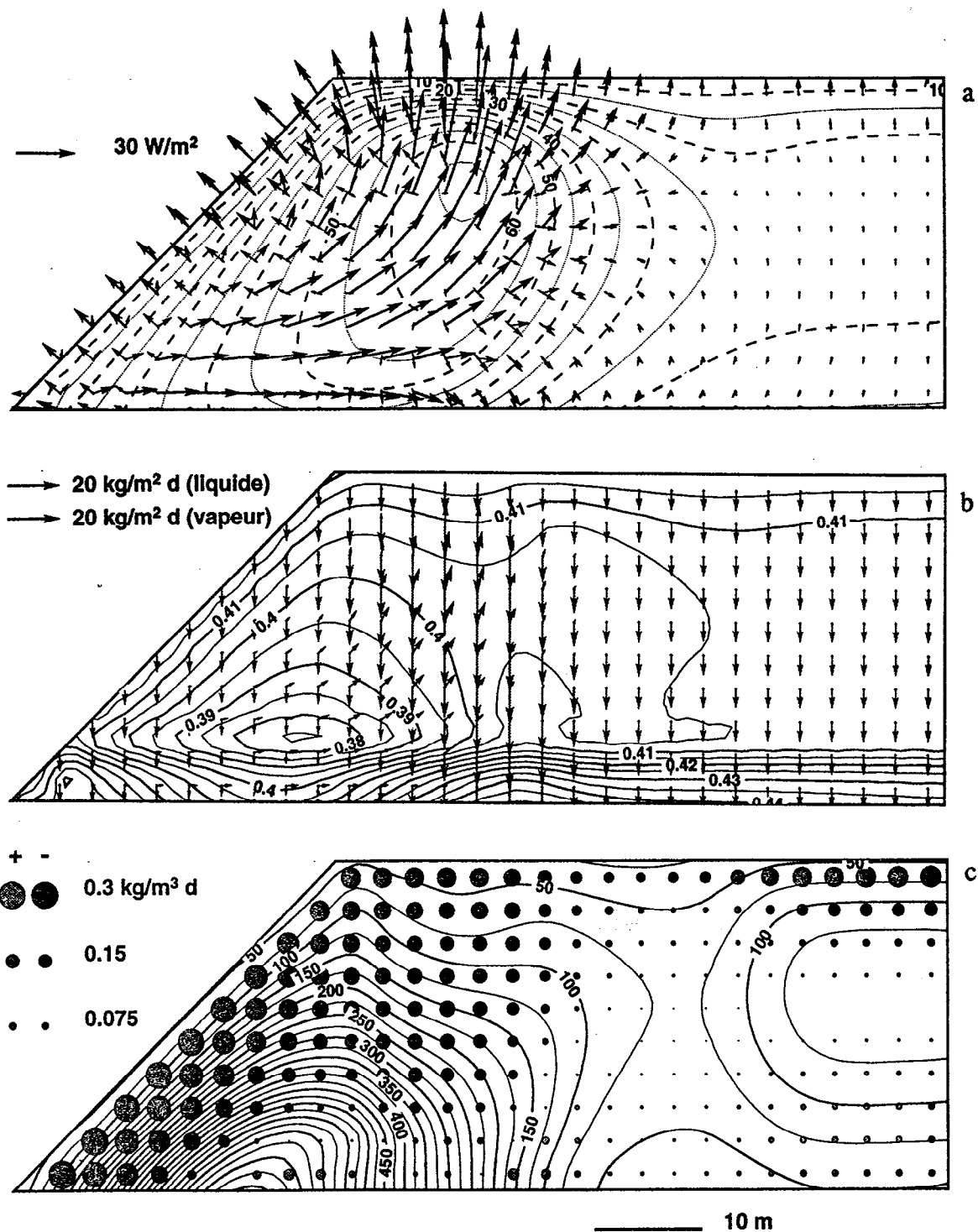
Fig. 7.7 Physical processes for the base case after 9 years of AMD production. a) Total, conductive and diffusive heat fluxes (W/m²) and temperature (°C). b) Liquid (gray) and vapor (black) water mass fluxes (kg/m² d) and water saturation (-). c) Net sulfate flux (kg/d) (negative: dark, positive: light) and concentration (g/L).

produced than may be leached during the early years of AMD production. This representation of mass transport is simplistic and requires more work. Also, no account is made for mass loss due to new minerals precipitation (gypsum, jarosite). It is clear that the very high concentrations indicated by the model could not be reached in a real system because oversaturation and precipitation would occur to limit the concentration.

7.5.4   EVOLUTION OF AMD PRODUCTION WITH TIME

The numerical model compiles global parameters for the entire dump through time. These results allow us to follow the evolution of AMD production with time and the changes in physical conditions which are induced. We will first look at the changes in average temperature and oxygen concentration through time since these parameters determine the rate of AMD production.

Figure 7.8a shows the evolution in time of the average temperature and oxygen mass fraction in air. These parameters show a continuous increase with time and explain the increase in the oxidation rate. The increase in temperature drives more gas convection which provides more oxygen to the dump and the rate of oxidation rises directly with oxygen concentration. A cycle of increased heat production, convection, temperature and oxygen concentration is generated leading to a continuous increase in AMD production. However, the overall oxidation rate will eventually decrease as less pyrite is available and the oxygen has to diffuse through the blocks to reach the oxidation sites. There is also a limitation to the oxidation rate where temperature reaches more than 65 °C. In those areas, the oxidation rate is lower than would be the case simply on the basis of oxygen concentration and pyrite remaining.

Figure 7.8b shows the evolution with time of remaining pyrite mass fraction and oxidation rate. There is a sharp increase in the oxidation rate in the first years and a slower but steady increase afterward. The reduction in available pyrite follows the trend in oxidation rate. After 15 years of AMD production, about 30% of the original pyrite has been consumed. This reduction is quite important especially considering that very little pyrite has been oxidized at the core of the dump. A dump with smaller lateral extent would have much less pyrite remaining. Pyrite oxidation releases sulfate and we will now look at the evolution in its concentration with time.

As mentioned, the small infiltration rate used in the model does not allow the complete leaching of the sulfate produced in a given year. As a result, there is a steady increase in sulfate concentration within the dump as shown on figure 7.8c. This increased concentration also implies a greater sulfate production with time as the same amount of liquid leaves the dump. However, this picture is distorted since the model does not consider mass loss through mineral precipitation. At La Mine Doyon, what is actually observed is an increase in sulfate concentration during the first years of AMD production but a stable concentration afterward. This observation is interpreted as the result of concentration being controlled by minerals precipitation since abundant gypsum and jarosite are observed in the dump. Geochemical capabilities need to be added to the model to take this effect into account. Still, mass accumulation within waste rock dumps must be taken into account in the planning of AMD control methods and for the evaluation of their effectiveness. It could take many years to see the beneficial effects resulting from efficient control methods if the mass accumulated in a dump continues to be leached.
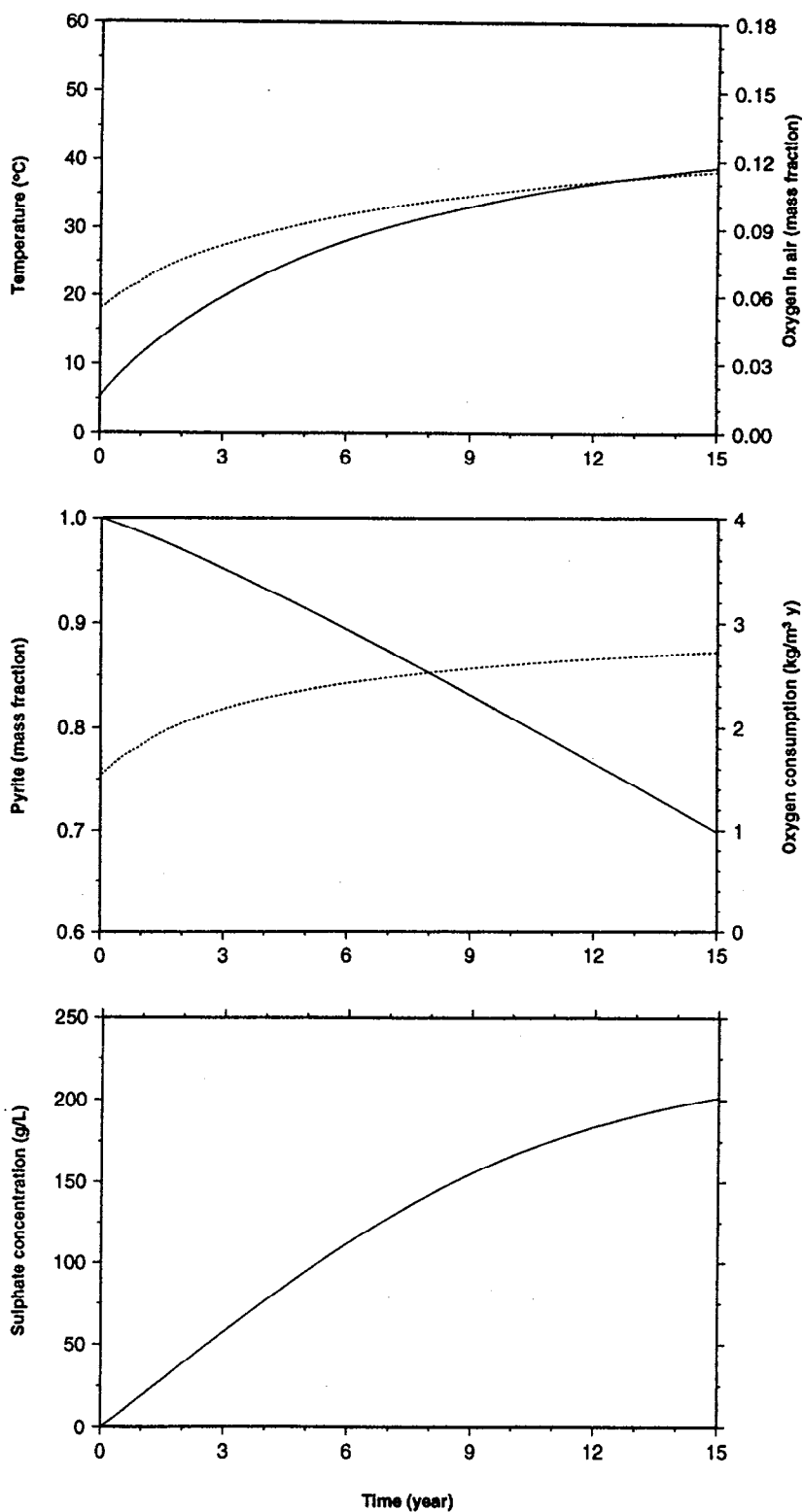
*Fig. 7.8 Evolution of average conditions with time for the base case. a) Temperature (solid) (°C)
and oxygen mass fraction in air (stippled) (-). b) Unreacted pyrite mass fraction (solid) (-) and
oxidation rate (stippled) (kg O_2/m^3 y). c) Sulfate concentration (g/L).*

7.5.5   IMPACT OF PERMEABILITY ANISOTROPY

The impact of various parameters on AMD production was investigated. We were mainly interested in convective systems and the controls on the physical processes of oxygen and heat transfer as well as the impact of the reaction kinetics. We found that permeability is of course the key parameter determining the onset of convection. However, it is not only the magnitude of permeability which is important: its anisotropy has also a major impact on the gas convection patterns. We then present the results of a case which has a lower vertical permeability than the base case, 5×10^{-10} m^2 instead of 1×10^{-9} m^2, but is more anisotropic and has a horizontal permeability of 5×10^{-9} m^2 instead of 2.5×10^{-9} m^2 for the base case. Anisotropy in permeability in a waste rock dump may have several causes: machinery rolling surfaces, the modes of dumping (surface or end dumping), the heterogeneity of the material (especially the mixing of overburden material within the wastes), the exposure of surfaces to atmospheric conditions for long periods during operations. Field methods must be developed to determine permeability and its anisotropy.

Figure 7.9 shows conditions for this case after 9 years of AMD production. Figure 7.9a shows that higher temperatures are reached over a wider area for this case compared to the base case. This results from the greater horizontal penetration of oxygen within the dump which causes oxidation deeper in the dump where heat losses are smaller. Also, the oxygen concentration and fluxes are higher over almost the entire section (figure 7.9b). The oxidation rate is thus higher and the depletion of pyrite is more widespread (figure 7.9c). However, the high temperature reached (above 65 °C) limits the oxidation rate over a wide area. This case points out the need for careful characterization of waste rock dumps to predict their behavior. It also indicates that avoiding lateral air entry from the sides of a dump might be a good way to reduce AMD. The following section shows modeling results for a case in which a border membrane is used to reduce ongoing AMD production. That case illustrates the applicability of modeling to the design of control methods.

7.5.6   EFFECT OF A BORDER MEMBRANE TO CONTROL AMD PRODUCTION

Studies have shown that completely covering a waste rock dump with a low permeability membrane may effectively prevent or control AMD (Harries and Ritchie 1986). However, this is a very costly solution which is not always applicable as in the case of a dump showing important compaction as for La Mine Doyon (Gélinas et al., 1990). This is why we studied theoretically the impact of covering only the slopes of a dump with a membrane. Since this is the site of most of the oxygen entry, it could potentially curb AMD production. Such a "membrane" could more easily be put in place during construction by placing low permeability material near the border but it would still be less costly than a full membrane for sites which are already producing AMD.

To model this case, the base case is modified by adding a new layer of elements at the border to represent a low permeability material such as till. The properties used for that material are a porosity of 20%, a permeability of 10^{-14} m^2, a residual water saturation of 45% and an initial saturation of 85%. With such properties, we do not have a "perfect" membrane but one through which some gas can diffuse and some water can infiltrate but still strongly restricts gas convection.
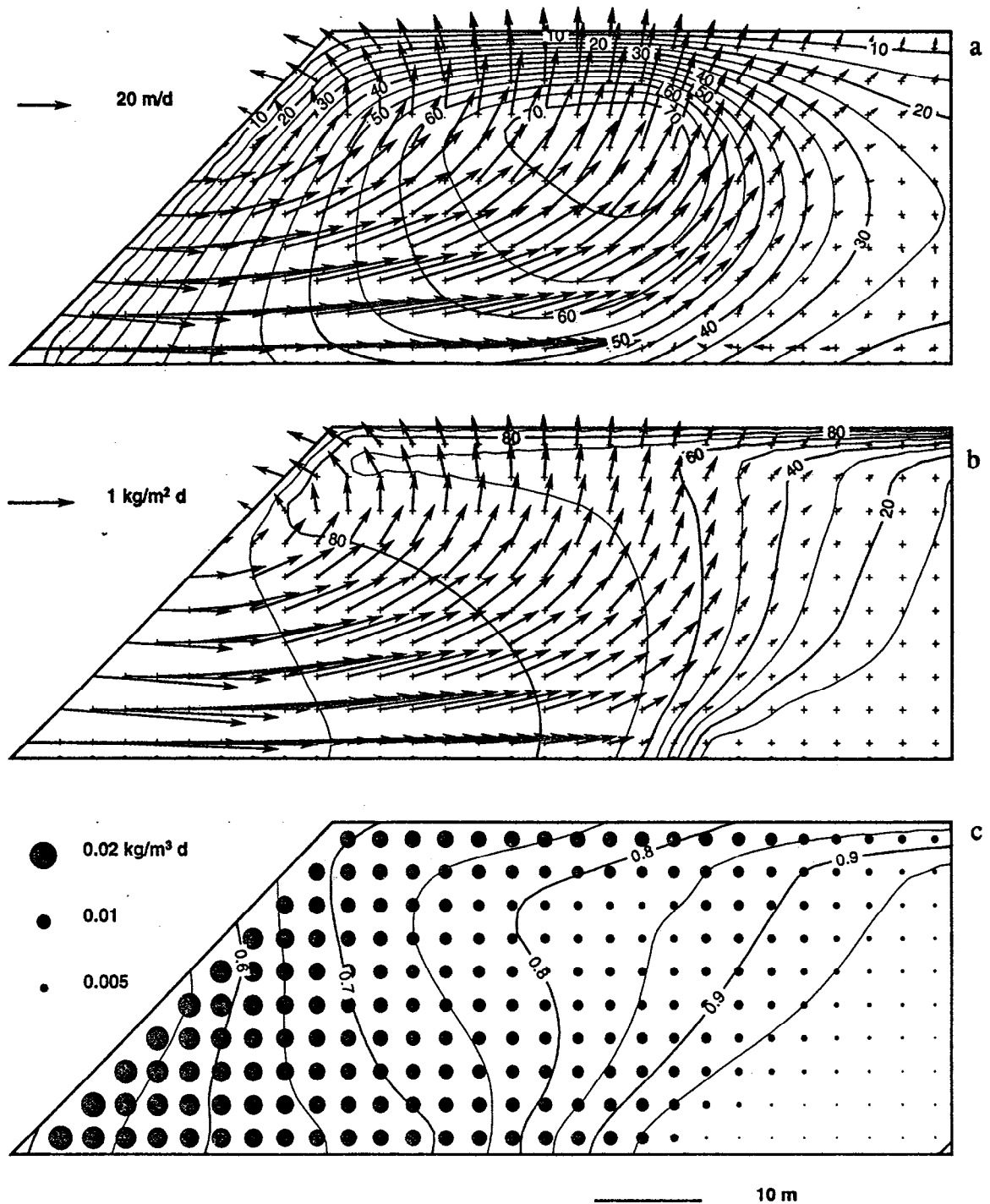
Fig. 7.9 Conditions for the permeable and anisotropic case after 9 years of AMD production. a) Gas velocity (m/d) and temperature (°C). b) Oxygen mass flux (kg/m² d) and oxygen mass fraction in air with respect to atmospheric value (%). c) Unreacted pyrite mass fraction and oxidation rate (kg O_2/m^3 d).

The initial conditions used are the ones of the base case after 9 years of AMD production. Water saturation in the top elements near the edge is also lowered to represent better drainage which could be achieved by slight changes of the surface near the border. This reduction in infiltration near the edge prevents the leaching of the mass accumulated at the border and slows AMD production at the base of the dump. Conditions 1 and 9 years after the installation of the border membrane are presented.

Figure 7.10 shows conditions 1 year after the membrane was put in place. We see that convection and temperature remain important. However, convection patterns have changed drastically (figure 7.10a). Since the air can non longer penetrate within the dump through the membrane, convection is initiated from the surface because the very high temperatures still present in the dump drive the entry of air. Even though this process is less efficient than convection from the slope, much oxygen is drawn in the dump from the surface (figure 7.10b) and the oxidation rate remains high near the surface (figure 7.10c). However, very little oxygen reach the hottest region since it is consumed beforehand. As a result, temperature has started to decrease in the hottest zone whereas the interior of the dump has warmed up significantly from 20 °C to 35 °C. These lower temperature gradients will lead eventually to the reduction of convection and a decrease of the global oxidation rate.

These results show that a border membrane could curb AMD production but that it would be much more efficient if convection from the surface could be avoided initially. This could be done by a reduction, even temporary, of the surface permeability. Even without surface permeability reduction, convection will almost cease after a few years. Figure 7.11 shows the conditions 9 years after the border membrane was installed. Temperature has decreased significantly and convection is very weak (figure 7.11a). As a result, the penetration of oxygen in the dump is shallow (figure 7.11b) and oxidation only occurs near the surface (figure 7.11c).

Figure 7.12 shows the change in conditions with time during the first 9 years after the border membrane was installed compared to the base case without AMD control methods. It takes about one year for oxygen concentration to decrease whereas the reduction in temperature occurs over many years (figure 7.12a). The oxidation rate of course follows the oxygen concentration decrease (figure 7.12b). This relative success in reducing AMD production is not readily translated in a reduction in sulfate concentration (figure 7.12c). This results from the high accumulation of sulfate within the dump and the small water infiltration rate having a limited leaching capacity. We may conclude that the installation of a border membrane may lead to a significant reduction in the oxidation rate by preventing the supply of oxygen by convection. However, this method will be more efficient if coupled with a reduction, at least temporary, of permeability at the surface of the dump. However, the impact of the reduction in oxidation will not translate into reduction in sulfate concentration and AMD production unless some mean of internal neutralization is also used to decrease the amount of stored AMD which may be leached later.
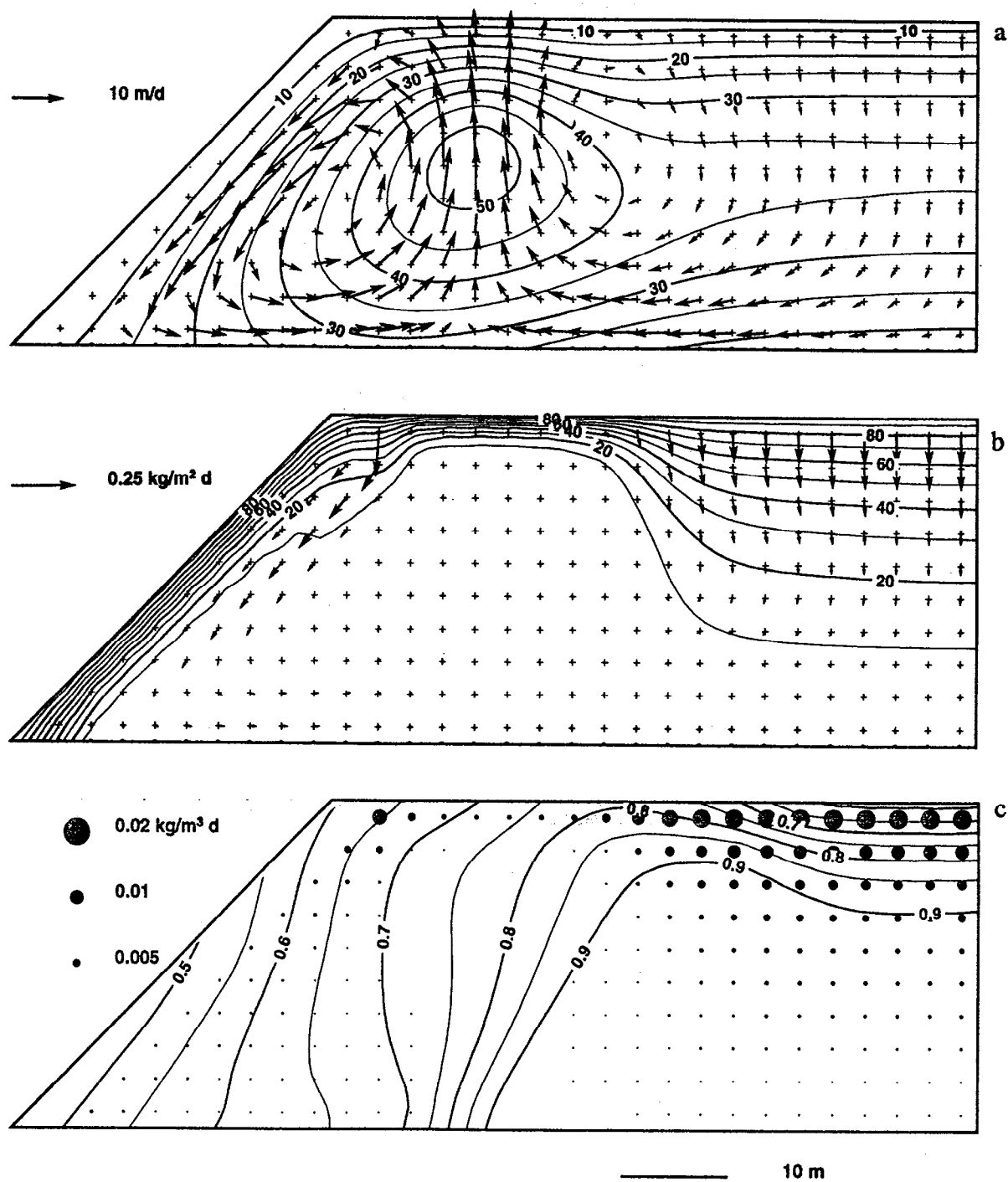
Fig 7.10 Conditions for the border membrane 1 year after installation. a) Gas velocity (m/d) and temperature (°C). b) Oxygen mass flux (kg/m² d) and oxygen mass fraction in air with respect to atmospheric value (%). c) Unreacted pyrite mass fraction and oxidation rate (kg O₂/m³ d).
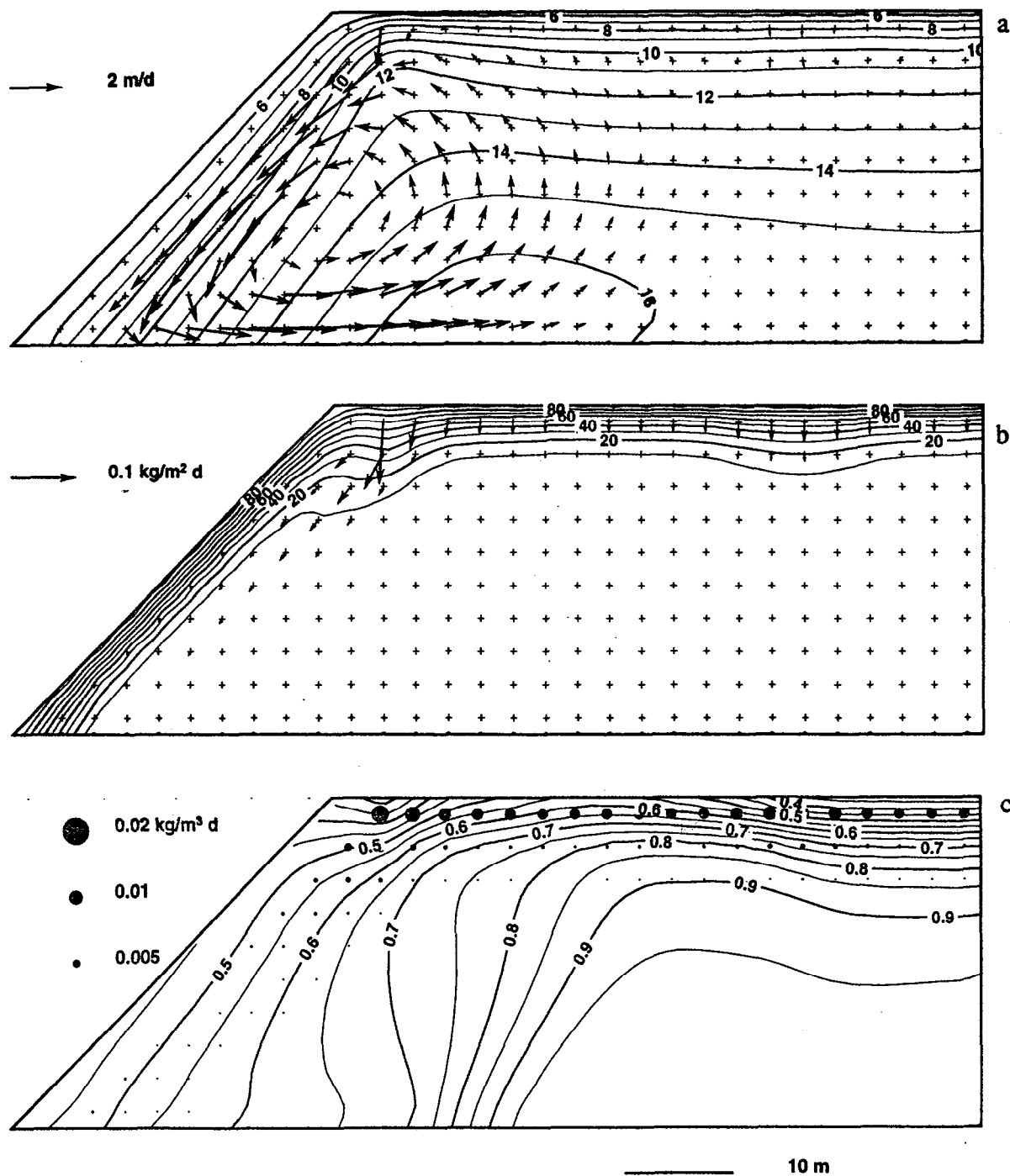
Fig. 7.11 Conditions for the border membrane 9 year after installation. a) Gas velocity (m/d) and temperature (°C). b) Oxygen mass flux (kg/m² d) and oxygen mass fraction in air with respect to atmospheric value (%). c) Unreacted pyrite mass fraction and oxidation rate (kg O₂/m³ d).

Fig. 7.12 Evolution of average conditions with time for the case with a border membrane compared to the base case. a) Temperature (solid) (°C) and oxygen mass fraction in air (stippled) (-). b) Unreacted pyrite mass fraction (solid) (-) and oxidation rate (stippled) (kg O_2/m^3 y). c) Sulfate concentration (g/L). The curves for border membrane case start at 9 years time.

7.5.7 MODEL LIMITATIONS AND FUTURE RESEARCH

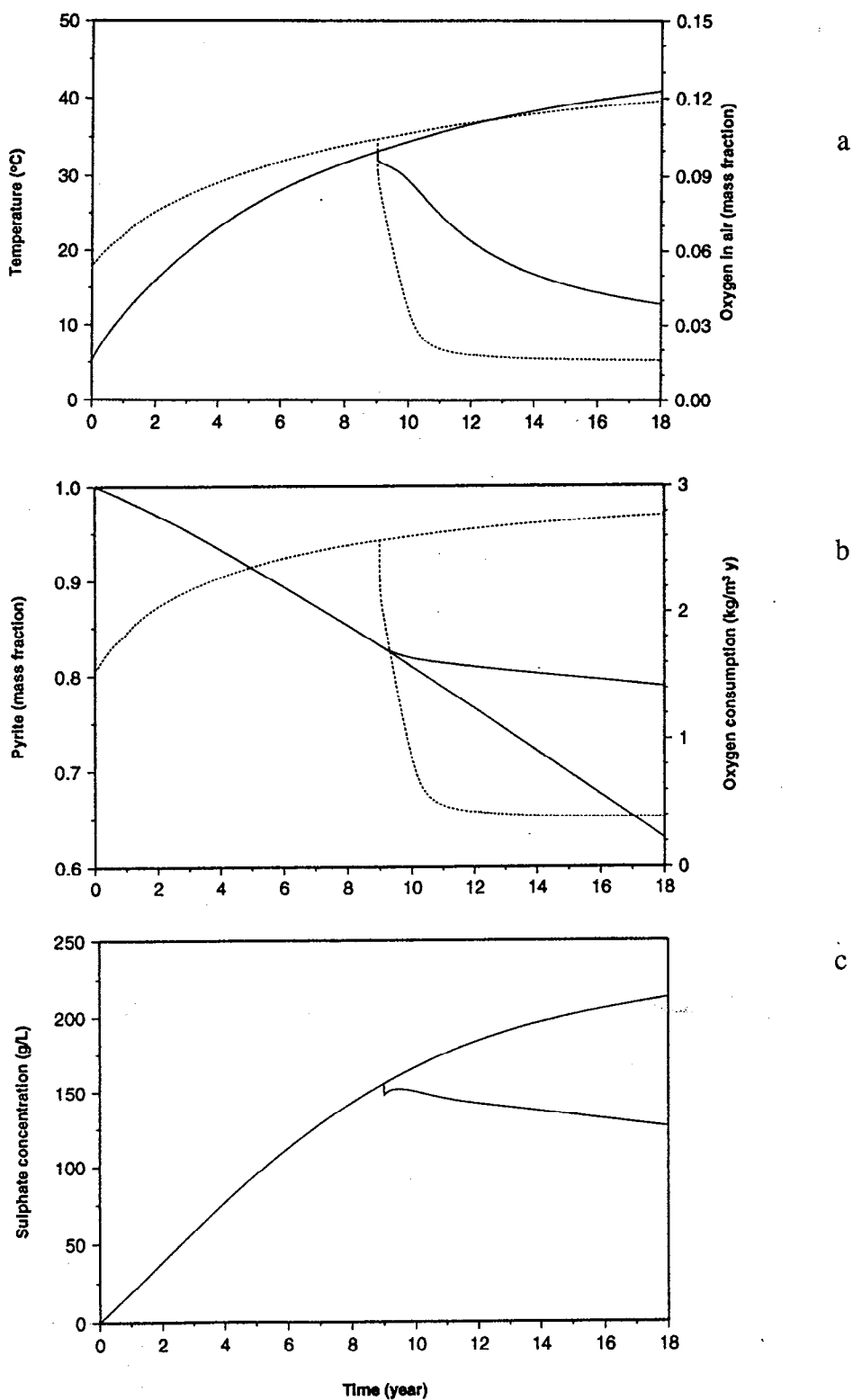Differences between the model predictions and field observations point out limitations in the numerical model and in our general knowledge of some key processes related to AMD production. Further research is needed to develop the firm fundamental knowledge upon which applied numerical modeling must be based.

The processes of water infiltration in a coarse heterogeneous porous media, mass transport in the unsaturated zone, and the leachate geochemical behavior (interaction with rocks and mineral precipitation) need to be studied further both in the lab and in the field. The lack of knowledge on these key processes is the main impediment on the further development of AMD modeling and its capability to predict the behavior of waste rock dumps. Further field studies are also required as we need more site characterization with integrated monitoring and modeling programs. For those sites, we have to develop methods to better characterize air permeability and its anisotropy as it affects both gas convection and water infiltration. We also have to be able to characterize, in the field and lab, the changes in physical properties of waste rocks through time and especially the effect of mineral precipitation on permeability.

8 / Conclusions

This project provides a contribution to the understanding of physical, hydrological, chemical, mineralogical and microbiological processes active during acid rock drainage production in waste rock dumps. The case study of La Mine Doyon has been instrumental in testing new field techniques to measure key parameters needed for modeling ARD processes and eventually to help manage efficiently the production of acid drainage.

The principal results of the *Mine Doyon Monitoring and Modeling Project* can be grouped in three sections:

1. Contributions to the methods of waste rock dumps characterization by developing and testing new techniques and by collecting field and laboratory data on key parameters needed to better describe the generation of acid rock drainage.

2. Improvements in the understanding of processes controling acid rock drainage;
    a) physical processes such as heat and gas transfer,
    b) hydrological processes like infiltration, baseflow, groundwater losses, and response to snowmelt or storm events,
    c) geochemical processes like oxidation rates, mass transport and storage in the unsaturated zone, mineral transformations, chemical evolution of the acid drainage,
    d) microbiological processes such as conversion of ferrous to ferric iron, oxygen consumption with depth, aerobic/anaerobic reactions.

3. Modeling water transport at the base of a waste rock dump, mass and energy transport in the unsaturated part of WRD with special emphasis on heat transfer as an efficient method to estimate rates of oxidation in an active WRD.

8.1   CONTRIBUTIONS TO WRD CHARACTERIZATION

At the international level, there are still a very small number of case studies giving detailed characterization of active waste rock dumps. The Mine Doyon project is an attempt to correct some of these shortcomings by exploring new characterization methods, by measuring important physical and chemical parameters, and by making available large sets of coherent data describing major processes of acid rock drainage generation.

A   CHARACTERIZATION METHODS AND FIELD INSTRUMENTATION

Physical characterization

New methods of physical characterization were developed or adapted for WRD in this project. Geophysical methods such as micro-gravimetric surveys gave information on bulk density, degree of saturation, and porosity of the entire dump. Internal temperatures were monitored with chains of thermistors to derive temperature gradients and thermal properties (conductivity, heat production and heat fluxes). Large scale convection was described using airborne infrared thermography coupled with ground controls using infrared pyrometers to map surface temperature variations. Gas tubes were installed at different depths to measure oxygen concentration and the composition of gases. In each borehole, gas pressure (absolute and differential) was measured with a precision of 10^{-4} atmosphere (10 Pa) with a pressure transducer connected to a manifold valve system. Large scale granulometry tests were carried in the field with equipment built for that purpose. Special standard test used in concrete technology were used to measure rock toughness and resistance to physical breakdown. An acoustic celerometer was used to determine elastic wave velocities (compression and shear) in rock fragments as an index of their physical resistance. Several properties derived from these techniques were never documented before in WRD literature.

Hydrological characterization

The Mine Doyon site is equiped with monitoring equipment including: a weather station, collection ditches, weir stations, boreholes and piezometers. For the detailed analysis of water balance, more instrumentation is needed to estimate infiltration and evaporation rates and to help evaluate the volume of acid drainage originating in the dump when it is mixed with runoff generated in the hydrologic basin where WRD is located. Shallow gravity lysimeters were installed on the dump to measure direct infiltration to understand better the hydrological processes acting at the surface.

Geochemical and mineralogical characterization

Large waste rock samples were collected in surface trenches to identify rock types and their distribution. Drill cuttings were used extensively to study mineral transformations across the whole thickness of the WRD. Wa-Terra pumps were used for the first time in WRD research; they allow the use of dedicated sampling equipments without the problem of cross-contamination. Simple analytical procedures were developed to do routine water quality monitoring: the use of index parameters (pH, Eh, total dissolved solids, electrical conductivity) with regression curves is both effective and economical; quick analyses using X-ray fluorescence for major ions proved to be accurate, rapid, and cost effective. A new technique is proposed to measure the acid reaction products stored in the unsaturated zone using a leaching procedure with distilled water. Leachate samples from the unsaturated zone were also obtained by squeezing moist waste rock samples with a hydraulic press.

Microbiological characterization

Microbial populations were sampled over the entire thickness of the waste dump using drill cuttings and specific field preservation techniques. A special "bacterial trap" was developed to sample bacteria in the saturated groundwater zone at the base of the dump. A new laboratory method for counting bacteria was developed and applied at Mine Doyon.

B   MEASUREMENTS OF PARAMETERS AND PHYSICAL PROPERTIES

To better unsderstand acid rock drainage processes and model them, many parameters are required and a very limited number of studies have gathered significant and coherent field data. A major part of this project was dedicated to the measurement of all the parameters which are assumed to control acid generation and its transport. Here is a list of such parameters:

> Particle size distribution (granulometry); water content; degree of water saturation; bulk porosity of the dump; bulk density of the waste rocks; specific gravity of solids (rocks and minerals); hydraulic conductivity of underlying soils and rocks; air permeability (method being developed); oxygen concentration profiles; gas pressure; temperature gradients; thermal conductivity; heat capacity; surface temperature distribution and mappping; precipitation; air temperature; atmospheric pressure; piezometric (water) levels.

Other parameters are used for geochemical modeling. They include rocks and minerals characterization using total chemical analyses, X-ray diffraction and fluorescence, EDAX, scanning electron microscopy, image analysis, and optical petrographic microscopy. Chemical analyses of the acid leachate used ion chromatography, X-ray fluorescence, atomic adsorption, spectrophotometry, and standard wet chemical methods.

Microbial activity was studied through different procedures of bacteria enumeration, identification, population growth and decay, optimal temperature conditions, and kinetic transformation of ferrous to ferric iron.

C   MONITORING DATA FILES

The Mine Doyon project makes available extensive data files on physical properties such as temperature monitoring, weather data, flow rates, chemical data on acid drainage, gas composition and pressure. Most of these parameters are still being collected by the mine and therefore could become very valuable in the future for model calibration and validation.

8.2 CONTRIBUTIONS TO THE UNDERSTANDING OF KEY PROCESSES CONTROLING ACID ROCK DRAINAGE

The Mine Doyon project has produced important results on three types of processes responsible for acid rock drainage:

A   PHYSICAL PROCESSES

• Thermal profiles through the dump can be used effectively to calculate heat production and heat flow.
• Oxidation rates in the dump can be monitored by computing heat production at different levels and assuming that most heat results from the oxidation of sulphides by oxygen and ferric iron; sulphate production is derived from oxidation rates.
• Thermal analysis identifies air convection as the major mechanism of oxygen transfer at the site studied.
• Total heat production and internal temperatures have decreased significantly over a two year period (1991-1993) suggesting that maximum oxidation rates have peaked already.
• Air permeability is a key factor responsible for the beginning of convection in waste dumps; it is controled by grain size distribution, water content and degree of saturation.
• Waste rock disintegration is accelerated by water saturation of microfractures and splitting by secondary mineral precipitation.
• Mechanical properties of waste rocks (such as brittleness) are a major factor affecting oxidation rates in providing new surface exposures for sulfides.
• Schistose rocks containing sulphides such as the sericite schists found at La Mine Doyon are extremely reactive because of their brittleness.

B   HYDROLOGICAL PROCESSES

• In spite of large infiltration rates, only about 30% of total precipitation on the dump is recovered in the drainage ditches; losses to groundwater through the base is small (5 to 10% of total precipitation).
• Water permeability of the unsaturated material is very small unless the material is nearly saturated.
• Rapid water flow through the dump occurs only during major rainfall events or spring snowmelt.
• Percolating water during a year is not abundant enough to flush completely the reaction products which are generated suring the same time interval.
• Slow water movement appears to dominate mass transport; significant redistribution of water is done in the vapor phase.
• It may take up to 10 years to reach field capacity.
• Volumetric water content ranges from 10 to 12% in the dump and it is controlled by capillary properties in the unsaturated zone.

- Capillary properties are dependant on grain size and as the oxidation processes continue, more and more fine particles are generated and therefore may cause a slow increase in water content with time.
- Analysis of stream hydrographs at three weir stations show that most peak-flow events correspond to runoff generated outside the dump and that the baseflow component varies only slightly throughout the year.

C   GEOCHEMICAL PROCESSES

- Most oxidation reactions seem to occur at shallow depths (1 to 10 meters) where temperatures are optimal for bacteriological activity.
- Neutralization reactions involving silicates (mainly phyllosilicates such as chlorites and micas) are of major significance in explaining geochemical evolution of acid leachate and the precipitation of secondary minerals such as jarosite and gypsum.
- Dissolution of one mole of chlorite by acids consumes 16 moles of H^+; aluminum and magnesium are released in large quantities to the solution by this reaction.
- About two thirds of all sulphates produced are stored in the dump as secondary mineral precipitates and contribute to increase leachate concentration.
- Concentration of acid drainage in ditches varies mainly because it is more or less diluted by surface runoff originating outside the dump; composition of the baseflow generated by the dump is fairly constant throughout the year.
- Concentration of acid leachate in the unsaturated zone of the dump increases with time since oxidation products are generated faster than they are flushed out by percolating water.
- Notwithstanding the preceding observations, large dumps show remarkable thermal, hydraulic and chemical inertia, which means that changes in properties occur slowly and regularly with time.

D   MICROBIOLOGICAL PROCESSES

- *Thiobacillus ferrooxidans* and several other species are active throughout the dump including high temperature zones, groundwater, and surface seepage.
- Field evidence is conclusive that *Thiobacillus ferrooxidans* is active in the absence of oxygen by using ferric iron as an electron acceptor.

8.3   MODELING WATER, MASS, AND ENERGY TRANFERS IN WRD

- Physical modeling using TOUGH AMD can simulate actual conditions in a waste rock dump from the knowledge of physical parameters and initial conditions.
- The TOUGH AMD model can be used to simulate the result of corrective measures such as the placement of a partial cover and therefore it has an interesting potential as a management tool.

References

Bhatti, T.M., Bigham, J.M., Vuorinen, A,. and Tuovinen, O.H., 1992: Alteration of micas and feldspars associated with microbiological oxidation of pyrrhotite and pyrite. In *Environmental Geochemistry of Sulfide Oxidation*. ACS Symposium series 550. C. N. Alpers and D.W. Blowes eds. 204 th Nat. Meeting of the ACS, Washington, D.C., Aug. 1992. pp.90-105.

Beaudoin, P., and McMullen, J., 1990: L'approche environnementale pour le contrôle des effluents acides à la mine Doyon. *Conférences NEDEM, Colloque sur la réduction et le drainage des effluents acides générés par les activités minières.* CRM ed., Val d'Or, Québec, Nov. 28, 1990. pp. 85-95.

Belle-Ilse, F., Bienvenue, L., Paquet, A. and Robert, J.M., 1993: Programme de recherche visant la neutralisation des eaux de drainage dans l'environnement minier (NEDEM). Rapport Annuel 1992-1993. Published by: Centre de Recherches Minerales, Ministère de l'Énergie et des Ressources, Sainte-Foy, Québec.

Blowes, D.W. and Jambor, J.L., 1990: The pore-water geochemistry and the mineralogy of the vadose zone of sulfide tailings, Waite Amulet, Québec, Canada. *Appl. Geochem.* **5**, 327-346.

Bourque, E., 1994: Hydrologie d'une halde de stériles miniers affectée par le drainage minier acide. Essai de maîtrise, Département de génie civil, Université Laval.

Brock, T.D., and Gustafson, J., 1976: Ferric iron reduction by sulfur- and iron-oxidizing bacteria. *Appl. Environm. Microbiol.*, **32**, 567-571.

Cathles, L.M., and Apps, J.A., 1975: A model of the dump leaching process that incorporates oxygen balance, heat balance, and air convection. Metal. Trans. B, vol. 6B, p. 617-624.

Cathles, L.M., and Schlitt, W.J., 1980: A model of the dump leaching process that incorporates oxygen balance, heat balance, and two dimensional air convection.Dans Schlitt, W.J., ed., Leaching and recovering coper from as-mined materials. Proc. of the Las Vegas Symp., 26 Feb., 1980, Solution Mining Commitee, Soc. of Mining Eng. of AIME, pp. 9-27.

Choquette, M. and Gélinas, P., 1994: Mineralogical transformations associated with AMD production in a waste rock dump. La Mine Doyon South waste rock dump. Report GREGI 1994-06, Dep. de Génie Géologique, Université Laval, Québec. Report submitted to CANMET.

Choquette, M., Gélinas, P. and Isabel, D., 1993a: Two rapid methods to evaluate acid mine drainage composition: total dissolved solids and energy dispersive X-ray fluorescence spectroscopy. Report GREGI 1993-04, Dep. de Génie Géologique, Université Laval, Québec. Report submitted to CANMET.

Choquette, M., Gélinas, P. and Isabel, D., 1993b: Monitoring of acid mine drainage: chemical data from la Mine Doyon - South waste rock dump. Report GREGI 1993-05, Dep. de Génie Géologique, Université Laval, Québec. Report submitted to CANMET.

Dake, L.P., 1978: Fundamentals of reservoir engineering. Elsevier, Amsterdam, 443 p.

Duchesne, J., 1993: Le rôle des ajouts mineraux face aux réactions alcalis-granulats dans le béton: mécanismes de réaction, performance et essais d'évaluation de la performance. Thèse de doctorat. Dept. de Géologie, Université Laval, Québec.

Fanning, D.S., Keramidas, V.Z. and El-Desoky, M., 1989: Micas. In: *Minerals in soil environments*, 2nd ed. J.B. Dixon and S.W. Weed ed. pp. 551-634.

Feasby, D.G., Blanchette, M. and Tremblay, G., 1991: The mine environment neutral drainage (MEND) program. *Proc. of the Second Int. Conf. on the Abatement of Acidic Drainage.* Montréal, Sept. 16-18, 1991. 1, pp. 1-27.

Firlotte, F.W., Gélinas, P., Knapp, R., and McMullen, J., 1990: Acid drainage treatment at La Mine Doyon: Evolution and future direction. Dans MEND, éd., Proc. of the Second Int. Conf. on the Abatement of Acidic Drainage, Montréal, sept.16-18, vol. 4, pp.119-139.

Gélinas, P., Bérubé, M.-A., Choquette, M., Leroueil, S., Locat, J., and Lefebvre, R., 1990: Évaluation in-situ de la performance des barrières sèches pour les parcs à roches stériles qui produisent des effluents acides. Report GGL 90-23 submitted to the Service de la technologie minière, Centre de recherches minérales, Nov. 1990, 39 p.

Gélinas, P., Choquette, M., Lefebvre, R., Isabel, D., Leroueil, S., Locat, J., Bérubé, M.A., Thériault, D. and Masson A., 1991: Évaluation du drainage minier acide et des barrières sèches pour les haldes de stériles: Étude du site de la Mine Doyon. Report GREGI 1991-19. Report submitted to Centre de Recherche Minérales, Ministère de l'Énergie et des Ressources du Québec.

Gélinas, P., Lefebvre, R. and Choquette, M., 1992: Characterization of acid mine drainage production from a waste rock dump at La Mine Doyon, Québec. *Second Int. Conf. on Env. Issues and Manag. of Waste in Energy and Mineral Prod.* Calgary, Alberta. Sept. 1992.

Grant, F.S. and G.F. West, 1965: Interpretation and theory in applied geophysics. Toronto, McGraw-Hill Book Co., 584 p.

Guay, R., M.Silver and A.E.Torma. 1977. Ferrous iron oxidation and uranium extraction by *Thiobacillus ferrooxidans* . Biotechnol.Bioeng. **19**: 727-740.

Guay, R. 1993. Development of a modified MPN procedure to enumerate iron oxidizing bacteria. Report submitted to MEND prediction committee. February 1993.

Guay, R. 1994. Diversité microbiologique dans la production de drainage minier acide à la halde sud de la Mine Doyon. MEND report 1.14.2. March 1994. 64 p. and app.

Guay, R., J.Ghosh and A.E.Torma. 1989. Kinetics of microbiolgical production of ferric ion for heap and dump leaching. in: Biotechnology in Mineral and Metal Processing. B.J.Scheiner, F.M.Doyle and S.Kawatra, Eds,. Society of Mining Engineers, Inc.,Littleton, Colorado. pp. 95-106.

Harries, J.R., and Ritchie, A.I.M., 1986: The impact of rehabillitation measures on the physicochemical conditions within mine wastes undergoing pyritic oxidation. Proc. of the sixth int. symp. on biohydrometallurgy. Vacouver, Canada, 21-24 august 1985, pp. 341-351.

Hirschfelder, J.O., Curtis, C.F., and Bird, R.B., 1954: Molecular theory of gases and liquids. John Wiley & Sons, New York, NY.

Hiskey, J.B. and Schlitt, W.J., 1981: Aqueous oxidation of pyrite. In Schlitt, W.J. ed.,*Interfacing technologies in solution mining*. Proc. of the second SME-SPE int. solution mining symp. Denver, Colorado, Nov. 18-20, 1981. pp. 55-74.

International Formulation Committee, 1967: A formulation of the thermodynamic properties of ordinary water substances. IFC Secretariat, Düsseldorf, Germany, 1967.

Isabel, D., Gélinas, P.J., Bourque, E., Nastev, M., and Précourt, S., 1994: Water budget for the waste rock dump at La Mine Doyon, Québec. Rapport GREGI 94-05, Département de géologie et de génie géologique, Université Laval, présenté à CANMET, Programme NEDEM, 50 p. et annexes.

Isabel, D, and Blanchet, J., 1991: Évaluation de la performance hydrologique d'une couverture en matériaux naturels sur la halde sud de la Mine Doyon a l'aide du logiciel HELP. Rapport GREGI-91-33, Département de géologie, Université Laval.

Isabel, D., and Masson, A., 1991: Analyse des précipitations journalières pour la mine Doyon. Rapport présenté au Service de la Technologie Minière du MER, Rapport GREGI 91-13, Département de Géologie, Université Laval.

Jambor, J.L. and Blowes, D.W., 1991: Mineralogical studyof low-sulphide, high-carbonate, arsenic bearing tailings from the Delnite minesite, Timmins Area, Ontario. *Proc. of the Second Int. Conf. on the Abatement of Acidic Drainage*. Montréal, Sept. 16-18. 4, pp. 175-197.

Jaynes, D.B., 1983: Atmosphere and temperature within a reclaimed coal-stripmine and a numerical simulation of acid mine drainage from stripmined lands. Ph.D. Thesis, Pennsylvania State University, 198 p.

Lafleur, R., E.D.Roy, D.Couillard and R.Guay. 1993. Determination of iron oxidizing bacteria numbers by a modified MPN procedure. in Biohydrometallurgical Technologies. eds A.E.Torma, M.L.Apel and C.L.Brierley. The Minerals, Metals & Materials Society.

Lefebvre, R., 1994: Caractérisation et modélisation numérique du drainage minier acide dans les haldes de stériles. Ph.D. Thesis, Université Laval.

Lefebvre, R., Gélinas, P., and Isabel, D., 1992: Heat transfer analysis applied to acid mine drainage production in a waste rock dump, La Mine Doyon (Québec). 1992 Int. Ass. of Hydrogeol., Hamilton, May 1992.

Lefebvre, R., Gélinas, P., and Isabel, D., 1993: Heat transfer during acid mine drainage production in a waster rock dump, La Mine Doyon (Quebec). Rapport GREGI 93-03, submitted to MEND Prediction committee, March 1993, 46 p. and app.

Levenspiel, L., 1972: Chemical reaction engineering, Second edition. John Wiley & Sons, New York, 578 p.

Llamas, J., 1985: Hydrologie générale: Principes et méthodes. Gaëtan Morin éditeur, Chicoutimi.

Locat, J., Bérubé, M.A., Gélinas, P. and Choquette, M. 1994. Caractéristiques 'physico-chimiques et mécaniques des principales unités lithologiques à la Mine Doyon. Report GREGI 1994-04, submitted to MEND prediction committee, January 1994, 26 p. and app.

Locat, J., Beauséjour, N. and Bérubé, M.A., 1986. Utilisation du céléromètre ultrasonique sur des sols cohérents. *Canadian Geotechnical Journal*, **23**. pp. 247-250.

McDonald, M.G., and Harbaugh, A.W., 1984: MODFLOW, A modular three-dimensional finite-difference ground-water flow model. USGS, Techniques of Water-Resources Investigations, Book 6, Capter A1.

Mangold, D.C., and Tsang, C.-F., 1991: A summary of subsurface hydrological and hydrochemical models. Reviews of Geophysics, 29, no.1, pp. 51-79.

Marsily, G. de, 1986: Quantitative Hydrogeology. Academic Press, San Diego, 440 p.

Morin, K.A., 1988: Physical and chemical hydrogeology of uranium tailings in Canada and in the United States of America. *Proc. Int. Groundwater Symp, Int. Ass. of Hydrogeologists.* Halifax, Nova Scotia, May 1-5, 1988. pp. 175-188.

Narasimhan, T.N. and Witherspoon, P.A., 1976: An integrated finite difference method for analyzing fluid flow in porous media. Water Resour. Res., 12, no.1, pp. 57-64.

Nastev, M., and Isabel, D., 1993: Modélisation des écoulements souterrains sous la halde sud de la Mine Doyon. Rapport GREGI 93-11, Département de géologie et de génie géologique, Université Laval.

Otwinowski, M., 1993: Quantitative analysis of chemical and biological kinetics for acid mine drainage problem. MEND/B.C. AMD Task Force Report, 143 p.

Pantelis, G., and Ritchie, A.I.M., 1991: Macroscopic transport mechanisms as rate-limiting factor in dump leaching of pyritic ores. Appl. Math. Modeling, 15, March, pp. 136-143.

Pantelis, G., and Ritchie, A.I.M., 1992: Rate-limiting factors in dump leaching of pyritic ores. Appl. Math. Modeling, 16, October, pp. 553-560.

Parker, J.C., 1989: Multiphase flow and transport in porous media. Reviews in Geophys., 27, no.3, pp. 311-328.

Précourt, S., 1993: Rapport hydrologique de la halde sud, Mine Doyon, Cadillac, Québec. Essai de maîtrise, Département de géologie et de génie géologique, Université Laval.

Pronk, J.T., K.Liem, P.Bos and J.G.Kuenen. 1991. Energy transduction by anaerobic ferric ion respiration in *Thiobacillus ferrooxidans* . Appl.Environm.Microbiol., **57**: 2063-2068.

Pruess, K., 1987: TOUGH User's Guide. Lawrence Berkely Laboratory LBL-20700, Nuclear Reg. Comm. NUREG/CR-4645, 78 p.

Pruess, K., 1991: TOUGH2 - A general-purpose numerical simulator for multiphase fluid and heat transfer. Lawrence Berkely Laboratory LBL-29400, 102 p.

Rimmer, S.M. and Eberl, D.D., 1982: Origin of an underclay as revealed by vertical variations in mineralogy and chemistry. *Clays and Clay Minerals*. **30** (6), 442-430.

Ross, J.G., 1969: Acid dissolution of chlorites: release of magnesium, iron and aluminium and mode of acid attack. *Clays and Clay Minerals* **17**, 347-354.

Ross, J.G. and Kodama, H., 1974: Experimental transformation of a chlorite into a vermiculite. *Clays and Clay Minerals* **22**, 205-211.

Savoie, A., Trudel, P., Sauvé, P., Hoy, L. and Kheang, L., 1991: Géologie de la mine Doyon (région de Cadillac). Rapport ET 90-05. Ministère de l'Énergie et des Ressources du Québec.

Silverman, M.P. and D.G.Lundgren. 1959. Studies on the chemoautotroph iron bacterium *Ferrobacillus ferrooxidans* . I. An improved medium and a harvesting procedure for securing high cell yields. J.Bacteriol., **77**: 642-647.

Stallman, R.W., 1965: Steady One-Dimensional Fluid Flow in a Semi-Infinite Porous Medium with Sinusoidal Surface Temperature. Jour. of Geoph. Res., v.70, no.12, p.2821-2827.

Sugio, T., White, K.J., Shute, E., Choate, D. and Lake, R.C.B., 1992: Existence of a hydrogen sulfide: ferric ion oxydo-reductase in iron-oxidizing bacteria. *Apply. Environm. Microbiol.*, **58**, 431-433.

Suzuki, I., L.Travis, T.Takeushi, T.D.Yuthasastrakosol and J.K.Oh. 1990. Ferrous iron and sulfur oxidation and ferric iron reduction activities of *Thiobacillus ferrooxidans* are affected by growth on ferrous iron, sulfur and a sulfide ore. Appl.Environmen.Microbiol., **56**: 1620-1626.

Theisen, A.A. and Harward M.E., 1962: A paste method for the preparation of slides for clay minerals identification by X-ray diffraction. *Soil Science Society of America Proceedings* **26**, 90-91.

Weeks, E.P., 1979: Field determination of vertical permeability to air in the unsaturated zone. U.S. Geol. Surv. Prof. Paper 1051, 41 p.

Wessel, P., and Smith, W.H.F., 1991: Free software helps map and display data. EOS Trans. Amer. Geophys. U., 72, pp. 441, 445-446.